CRANFIELD UNIVERSITY

DEFENCE COLLEGE OF MANAGEMENT AND TECHNOLOGY

DEPARTMENT OF ENGINEERING AND APPLIED SCIENCE

EngD THESIS

Academic Year 2010-2011

STEPHANIE FOLLETT

BLAST ANALYSIS OF COMPOSITE V-SHAPED HULLS: AN EXPERIMENTAL AND NUMERICAL APPROACH

SUPERVISOR: DR AMER HAMEED

July 2011

"THE LENGTH OF THIS DOCUMENT DEFENDS IT WELL AGAINST THE RISK OF ITS BEING READ"

WINSTON CHURCHILL (30 NOVEMBER 1874 – 24 JANUARY 1965)

ABSTRACT

During armed conflicts many casualties can be attributed to incidents involving vehicles and landmines. As a result mine protective features are now a pre-requisite on all armoured vehicles. Recent and current conflicts in Iraq and Afghanistan have shown that there is a requirement for vehicles that not only provide suitable protection against explosive devices but are also lightweight so that they may travel off-road and avoid the major routes where these devices are usually planted.

This project aims to address the following two topics in relation to mine protected vehicles.

1. Could composite materials be used to replace conventional steels for the blast deflector plates located on the belly of the vehicle, and
2. How effective and realistic is numerical analysis in predicting the material response of these blast deflectors.

It also looks into the acquisition and support of new equipment into the armed services, where the equipment itself is but one small element of the system involved.

The first topic has been addressed by conducting a number of experimental tests using third scale V-shaped hulls manufactured from steel and two types of composite, S2 glass and E glass. These experiments found that, on a weight-for-weight equivalency, the S2 glass was by far the superior material, with very little damage to the outside shape of the hull. The steel was significantly deformed after testing and the E glass, although also did not deform as such, did experience a severe amount of matrix cracking leading to significant loss of structural integrity in that the hull could be easily flexed by hand after the tests.

One S2 glass hull was also subjected to a further two explosive tests and although the amount of delamination was severe at the base of the hull there was very little geometry lost to the outside of the shape.

The numerical modelling work consisted of the modelling of the mine blast phenomenon in autodyn and comparisons with published experimental and numerical work, with the results in reasonably good agreement. The second part consisted of comparing flat S2 glass plates subjected to varying charge sizes both experimentally and numerically in order to validate the material model, with good agreement. The final stage involved using the validated material model and re-creating the tests done on the V-shaped hulls. The results here at first were not in agreement, but with development of the model and the limitations from the experimental data collection methods applied a model that, when viewed with the experimental results, gave a reasonable representation of the experimental work was created.

The management section of the thesis considers previous equipment purchases and what went wrong during their implementation. The Through Life Capability Management model is assessed in relation to an all composite vehicle and identifies some key questions and areas of concern, such as how the management of the DLOD trade-off process should be conducted.

ACKNOWLEDGMENTS

The author would like to thank the following people for all their help and support throughout the duration of this project, without whom I doubt this thesis would have ever materialised

First and foremost my supervisor, Dr Amer Hameed, whose help and guidance has been invaluable throughout the course of this project. You have always gone out of your way to help, despite on occasion it not being relevant to this work. Thank you.

To everyone at NP Aerospace, the sponsors of this work, who have helped throughout this work. You have given me an insight into the world beyond academia and through you I have learnt and experienced so much. This project would never have got off the ground without your financial support and your ideas have kept it moving throughout. You have my eternal gratitude for giving me this step in my future career.

The list of people at Shrivenham who have helped me throughout this work is a very long one and there is not room to mention them all here, below is a list of some, which is by no means comprehensive. To you all, I would not have got through the past years without your help, support and the ability to make me laugh when everything has gone wrong.

- Ian Horsfall – your time and expertise during the testing phase is greatly appreciated, when you were able to be found, you gave your time gladly, and I will always be thankful for that.
- Alan Peare – for understanding that computers do not like me, and have even set themselves on fire to be rid of me. I would have given up a long time ago without your ability to always find me another.
- To everyone at the Bashforth Laboratory, your help with all the heavy lifting during testing and the endless cups of tea, despite me not being in your group will always be remembered, thank you.
- To the workshop staff, especially Bob and Chris, your ability to fix quickly whatever I managed to break was invaluable, plus you would both make great agony aunts. So thank you not only for helping me with work, but for always having the time to listen.
- The ASET staff in particular Graeme but not forgetting Paul and Jim. Always willing to lend a hand especially with the heavy lifting I would never have finished on time without all your help.

- Mike Gibson – the one and only person at Shrivenham who understood my many ramblings about AUTODYN. You always had time to listen and to help, and your cheerful outlook on everything makes me realise how glad I am to have known you. Thank you very much.

To everyone else at Shrivenham, you know who you are; I have never met a more helpful group of people. During the past eight years I have come to view you all as a family and although I am excited about the next stage of my life and career, I will miss you all and very much hope to come back at some point. Please stay in touch.

Kate, Helen and Liza, your influence has probably damaged my liver irreparably however you are the very best of friends and wish you all the luck with your future careers and lives.

To my family and friends, especially my parents, your unparalleled support is certainly one of a kind and would not change a single moment of it. You have always been there to support me and my decisions and I would not be the person I am today without your backing and your love. I thank you from the bottom of my heart.

Last but by no means least, Jenks. You know how much you mean to me, thanks are nowhere near enough for all you have done. You have been there before, during and now I hope after, you have been the inspiration to keep going when everything has fallen down around me and I am very much looking forward to the next stage in our lives together.

CONTENTS

LIST OF FIGURES

LIST OF TABLES

LIST OF GRAPHS

LIST OF ABBREVIATIONS

STANAG	Standardisation Agreement
TLCM	Through Life Capability Management
DLoD	Defence Lines of Development
IED	Improvised Explosive Device
AFV	Armoured Fighting Vehicle
LPPV	Light Protected Patrol Vehicle
MoD	Ministry of Defence
CAV	Composite Armoured Vehicle
CFL	Courant-Fredichs-Lewy
ALE	Arbitrary Lagrange Euler
SPH	Smooth Particle Hydrodynamics
EoS	Equation of State
TMD	Theoretical Maximum Density
JWL	Jones-Wilkins-Lee
AEP	Allied Engineering Proposal
DoB	Depth of Burial

"SCIENCE MAY SET LIMITS TO KNOWLEDGE, BUT SHOULD NOT SET LIMITS TO IMAGINATION"

BERTRAND RUSSELL (1872 –1970)

1 INTRODUCTION

This thesis will look at using composite materials as a replacement for steels in the manufacture of armoured vehicles. Specifically it will concentrate on the response of composite materials under blast loading by using numerical analysis techniques. Numerical analysis - finite element analysis - is a cost effective method of testing an idea without having to construct various models for testing throughout the design process. The key question is whether the numerical analysis is accurate. This thesis not only conducts the experiments numerically but also provides comparable results from actual experiments in order to validate the models used.

This thesis also looks and addresses the method by which new equipment is introduced into the armed services, by means of research into the topic and a case study based on introducing an all composite vehicle. By investigating this topic a better understanding of how the need for new equipment is identified and how mistakes that should have been avoided can be avoided with the use of the Through Life Capability Management model.

This chapter will assess the need for the project, whilst looking at the background to the problem. The chapter concludes with the thesis outline.

1.1 BACKGROUND

1.1.1 COMPOSITE MATERIALS

Composite materials are considered to be one of the foremost advances in engineering materials over the past century, even though the primitive idea can be dated back over 6000 years ago, when bricks for building were constructed from a straw and mud mix. The main reason for their popularity is they can offer a much higher strength to weight ratio than their steel counterparts, they can also be designed to suit a specific purpose.

In a military context there is a great need to reduce the weight of armoured vehicles without compromising on levels of protection. With threats similar to those currently being encountered in Iraq and Afghanistan, to provide complete protection with conventional materials would mean that the vehicles would be almost impossible to transport easily. The infrastructure in Afghanistan is also unable to cope with this weight on most roads, and travelling off-road becomes almost impossible.

Composites for vehicle armour were first used in the mid 1950's with the Americans experimental T95 series which used a ceramic composite (Ogorkiewicz, 1991). Although this vehicle never went into production the idea remained and the first widespread use of composites for armoured vehicles was on the soviet T-64. It used armour made from glass reinforced plastic, sandwiched between inner and outer steel layers; this was known as Combination K (Army Guide).

Figure 1-1 T-64 Soviet Main Battle Tank (Battletanks.com, 2010)

Over the years composites have been further developed and improved considerably, so much so that it is now currently possible to have vehicle body made entirely from composite materials. For example the SPV400 from Supacat and NP Aerospace has a crew pod made entirely from composite materials, with no internal frame, so all road loads are transmitted through the composite. Whereas, previously some form of framework needed to be included as composites were not able to take the structural loads associated with armoured vehicles.

Figure 1-2 Supacat SPV400 photo taken at vehicle launch April 2010 by author

1.1.2 LAND MINES AND IED'S

Land mines have always been one of the most dangerous weapons, since WWII more vehicles have been lost to landmines than any other threat (Bird, 2001). Many research studies have looked into ways of protection against anti-tank (AT) and anti-personnel (AP) mines, however with the advent of the conflicts in Iraq and Afghanistan the threat of landmines has been superseded by improvised explosive devices (IEDs). Table 1-1 below shows how many of the coalition forces personnel were killed by IEDs in Afghanistan over the past ten years. It is important to note that this table does not break down the number of people killed into mounted and dismounted patrols.

PERIOD	IED	TOTAL	PERCENTAGE
2001	0	4	0.00%
2002	4	25	16.00%
2003	3	26	11.54%
2004	12	27	44.44%
2005	20	73	27.40%
2006	41	130	31.54%
2007	78	184	42.39%
2008	152	263	57.79%
2009	275	449	61.25%
2010	368	630	58.41%
2011	252	492	51.22%

Table 1-1 IED Fatalities Afghanistan (iCasualties, 2011)

IEDs are constructed from almost anything, with any type of material and initiator. They are unique to the creator as they are constructed with whatever is at hand.

IEDs fall into three types of categories (Global Security, 2010):

1. *Package Type IEDs* – these include munitions placed in potholes and covered with dirt on the road and containers filled with explosive and shrapnel. The most common explosives used are military munitions, of 120mm and above, as they have a readymade fragmentation effect. They can be placed on their own or as part of a group all linked together, known as daisy chaining. Figure 1-3 shows two different IEDs found in Afghanistan in 2008.
2. *Vehicle-Bourne IEDs (VBIEDs)* – these are where vehicles are used as the package. The vehicle will be packed with explosives and the vehicle left near or driven towards the target.

3. *Suicide Bomb IED* – The suicide bomber usually wears a vest packed with explosive and shrapnel for fragmentation, intending to maim and kill as many civilians and/or coalition force members as possible. The only way to stop these attacks is to use deadly force.

For the purposes of this project, the focus will be on the package type IEDs and the effect that they have on the vehicles which drive over them.

Figure 1-3 Buried IEDs in Afghanistan (X Coy 45 Commando Op Herrick 9, 2008)

For the protection against blast on vehicles there is a STANAG level that was introduced in 2004. STANAG Levels are; S*tandardisation Agreements* that cover processes, procedures, terms and conditions for common military or technical procedures or equipment between members of the alliance. (NATO, 2010)

STANAG Level 4569 covers the *Protection Levels for Occupants of Logistic and Light Armoured Vehicles*. The Standard covers strikes from kinetic energy (KE), artillery and blast mines, Table 1-2 below shows only the blast threat levels. A full copy of the agreement can be found in Appendix 2.

However the variation in every aspect of an IED makes it very difficult to predict and therefore protect vehicles and people against this threat.

LEVEL		GRENADE AND BLAST MINE THREAT	
4	4b	Mine explosion under centre	10kg (explosive mass) Blast AT Mine
	4a	Mine explosion pressure activated under any wheel or track	
3	3b	Mine explosion under centre	8kg (explosive mass) Blast AT Mine
	3a	Mine explosion pressure activated under any wheel or track	
2	2b	Mine explosion under centre	6kg (explosive mass) Blast AT Mine
	2a	Mine explosion pressure activated under any wheel or track	
1	Hand grenades, unexploded artillery fragmenting submunitions, and other small anti personnel explosive devices detonated anywhere under the vehicle		

Table 1-2 STANAG 4569 Floor Protection Levels for Logistic and Light Armoured Vehicle Occupants for Grenade and Mine Blast Threats (NATO Standardization Agency, 2004)

1.2 RESEARCH AREAS

Due to the reasons detailed above mine protection features are now a pre-requisite on all vehicles sent to theatre. There are three main areas where research has been conducted over the past few years:

1. *Prediction of the blast load* – this area deals with the propagation of the blast through the ground and surrounding air. Taking into account moisture content and soil particle size.
2. *Vehicle response to the blast* – this area considers the design features that may be implemented on a vehicle in order to deflect the blast around the vehicle, absorb as much of the remaining blast as possible and therefore mitigate the effects seen inside the vehicle.
3. *Vulnerability of occupants* – assesses the impact that blast loading has on individuals. Including fragments, high shock pressures, and motion of the vehicle as a result of the explosion.

The area that this project focuses on is the response of the vehicle hull to blast. The prediction of the blast load is briefly analysed looking at the work done by (Fiserova, 2006) and in the conference proceedings (Follett et al., 2010) shown in Appendix 1.

1.2.1 METHODS OF APPROACH

There are two main methods that are used to approach the blast analysis part of the problem

1. Experimental approach – gives a definite idea of how the vehicle will respond to blast loading. Unfortunately, this approach is both labour intensive and resource heavy to set up, it can also be very expensive to test at intermediate stages.

2. Theoretical approach – this method uses numerical simulations to predict what the vehicle will do under different loads. It allows the user to analyse what occurs at different stages of the blast and provides lots of useable data. However it is a time consuming process and the user must have knowledge of the software and what it is they are trying to model.

These two methods do in fact complement one another and it would not be wise to use one without the other, especially when using numerical simulations. These cannot be guaranteed to survive without the validation gained from the experimental approach. The experimental approach and the understanding of the situation can be improved with results from the theoretical approach.

This project will mainly focus on the theoretical approach, though experiments have been conducted at every stage and to validate the numerical models used.

1.3 SPONSOR COMPANY

The company sponsoring this project is NP Aerospace based in Coventry. They are one of the largest thermosetting moulding companies in Europe and supply products to the defence, electrical, aerospace, automotive and medical industries.

NP Aerospace was the first company in the world to have mass produced a composite structured armoured vehicle. They have had vehicles in service since 1993 and have amassed a unique database on design and manufacturing techniques to ensure every vehicle that they put out is of unrivalled quality and reliability.

1.4 RESEARCH SPECIFICATION

The aims of this research are broken down into two main sections, experimental work and numerical work. Experimentally the aims are to discover if composites can provide better levels of protection than their steel counterparts, for weight-for-weight equivalency, under blast loading, and to address the shape vs. stand-off argument for the V-shaped hulls.

Numerically the aims and objectives can be broken down into three stages of increasing complexity. The first stage is to recreate the blast phenomenon in the commercially available software AUTODYN and to compare with published experimental data and data from other software. The next stage is to then validate the material model used by recreating experimental work on different charge sizes and their blasts impacting on flat plates. The

third and final stage involved recreating the experimental work conducted on steel and composite V-shaped hulls and then comparing all data.

1.5 WORK DISSEMINATIONS

Research findings were presented in the following peer-reviewed conferences and journals.

- Follett, S. *et al* Numerical Simulations as a Reliable Alternative for Landmine Explosion Studies: The AUTODYN Approach. In *ASME 2010 International Mechanical Congress and Exhibition* (Vancouver, British Columbia, Canada, November 2010)

Work was also presented at the following events without submission of a paper.

- Poster presentation at London Technology Network: Blast Resistant Structures, November 2009, Royal Geographical Society, London
- Group of Experts for Mitigation Systems (GEMS) Conference, January 2011, Imperial College London.

For a copy of all these disseminations please refer to Appendix 1.

1.6 THESIS OUTLINE

The thesis deals with the following topics

CHAPTER 2: THROUGH LIFE CAPABILITY MANAGEMENT

- This chapter discusses the considerations and the chain of events that occur when a new piece of equipment is implemented into the armed services

CHAPTER 3: LITERATURE REVIEW

- This chapter discusses and analyses the relevant literature and identifies the gap where this project will lie

CHAPTER 4: MODELLING USING ANSYS AUTODYN

- The software used throughout this project is explained in this section, with detailed step-by-step guides on how models were created, assembled and run.

CHAPTER 5: EXPERIMENTAL WORK

- This chapter covers all experimental work undertaken throughout the course of this work and the results of that work.

CHAPTER 6: MODELLING EXPERIMENTAL WORK

- This chapter recreates the experimental work within the numerical modelling software and the results are presented along with the discussion of these results

CHAPTER 7: DISCUSSIONS AND FUTURE WORK

- In this chapter the work conducted is reviewed and evaluated with references to any further work that could be undertaken to improve the results and/or to take the work further.

CHAPTER 8: CONCLUSIONS

- The conclusions of the project are addressed and presented in this chapter.

"FOR EVERY COMPLEX PROBLEM THERE IS A SIMPLE SOLUTION THAT IS WRONG"

GEORGE BERNARD SHAW (1856-1950)

2 THROUGH LIFE CAPABILITY MANAGEMENT

Throughout this thesis there is a concentration on the physical design and construction of an armoured vehicle made from composite materials. However, as will be explained in this chapter, the acquisition and support of a new platform or equipment needs to be considered in terms of a "system of systems" in which the equipment itself is but one element.

2.1 INTRODUCTION

There is rich vein of literature, in particular from the National Audit Office (NAO) that is highly critical of the Ministry of Defence's ability to deliver new equipments within the pre-agreed cost, time and performance boundaries. For example the press release pages of the NAO website (National Audit Office, 2004) and the annual Major Projects Reports presented to Parliament every year detailing the MOD's progress on procurement for major pieces of defence equipment (National Audit Office, 2011).

However, a number of examples over the past ten years have emphasised the need to look wider than, simply, the equipment related costs. As a result of this, a new process called "Through Life Capability Management" (TLCM) was developed and, within this eight key strands (or "Defence Lines of Development" (DLODs)) were identified. These will be discussed further in this chapter, but first, two cases will be offered as examples underlying the importance of recognising the need to understand all of the costs associated with the introduction of a new or replacement capability – and not simply those related to the equipment itself.

2.1.1 BOWMAN CASE STUDY

Bowman and the associated Combat Infrastructure Platform (CIP), and programmes were introduced both as a replacement for the ageing Clansman radio system, as well as part of a much wider implementation of information systems down to unit level within all three Armed Forces. The programme involved conversion of some 15,700 land vehicles, 141 naval vessels and 60 helicopters. Contracts worth £2.4 billion were placed with General Dynamics

UK in 2001 for Bowman and 2002 for the CIP (Armedforces.co.uk, 2012; National Audit Office, 2006).

By not examining every stage before implementation the Department seriously underestimated the challenges involved in both delivering and sustaining the new system in service. For example, the failure to survey the state of the Army's vehicles adequately led to difficulties in conversion from the Clansman system to Bowman. For example a 'standard' vehicle of each type was selected and used as the basis for all subsequent plans, drawings and fittings. In reality, however, there were multiple variants of each class of vehicle with different pre-existing equipment and equipment locations within these 'fleets within a fleet'. By the same token, the costing of the provision of training was based on that for Clansman. However, Bowman was a significantly more complex system, and the consequential training burden was manifestly greater leading to additional costs of £121 million and a two year extension in the timescale (National Audit Office, 2006; House of Commons Committee of Public Accounts, 2007).

2.1.2 APACHE CASE STUDY

The introduction of the Apache Helicopter is a similarly well documented case of oversights with training leading to significantly increased costs. The key issue with the introduction of the Apache was the decision to proceed with the separate contracts for the weapons system and the training. The underlying premise for this approach had merit as it was clear that the equipment itself could only be provided by the sole supplier, McDonnell Douglas. However, it was reasoned that the training system could be subject to tender. Unfortunately, this proved to be a misjudgement as the intellectual property rights (IPR) for the software underpinning the training systems were also held by McDonnell Douglas (who in 1997 merged with rival Boeing). In April 1997 a PFI proposal was submitted by Westland, teamed with Boeing in a joint venture company, ATIL, which was, eventually, awarded the contract. Nevertheless, by separating the equipment and training contracts and, hence, the oversight of them, a mismatch in delivery timing occurred. As a result, the Apache airframes were delivered over 12 months before the pilots were trained to fly them. The resultant bill for garaging the unusable aircraft at RAF Shawbury was £6 million (National Audit Office, 2002).

A further result was that the arrangement for providing spares to support the helicopter for the first 30 months of operation was flawed as it was linked to a forecast schedule of flying and not actual rates of flying (National Audit Office, 2002; House of Commons Committee of Public Accounts, 2003).

2.2 THE THROUGH LIFE CAPABILITY MANAGEMENT MODEL.

As a result of the above, and similar, experiences, the MOD developed the Through Life Capability Management (TLCM) model, as shown in Figure 2-1 below.

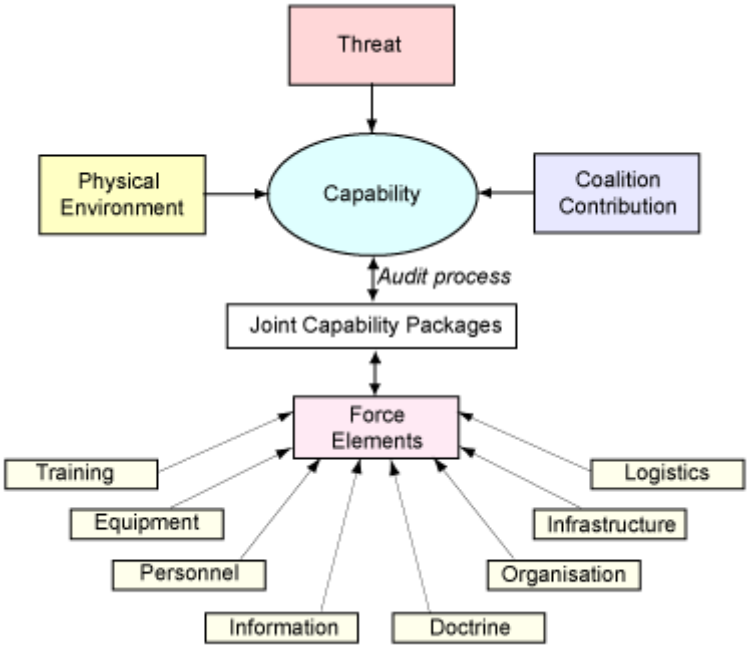

Figure 2-1 Through Life Capability Management (Ministry of Defence, Acquisition Operating Framework, 2009b)

From an academic perspective, it can be seen that the approach has broad alignment with Barney's resource based view of the firm. Barney argues that a firm can be conceived as a bundle of resources and it is these resources that if managed correctly lead to a sustained competitive advantage (Barney, 1991).

2.3 EXPLANATION OF MODEL

The TLCM model is aimed at translating the requirements of Defence policy into an approved programme that delivers the required capabilities, through-life, across all Defence Lines of Development (DLoDs) (Ministry of Defence, Acquisition Operating Framework, 2009a).

The underlying purpose of this model is to allow the **full** scope of the costs associated with both the introduction and through life management to be appreciated and understood.

This ensures that areas such as the training costs and the ongoing maintenance of the equipment can be budgeted for, prior to any implementation. However it can also indicate where trade-offs could be made in order to optimise the performance, cost and time characteristics of a project or programme. For example in the Apache case discussed above, it would clearly have been ideal if the companies responsible for the training and equipment elements had stayed in step with one-another, trading costs as and when appropriate in order to minimise the overall programme costs and achieve on time delivery.

The model works, by the following:

1. Defining the capability: This occurs by determining the threat, identifying the physical environment where the threat is located and analysing any contribution from coalition forces.
2. The capability can then be delivered by the force elements; which come from various aspects of the armed forces. These are:
    - Ships and submarines
    - Aircraft
    - Army formations
    - other Military Units
    - Force Enablers

Each Force Element is delivered either by, a single service, or by a joint organisation, and requires the integration of the eight defence lines of development (DLoDs). These DLoDs are training, equipment, personnel, information, doctrine, organisation, infrastructure and logistics (i.e. the lower half of Figure 2-1)

The key concept behind the model is the recognition of the inter-connectedness between the DLODs. Thus, for example, new and more sophisticated equipment may well require:

- A different training regime or approach
- Manpower (operators and maintainers) with different skill sets
- Different information feeds to maximise its capability
- A new doctrine or way of integrating the equipment and operating it in concert with pre-existing capabilities
- A new organisation construction to support and operate it

- New infrastructure
- New logistic support

It is by recognising and quantifying all of these cost elements that the true cost of the capability can be better estimated and, hence, the options for trade-offs. For example, a slight reduction in technical sophistication might save significant costs across the remaining DLODs. Clearly such a proposed reduction in technical capability would need to be acceptable to the front line forces who will be using the equipment, but in a zero sum (or reducing) defence budget regime, consideration of such trade-offs is increasingly important.

In practice, operationalising this model is not simple. For example, the introduction of new equipment will take place over a potentially significant time frame. As a result, the nature of the threat may well change – as is, arguably, the case for the RAF's Typhoon aircraft programme.

By the same token, the box headed "contribution from coalition forces" contains significant challenges as it is not always clear with which countries an operation will be conducted and, hence, what capabilities they will bring and UK need not provide.

Attempts to resolve this problem by means of multi-national programmes are, however, often equally fraught with challenge. Thus, for example, the A400M Airbus transport plane has caused many difficulties for the countries involved. The A400M is a European collaborative project to deliver a capability that bridges the gap between tactical and strategic military airlift. The reasons why this project is running so far behind schedule, current estimates are six years, are due to management and technical issues. However the customers have also introduced a great deal of risk. Governments insisted that the allocation of work to be undertaken in their respective countries should reflect on the number of planes they were ordering. An example being Airbus' preference for a Canadian engine that was turned down by French, German and UK governments who insisted that it should go to the European consortium to support and develop the European industrial structure. Customers also put in requests for national variations on the original design. For example Germany requested the problematic terrain masking low-level flight technology whereas the UK wanted the A400M to be able to carry its future generation armoured vehicle which has risen in weight from 17 tonnes to 30 tonnes, meaning that the cargo bay

floors and ramps will have to be strengthened (International Institute for Strategic Studies, 2010).

All these changes have led to less commonality for the equipment, increasing time and costs.

The A400M original in service date was December 2009, however in 2007 this slipped by 15 months to March 2011. With the reasons cited as "due to historic reasons associated with the time required for German approvals and changed customer requirements" (House of Commons Defence Committee, 2007). As of 2011 however, the current in service date is March 2013 for France and 2014/15 for the UK (Hall, 2011).

Figure 2-2 below, taken from the National Audit Office Major Projects Report, shows the increase in time and cost for the A400M (circled) between 2008 and 2009.

Source: National Audit Office analysis of Departmental data

NOTE
The arrows indicate in-year changes to cost and time performance since 2008. The Future Strategic Tanker Aircraft and Queen Elizabeth Class aircraft carrier are both new to this year's Major Projects Report; as such, no prior year figures are available. Astute Class submarines, Falcon and the United Kingdom Military Flying Training System all contain increments which were not reflected in last year's Report; as such, no comparable figures are available.

Figure 2-2 Time/cost performance for projects where the main investment has been taken (National Audit Office, 2009)

A further aspect of the TLCM model to appreciate is that, in analysing the costs for the introduction of a piece of equipment, it is also important to understand the cost behaviour and profile of each DLoD as it contributes to the total cost. This is important both in terms of

the macro-level trade-off requirement as well as the need for individual organisation elements to remain within their budgetary ceiling.

In addition, it will be recognised that the Through Life Capability Model reflects the position at a given snapshot in time. Whilst it can make some provision for changing threats, environments and coalition contributors that would change the capability, it is important where possible to allow for either room for future proofing when designing new equipment or technology, or adopt the ability for an agile approach to allow for changes in requirements. It is therefore essential to re-visit the assumptions, trade-offs and outcomes of the TLCM model on a regular basis to enable the equipment to be adapted to meet changing requirements, through either physical adaptation or through adaptation to doctrine to ensure that the best possible use of the equipment is being garnered.

2.3.1 FUTURE PROOFING VS. AGILE APPROACH

Negative reports in the media are common with regards to the defence procurement process. For example typing defence procurement into the search tool on BBC news brings up tens of reports just from the past year covering nearly every major defence equipment purchase of the past decade.

In 2009 Bernard Gray, now Chief of Defence Materiel, wrote an independent report for the secretary of state for defence looking at the acquisition process of the MOD. In it he stated that on average the cost of procurement programmes is 40% more than originally expected and will be delivered on average 80% later than first estimates predicted. In sum this could be expected to add up to c£35bn over the life of projects currently approved at initial gate (Gray, 2009). This leads to the query as to why industry does not experience the same problems, or at least to the same extent.

Industry is in the advantageous position of being able to predict market fluctuations and demand for a particular product, with a fair amount of accuracy. The MOD, however, has significant challenges in identifying future threats over the 20-30 year life of an equipment. For example the Snatch Land Rovers, which were frequently mentioned in the media for having insufficient levels of protection (Irvine, 2010; BBC News, 2010; BBC News, 2009): These vehicles were designed for the Northern Ireland conflict in the early 1990s. Their main purpose was to offer higher levels of ballistic protection without looking noticeably different from the conventional Land Rovers. Twenty years after this and they are required to protect

against roadside bombs and other improvised explosive devices. This was not part of the original capability so they did not stand up well to some of the threats encountered in Iraq and Afghanistan.

In order to future-proof a particular piece of equipment, designs would have to include protective measures that will deter threats that may not even be encountered in today's conflicts, but may be beneficial in twenty years time. This would make equipment heavy and impractical for carrying out day-to-day missions in the current areas of conflict. Vehicles would become impossible to transport by air due to their weight, training would take much longer to cover all the available equipment and the costs could be astronomical. Half of the features may never be required or worse a new threat that had not been predicted could emerge and the equipment would need to be updated or replaced anyway.

It is possible to mitigate these challenges by using the concept of an agile approach. Agility is needed in less predictable environments where demand is volatile and the requirements for variety are high – ideal for the defence industry. There are two ways in which this mitigation may occur: The first is the agility of the equipment and how it can be adapted to suit changing requirements. The second is agility within the supply chain and how manufacturers and suppliers can cope with changing demands (Christopher and Holweg, 2011).

By adopting such an "agile" approach, predictions of future conflicts are not attempted, as it is recognised that these are virtually impossible. Thus, this approach argues for equipment that can be altered quickly to suit the needs of the current user. For example by adopting a modular construction, Force Protection with the Ocelot vehicle has ensured that the vehicle can be deployed in many varied scenarios quickly and efficiently, without the need for redesign (Force Protection Incorporated, 2010).

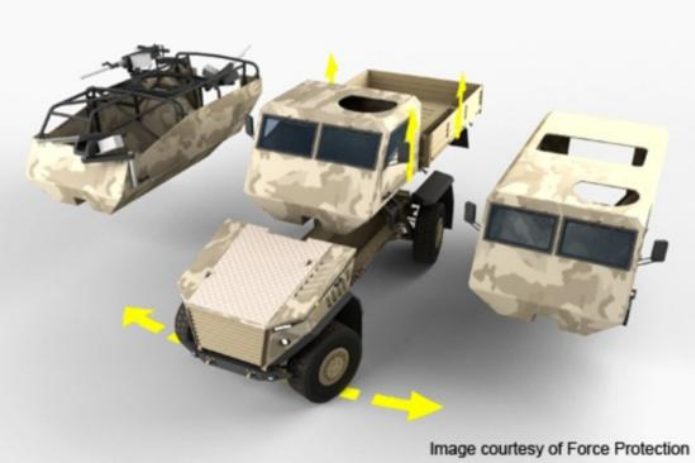

Figure 2-3 Ocelot Vehicle (Force Protection Incorporated, 2010)

As can be seen in Figure 2-3 it is possible to change the cab of the vehicle to suit the requirements. There is also the option to change the skateboard configuration from a 4x4 to a 6x6 to allow for changes in physical environment and the terrain.

Another way of adopting the agile approach is to allow for a certain amount of spare capacity to be built into the design from the beginning. For example the Type 45 destroyers for the Royal Navy have a 12% spare capacity built into the design for future upgrades (Defence Management.com, 2009). This would allow for extra equipment to be added as and when needed, or for new technologies to be implemented as they become available.

For example, some of the vehicles used at the start of the Iraq conflict were not designed for use in desert environments and as such had no air conditioning, making conditions unbearable inside. However by adding an air conditioning unit, valuable space was taken up and extra power was drawn from the engine to cope. By implementing spare capacity into the design of new equipment would allow for eventualities such as this.

A similar option is to adopt a bolt on bolt off approach, this would allow equipment to be removed when it is not required and replaced with equipment that is required, ideally not taking up any extra space and not affecting the vehicle's capabilities.

It is appreciated that the major disadvantage of including spare capacity into a design is the initial cost involved, although it should save money long term.

Within the supply chain the key to agile response is the presence of agile partners, where information is shared freely between buyers and suppliers in order that they may react to changes in demand as quickly as possible, both upstream and downstream. The procurement of defence equipment can be highly unpredictable however with the

introduction of urgent operational requirements (UORs) the lead time on equipment can be short in comparison. Figure 2-4 shows that this lends itself favourably to an agile supply chain.

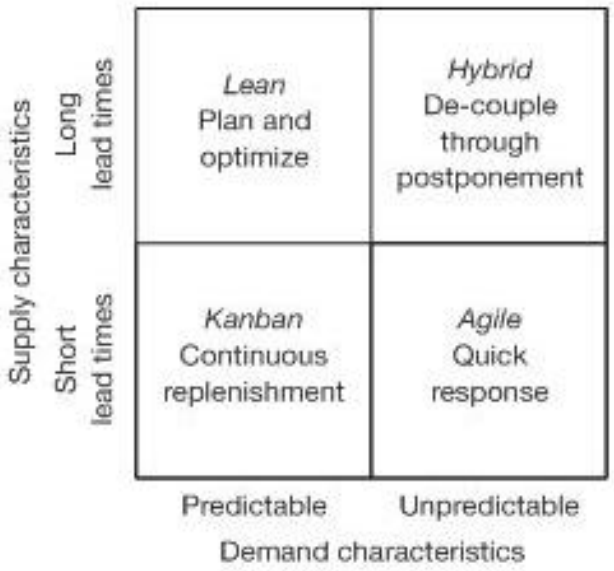

Figure 2-4 Supply and demand characteristics (Christopher, 2005)

The extreme case of an agile supply chain is the make-to-order response, this would not be ideal for the procurement of defence equipment as it tends to be a relatively expensive approach and because there are long lead times associated with 'military specials', but by making the supply chain more responsive to changes in demand, could reduce lead times and costs, meaning that equipment could be manufactured and in use in a much more efficient manner. In order to make a supply chain more responsive to changes in demand it is critical that information is shared freely and efficiently between the buyers and the suppliers.

For a supply chain to be agile it must be driven by demand, not forecasts, although this is fairly difficult within the defence procurement there are aspects that can be taken on board to try to make the supply chain more agile.

For example, the introduction of health usage monitoring systems (HUMS) on vehicles has enabled information to be fed straight back into the supply chain about the condition of the vehicle and the way it is being used. Figure 2-5 shows the flow of information from using HUMS in a vehicle. HUMS are currently in use on Panther vehicles.

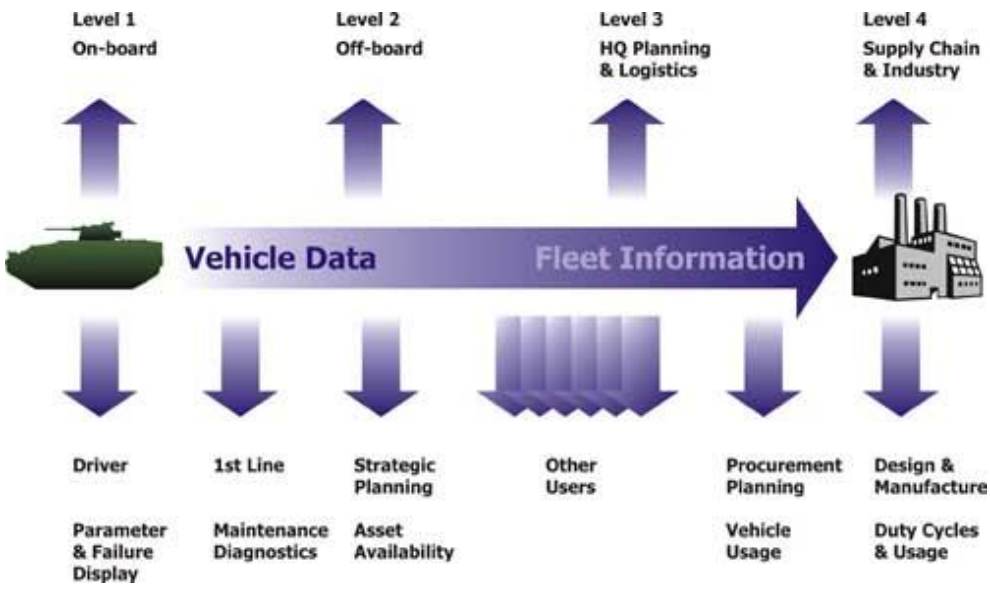

Figure 2-5 Health Usage Monitoring Systems (SYEN)

By sharing data along all levels of the supply chain companies should have a better understanding of what is required and can set up processes and procedures to deliver the requirements.

By adopting an agile approach it should be possible to adapt the vehicle for a variety of different situations quickly and at less expense than starting from scratch.

2.4 THINGS TO CONSIDER

So far this chapter has dealt with the underlying reasons why TLCM was introduced and what it aims to achieve when implementing new equipment to meet the identified capability gap. This section will look at the areas, with regards to the defence lines of development, that need to be considered and acted upon were the all composite vehicle from this project to be introduced.

Unfortunately due to the varied nature of equipment that is procured it would be very difficult to write a prescribed plan of action that would cover every type of equipment in every type of scenario. Therefore there is no step-by-step guide that can be followed. Rather the Through Life Capability Management (TLCM) (Ministry of Defence, Acquisition Operating Framework, 2009b) model is meant to be used as a tool to provide direction of the thought process by the users as well as to ensure that the user is aware of all the possible current and future effects that the introduction of a piece of equipment may have on the armed services, and the tax payer. There are six stages which together identify the changes necessary across all DLoD to provide the right capabilities, at the right time, within available resources. These stages are shown figuratively below (Ministry of Defence, Acquisition Operating Framework, 2011).

Figure 2-6 Capability Management (Ministry of Defence, Acquisition Operating Framework, 2011)

One of the most important considerations when applying the TLCM model is knowing when to stop. There are many possible scenarios that could crop up with the introduction of new

equipment, some relevant and some obscure. Depending on the threat, or future threat, these scenarios could go on indefinitely. It is therefore essential to be aware of the reasons **why** a piece of equipment is being brought in, **what** its purpose will be, and **what** it can reasonably be expected to achieve (Concepts and Doctrine), so that only logical questions are asked and relevant dependencies are noted.

2.4.1 ADVANTAGES AND DISADVANTAGES OF PROPOSED DESIGN

In all designs there are always positives and negatives that have to be taken into account and compromises made as a result, and this proposed design is no different. The major advantage is that composites have a much higher strength to weight ratio than steels, and as a result can either offer increased protection for the same weight or in theory lower weight for the same level of protection. This project focused on the increased protection for the same weight, mainly due to the LPPV contract and the fact that both proposed solutions incorporated a composite crew compartment and a steel blast deflector, within the weight allowance. The LPPV contract was issued in 2010 with two companies putting forward their solutions. The vehicle was to be under 7.5 tonnes in weight and still provide protection against a number of known and emerging threats. This is discussed in detail in Chapter 3 Literature Review, section 3.3.3 Light Protected Patrol Vehicle (LPPV).

The disadvantage of this increased protection is the increased thickness of the material. The experimental work conducted as part of this project used composites that were four times thicker than the steel. As a result of this three options are available to the designer, make the internal volume smaller or make the outside dimensions larger or a combination of the two. By making the internal volume smaller there is the risk that a reduction in the capability would occur. By making the external dimensions larger the risk is that the vehicle becomes difficult to transport and will not fit in the trains and planes available for transport. For the LPPV contract the width of the vehicle was pre-decided at "*ideally less than 2m*". Strictly speaking in terms of this project the extra width of the material is not as much of an issue. Both vehicles put forward for the LPPV contract consisted of an all composite crew compartment, so the extra width has already been incorporated into the design limits.

The issue arises that to keep the internal volume of the V-hull constant the bottom of the vehicle will have to be closer to the ground and as a result closer to the blast. This will also

have an impact on the required ground clearances, depending on the theatre/scenario in which the vehicle is deployed.

Other considerations include the material itself and the affect that this will have on repair work, add on armour and any other extras that may or may not need to be added over the course of its service life.

These factors should be discovered and noted during the analysis of the threat and the physical environment that make up the definition of the capability, and as a result should filter down into the Concepts and Doctrine DLoD. The following section looks at the defence lines of development in relation to this proposed design.

2.4.2 DEFENCE LINES OF DEVELOPMENT FOR VEHICLE

The vehicle that is the subject of this thesis is made mainly from composite materials; therefore *training* will need to be delivered for any repairs and maintenance to the vehicle, as well as how to drive it if it is different from others. This could be in the form of a user guide supplied by the manufacturer or instructional classes given to a few individuals who can then pass on knowledge to those they work with. The set-up of the training would be as a direct result of the training DLoD whereas the provision of the user guide would come under information.

It would also be necessary to ensure that all *equipment* fitted to the vehicle is compatible with the platform, and an understanding of the interaction(s) with any other platform would also have to be considered. For example the communications system would not only have to fit in the vehicle, but will also have to be compatible with other platforms, both the UK and her potential allies. The common communication system is the Bowman, which was discussed earlier, so compatibility with other platforms should not be an issue, though may have to be a consideration when dealing with allied forces. Other equipment such as the weapon system and any other attachments such as bolt on armour, which should all be laid out in the *Concepts and Doctrine*, will have to be able to physically be attached to the vehicle and therefore provision for this will have to be made. This is also where consideration for future conflicts and the resulting equipment requirements will also have to be analysed.

As previously mentioned, the *information* DLoD would cover the provision of any information relating to the vehicle and its continued use, for example user manuals for repair work and material safety information. The medium these would be available in i.e. paper, a disc, via an internet connection or passed on from someone who has taken a course will have to be considered. These sources of information will need to be available whenever required; therefore a number of different sources should be adopted.

In terms of the *organisation* DLoD this is a matter of deciding who is responsible for the vehicle, which will be a direct result of what the vehicle is required to achieve during service. Other areas that need to be considered are; who is to carry out the maintenance on the vehicle, who is responsible for ordering spare parts etc and the overarching issue of how are all these factors connected. There is most likely a system currently in place to meet these factors, but it would be essential to check beforehand.

Where the vehicle is stored when not in use and where the vehicle is repaired would all come under *infrastructure*. Questions such as, does repair work require a clean room will have to be answered so that suitable measures may be taken in order to provide it. If the vehicle is not designed to be left outside when not being used for prolonged periods of time, then where and how is it supposed to be stored. This will also link in with Information and Organisation, the information to answer these questions and the organisation with regards to who is responsible for the storage units and the vehicles, and what is the relationship between the two.

The final DLoD is *logistics*; this would cover the planning and carrying out of the physical act of getting the vehicle to where it is needed and providing all equipment to keep it running during its service life. This would again link in with a number of other DLoDs, significantly information. Information is required from the vehicle in order to furnish logistics with how often spare parts are needed, when they are needed and how long it takes for them to arrive and be fitted.

From the discussion of each of these DLoDs it can be clearly identified that there is a significant amount of interdependency upon other lines of development. It is important to be aware of this and to address it when it arises. During implementation each DLoD should have a voice willing to champion it less it get forgotten about or disregarded in favour of another with perceived greater importance. Finally the timing of the implementation of the

DLoDs is absolutely critical in ensuring the vehicle can be integrated without too many problems causing delays. A lot can be learnt from history, and whilst it will be inevitable that something will arise that was not foreseen or could not be predicted, by applying the TLCM model it should be possible to not repeat the same mistakes and minimise the problems that with hindsight could have been easily avoided. For example; as previously mentioned the new Type 45 destroyers have been designed with an extra 12% spare capacity to allow for any changes in requirements or technology that may arise during their lifetime.

It should be mentioned here, although not discussed, that this elegantly leads into a wider problem of how the MOD should manage the DLOD trade-off process. For example: who makes the decisions and on what basis? Not least as a given capability is part of a wider Royal Navy/Army/RAF capability which is, in turn part of a joint capability.

2.5 SUMMARY

This chapter has given a brief overview of how through life costs are analysed within defence procurement. The introduction of the Through Life Capability Model as a lesson learnt from previous mistakes, how manufacturers and suppliers can adapt to the changing needs of the armed forces. Finally the defence lines of development have been discussed in relation to this project and the implementation of an all composite armoured vehicle.

"EVERYTHING THAT CAN BE COUNTED DOESN'T NECESSARILY COUNT; EVERYTHING THAT COUNTS CAN'T NECESSARILY BE COUNTED"

ALBERT EINSTEIN (1879 –1955)

3 LITERATURE REVIEW

This chapter will review the literature and technology relating to all aspects of this research project. Starting with blast analysis then moving onto the process of sand and explosion modelling in finite element software, concentrating on previous studies. The following sections will then cover the development of armoured fighting vehicles including vehicle design to mitigate blast and composite armoured vehicles. The final section will cover the development and design of composite materials and an introduction to how they can be modelled in finite element software packages.

3.1 BLAST ANALYSIS

Explosions in air and various soil mediums have been well covered in literature see (Fiserova, 2006; Smith and Hetherington, 1994; Henrych, 1979; Grujicic et al., 2007; Bergeron et al., 1998). The following sections will cover what occurs during the detonation process, how the blast wave is formed and finally how it is possible to scale these blast waves for the experimental work conducted later in this project. Section 3.2 will then go on to look at how the blast wave interacts with the surrounding medium, and the modelling techniques used.

3.1.1 BLAST WAVE PARAMETERS

The detonation of an amount of high explosive is a chemical reaction that produces gases that are at very high temperatures and pressures. The violent expansion of these gases transfers energy to the surrounding medium causing it to be compressed and set in motion. The transfer of the energy into the surrounding medium is so rapid and of such intensity that the air shocks up to produce a blast wave which is characterised by an effectively instant increase in pressure at the wave front. Figure 3-1 shows the formation of the blast wave during detonation (Smith, 2009).

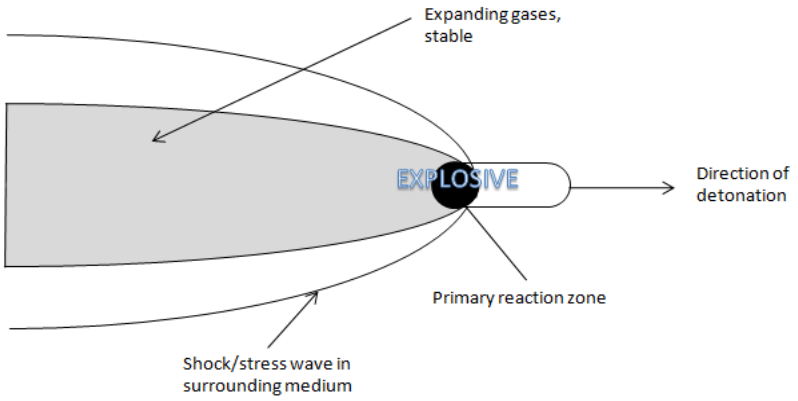

Figure 3-1 Blast wave formation

A typical pressure-time graph for an explosion in air is shown in Figure 3-2, where P_0 is the ambient pressure, P_s is the side on peak over pressure, t_a is the arrival time, T_s is the positive phase duration, ΔP_{min} is the greatest value of under-pressure and i_s is the specific impulse of the wave calculated by the area under the graph during the positive phase duration. The almost instantaneous increase in pressure is shown clearly by this graph.

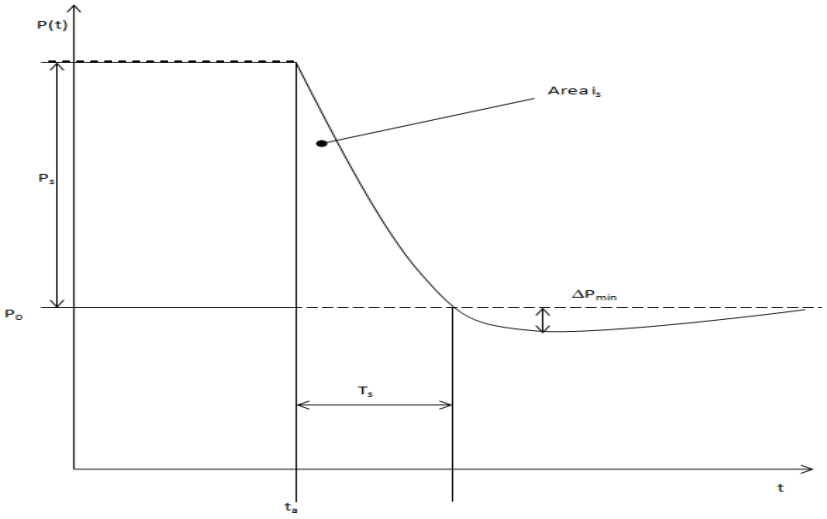

Figure 3-2 Blast wave pressure-time profile

In order to determine the conditions at the wave front the Rankine-Hugoniot equations are used. These give the conditions at a shock wave front travelling through a one-dimensional compressible medium. The equations that describe the three dimensional equations were first solved by Brode in 1955 (Brode, 1955). For the full list of equations please see (Smith and Hetherington, 1994).

3.1.2 SCALING BLAST WAVES

By scaling a blast wave it is possible to create an efficient representation of the data for a wide variety of scenarios. The most widely used scaling law is the Hopkinson-Cranz law, commonly referred to as cube-root scaling: The law states (quoted by Baker *et al*.(Baker et al., 1983)):

> *Self similar blast waves are produced at identical scaled distances when two explosive charges of similar geometry and of the same explosive but of different sizes are detonated in the same atmosphere.*

Therefore if two charge masses are W_1 and W_2 and of diameter d_1 and d_2 respectively, then for the same explosive material:

$$W_1 \propto d_1^3 \text{ and } W^2 \propto d_2^3 \text{ then:}$$

$$\frac{d_1}{d_2} = \left(\frac{W_1}{W_2}\right)^{1/3}$$

Equation 3-1

Therefore if the two charge diameters are in the ratio $^{d_1}/_{d_2} = \lambda$, then as indicated, if the same overpressure is to be produced from the two charges the ratio of the ranges at which the particular overpressure is developed will also be λ, as will the positive phase duration and the impulse ratio, as shown in Figure 3-3.

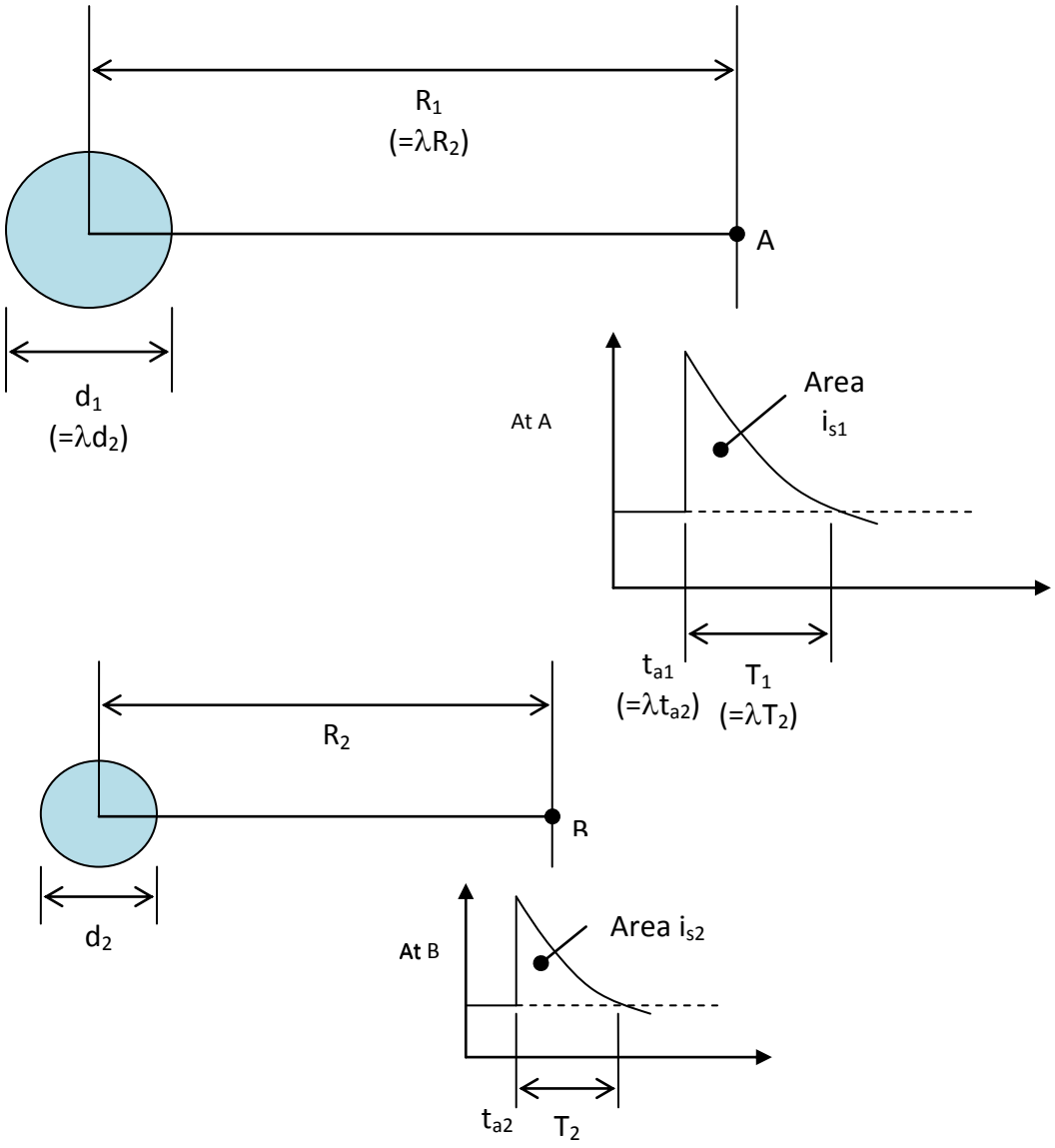

Figure 3-3 Scaling law

This leads to the scaled distance formulation:

$$Z = \frac{R}{W^{1/3}}$$

Equation 3-2

3.2 SAND AND EXPLOSION MODELLING

This section aims to introduce how the mine explosion phenomenon can vary depending on the medium in which it is buried, and how it is possible to model this effect in numerical analysis software.

There have been many studies looking at mine explosions both numerically and experimentally. They can generally be grouped into two separate areas;

- Internal process of the explosion – this deals with detonation theories and chemical compositions.
- External processes – this area looks at the effect of the shock wave travelling through materials and subsequent loading parameters.

This study focuses on the external processes and the interaction of the blast with the structure above.

3.2.1 BACKGROUND

The landmine is considered to be one of the most dangerous weapons in use during armed conflicts. In armed conflicts over the last decade of the 20th Century, US military losses attributed to landmines were 59% in Persian Gulf War and 60% in Somalia (Bird, 2001). Landmine Monitor, despite data collection issues, has identified at least 73,576 casualties of landmines, Explosive Remnants of War (ERW), and victim activated improvised explosive devices in 119 states and areas in the past ten years (International Campaign to Ban Landmines, 2009).

With the advent of conflicts in Iraq and Afghanistan the landmine has been usurped by the improvised explosive device, commonly known as an IED. IED's accounted for just over 61% of all fatalities in Afghanistan in 2009 and just over 58% in 2010 (iCasualties, 2011).

Again information is not given as to whether these casualties are mounted or dismounted individuals.

As a result, blast protection features are now a pre-requisite on all armoured vehicles. In particular crew survivability remains paramount when designing vehicles. Reducing crew mortality still remains a great challenge for vehicle manufacturers (Chassillan, 2004; Greuter, 2004; Hetcher, 2004; Ravid and Ziv, 2004).

Section 3.1 addressed the detonation of the explosive and the formation of the blast wave, this section will address what happens after the explosive has fully detonated and is interacting with the surrounding medium, in this case a soil.

The shockwave is released into the soil and will compress the material in its path, when this compression wave hits the surface most of the wave is reflected downwards, back into the ground. This has an almost identical effect to the spalling of metal; a soil cap is produced and projected upwards towards the structure/individual that caused the explosive device to detonate. Soil particles are ejected at supersonic speeds, between 800-2000mph (350-900ms^{-1}), depending on soil composition and explosive mass (Ramasamy et al., 2009).

During the production of this cap failure planes are created through which the gas expands. Some of the high pressure gas is propelled through these failure planes within the soil, this sustained high pressure collapses the soil in the immediate vicinity, meaning that if a mine is buried deep enough the collapse of the soil around the mine will prevent the energy escaping, thus causing little damage. Therefore IEDs and other explosive devices are much more likely to be just below the surface to cause maximum damage.

3.2.2 RESEARCH AREAS

There have been some initiatives over recent years into the understanding of mine blast loading behaviour in order to enhance demining equipment and mine resistant armoured vehicles. This research can be divided into three inter-dependant areas:

Prediction of the blast load – dealing with the shock wave propagation through soil and air by taking into account the characteristics of the explosive and the nature of the soil such as moisture content, soil particle sizes and their linkages.

Response of the structure – investigating the structural and kinematic responses of the demining equipment and vehicle, including the shape of the vehicle's chassis and the blast attenuation material.

Vulnerability of human being – assessment of the effects caused by the high shock pressures, the spalling of materials and the vertical and lateral motion of the vehicle as a result of the explosion.

The research in these three areas can generally be split into two approaches; numerical and experimental.

EXPERIMENTAL ACTIVITIES: Experiments have been conducted to investigate the response of a vehicle subjected to a mine explosion in order (i) to analyse the gross motion and damage to the vehicle, (ii) to assess effects on the occupants and (iii) to evaluate attenuation materials (Bird, 2001; Alem, N. M., Strawn,G.D., 1996; Holland, 2001; Nell, 2000). These experimental results have led to design proposals, in earlier vehicles, such as deflector plates fitted under the wheel wells and fuel tanks placed in rear of vehicle. More recent developments have wheels located outside of the crew compartment and the V-shaped hull designed to fit in between. Experiments studying explosion output have shown that mine deployment and soil compositions, especially moisture content, have a significant effect on the magnitude of vehicle loading. The most severe loading is obtained from explosion of mines buried in a cohesive soil, such as clay (Bergeron et al., 1998; Bergeron and Tremblay, 2000; Held, 2002).

NUMERICAL SIMULATIONS: Finite Element Analysis (FEA) is widely used in defence related engineering problems, high velocity impact and penetration problems being some of the more common analyses. In preliminary works empirical formulae were implemented in simulation format to model the explosion process (Gupta, 2002; Williams, 1999). Following on from this (Cheng et al., 2002; Fairlie and Bergeron, 2002; Laine, L., Ranestand, O., Sandvik, A., Snekkevik,A., 2001) conducted bespoke simulations which can now allow for the study of the explosion process from the initiation of the charge. Table 3-1 outlines studies looking at the simulation of mine explosions, focusing on the parameters dominant to explosion loading.

Source	Code	Mesh size (mm)	Explosive EOS	Soil model	Stand-off distance (m)	Note
Laine *et al*. (Laine, L., Ranestand, O., Sandvik, A., Snekkevik,A., 2001)	AUTODYN	8	10.4kg Composition B: JWL EOS	Sand (Laine, L., Sandvik,A., 2001)	0.4 till 1; 100mm soil cover	Analyses of pressure and impulse magnitude were conducted for buried, flush and surface laid charge.
Fairlie *et al*. (Fairlie and Bergeron, 2002)	AUTODYN	25 (air)	1kg C-4 Ideal gas EOS	Sand (Laine, L., Sandvik,A., 2001)	0.4; 50mm soil cover	Total momentum imparted to the pendulum was observed and compared with experiments
Grujicic *et al* (Grujicic et al., 2007)	AUTODYN	-	C-4 JWL	CU-ARL(Grujicic et al., 2006)	0 – 0.4; 0.1-0.8 soil cover	The impulse delivered to a vertical impulse measurement fixture (VMIF) was measured and compared with experimental results.
Wang (Wang, 2001)	LS-DYNA	-	100g C-4 JWL	Sand	0.3 and 0.7	Pressure and ejecta forming were investigated and compared with experiments (Bergeron et al., 1998).
Follett *et al.* (2010)	AUTODYN	1	100g C-4 JWL	Sand	0.3 and 0.7	Comparison between LS-DYNA model (Wang, 2001) and experimental results (Bergeron et al., 1998)
Cheng *et al.* (Cheng et al., 2002)	AUTODYN & MSC. Dytran	10	5kg TNT: JWL	Rigid surface	0.56	Output parameter was the deflection of box
Williams *et al.* (Williams, K., Poon,K.A., 2000)	LS-DYNA	-	7.5kg C-4	$\rho = 2170 kg.m^{-3}$ -		Blast was introduced through initial velocity boundary condition obtained from *empirical impulse* model. Output parameter was floor deflection
Gupta (Gupta, 2002)	LS-DYNA	-	907.2g Pentolite	-	1.52	CONWEP algorithm was implemented into LS-DYNA to generate blast pressure loading. Response of composite panel was investigated.
Niekerk (Niekerk, 2001)	MSC. Dytran	-	800g pentolite	Rigid surface	0.5	Pressure analysis resulted in 24% underestimated prediction. Experiment data varies from 38-81MPa.
Absil *et al.* (Absil et al., 1997)	AUTODYN	2	475g Composition B	-	0.2	Impact of fragments from steel casing on aluminium plates was investigated.
Dorn *et al.* (Dorn et al., 1999)	FLUENT & LS-DYNA	Interaction of blast wave with vehicle and occupant injuries (DYNAMAN model)				
Jacko *et al.* (Jacko and Bella, 2002)	AUTODYN		500g TNT			Response of armour plate subjected to contact explosion, was studied.

Table 3-1 Landmine explosion studies

3.2.3 SOIL CONDITIONS

For every deployment of a mine the soil conditions will have an effect on the result of the explosion, even though part of the explosive energy will be dissipated through the soil. The soil impinging on the target will considerably contribute to the loading that the target sees. Depth of burial and soil composition, therefore have significant roles in the loading magnitude.

A number of studies have been conducted into the effect the water content of soil has on the mine explosion phenomenon (Fiserova, 2006; Grujicic et al., 2007; Grujicic et al., 2006; Grujicic et al., 2009; Grujicic et al., 2009; Grujicic et al., 2008; Grujicic et al., 2008). All found that the water content had a significant effect on the loading, and that the composition of the sand had relatively small effects on the loading in comparison.

Water saturation levels have a significant effect at high deformation rates i.e. during a mine blast because as previously mentioned energy is dissipated through the soil when forcing the soil particles to compact. In saturated soil there is no room for compaction so less energy is lost through compaction of the soil. Section 4.3.3 discusses this further.

3.3 ARMOURED FIGHTING VEHICLES

This section aims to introduce the development of armoured fighting vehicles throughout history, and the different designs used to combat different threats experienced.

The development of AFVs can be traced through the centuries in one form or another. In 1700 BC war chariots were used in the Near East as mobile weapon platforms.

During the Middle Ages wheeled siege towers were used to offer protection to Archers and those operating the battering rams, as well as provide a mobile platform for those same archers.

Leonardo Da Vinci presented the first mobile vehicle with all round protection in 1487 (Leonardo Da Vinci, 1487), as shown in Figure 3-4 below.

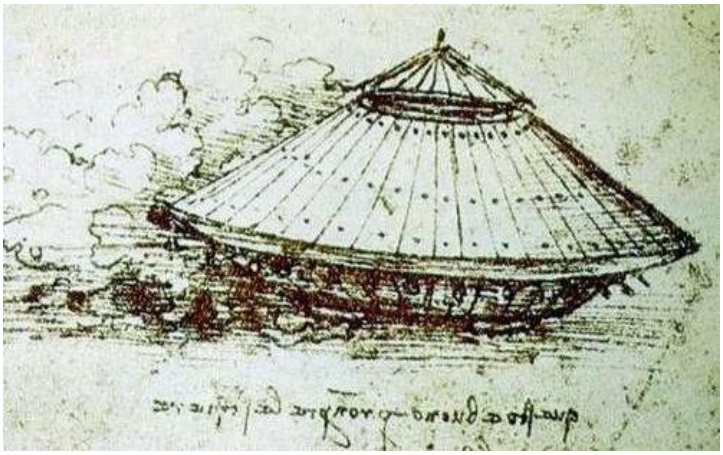

Figure 3-4 Pen Drawing of Armoured Car by Leonardo Da Vinci 1487 (Leonardo Da Vinci, 1487)**.**

The invention of the traction engine and the motor car at the turn of the previous century enabled armoured vehicles to take shape into what is recognisable today.

The first armoured vehicle was a road locomotive built by John Fowler and Company, of Leeds for use in the South African War of 1899-1902. Whilst the first armed vehicle was a de Dion-Bouton powered quadricycle on which F. R. Simms mounted a Maxim machine gun in 1899. The next stage would be to combine the armoured and armed vehicle into one to provide the mobile fighting platform with adequate protection for those operating it. The first was produced by Vickers in 1902 and consisted of an open top structure with a boat shaped hull (Ogorkiewicz, 1968).

During the First World War there was a requirement for a vehicle that could traverse a mud and shell cratered battlefield, break through the wire fortifications and overcome trenches in order to engage the enemy. In 1915 efforts were made to find a solution and the

prototype Number 1 Lincoln Machine was the result. This was the first tracked vehicle, offering an alternative to the wheel, which would get stuck in the battlefield (Terry et al., 1991).

3.3.1 PROTECTION VS. MOBILITY VS. FIREPOWER

According to Ian Hogg there are three basic elements of warfare – mobility, protection and firepower (Hogg, 1977).

In order to provide the best equipment in terms of vehicles the designer must encompass all three of these elements to a high degree. However this is impossible and trade-offs have to be made. Weight is usually the critical factor; an impenetrable vehicle with state of the art weapon system is unlikely to be able to move.

This has again been shown throughout history. The war chariots previously mentioned developed over time to include added protection for the driver, these then became difficult to manoeuvre leaving the horses vulnerable to attack. Cavalry soldiers dressed themselves and their horses with more and more armour over the centuries, making the horses tire easily and quickly, then again mobility would be compromised.

Main Battle Tanks have similar problems, the bigger the gun barrel, the larger the turret required to balance the weight of the barrel and to counter the recoil forces associated with firing, the bigger the turret the bigger the vehicle needed beneath to support it. Armour is also required to some degree, all adding to the overall weight of the vehicle and the reduction in mobility.

Armoured vehicles can be classified in terms of their abilities and functions or in terms of weight. According to Ogorkiewicz (Ogorkiewicz, 1994) there are at least six types of armoured vehicles all used for different purposes to achieve the best possible outcome.

- Ultra-light armoured vehicles – these are the lightest of armoured vehicles. Usually used for reconnaissance and patrolling.
- Wheeled armoured carriers
- Infantry's tracked armour – used where wheeled armoured carriers cannot gain access.
- Light tanks –used for reconnaissance and light fighting
- Wheeled gun vehicles
- Battle tanks

The British Army however classifies it's vehicles in terms of type (MOD, 2010).

- Combat vehicles – such as Challenger 2 and Warrior, these usually have heavy firepower and lots of protection
- Reconnaissance vehicles – such as Jackal and Scimitar, these usually have a high level of mobility with low levels of armour protection and a medium level of firepower.
- Protected Patrol Vehicles – such as Snatch, Mastiff and Vector, these are designed to carry troops and their equipment from place to place when needed. They should have high levels of protection but with high levels of mobility.

3.3.2 VEHICLE DESIGN TO MITIGATE BLAST

The standard V shape structure seen on many of the armoured vehicles in service today was first introduced in the 1970's on vehicles such as the Leopard Security vehicle used in the Rhodesian Bush War and the Buffel from the South African Land Systems OMC.

Figure 3-5 Buffel Mine Protected Personnel Carrier (photo taken by author)

The V-shape helps to mitigate the impulse delivered to the vehicle during a mine blast by deflecting the detonation products away from the body of the vehicle, thereby reducing the total amount of impulse delivered to the vehicle. Conversely a flat surface will result in significant pressure concentration beneath the surface, where the pressure becomes 'trapped' resulting in a significant load being transferred to the vehicle. This ultimately means that the vehicle is thrown upwards into the air. Even if the crew compartment were to remain intact, the passengers inside can still be killed by the upwards acceleration of the vehicle and occupants, which can cause fatal damage to the spine. Figure 3-6 shows how the

flow of detonation products is related to the geometry of the object they are impinging upon.

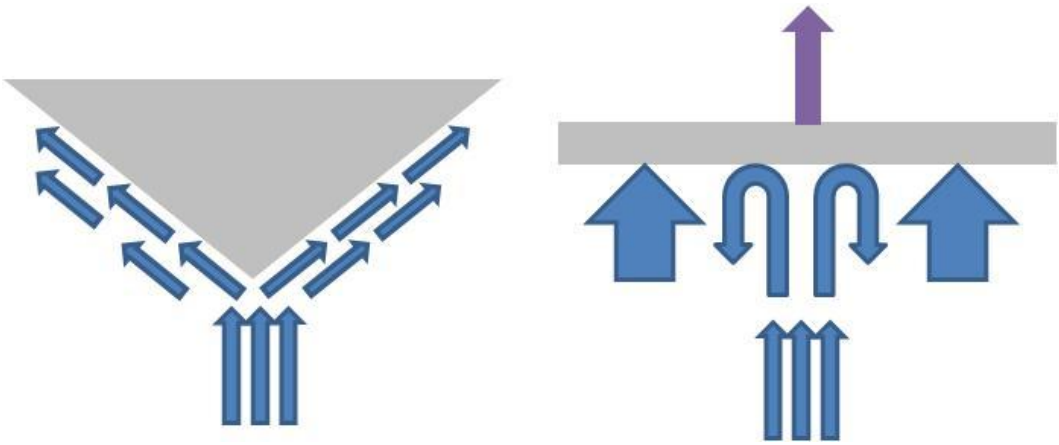

Figure 3-6 Flow of detonation products

This idea of making the geometry of the vehicle deflect blast away has been developed into vehicles such as the Buffalo used in Afghanistan for IED mine clearance. The light protected patrol vehicles (LPPVs) also implement this V shape structure but not to the same extent as the mine clearing vehicles.

Figure 3-7 Buffalo Mine Protected Clearance Vehicle (Net Resources International, 2010)

The Foxhound, discussed in detail in section 3.3.3 below, is specifically designed to meet UK requirements. It weighs 7.5t compared to the Buffalo at 30t, Mastiff at 27t and Ridgeback at 20t. It has a definite V shaped hull which is also used to house and protect the drive train from the engine to the wheels.

Figure 3-8 Foxhound Mine Protected Vehicle for LPPV (Ricardo)

However, all vehicles currently in service with this design feature are manufactured from steel or a mixture of composites and steel. The aim of this project is to discover if composites can be used instead of the steel for both the vehicle and the blast pan, underneath the vehicle.

Other design features include the recently introduced structural blast chimney (SBC), designed for the Humvee by Maryland-based Hardwire LLC. The chimney works by providing an outlet for the energy from the blast, by channelling it through the chimney. By doing this the vehicle does not accelerate rapidly off the ground because the energy travelling through the chimney creates an enormous downward pressure, counteracting the upward pressure from the blast, meaning passengers are subjected to fewer traumas (Wasserbly, 2010; Brannen, 2010).

Figure 3-9 shows schematically how a blast chimney, incorporated into a V-shaped hull vehicle would work.

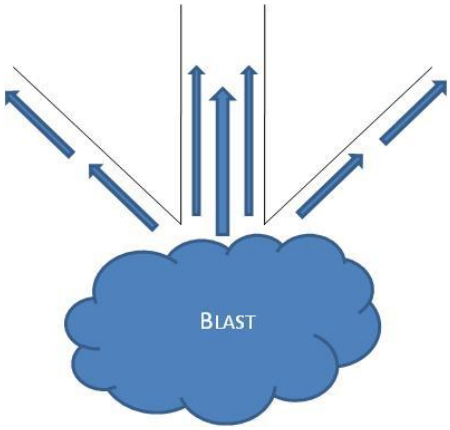

Figure 3-9 Blast chimney

3.3.3 LIGHT PROTECTED PATROL VEHICLE (LPPV)

This project is focusing on the protected patrol vehicles. With the advent of conflicts in Iraq and Afghanistan there has been a demand for highly protected vehicles that are much lighter. The government in 2010 introduced a competition for a new Light Protected Patrol Vehicle (LPPV). The requirements for the tender are (Think Defence, 2010):

> *The LPPV will be a wheeled vehicle with an estimated gross vehicle weight of around 6 to 7 tonnes, capable of carrying up to 6 crew (2+4), integrated with a range of communication and electronic equipment providing protected mobility. LPPV will replace in-service light legacy platforms based on the Land Rover based SNATCH vehicle. Additionally, the platform may be used as the basis for the replacement to Land Rover WMIK.*
>
> *The vehicle must provide the optimum levels of protection against a number of known and emerging threats of a varied nature including Ballistic, Blast, Mine and Fragmentation. As a guide the requirements for protection should be a minimum of level 2 ballistic and level 2 blast as detailed in STANAG 4569.*
>
> *LPPVs are principally required for a wide range of patrol tasks and are normally expected to operate on roads and rough tracks and trails in urban, semi-urban and rural environments; they need to be sufficiently agile to provide high cross country mobility. To achieve the desired levels of urban manoeuvrability the vehicle will ideally have a width less than 2m and a turning circle less than 12m.*

On the 26th May 2010 the UK Government invited Force Protection Incorporated to tender with their Ocelot vehicle, followed by on the 7th June Supacat were also invited to tender for their SPV 400 vehicle. On the 22nd September 2010 Force Protection and Ricardo were awarded the £100million contract to manufacture the Ocelot vehicle for UK armed forces, since been renamed Foxhound to fit in with other names of UK vehicles.

(a) (b)

Figure 3-10 Images of (a) SPV400 (authors own image) and (b) Foxhound (Ricardo, 2009)

Both of these vehicles make extensive use of composite materials in the construction, in order to reduce the weight as much as possible. For example Figure 3-11 below shows the use of composites in the SPV400. Composites are discussed in detail in the following section.

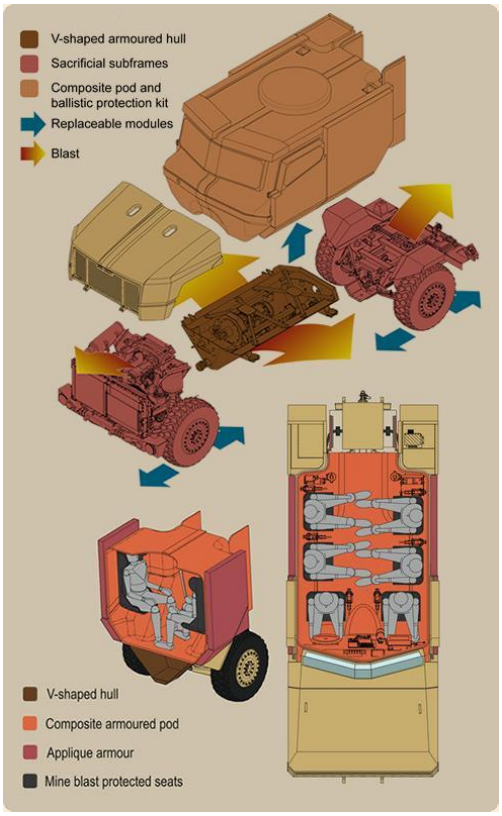

Figure 3-11 Supacat SPV 400 (Supacat, 2010)

3.3.4 ALL COMPOSITE ARMOURED VEHICLES

The use of composite materials for military vehicles has been proposed for a number of years, but has been typically limited to spall liners and a limited number of components such as ammunition bins. Before the introduction of the LPPV contract there was one exception to this which is the CAV 100 vehicle commonly known as Snatch Land Rover from NP Aerospace, which uses a composite pod on a metal chassis. In this case, the composite pod fulfils multiple roles, forming the structure of the rear of the vehicle as well as providing protection against ballistic, blast and fragmentation threats. (French, 2010)

Examples of other vehicles that have been developed as far as the prototype or demonstrator level include:

ADVANCED COMPOSITE ARMOURED VEHICLE PLATFORM (ACAVP)

Developed by Defence Evaluation and Research Agency (DERA, since split into Qinetiq and DSTL) in conjunction with Vickers Defence Systems in April 2000, this vehicle was designed in order to test the viability of using an all composite hull. All sub-systems were taken from existing and well proven vehicles such as the Warrior, from which the running gear was taken.

The hull manufactured from E-glass, bonded with epoxy resin, provided a much higher level of protection for a lower weight, saving approximately 4 tonnes from a similar metallic vehicle (French and Lewis, 1996).

The hull consists of only two major mouldings; a top moulding which incorporates the glacis and the sponsons and a bottom moulding incorporating the floor, toe plate and the side walls (Jane's Information Group, 1999).

The demonstrator vehicle exceeded all expectations in trials, but was never put into production. However the purpose of the programme was only to discover if composite materials could be used to develop armoured vehicles and with that in mind the programme was highly successful.

HIGH SURVIVABILITY CONCEPT (HSC) DEMONSTRATOR VEHICLE

This, according to (French, 2010), was an all composite patrol vehicle designed for use in Northern Ireland, looking specifically at the potential use of composites as structural and ballistic materials for future protected patrol vehicles. The key requirement was to minimise the amount of metal components to reduce the threat of spall from metallic fragments.

This vehicle was seen as taking the CAV 100 further by eliminating the metallic chassis that the crew compartment rested on.

The vehicle was not developed further though as hostilities in Northern Ireland were reducing, though the idea can be seen as the precursor for the LPPV contract mentioned in section 3.3.3.

ALL COMPOSITE MILITARY VEHICLE (ACMV)

TPI inc. in conjunction with Armor Holdings developed an all composite vehicle based upon the American high mobility multi-purpose wheeled vehicle (HMMWV, more commonly known as Humvee), in order to research and develop the incorporation of lightweight materials into its fleet of systems, as part of the US Army's All Composite Military Vehicle programme (White, 2007).

Figure 3-12 ACMV from TPI Composites (TPI Composites, 2007)

The vehicle saves 408kg in weight over the steel and aluminium equivalent allowing for additional protective equipment such as; add on armour, sniper detection systems and other important life-saving equipment.

The ACMV performed very well exhibiting no significant structural failures during all performance testing, including dynamic stability testing. Blast testing was set to take place in the early part of 2010, but there is no published information on how the vehicle performed.

However as yet a composite patrol vehicle for use by the US Army has yet to be announced

3.4 COMPOSITE MATERIALS

This section aims to introduce composite materials and how they have become a desirable material in many applications, especially defence.

Composites are desirable, especially for defence applications, as they have a much higher strength to weight ratio than their metal counterparts. For example rolled homogenous armour steel has a strength to weight ratio of around 250 $kNmkg^{-1}$ whereas Kevlar is a factor of ten larger at around 2514 $kNmkg^{-1}$. They also can be designed and manufactured to suit a particular purpose as there are so many different materials to choose from. As previously mentioned the main purpose of this project is to discover if composite materials, already in use for ballistic protection of vehicles, can be used for the blast protection underneath the vehicle, as a replacement for steel.

There are of course some disadvantages associated with the use of composites, the main issue being that of cost (which very much depends upon the materials used in the composite). Other issues include the differences in repair work between composites and metals. This however should be outlined through the use of the Defence Lines of Development and the Through Life Capability Management Model as discussed previously in Chapter 2.

3.4.1 WHAT IS A COMPOSITE MATERIAL

Composite materials are composed of two or more different materials. Most consist of a matrix material reinforced with fibres. The fibre is defined by a thread like strand of material with length to diameter ratios of the order 10^3. Many materials exhibiting low or moderate strengths and elastic moduli in bulk form, demonstrate greatly enhanced properties when in the form of small diameter fibres (John, 2003). Many types of different materials can be used for the fibres including metals, ceramics, polymers, glass and carbon. The materials being used in this project are S2-glass fibres and E-glass fibres; S2-glass fibre has a much

higher tensile strength than E-glass, 4890MPa to 3445MPa respectively. This is due to the higher content of silica present in the material 65% to 54% respectively. The silica content is also the reason why S2-glass is more expensive. Silica has a very high melting temperature and as a result more complicated manufacturing methods are required for higher content materials.

The matrix material again can be made from any number of different types of materials. It really does depend on what use the material is going to have as a finished product. The main requirement is that it can fully infiltrate between fibres and provide a good interfacial bond. Also there should be no chemical reaction between the fibres and the matrix (John, 2003). The sponsor company uses a thermosetting resin as the matrix material. A thermoset is a material that when first heated becomes plastic and is able to be moulded. Then upon being exposed to a certain temperature for a certain length of time the material cures, setting into a hard rigid structure that cannot be turned back into a plastic. The S2 glass had a phenolic resin as the matrix material. For all material data sheets please refer to Appendix 3.

Composites are generally used because they have desirable properties which could not be achieved by either of the constituent materials acting alone. The most common example being that of a fibre embedded within a matrix material (Gibson, 1994). A large scale example of this would be reinforced concrete. The steel bars are effectively the fibres whilst the concrete itself would be the matrix material.

Composite materials are an anisotropic material which means that they can have different properties depending upon which axis is being analysed. One of the benefits of using composite materials is that they can be designed to suit a particular purpose, for example they can be made stronger in a particular direction.

3.4.2 TYPES OF COMPOSITE MATERIALS

There are various types of composite material.

Figure 3-13 shows three different types.

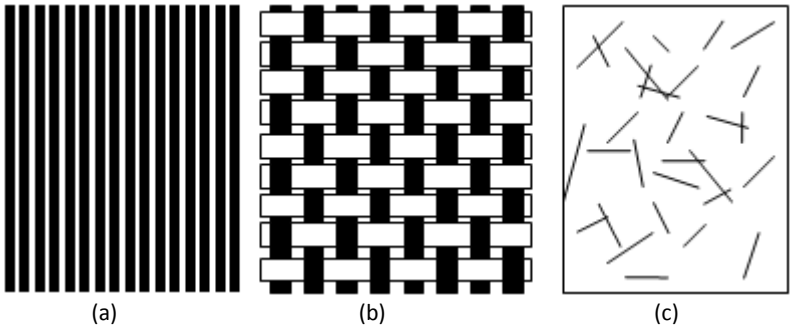

Figure 3-13 Types of fibre-reinforced composite

Type (a) is the continuous fibre composite, this will have very high strength in the direction of the fibres but its interlaminar and transverse strength will be very low in comparison. Whereas (b) shows the woven fibre composite, this will have much better interlaminar strength however its strength along the fibres will be reduced due to the fibres not being in a straight line. The chopped fibre composites, (c) are cheap to produce but the mechanical properties are considerably less than that of the continuous fibre and woven fibre composites.

Other types exist, such as the sandwich structure which consists of high strength composite sheets bonded to a lightweight foam or honeycomb core. However for this project the sandwich structure is not relevant.

3.4.3 USES OF COMPOSITE MATERIALS

DEFENCE

Composites are widely used throughout the defence industry. They can have excellent ballistic properties making them ideal choices for body armour, vehicle armour and spall liners.

For example a typical combat helmet consists of para-aramid fibres providing a tough but lightweight means of protection against impact and fragmentation. The ceramic plates used in body armour typically have a composite backing either polyethylene in a 0/90 configuration or a plain woven aramid fibre. This is to prevent spalling of the ceramic plate and fragments entering the soft tissue behind.

AUTOMOTIVE

The automotive industry has also made use of composites for luxury sports cars and formula one where weight is a critical factor.

For example the McLaren SLR pictured in Figure 3-14, on this car the entire body is made from carbon fibre reinforced plastic materials. Other cars similar to this that are built for race events use composites throughout the vehicle to make it as light as possible. However the average car on the roads today does not use them anywhere near as much.

There is an argument against using this type of composite material for automotive construction and that is the inability to recycle any of the material used, so all manufacturing excesses and unusable vehicle components go to landfill (Department of Trade and Industry, 2006).

Figure 3-14 McLaren SLR (Mercedes Benz, 2011)

AEROSPACE

With concerns over the environment and global warming, by making aircraft lighter they use less fuel. Composites therefore have an ever increasing role in aircraft design. For example the Airbus A330 uses 10 tonnes of lightweight composite structures (Airbus, 2011).

3.4.4 MODELLING OF COMPOSITE MATERIALS

Unlike metals, which have the same material properties in any direction, composites are orthotropic. This means that they can have different properties depending upon the direction. For example in a unidirectional laminate the strength of the material will be much greater along the fibre direction than across the fibres.

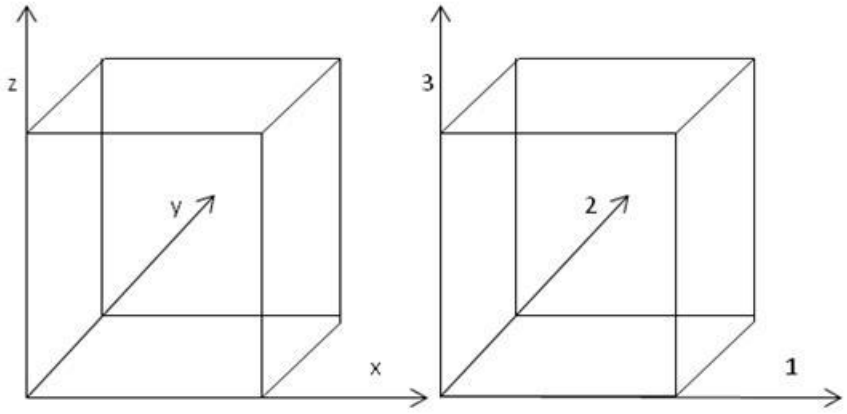

Figure 3-15 Co-ordinate systems

The standard notation is that the fibres run along the 1 and 2 directions and the 3 direction is the through thickness.

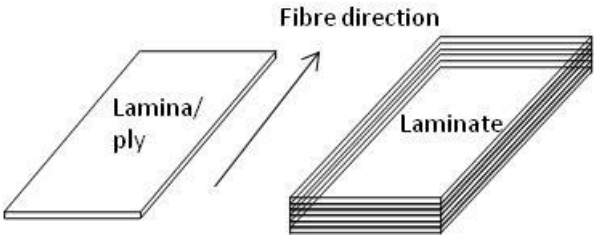

Figure 3-16 Difference between lamina and laminate

When modelling composites, for use in finite element software, there are two methods that are generally used: The input of the materials stiffness matrices or the input of the engineering properties in all three directions. This is discussed further in Chapter 4 Modelling using ANSYS AUTODYN.

For unidirectional composites or laminates that consist of unidirectional plies layered together at angles, classical lamination theory (Gibson, 1994; Daniel and Ori, 2006; Vasiliev and Morozov, 2001; Christensen, 1979) allows the user to calculate the material properties for an entire laminate from just the properties of a single lamina. This process eventually calculates the stiffness matrices for the laminate.

Woven fabrics have gained increasing technological importance over the years, as a result of their more balanced properties. The bi-directional reinforcement in each layer gives rise to excellent impact resistance. As a result they have been used in increasing quantities for ballistic protection, for example combat helmets, spall liners and some backing fabrics for body armour plates.

However, woven fabrics are a little more complicated to calculate manually. There have been a few studies into how it may be done (Ishikawa and Chou, 1982; Raju and Wang, 1994) with seemingly accurate results when compared to finite element models. In order to calculate the stiffness matrices using these approaches the bend in the fibres is taken into account. These have different methods but a similar approach. The lamina is broken down into regions, classical lamination theory is applied to the straight fibre regions and their own method is applied to the undulating fibre regions.

As this project will be using a woven fabric composite the decision to use the engineering properties was taken due to the inaccuracies of not having all the required information to calculate the stiffness matrices.

The material data was supplied by the sponsor and was calculated using standard testing methods.

3.4.5 COMPOSITES FOR ARMOURED VEHICLES

Composites are used extensively in ballistic protection, both for personal and vehicle armour systems. In personal armour systems composites are used as they are light and absorb the energy impact from small calibre rounds and shrapnel from explosions. Ceramic plates can be added for enhanced protection against rifle fired rounds (British Army, 2010).

In vehicle armour systems, composites have been used as spall liners for many years. A spall liner works by lining the inside of a vehicle and causes fragments from an explosion to be either fully contained or at the very least minimise the dispersion of fragments within the vehicle for maximum survivability. Figure 3-17 below shows the impact that a spall liner can have from a ballistic round. By limiting this cone of damage and the amount of fragments that are created, more personnel are likely to survive an attack.

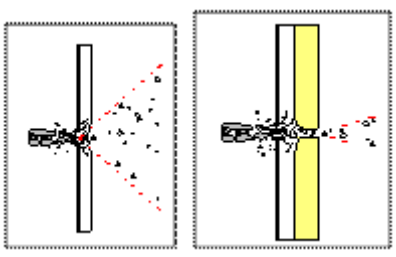

Figure 3-17 Spall liner effects

As stated in the requirements for tender the LPPV vehicle must meet STANAG 4569 level 2, which as laid out in Table 1-2 in chapter 1 is 6kg under any wheel and the centre of the vehicle. The level of damage caused to a structure located above an explosion varies considerably depending upon the medium in which it is buried. Explosives buried in different types of soils are covered in sections 3.2 and 4.3.3.

3.4.6 COMPOSITES UNDER BLAST LOADING

If composites can withstand blast as well as or better than steel then replacing the steel V-shaped hull with composite could reduce the overall weight of the vehicle, or offer better protection for the same weight.

There have been few studies conducted into blast loading on composites. Those that have are based on using flat plates, and making comparisons with numerical simulation software.

Adamík *et al.* (Adamik et al., 2004) conducted tests on plates made from steel and a steel-composite combination under blast loading, and compared the results with numerical simulations. However there was no comparison made between the two plates. It can be seen from graphs though that the steel plate deformed significantly more than the steel-composite.

Comtois *et al.* (Comtois et al., 1999) looked at the effect of explosives on polymer matrix composite laminates and discovered significant differences between composite and steel plates. They also discovered that the extent of damage created by stood off charges was not only a function of peak pressure but also of impulse.

Batra *et al.* (Batra and Hassan, 2008) conducted a study into the blast resistance of unidirectional fibre composites. There was however little experimental work conducted to validate results.

3.5 SUMMARY

This chapter has given a detailed physical description of the blast – time history, including the differences when buried in different conditions, and the effect on vehicles as well as the development of vehicles to combat the threat of mine blast. The uses of composite materials in defence applications have also been investigated and a potential gap, in using composites to replace steel for blast deflectors under vehicles, has been identified.

"FOOLPROOF SYSTEMS DON'T TAKE INTO ACCOUNT THE INGENUITY OF FOOLS"

GENE BROWN

4 MODELLING USING ANSYS AUTODYN

This chapter aims to introduce and explain the various material models and modelling techniques used whilst using the software, AUTODYN.

4.1 INTRODUCTION

AUTODYN, from Century Dynamics, is an explicit analysis tool used for modelling the non-linear dynamics of solids, fluids, gases and their interaction. The conservation laws of mass, momentum and energy give rise to a set of governing differential equations. In order for materials to be modelled a constitutive law is also required that links stress to deformation and internal energy. Initial conditions and boundary conditions complete the equations which are then solved using explicit time integration.

It is important to note that although the conservation of mass and momentum are exactly satisfied at every time step, conservation of energy is not. An energy error is introduced into the model so that stability is increased. Models that conserve energy exactly tend to be unstable and noisy. By default the error is set at 5%, when this value is exceeded the simulation terminates with the error message '*Energy error is too large'*. It is possible to increase the energy error with the AUTODYN environment in controls →wrap-up criteria →energy fraction, however it is necessary to proceed with caution as you endanger the question *'what is the tolerable energy error for the model?'*

There are two methods for solving in finite element software; explicit and implicit. The differences between explicit and implicit methods are outlined in Table 4-1. AUTODYN uses the explicit method.

Explicit	Implicit
Local Response – Direct computation of dependant variables from known quantities	Global Response – Dependant variables defined by coupled equations – Requires a matrix or iterative technique to solve
More efficient and more accurate for transient solutions	More efficient for static and steady-state solutions
Require a time step that restricts pressure waves from propagating further than one computational element per time step.	No time step constraints

Table 4-1 Implicit versus explicit methods (Century Dynamics Limited)

The time step in the model plays a crucial role in the stability. It is based on the Courant-Fredrichs-Lewy (CFL) criterion (Oran and Boris, 2000):

A disturbance (sound wave) cannot travel more than one element in one cycle.

$$\Delta t \leq \frac{kl}{c}$$

Equation 4-1

Where t is the time step, k is the smallest element size, c is the speed of sound in the material and l is the stability fraction. The stability fraction is typically 0.6-0.9 (Oran and Boris, 2000) in AUTODYN this is set to a default value of 0.6666. It can be changed by setting the safety factor, in controls →time step options.

4.2 SOLVERS

With the various applications there is a requirement for different solvers that can meet these problems. For this project two different solvers have been used, Euler and Lagrange, though AUTODYN has four in total to perform analyses: Lagrange, Euler, Arbitrary Lagrange Euler (ALE) and Smooth Particle Hydrodynamics (SPH) which is a mesh free solver. The Lagrange and Euler solvers are discussed below.

4.2.1 LAGRANGE SOLVER

The Lagrangian solver is normally used for the modelling of solids. The mesh is applied to the part and during simulation the nodes move with the material, as depicted in Figure 4-1.

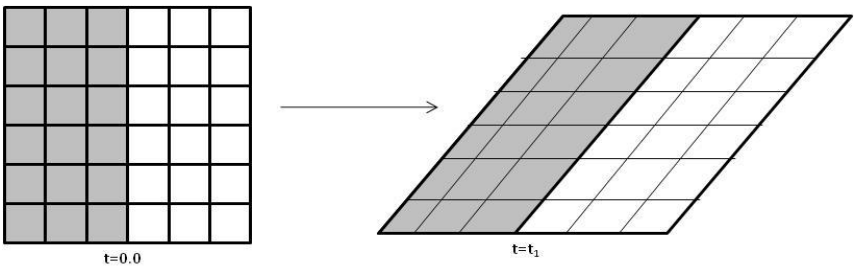

Figure 4-1 Lagrange representation of mesh

The computational cycle for the Lagrange calculations is as follows:

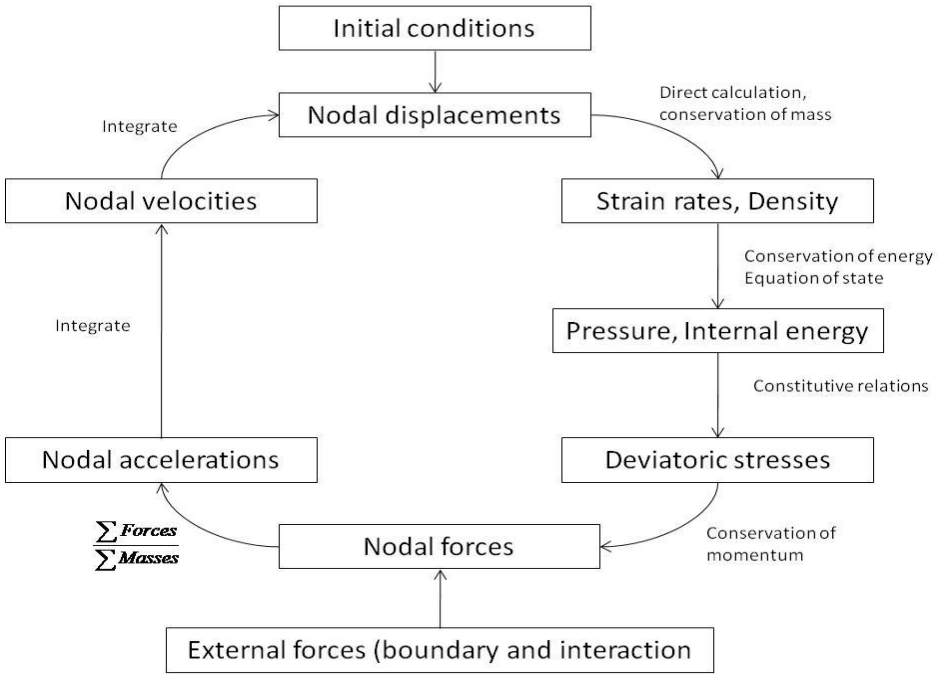

Figure 4-2 Lagrange computational cycle (Century Dynamics Limited, 1998)

At the start of the cycle the nodal velocities are integrated with respect to time in order to get the new nodal positions. These can then be used with the conservation of mass to calculate the new cell density and the strain rates associated with the node.

The change in volume from the cell deformation allows the volumetric stress or pressure to be calculated, this is governed by the equation of state and the conservation of energy. The change in shape gives rise to the deviatoric stresses, which is governed by Hooke's law and a plastic yield criterion. These are known as the strength model in AUTODYN.

The conservation of momentum, coupled with external forces and boundary conditions allow the new nodal forces to be calculated from the stress state of the cell. The nodal accelerations can then be determined from Newton's Second Law, and then finally

integrating these accelerations with respect to time allows the new nodal velocities to be calculated.

Integrating for a second time gives the new nodal displacements and allows for the cycle to start again.

4.2.2 EULER SOLVER

With the Eulerian solver, the mesh stays in the same place and allows the material to flow through the cells; this is shown in Figure 4-3. It is normally used for modelling of fluids, gases and large deformations of structural materials.

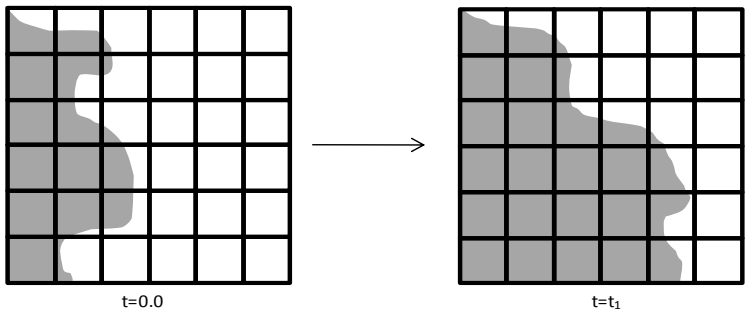

Figure 4-3 Euler solver representation

There are a number of different Eulerian solvers within AUTODYN to be used for modelling.

- Multiple material solver with strength – this model uses the Godunov method (see (Hirsch, 1992) for detailed explanation). It allows the use of multiple materials within a single cell, and algorithms are used to determine the state of those cells. It can be used in AUTODYN 2D and 3D.
- Ideal gas solver – this solver uses the Flux Corrected Transport (FCT) method developed by; (Boris and Book, 1997; Boris and Book, 1973) (see (Oran and Boris, 2000) for basic explanation). It only allows for the use of a single material within a cell. This solver can also be used in both AUTODYN 2D and 3D.

The Euler solvers apply a control volume method to solve the governing conservation equations. In this method the integral equations are discretized over finite volumes. Firstly the Lagrangian step is applied, where the mesh follows the material flow and as a result distorts, the second step is to re-map the solution back onto the initial mesh, which is fixed.

The multiple material solver is generally used throughout this project as it allows for the air, sand and explosive to all be modelled as one part.

When modelling in AUTODYN Lagrange parts will always take precedence over Euler parts. This makes it easier to model complicated Lagrange shapes that can then be surrounded by an Euler mesh, for example air.

4.3 MATERIAL MODELLING

In general materials have a complex response to dynamic loading and as a result the following phenomena may need to be modelled (Century Dynamics Limited, 1998):

- Non-linear pressure response
- Strain hardening
- Strain rate hardening
- Pressure hardening
- Thermal softening
- Compaction
- Orthotropic response
- Crushing damage
- Chemical energy deposition
- Tensile failure
- Phase changes

The modelling of such phenomena can generally be broken down into four components:

- ***Equation of State (EOS)*** – describes the hydrodynamic response of a material by, for the majority of materials, expressing the relationship between the state variables – density, pressure and specific energy.

$$p = f(v, T)$$

Equation 4-2

Where p is the hydrostatic pressure, v is the specific volume and *T* is the temperature.

For liquids and gases this is the primary response of the material as they cannot sustain shear and as a result their response to dynamic loading is strictly hydrodynamic.

This is also the primary response of solids that have a high deformation rate, when the hydrodynamic pressure is far greater than the yield stress of the material.

- ***Material Strength Model*** – describes what happens to a material during the elastic-plastic phase. It is represented by the yield criterion which is a function of the material properties.
- ***Material Failure Model*** – as materials cannot withstand tensile forces beyond their tensile limit a failure model must be introduced to simulate how the material would fail when subjected to excessive loads.
- ***Erosion*** – this is a numerical method that allows elements to be eliminated from the simulation once they have distorted beyond a specified limit. This prevents cells from becoming degenerate, or from causing the time step to drop below a stated minimum value. The criteria can be based upon minimum time step values, strain or material failure. When dealing with the interactions as discussed later in section 4.4, it is also an option to retain the inertia of these eroded cells as point masses to enable more accurate loading criteria.

AUTODYN has a number of material models that the user can choose from depending upon the problem being modelled. There is also the option to introduce a user's own model through the custom subroutines. There is also an extensive material library within AUTODYN that has these models already created for the user to use and modify if desired.
The following sections will discuss how the materials used in this project were modelled. For all material models used that were not available in the AUTODYN library please refer to Appendix 4 for details.

4.3.1 COMPOSITE MATERIALS

Composite materials are orthotropic, therefore a material model that allows for different properties in the principal directions is essential. The orthotropic equation of state does just this, through a set of orthotropic constitutive relations. These constitutive relations for these materials are a totally stress based formulation as opposed to the division of the total stress into hydrostatic and deviatoric components, as for the modelling of steel shown in the next section.

The incremental stress-strain relations may be expressed as:

$$[\sigma]^{n+1} = [\sigma]^{n} + [C][\dot{\varepsilon}]\Delta t$$

Equation 4-3

Where [C] is the stiffness matrix (shown in Equation 4-4 below), $[\dot{\varepsilon}]$ is the strain rate tensor and Δt is the time step.

The linear elastic constitutive relations for an orthotropic material can be expressed as:

$$\begin{bmatrix}\sigma_{11}\\ \sigma_{22}\\ \sigma_{33}\\ \sigma_{23}\\ \sigma_{31}\\ \sigma_{12}\end{bmatrix} = \begin{bmatrix}C_{11} & C_{12} & C_{13} & 0 & 0 & 0\\ C_{12} & C_{22} & C_{23} & 0 & 0 & 0\\ C_{13} & C_{23} & C_{33} & 0 & 0 & 0\\ 0 & 0 & 0 & C_{44} & 0 & 0\\ 0 & 0 & 0 & 0 & C_{55} & 0\\ 0 & 0 & 0 & 0 & 0 & C_{66}\end{bmatrix}\begin{bmatrix}\varepsilon_{11}\\ \varepsilon_{22}\\ \varepsilon_{33}\\ \varepsilon_{23}\\ \varepsilon_{31}\\ \varepsilon_{12}\end{bmatrix}$$

Equation 4-4

The inverse of the stiffness matrix shown in Equation 4-5 is known as the compliance matrix and is expressed as:

$$[S] = \begin{bmatrix} \frac{1}{E_{11}} & \frac{-v_{12}}{E_{11}} & \frac{-v_{31}}{E_{33}} & 0 & 0 & 0 \\ \frac{-v_{12}}{E_{11}} & \frac{1}{E_{22}} & \frac{-v_{23}}{E_{22}} & 0 & 0 & 0 \\ \frac{-v_{31}}{E_{33}} & \frac{-v_{23}}{E_{22}} & \frac{1}{E_{33}} & 0 & 0 & 0 \\ & & & \frac{1}{2G_{23}} & 0 & 0 \\ & SYM & & & \frac{1}{2G_{31}} & 0 \\ & & & & & \frac{1}{2G_{12}} \end{bmatrix}$$

Equation 4-5

Where E_{ii} are the Young's Moduli in the principal material directions, G_{ij} are the shear moduli and v_{ij} are the Poisson's ratios, where v_{ij} is defined as the transverse strain in the j-direction when stressed in the i-direction:

$$v_{ij} = -\frac{\varepsilon_j}{\varepsilon_i}$$

Equation 4-6

Inherent in this model is the linear volumetric response. It is possible to change this to include shock effects for hypervelocity impact which uses the Hugoniot formula, or for a polynomial to account for other non-linear effects.

For this project an elastic strength model was used, as the main concern was to look at the amount of deflection of the composite under the blast load when compared to the steel

The failure model implemented for this work was the material stress strain model. This allows the user to input the following failure stresses and strains:

- Tensile failure stress 11, 22 and 33
- Maximum shear stresses 12, 23 and 31 (23 and 31 available in AUTODYN 3D only)
- Tensile failure strains 11, 22 and 33
- Maximum shear strains 12, 23 and 31 (23 and 31 available in AUTODYN 3D only)

Failure is initiated if any of the principal material stresses or strains exceed these values.

Within AUTODYN it is possible to model a composite part in two ways. The first is to model the part as a shell i.e. with no thickness, and then input the layer data, including fibre

orientation and number of layers, in the composite layer fill option. However this process uses a lot of computer memory. The second option is to model the part as a solid and then fill as you would any other part with the equivalent data for the material as a whole. This option does not allow the user to see how failure initiates between layers but is much more efficient.

4.3.2 STEEL

In order to model the steel in this project the linear equation of state was used.

The linear equation of state is the simplest form and can be determined by assuming that the pressure is independent of the internal energy and that changes in the material density are small and reversible. The EOS is of the form:

$$p(\rho) = K\mu$$

Equation 4-7

Where K is the bulk modulus and μ is the compression $\left(\mu = {}^{\rho}/_{\rho_0} - 1\right)$

The strength model is the Johnson-Cook model (Johnson G. R., Cook W. H., 1983) and is of the form:

$$\sigma = [A + B\epsilon^n][1 + C \ln \dot{\epsilon}^*][1 - (T^*)^m]$$

Equation 4-8

Where ϵ is the equivalent plastic strain, $\dot{\epsilon}^* = {}^{\dot{\epsilon}}/_{\dot{\epsilon}_0}$ is the dimensionless plastic strain rate for $\dot{\epsilon}_0 = 1.0s^{-1}$ and T^* is the homologous temperature, calculated by $T^* = \frac{T - T_{room}}{T_{melt} - T_{room}}$.

A, B, C, n and m are the five material constants and are what are needed to model this strength model in AUTODYN. These constants are available for many materials within the AUTODYN library.

The expression in the first set of brackets gives the stress as a function of strain when $\dot{\epsilon}_0 = 1.0s^{-1}$ and $T^* = 0$ (i.e. for laboratory experiments at room temperature).

The constant A is the basic yield stress at low strains while B and n represent the effect of strain hardening.

The expressions in the second and third sets of brackets represent the effects of strain rate and temperature, respectively.

In particular the latter relationship models the thermal softening so that the yield stress drops to zero at the melting temperature T_{melt}. The constants in these expressions were obtained by Johnson and Cook empirically by means of dynamic Hopkinson bar tensile

tests over a range of temperatures and other tests and checked by calculations of Taylor tests of impacting metal cylinders on rigid metal targets which provided strain rates in excess of 10^5 sec^{-1} and strains in excess of 2.0.

This Johnson-Cook model may also be used for the failure model.

An erosion model was also introduced with a geometric strain of 0.5 or 50%.

4.3.3 SAND MODEL

Sand is a porous material and as such requires an equation of state to account for this. The sand model within AUTODYN was developed by Laine *et al.* (Laine, L., Sandvik,A., 2001).

The equation of state used to model sand is the compaction EOS and is based on a ten point piece-wise linear pressure-density relationship as shown in Graph 4-1.

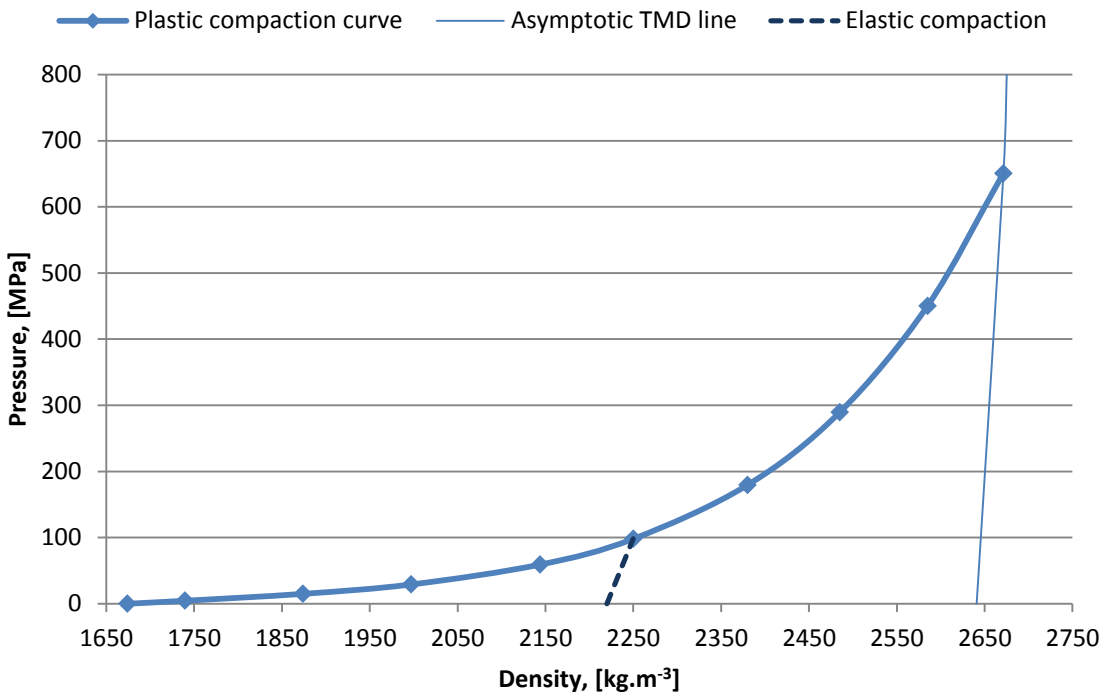

Graph 4-1 Input data for EOS Compaction of Sjöbo sand (Laine, L., Sandvik,A., 2001)

The first point on the graph corresponds to the loose soil and the last corresponds to the fully compacted or the theoretical maximum density (TMD).

The elastic loading/unloading compaction curve comes from the density dependent bulk sound speed, *c(ρ)*:

$$P = c^2 \cdot (\rho) \cdot \rho$$

Equation 4-9

Where P is pressure, c is sound speed and ρ is the density.

This density dependent bulk sound speed must also be provided within the model in AUTODYN as a ten point linear piece-wise curve as shown in Graph 4-2.

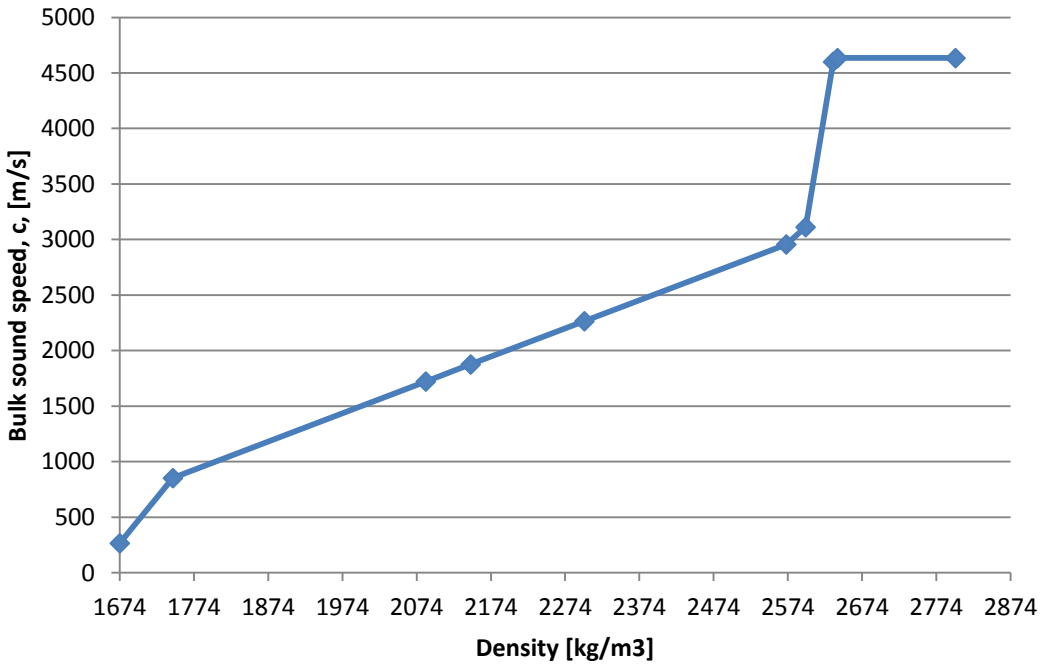

Graph 4-2 Input data for the density dependent bulk sound speed, c(ρ) of Sjöbo sand (Laine, L., Sandvik,A., 2001)

For further information on how the compaction EOS for the sand model implemented in AUTODYN was calculated please see (Laine, L., Sandvik,A., 2001).

The strength model used to model a porous material such as sand is the granular strength model. This model describes the non-linear behaviour of the material under deviatoric strain. It assumes that the shear modulus of the material varies non-linearly from that of the loosely packed grains to that of the fully compacted material. The model also assumes that the yield strength varies with both pressure and density.

$$Y = F_1(p) + F_2(\rho)$$

Equation 4-10

The non-linear behaviour of the shear modulus is also described by a ten point piece-wise linear curve for which the shear modulus varies with the density (Century Dynamics Limited, 2005).

The failure model implemented is the hydro tensile limit. This is the minimum pressure to which the material can withstand continuous expansion.

$$p > p_{min}^{tensile} = constant$$

Equation 4-11

If the material pressure drops below this limit in a cell it is assumed that the material, in this case, will sustain bulk failure. A re-heal option can also be implemented where the pressure is set to zero and the internal energy recalculated so that the cell can withstand a negative pressure for the next time step. Using this fairly simple criterion allows the simulation to continue without error for a long period of time.

There are two sand models implemented within this project: One is the Laine *et al.* (Laine, L., Sandvik,A., 2001) for sand with a water content of 6.57% which is implemented in the material library in AUTODYN. However as this model does not allow for changes in moisture content the second model was used for a fully saturated sandy clay derived by (Grujicic et al., 2009), to allow for comparisons with experimental work. Another wet sand model was also implemented for comparative purposes, also by (Grujicic et al., 2009) but was an online paper and could not be found in a journal or conference proceedings. Details can be seen in Appendix 4.

(Grujicic et al., 2006) stated that when the saturated sand is subjected to low deformation rates the water particles are given enough time to leave the pores, hence the density of the fully compacted sand and the pressure at which full compaction is attained is identical to their counterparts in the dry sand. However during an explosion the deformation rates are much higher, causing the water to remain trapped inside the pores and the sand to behave as fully compacted sand which can only undergo an elastic compaction. Graph 4-3 shows this schematically and is taken from (Grujicic et al., 2006). The values used in the AUTODYN material model are also displayed in Appendix 4 but for comparative purposes Graph 4-4 and Graph 4-5 here show the material model in the same format as above.

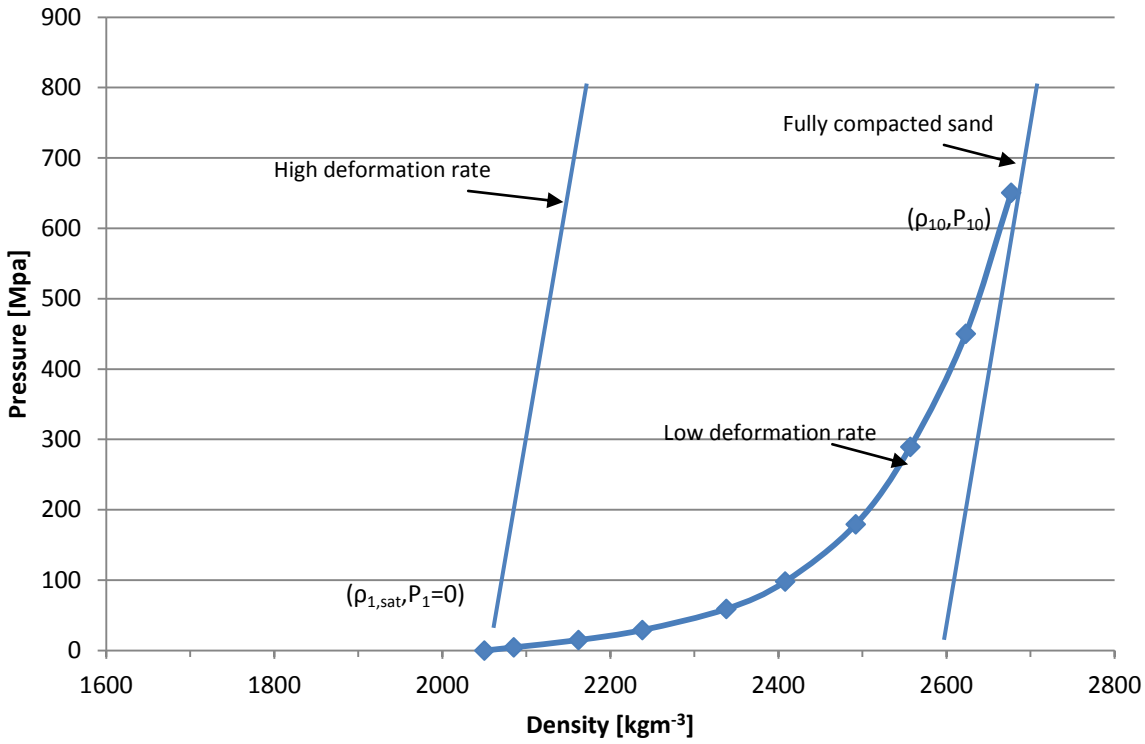

Graph 4-3 Pressure vs. Density relations for saturated sand at low and high deformation rates (Grujicic et al., 2006)

This is also shown in Graph 6-2 on page 134 where an AUTODYN model has been created to show the differences in maximum side on pressure when a charge is a) detonated in air b) buried in dry sand and c) buried in wet sand.

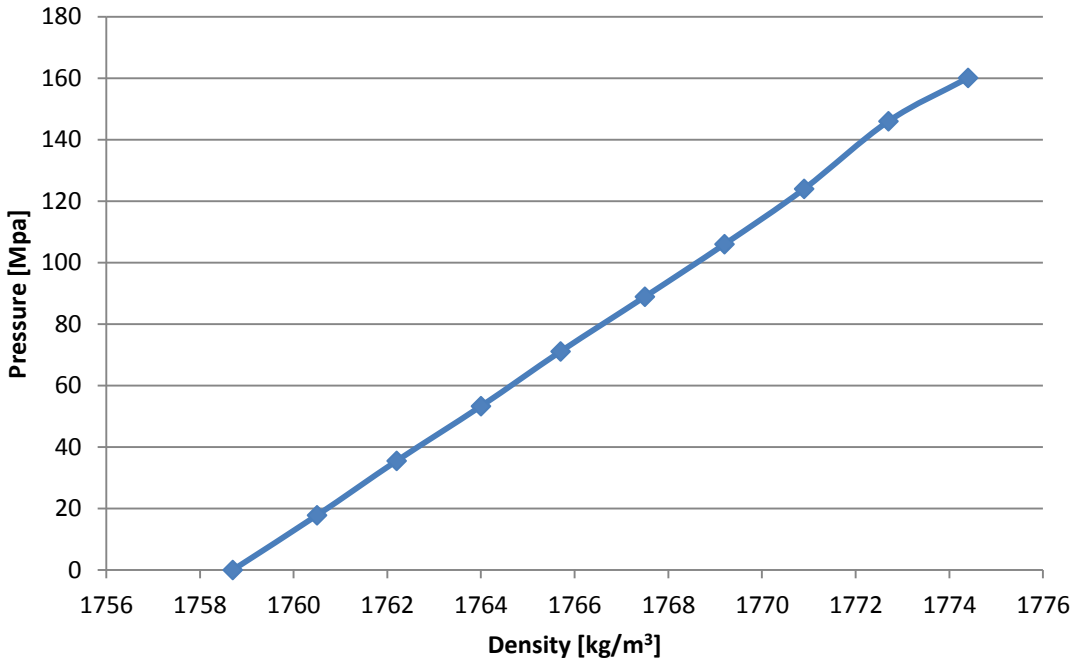

Graph 4-4 Pressure vs. Density relations for AUTODYN numerical model (Grujicic et al., 2009)

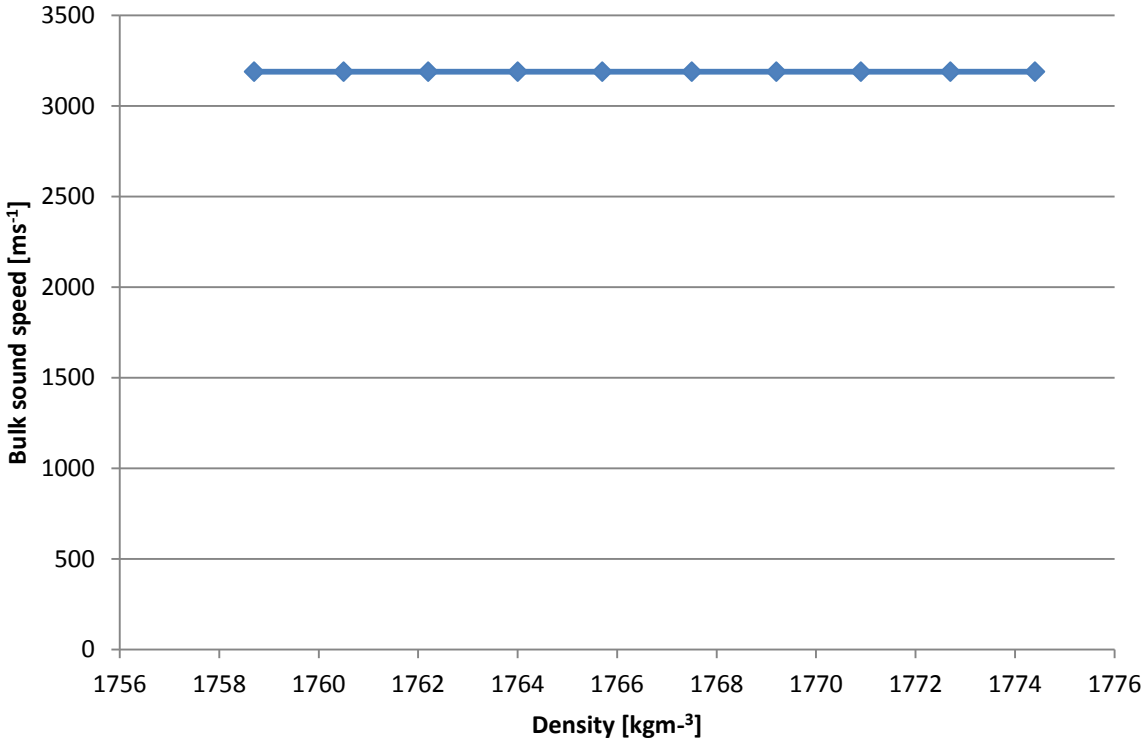

Graph 4-5 Density vs. Sound-speed for AUTODYN numerical model for wet sand (Grujicic et al., 2009)

4.3.4 AIR

Air is modelled by using the ideal gas equation of state. This is of the form:

$$P = (\gamma - 1)\rho e$$

Equation 4-12

Where γ is the ideal gas constant, ρ is the density and *e* is the specific internal energy.

$$e = \frac{RT}{\gamma - 1}$$

Equation 4-13

Where R=287.1 $J.kg^{-1}.K^{-1}$ and is the individual gas constant, γ = 1.4. When T=288.15K (t=15°C) the specific internal energy is equal to $206.82x10^{3}$ $J.kg^{-1}$.

As air cannot withstand shear there is no strength or failure model for modelling air.

4.3.5 EXPLOSIVE

The explosives modelled within this project are C-4 and TNT which are present in the material library of AUTODYN. In order to model the expansion of the detonation products the Jones-Wilkins-Lee (JWL) equation of state is used. This is of the form:

$$p = A\left(1 - \frac{\omega}{R_1 V}\right)e^{-R_1 V} + B\left(1 - \frac{\omega}{R_2 V}\right)e^{-R_2 V} + \frac{\omega E}{V}$$

Equation 4-14

Where A, B, R_1, R_2 and ω are coefficients dependent upon the composition of the explosive, the variable $V = \frac{v}{v_0}$ is the expansion of the explosive products and E is the detonation energy per unit volume.

Dobratz *et al.* (Dobratz, B. M., Crawford,P.C., 1985) is just one of many authors that have derived the coefficients of this equation of state. Table 4-2 below gives the parameters used within AUTODYN for the JWL EOS for C-4 and TNT.

Parameter	TNT	C-4	Unit
EOS	JWL	JWL	
Density, ρ_0	1630	1601	$Kg.m^{-3}$
A	373.77×10^6	609.77×10^6	kPa
B	3.7471×10^6	12.95×10^6	kPa
R_1	4.15	4.5	-
R_2	0.9	1.4	-
ω	0.35	0.25	-
CJ Detonation velocity	6930	8193	$m.s^{-1}$
CJ energy, e_0	6.0×10^6	9.0×10^6	$J.kg^{-1}$
CJ Pressure	21.0×10^6	28.0×10^6	kPa
Auto-convert to ideal gas	Yes	Yes	

Table 4-2 Parameters for JWL equation of state for explosives used in AUTODYN

Like air there is no strength or failure model implemented for explosives.

4.4 BUILDING MODEL IN AUTODYN

When modelling in AUTODYN the user can choose whether to model in 2D or 3D. 2D allows for a smaller mesh size and therefore greater accuracy, 3D however allows for more complicated geometries. Both options are used in this project.

This section describes the features within AUTODYN that permits the user to build and analyse a successful model.

STEP 1 – MATERIAL SELECTION

AUTODYN has an in-built library of materials covering a wide variety of options. It is possible to modify a material once it has been imported into the model, by highlighting the material in the dialog panel and selecting modify. It is also possible to create a user defined material as described in section 4.3. Once created or modified it is possible to save the material into a separate library for future use.

STEP 2 – PARTS

Parts can either be created in AUTODYN as a structured part using the part wizard, or they can be created in the Design Modeller interface in workbench and then imported through the meshing interface and into AUTODYN as an unstructured part. 2D models can only be created in AUTODYN whereas 3D models can be created in AUTODYN or in the Design modeller.

To create structured parts in AUTODYN, first the solver must be chosen: Lagrange, Euler etc. The available options will change depending upon whether conducting a 2D or 3D analysis. Then there is a part wizard which allows for the automatic generation of quality structured meshes for a range of predefined geometries:

- 2D Volume: Box, Quad, Circle, Ogive, Rhombus, Triangle and Wedge
- 3D Volume: Box, Hex, Cylinder, Sphere, Ogive, Fragments/Bricks
- Shells: Plate, Cylinder
- Beams: Single, Multiple, 2D Frame, 3D Frame

The part wizard also enforces the user to specify the mesh distribution within the part and what the part is to be filled with, material or initial condition.

The wizard allows the user to fill a part with one material, after generation it is then possible to fill a part with blocks of another material, either by using a block fill or fill by geometrical space.

Block fill requires the user to specify the range of nodes within the part that are to be filled by the new material. Filling by geometrical space allows the user to choose between a number of shapes: Rectangle, Quad, Ellipse, Parabola and Halfspace, and then the co-ordinates and dimensions of the shape.

For example in this study a 2D Euler multi-material box filled with air is created with the part wizard and then afterwards a range of cells is filled with the soil conditions and with explosive as shown in Figure 4-4 below.

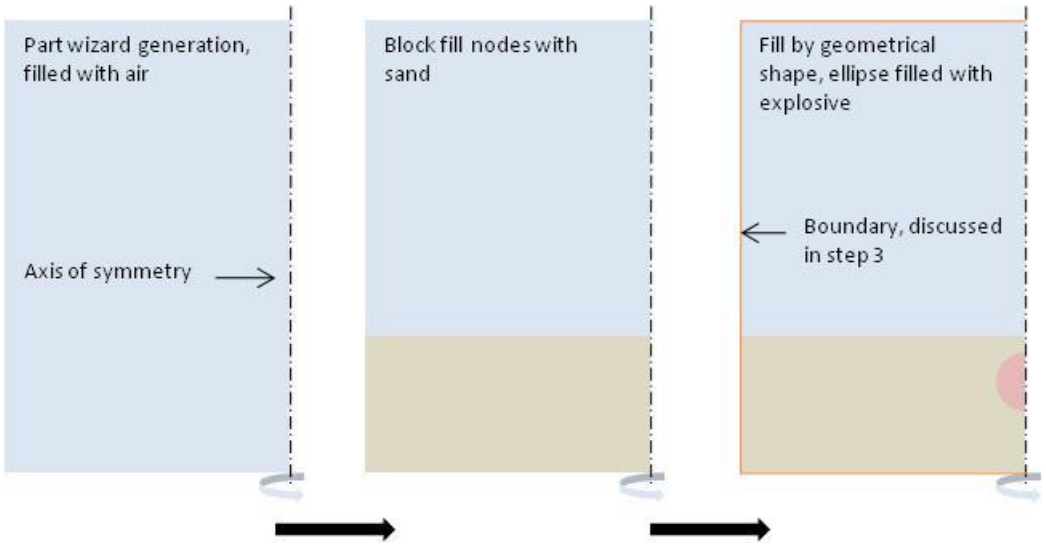

Figure 4-4 Additional fill options within AUTODYN

Within the parts dialog panel there is also the option to add gauges to parts so that the movement of parts or cells can be tracked and chosen data logged for post-processing after the simulation has finished.

A gauge can be added by selecting the required part in the parts dialog box and then selecting the gauges tab, located below zoning. There are two types of gauges available in AUTODYN; fixed and moving. Fixed gauges are exactly that, 'fixed'. Their coordinates do not change throughout the simulation. These are ideal for measuring pressure at a fixed location throughout a blast analysis. Moving gauges move with the flow if attached to an Euler part or with the part if attached to a Lagrange part. This makes them ideal for measuring deflections of structures under loading. The gauges can be located by x, y, z co-ordinates or by i, j, k locations.

The gauge parameters can be set in the output tab in AUTODYN under history and the results can be viewed under history in the plots dialog after the simulation has been stopped.

STEP 3 - BOUNDARY CONDITIONS

Boundary conditions are used to both constrain the problem and apply initial conditions to the problem. There are a range of boundary conditions to choose from in order to allow simulations to be as accurate as possible. The following boundary conditions are available within AUTODYN:

- Stress
- Velocity
- Flow_in
- Flow_Out
- Transmit
- Force
- Force/Length

Though only, velocity and Flow_Out are used in this project.

The velocity boundary condition can be applied to Lagrange, ALE, Shell, Beam and SPH parts and has a variety of different options available:

- X, Y, Z Velocity constraints
  - Constant - Fixed at a constant value
  - Limit - Limit position between maximum and minimum co-ordinates
  - Piecewise - Piecewise linear segments
- General velocity constraints
  - Fixed constant velocities in X, Y, Z (3D) and fixed rotational velocities about co-ordinate axes
- User subroutine
- User Time-Dependant X, Y, Z velocity

For this study the constant velocity boundary was applied for various arrangements to ensure that a part was fixed in space.

The flow boundary conditions allow the user to specify what happens at the edge of an Euler part. For the purposes of this project the flow_out condition allows pressurised air, and ejecta from the mine explosion simulation to flow out of the Euler mesh area, without being reflected back in and causing more damage to the structure being loaded. It is

important to note that this boundary condition is only approximate and therefore should be placed as far as possible from the area of interest (Century Dynamics Limited).

STEP 4 – INTERACTIONS

When there is more than one part in a model interaction between the parts is necessary. There are two forms of interaction: Euler/Lagrange and Lagrange/Lagrange.

Lagrange/Lagrange interaction is implemented when there are Lagrange parts in the model, in 2D simulations this of the form of an interaction gap. The gap is defined as the radius of a contact detection zone that surrounds each surface element. This is shown figuratively by the blue shadow in Figure 4-5 below. Any nodes that enter this contact zone are repelled by a force proportional to the depth of penetration of that node within the contact detection zone.

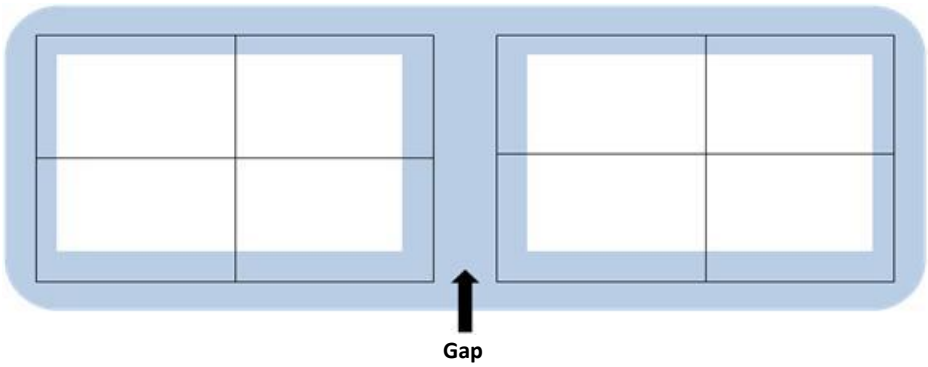

Figure 4-5 External gap for a Lagrange part

This gap size must be in the range of 1/10th to ½ of the dimension of the smallest surface element. AUTODYN can calculate this value for you, but will calculate the recommended size which is 1/10th. It is possible to override this value by inputting in your own value and as long as it falls within the specified range it should be ok. AUTODYN also offers a check to ensure the gap size is valid.

There is also the option within this interaction to *retain inertia of eroded nodes*, when an element erodes its internal energy is always discarded. By checking this option its inertia can be retained as a free mass point. By allowing the elements to erode ensures that degenerate cells do not occur forcing the solution to terminate. The erosion constraints are set at the material modelling stage as outlined in section 4.3.

In 3D there are two options available for Lagrange/Lagrange interaction, the external gap method and the trajectory method.

The external gap method works in exactly the same way for 3D as it does for 2D.

The trajectory method detects contact over time by tracking node and face trajectories. This is a much simpler method and gives significant performance improvements for the simulation.

The same option to retain inertia of eroded nodes is also present in this option.

Euler/Lagrange interaction is different for 2D and 3D models. In 2D there are three coupling types available:

- None
- Automatic (polygon free)
  - Easy to use
  - Can be used with erosion
  - Must be used for all parts
  - Cannot be used with shell parts
- Polygons
  - Cannot be used with erosion
  - Can be used for Lagrange, ALE and Shell parts

The automatic method is used throughout this project whenever modelling in 2D. It works by the entire surface of the Lagrange part interacting with the Euler part automatically. As the Lagrange part enters the Euler grid the Lagrange parts covers faces and elements within the grid. This then imposes flow constraints upon the Euler grid and as a result the Euler grid exerts a pressure on the Lagrange part as the material contained within the Euler grid tries to move through the grid.

For 3D models the menu options for coupling types are (Century Dynamics Limited, 1998):

- None – where no coupling is defined
- Rigid – where the filled parts are used to define rigid boundaries for Euler
- Fully Coupled – where Lagrange parts interact with Euler parts dynamically
- Weak Coupling – is a faster, but less accurate method for Lagrange parts to dynamically interact with Euler.

For this project fully coupled is always used.

STEP 5 – DETONATION

When analysing mine blast problems it is essential to include the detonation of the high explosive for an initiation time in the simulation.

The detonation is initiated at a user specified time and node or plane.

Using the JWL EOS as described in section 4.3.5 the expansion of the detonation products, or gases, is calculated.

STEP 6 – CONTROLS

These are the solution controls. In here it is possible to specify the wrap-up criteria. The other solution controls usually have sufficient default values.

The wrap-up criterion consists of the cycle and time limit, which is where the user specifies how long they want the solution to run for. The energy fraction and the energy reference cycle.

As previously mentioned at the start of this chapter, energy cannot be perfectly conserved during these simulations. The energy fraction allows the user to input an allowable amount of error due to energy into the model. The energy reference cycle is the cycle at which this energy fraction is implemented in the model. If the solution exceeds the allowable energy error it will terminate with the error message 'energy error too large'.

STEP 7 – OUTPUT

In this section the results files are identified and saved. By defining the frequency of saves, by either times or cycles, a simulation may be saved for future reference.

In the History dialog box within this section the gauge variables can be set, these allow the user to plot graphs of a large variety of variables. However only the variables selected here will be saved.

STEP 8 - POST-PROCESSING

In the history section of the main screen, graphs can be plotted for the various gauge points placed in the model at the start of the simulation. Using the Single variable plots it is possible to look at a single parameter for every gauge. In the Multiple variable plots it is possible to look at a variety of parameters for any number of gauges on the same graph. There are also options to pull out the minimum and maximum values on the graph, to integrate or differentiate depending on what the user is looking to find out. It is also

possible to export the data to other software such as Microsoft Excel. This is done by selecting the write text output option, the menu depicted in Figure 4-6 then appears.

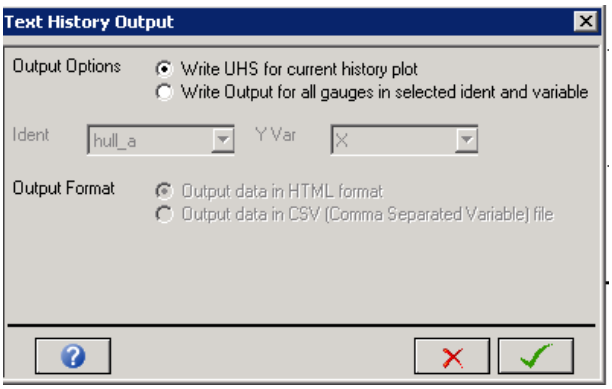

Figure 4-6 Text history output

From here the user can select the data for the current plot, that which is on the history graph at that moment in time or, as what was done in this project, select the write output for all gauges option. This writes all the data for every gauge for a particular Y variable, the X variable is time. By outputting the data in the CSV format option enables easy conversion into an Excel file. It is however important to note that there are tens of thousands of lines of data for each gauge. It is possible to reduce this back in the history section. By selecting the reduce option, the user will be asked to input a number to reduce by. For example, if 2 were entered the history file will be reduced by a factor of 2. It is essential not to reduce the data by too much as it cannot be undone.

To open the data in Excel, open the .uhs file through Excel and the text import wizard will appear as shown in Figure 4-7. By selecting the Delimited option as opposed to the default Fixed width option it is then possible on the next window to use commas to separate a column, allowing each gauge and the associated data to be displayed in a separate column. This makes formatting the data much easier to manage.

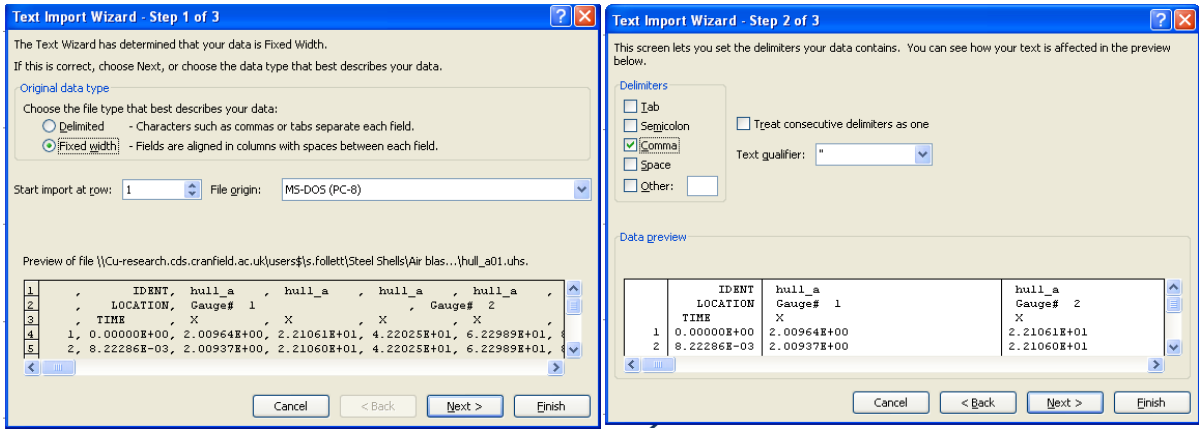

Figure 4-7 Text Import Wizard

On step 3, select finish and then the data can be manipulated for display purposes.

4.5 SUMMARY

This chapter has discussed and described the AUTODYN software, with specific reference to its intended use for this project. A step-by-step guide has been described to show the processes involved in creating a model, should the models need to be recreated for future work. The actual models used for simulations are described in detail in chapter 6 Modelling Results later in this thesis.

"NO AMOUNT OF EXPERIMENTATION CAN EVER PROVE ME RIGHT; A SINGLE EXPERIMENT CAN PROVE ME WRONG"

ALBERT EINSTEIN (1879 –1955)

5 EXPERIMENTAL WORK

For numerical simulations to be accepted as realistic and as an alternative to carrying out expensive testing throughout development, they must be comparable with actual results.

This chapter will cover the experimental work carried out during the course of the project for comparisons with the numerical models used later.

The experiments conducted aimed to evaluate the response of flat composite plates subjected to a buried mine blast. These tests were conducted using dry sand similar to that used by Laine *et al*. (Laine, L., Sandvik,A., 2001) in order to replicate the experiment using ANSYS AUTODYN. The results for the modelling are shown in the following chapter. The second experiment conducted was to create small scale experiments of a variety of different V-shaped hulls. Different materials were used during the experiments in order to discover an ideal solution. The explosive this time though was buried in saturated sand, in order to address STANAG 4569 requirements as a worst case scenario. Material models developed by Grujicic *et al*. (Grujicic et al., 2007; Grujicic et al., 2006; Grujicic et al., 2009; Grujicic et al., 2008) were used to model the wet sand in AUTODYN. Again the numerical results are detailed in the subsequent chapters.

All tests were conducted on the Explosives Range and Demonstration Area (ERDA) located at the Shrivenham campus of Cranfield University, in May and December 2010 and May 2011. Prior to testing a test plan must be submitted to the ERDA outlining plan for duration of time, for a copy of all test plans please refer to Appendix 6.

Table 5-1 below shows a brief description of the experimental work conducted, with details of who was responsible for the work.

Experiment	Dates	Description	Who was responsible
Flat plates	May 2010	Six flat S2-glass composite plates 500mm^2 subjected to varying PE4 charge sizes buried in dry sand	Author, MSc student was present though this experiment not shared.
1	May 2010	Steel and S2-glass V-shaped hulls shapes A-C, see Figure 5-9. 240g PE4 buried in wet sand with high stand-off	Author and MSc Student and results shared, see (Khare, 2010).
2	December 2010	Steel, S2-glass and E-glass shape D. 240g PE4 buried in wet sand with high stand-off	Author
3	May 2011	Steel, S2-glass and E-glass. Shapes A-D. 240g PE4 buried in wet sand with low stand-off	Author

Table 5-1 Description of experimental work conducted

5.1 FLAT PLATE TESTING

The following experiments were conducted as part of this section of work:

PLATE	MATERIAL	SAND	STAND-OFF	CHARGE SIZE
1	S2-glass	Dry	350mm	75g
2	S2-glass	Dry	350mm	130g
3	S2-glass	Dry	350mm	185g
4	S2-glass	Dry	350mm	185g
5	S2-glass	Dry	350mm	240g
6	S2-glass	Dry	350mm	300g

Table 5-2 Flat plate experiments

The rig consisted of a steel box framework with four steel bars attached by bolts through the box section at the top of the rig. An EN8 steel plate with a 400mm^2 window is then suspended by the bars. Flat composite panels of 500mm^2 were placed over the window in the plate. This was then bolted in place with another steel plate located on the top surface, again with a 400mm^2 window cut into it. The setup of the rig is shown in Figure 5-1 below, with a close up of the steel and composite plates in Figure 5-2. The rig was originally built for an MSc project in 2009 where the student looked at steel V shaped hulls, and the impact of blast location. For full details please refer to the project report (Child, 2009). To see dimensions of the rig please refer to Appendix 5 for the technical drawings submitted to the workshops. The rig was adapted for this experiment by changing the supports that held the

composite plates in place. It was found during tests conducted for (Child, 2009) that the original supports, threaded bars, were too weak and would buckle under the force of the explosion. In order to recreate the model in Autodyn, the plate needed to be fully constrained and the framework holding it in place unable to move in any direction. Therefore new bars were constructed by the workshops that were much stiffer and would not buckle. Again for detailed drawings of the changes made to the rig including all technical drawings for new parts please refer to Appendix 5.

Figure 5-1 Test rig set-up

Figure 5-2 Plate configuration

The charge used was PE4 which has a TNT equivalence of 1.3 (Weckert and Anderson, 2006). It is usual to convert explosives into a TNT equivalency; however there are some difficulties with this, as it very much depends upon the parameters that are being measured. For these experiments PE4 was used which can have an equivalency of a variety of values between 1.09 – 1.37. (Weckert and Anderson, 2006) stated that since the effects of a landmine on a vehicle may include both acceleration of the vehicle and deformations, it is suggested that an equivalency ratio of 1.3 may be appropriate, since this will be reasonably close to both the acceleration and deformation results. Work conducted by (Wharton et al., 2000) also indicated an overall TNT to PE4 equivalency of approximately 1.3.

The PE4 was rolled by hand into a sphere for these tests and then buried in dry sand 50mm below the surface. Six plates were tested for this experiment, with the following charge masses:

- 75g
- 130g
- 2 x 185g
- 240g
- 300g

High speed cameras were positioned behind pendine blocks in order to capture the explosion and provide information on the deflection of the plates.

Figure 5-3 Camera position

Figure 5-3 shows the position of the camera behind the wall. A mirrored tile was placed on top of the wall in order to film the experiments without jeopardising the integrity of the

camera. The gazebo was to protect the camera and the laptops against the rain and debris from the explosion.

5.1.1 CALCULATIONS

This section will discuss how the actual displacements were calculated from the images collected during testing.

Figure 5-4 shows an image from the high speed camera for the test using 130g of PE4. The plate was sprayed with paint in a random pattern in order to make it possible to track a point with the video camera, so that the displacement can be calculated. It can also be seen from this image that the flat plate does not lie directly in the x-y plane. Therefore trigonometry needs to be conducted to find the vertical displacement experienced by the plate.

Using the picture in Figure 5-3 it is possible to work out the position of the camera and therefore the angle at which the displacement is being filmed.

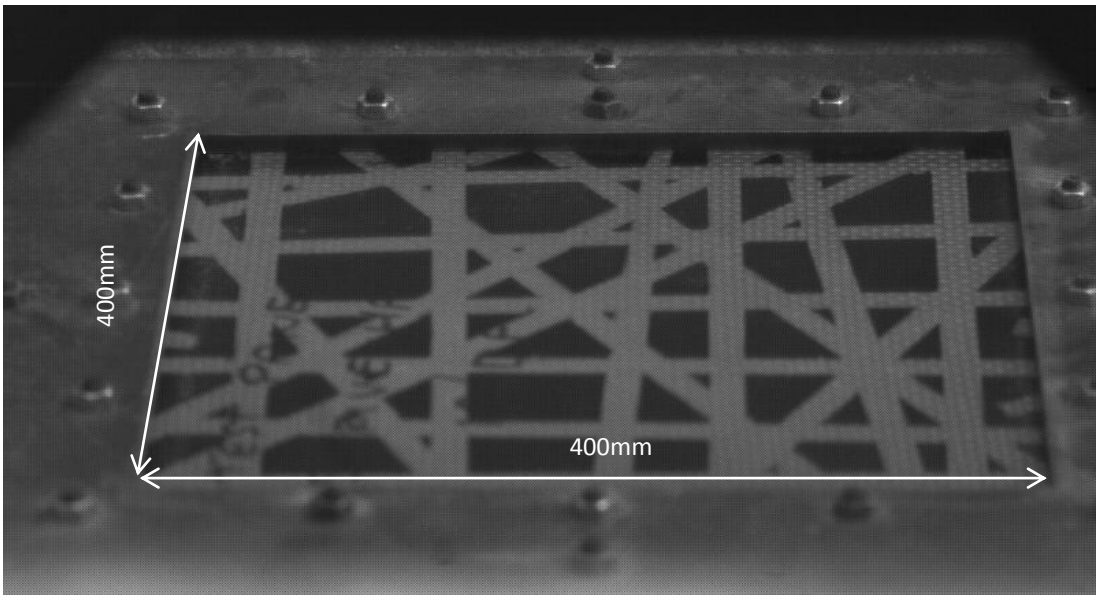

Figure 5-4 Image from high speed camera before firing

Figure 5-5 Calculating angle for actual displacement

Looking at Figure 5-5 where α is the angle difference between the vertical and the filmed displacement, h is the vertical displacement and d is the observed displacement. It is then possible to calculate the actual displacement by using the following expression:

$$h = \frac{d}{\cos \alpha}$$

Where α was measured to be 27°.

It is also necessary to set scaling for the image in Figure 5-4. It is known that in this instance the horizontal and vertical distances from corner to corner are all 400mm. The larger the gauge length set the more accurate the measured values are. It is then possible to track a point on the plate frame by frame using the high speed video camera software in order to calculate the displacement. Due to the angle of the image, the horizontal distance is used for the gauge length as this does not need any trigonometry corrections applied to it.

5.1.2 RESULTS

All the plates moved in a sinusoidal fashion, as depicted in Figure 5-6 below with the displacement fading over time.

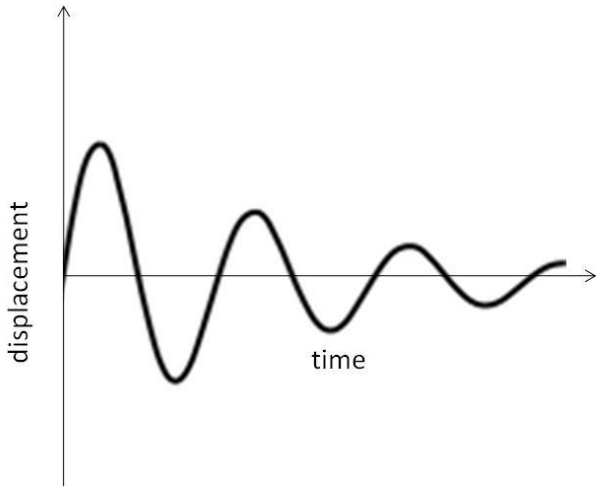

Figure 5-6 Plate oscillation

Table 5-3 below shows the observed maximum dynamic displacements from the experiments and the vertical dynamic deflections after applying the scale factor due to the angle.

Charge Weight	Filmed Deflection (mm)	Actual Deflection (mm)
75g	*Data not captured*	-
130g	14.094	15.82
185g	23.061	25.88
185g	24.874	27.92
240g	25.3	28.39
300g	39.926	44.8

Table 5-3 Flat plate results table

These results are compared to the numerical simulation results in chapter 6 Modelling Results. Unfortunately the data from the 75g experiment was not captured, so it was not possible to compare those results.

None of the composite plates had any permanent damage done to them. The plates were all sectioned into quarters to check for delamination, of which there was none.

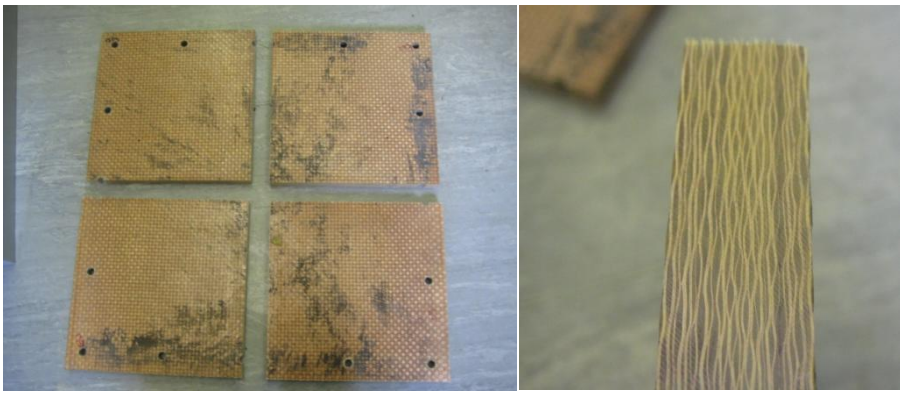

(a) (b)

Figure 5-7 130g Flat plate (a) sectioned into quarters (b) close up of edge at centre of plate

5.2 V-SHAPED HULLS

For these experiments the work was broken down into three sections. The first were run in conjunction with an MSc project looking at the blast effects on composite V-shaped hulls; please refer to (Khare, 2010) for the thesis. It is necessary to note that the author was present for all trials and that it was conducted as a joint endeavour.

The second involved introducing a new composite material, but for only one of the shapes (test pan D) and comparing all three material results.

The third involved using all three materials for all four shapes but at a lower stand-off distance, to more accurately represent the maximum stand-off currently available under an LPPV. Hereafter these experiments will be referred as 1, 2 and 3 respectively as shown in Table 5-1. The experiments are further detailed below in Table 5-4 where all charges were 240g PE-4 rolled into a sphere and buried 50mm below the sand surface.

EXPERIMENT	SHAPE	HULL ANGLE	MATERIAL	DISTANCE: HULL TOP TO SAND SURFACE	SAND
1	A	107	S2	590mm	Dry
1	A	107	S2	590mm	Wet
1	B	101	S2	590mm	Wet
1	C	95	S2	590mm	Wet
1	A	107	Steel	590mm	Wet
1	B	101	Steel	590mm	Wet
1	C	95	Steel	590mm	Wet
2	D	90	S2	590mm	Wet
2	D	90	E	590mm	Wet
2	D	90	Steel	590mm	Wet
3	A	107	S2	480mm	Wet
3	B	101	S2	480mm	Wet
3	C	95	S2	480mm	Wet
3	D	90	S2	480mm	Wet
3	A	107	E	480mm	Wet
3	B	101	E	480mm	Wet
3	C	95	E	480mm	Wet
3	D	90	E	480mm	Wet
3	A	107	Steel	480mm	Wet
3	B	101	Steel	480mm	Wet
3	C	95	Steel	480mm	Wet
3	D	90	Steel	480mm	Wet

Table 5-4 Experiments conducted on V-shaped hulls

It should be noted that apart from the stand off for the third set of experiments the set-up was exactly the same for each.

The hulls were scaled down to third scale in order to make the experiment cost effective and to fit in with the rig that had already been constructed. Also there is a limit of 450g to the amount of explosive that can be used on the outdoor explosives range at Shrivenham. When scaling the explosive, it is necessary to take into account the fact that it is a volume and therefore needs to be scaled by a factor of 3^3. For these tests an explosive mass of 240g was decided upon, this scales up to 6.5kg. Using TNT equivalency this is just short of 8.5kg which is greater than that required for STANAG 4569 level 3, and a level above that stated in the LPPV contract.

It should be noted that although mentioned the TNT equivalency is not used within this project for any comparative work, as not necessary and due to the ambiguity surrounding it.

Fully saturated sand was also used for this round of experiments, partly in accordance with AEP 55, which can be seen in Appendix 2, and with the sponsors' wishes. Though for a brief comparison, discussed in (Khare, 2010) pans A and B were also tested using dry sand.

As discussed in section 3.2.3 explosives buried in wet sand deliver a much greater pressure and therefore impulse to the target, than those buried in dry sand. This is because little energy, in comparison, is lost through the sand and the blast is more concentrated on the target, giving tests for a worst case scenario. Figure 5-8 shows pan A under testing using dry sand (a) and pan C under wet sand (b). From a very early stage in the explosion the dry sand is dispersed over a wider area, when compared to the wet sand at about the same stage in the explosion, the sand is much more focused and less 'dusty'.

(a) **(b)**

Figure 5-8 Dry sand test (a) vs. west sand test (b)

Four different shapes were used in three different materials, steel, S2 and E glass composites. Figure 5-9 shows the configuration of the four shapes. The aim of the experiments was not only to compare the steel with the different composites; but also to look at the effect of shape vs. stand-off. Pan A was the shallowest hull, with an angle of 107°, pan B at 101°, pan C at 95° and pan D, the steepest, but closest to the blast at 90°. The figure shows the dimensions for the steel hulls. The composite hulls were 22mm thick for weight-for-weight comparisons between each hull shape. The inside dimensions were exactly the same to allow fitting onto the rig and it is worth mentioning that if a composite solution was to be used instead of steel then the composite will be closer to the ground to allow for the extra thickness and to keep the same internal volume.

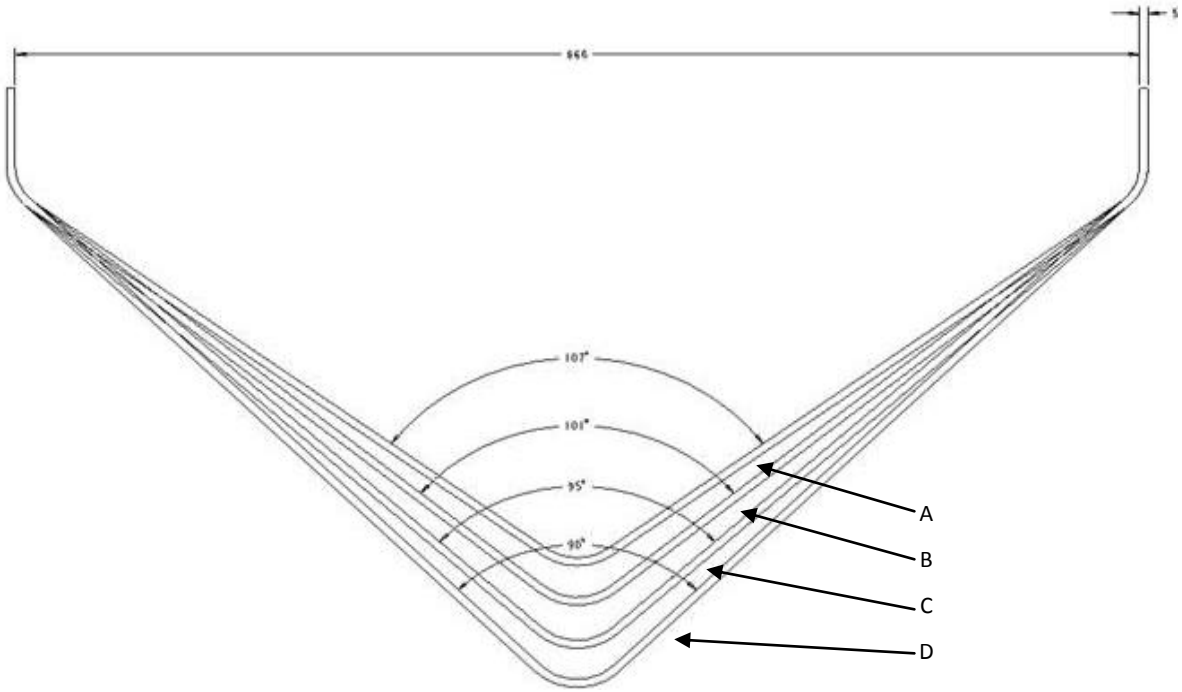

Figure 5-9 Test pan shapes

Figure 5-10 below shows how the rig was configured. In order to judge which shape was best suited for blast mitigation, the distance from the top of the hull to the top of the sand was kept at a constant 590mm for experiments 1 & 2 and 480mm for experiment 3. The table below gives the stand-off distances for the different pans and materials.

PAN	STAND-OFF DISTANCE EXPERIMENTS 1 & 2		STAND-OFF DISTANCE EXPERIMENT 3	
	COMPOSITE	STEEL	COMPOSITE	STEEL
A	264	279	154	169
B	239	254	129	144
C	214	229	104	119
D	189	204	79	94

Table 5-5 Stand-off distances [mm]

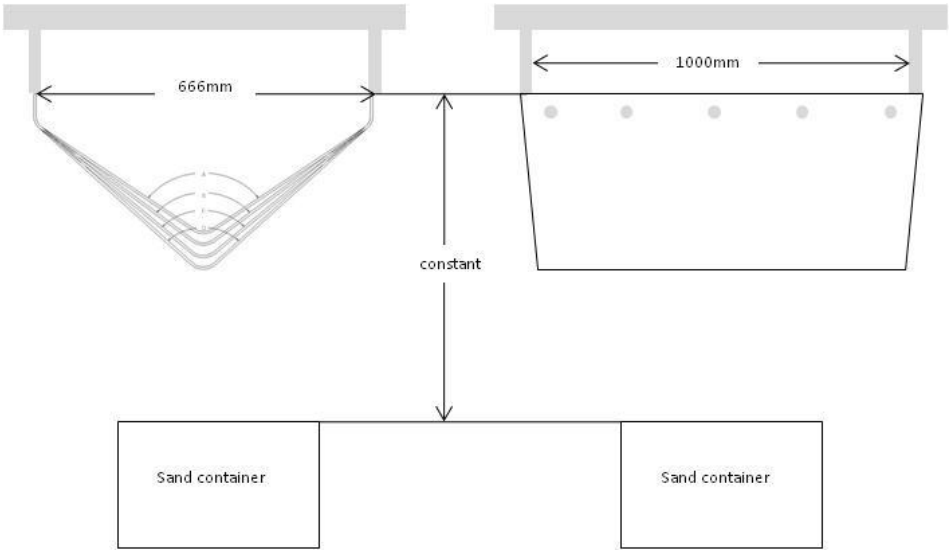

Figure 5-10 Rig configuration

5.2.1 TEST PROCEDURE

The rig used was the same as for the flat plate tests discussed above in section 5.1, with the same steel supports supporting a different frame. The frame used was placed on the inside of the hull and five M12 bolts went through the vertical top edges of the hull and through the frame, along each side, and tightened with a torque drill, to ensure a rigid support. For full drawings of the rig and experimental set up please refer to Appendix 5. However Figure 5-12 shows the configuration of the experiment before firing.

After experiment 1 it was found that the frame holding the test pan kept bending along the bolted edges and had to be replaced after two or three tests. It was therefore modified to include an extra support bar to prevent this, as depicted in Figure 5-11; Appendix 5 includes all drawings for modifications. The extra bars were not attached to the frame supporting the hull, only to the outside framework. They are solely to stop the frame supporting the hull from bending.

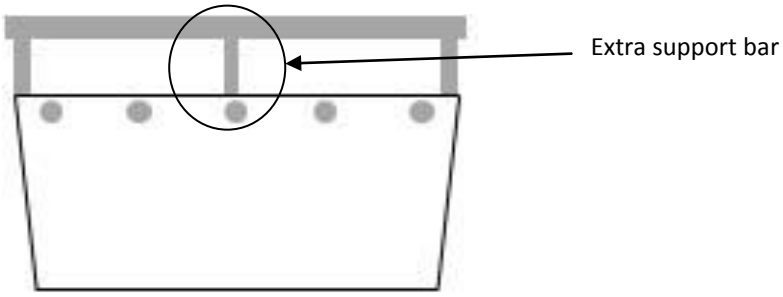

Figure 5-11 Rig modification

Figure 5-12 Experimental set up

After this first firing depicted in Figure 5-12 the steel box containing the saturated sand split along all four corners and was deemed unsafe for further experiments due to fragmentation risks. An alternative arrangement was decided upon where a sacrificial plastic box filled with the saturated sand was placed inside a new steel box, creating a substantial air gap between the explosion and the steel container. This set up is shown in Figure 5-13. This also ensured that the all the water stayed in the box and would not drain away before firing, and that the ratio of sand to water was much easier to keep constant.

Figure 5-13 Modified sand container

5.2.2 RESULTS

The following section has been broken down into two main parts. The first looks at all the experiments conducted at the larger stand-off distance, including the second set of tests looking at pan D comparisons with steel, S2 glass and E glass.

The second section will look at the third set of experiments, looking at all three materials in all four shapes at the lower stand-off distance.

During all tests the movement of the hull, both steel and the composites, as a result of the blast was in the direction as described in Figure 5-14. Using high speed video camera footage, it is possible to track points on the inside of the hull and therefore measure the amount of deflection. The parameters measured for all experiments are the dynamic and permanent deformations.

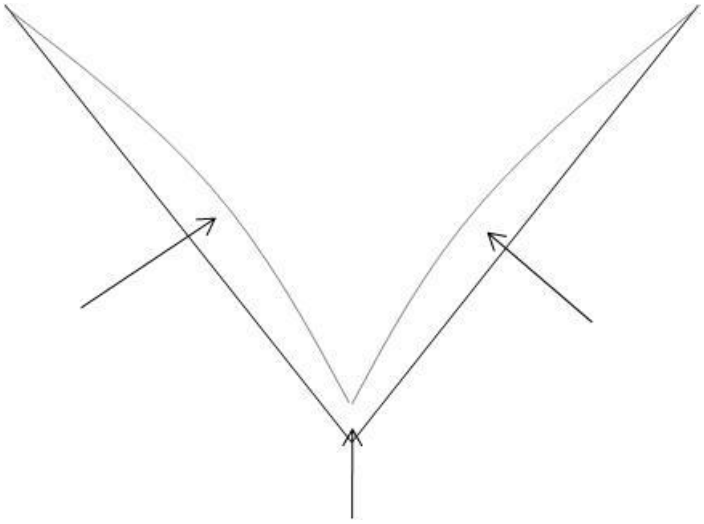

Figure 5-14 Hull movement

All pictures in yellow are S2 glass composite, green are E glass composite and grey are the steel. Graphs of all the experimental work from the high speed video cameras can be seen in Appendix 7

EXPERIMENTS 1 & 2

During these tests the composite withstood the blast much more effectively than the steel; in that they retained their outside shape very well with no 'denting' occurring on the side panels. There was some damage on the outside of the pans due to the sand impacting on the material causing some of the fibres in the first few layers to fray slightly, as shown in Figure 5-15. Most of the composite test pans experienced a small amount of delamination at the bottom of the V on the inside surfaces, this is shown for pan C in Figure 5-16.

Figure 5-15 Damage to underside of hull C after firing

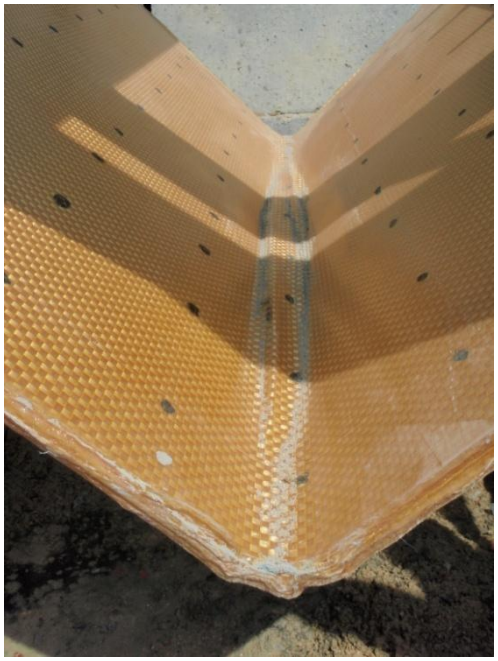

Figure 5-16 Delamination of Pan C after firing

The hulls were sectioned to look at the damage to all the layers and a dye penetration test was carried out in order to see the damage more clearly. It was found that very little damage was done to the inside and only at the point of the V-shape and this is shown in Figure 5-17. It can be seen that the damage forms a triangular shape covering approximately one third of the overall thickness. It can also be seen that the damage done to the outside surface is minimal, with only one or two layers showing the darker pink.

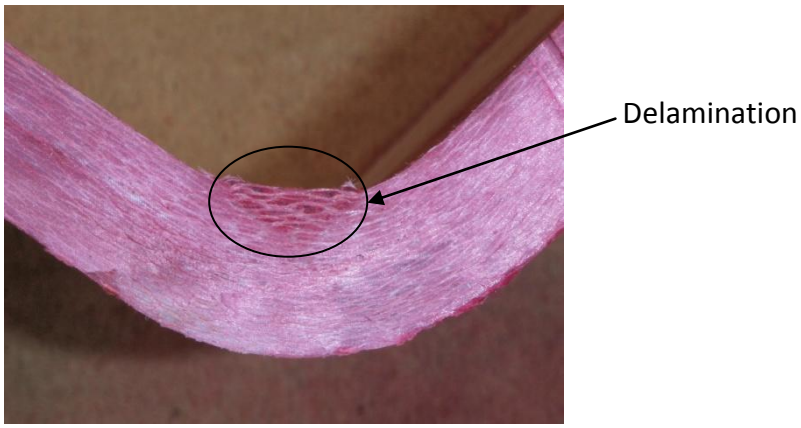

Figure 5-17 Dye penetration test to show delamination effects

As mentioned in section 5.2.1 during experiment 1, it was found that the frame holding the test pan in place kept bending due to the force from the explosion. On the last day of testing, this frame was deemed unusable for future tests, due to the bend and making it virtually impossible to get the bolts through the test pan and the frame. At the time the composite pan C was on the frame, and it was decided to test the pan again to see if it could withstand a second or third blast.

COMPOSITE PAN C AFTER SECOND AND THIRD FIRINGS

The experiment was set up in exactly the same way as previously though for these tests the composite test pan was left on the frame.

After the second firing, the pan was still intact with the hull retaining its outside shape and no perforations. The delamination on the inside surface at the bottom of the V-shape became greater and the slight fraying/tearing to the fibres on the outside few layers was more pronounced, as shown in Figure 5-18.

Figure 5-18 Pan C after second firing

It was also noticed that a crack in the matrix appeared on the inside of the hull, but did not appear to go through more than the top few surface layers.

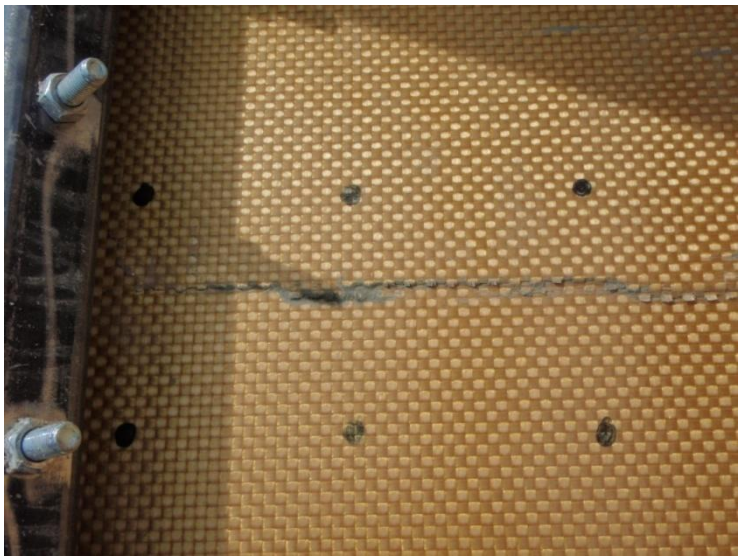

Figure 5-19 Matrix cracking in composite after second firing

After the third firing again there was very little in the way of damage to the overall shape, but again the delamination damage became more pronounced.

Figure 5-20 Pan C after third firing

When the test pan was taken off the rig and frame, it was turned over to look at the damage to the underside. Water was poured over the pan to see if there were any perforations through the material. This turned out to be negative, so the test pan was still intact, and had largely kept its shape even after being subjected to a 240g blast in saturated sand three times.

Figure 5-21 Underside of composite hull C after third firing

Figure 5-21 shows the underside of the test pan after the third firing. It can be seen that the damage to one side is distinctly worse than on the other. This was because during manufacturing the material sat on foam pad to ensure that the bottom of the V was as pronounced as possible. This foam pad left an indentation on both sides of the pan but on one side was much lower to the point of the V. This indentation appears to have caused the blast to catch and tear the material. It was suggested to the sponsors, NP Aerospace, that this indentation should be moved upwards to the same position as the other side, if it is not possible to get rid of it altogether.

From the experimental results a comparison of the maximum dynamic deflection at the side and base for the different hull shapes and the different materials was conducted and presented in Table 5-6. The distance column was calculated using Pythagoras theorem, from the x and y displacements. Where needed the same trigonometry as applied to the flat plates was also applied here. Though it is not needed for horizontal displacement as the horizontal movement was in the same plane as the camera. Figure 5-22 shows the movement of the test pans and the notation used for Table 5-6.

Dynamic deflection is the deflection of the material during the explosion. The permanent deflection is measured later in this section.

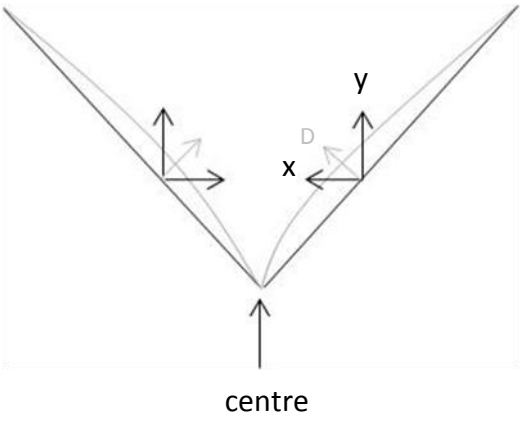

Figure 5-22 Deflections

In Table 5-6 it should be noted that on the composite test pans, the centre deformation is what is seen by the camera, and as a result includes the movement from the delamination. The hull as a whole did not move so far, but there was no method implemented to measure this.

The delamination occurs due to a compressive stress wave passing through the material as a result of the blast wave impinging on the front face. When the stress wave reaches the back face of the material it is reflected back as a tensile wave, this tensile wave if greater than the tensile strength of the material will cause local failure at the back face. In metals this leads to the formation of spall or fragments. In the composite the tensile strength of the stress wave has to be greater than the tensile strength of the resin to cause the delamination. In the case of the V-shaped hulls the fibres do not break as the material effectively lifts away from the rest of the structure, actually causing more slack in the fibres. In order to break the back face of the material, the stress wave would either have to break the fibres or peel away all the resin over the entire inside surface of the hull. As shown in Figure 5-17 previously, this does not occur for the S2 glass fibre hulls.

With the advent of the drive train being placed inside the V to help increase the deflection effects and to protect against large parts of the vehicle flying off the vehicle and causing yet more damage, it would be beneficial to find out what would happen to these back face layers when they come into contact with heavy items placed in the way. Due to the mass of the fibres in the few layers that do detach, they would not be likely to cause damage to anything but they could themselves become damaged further.

Measured values from video footage							Adjusted values for camera angle				
Pan	Material	Sand	Centre [mm]	Side [mm] Y	Side [mm] X	Distance, d	Camera angle, a	Centre [mm]	Side [mm] Y	Side [mm] X	Distance, d
A	*S2*	*Dry*	*14*	*14*	*-*	*-*	*30*	*16.17*	*16.17*	*-*	*-*
A	S2	Wet	32.2	21	3	21.21	31	37.57	24.50	3.00	24.68
B	S2	Wet	27.8	22.6	4.5	23.04	30	32.10	26.10	4.50	26.48
C1	S2	Wet	35	24.4	9	26.01	30	40.41	28.17	9.00	29.58
D	S2	Wet	33	18.5	5.56	19.32	39	42.46	23.81	5.56	24.45
C2	*S2*	*Wet*	*47*	*27.7*	*11.5*	*29.99*	*32*	*55.42*	*32.66*	*11.50*	*34.63*
C3	*S2*	*Wet*	*-*	*66*	*24*	*70.23*	*42*	*-*	*88.81*	*24.00*	*92.00*
D	E glass	Wet	30.2	31.68	4.5	32.00	41	40.02	41.98	4.5	42.22
A	Steel	Wet	43	53	14.6	54.97	36	53.15	65.51	14.60	67.12
B	Steel	Wet	57	72	14	73.35	40	74.4	93.99	14.00	95.75
C	Steel	Wet	60	47.4	17.1	50.39	32	70.75	55.89	17.10	58.45
D	Steel	Wet	36	48.07	17.9	51.29	35	43.95	58.68	17.9	61.35

Table 5-6 Maximum dynamic deflections experiments 1 & 2

The first row in Table 5-6 is the results from test pan A under dry sand loading for comparative purposes. Rows C2 and C3 are the results from the second and third firings of test pan C. It can be seen from these results that the dynamic displacement is much greater once the material has already delaminated in places, showing that the material properties have degraded significantly.

Table 5-7 below shows the permanent deflections of the test pans. It can be seen that there was none at the sides for the composite and again it should be noted that the deflection at the centre includes the added thickness due to the delamination.

PAN	MATERIAL	SAND	DEFLECTIONS [MM]	
			CENTRE	DISTANCE, D
A	S2	Dry	-	-
A	S2	Wet	-	-
B	S2	Wet	-	-
C	S2	Wet	-	-
D	S2	Wet	-	-
A	Steel	Wet	1	34
B	Steel	Wet	2	27
C	Steel	Wet	2	31
D	Steel	Wet	3	24
D	E glass	Wet	-	-

Table 5-7 Permanent deflections

The results from Table 5-6 show that the dynamic deflections of the steel test pans move at least twice as much as the S2 glass with phenolic resin.

Looking at the permanent deflections, from Table 5-7, whilst the S2 glass with phenolic resin delaminates slightly at the bottom of the V on the inside surfaces, see Figure 5-23 for an example of this, there is no other permanent deformation or deflection. The same is the case for the E-glass, though the delamination is worse than in the S2-glass. Whereas the steel does deform plastically and as a result, does not return to its original shape after the experiment. Table 5-10 and Table 5-12 in the following sections show the relationships between the steel and the composites and between the different shapes.

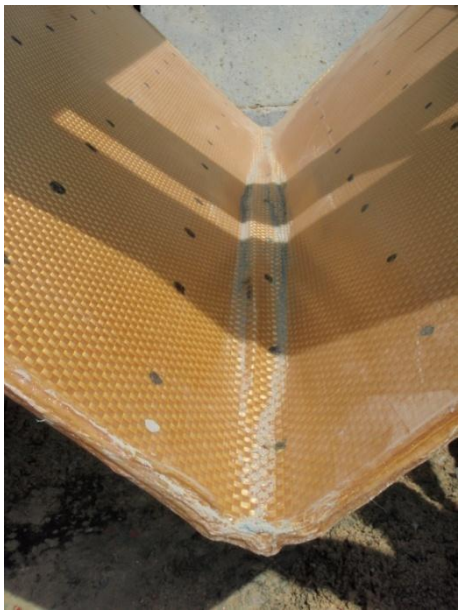

Figure 5-23 Delamination of pan C after first firing

EXPERIMENT 3

Again during these tests the S2-glass composite withstood the blast much more effectively than the steel. It also out-performed the E-glass composite significantly.

The main damage was again delamination in the inside, along the centre of the V in both the S2 and the E-glass. The E-glass experienced cracking up the sides of the test pan and also lost some of its structural integrity, in that it could be easily flexed after the test. The cracking of hull D is shown in Figure 5-24.

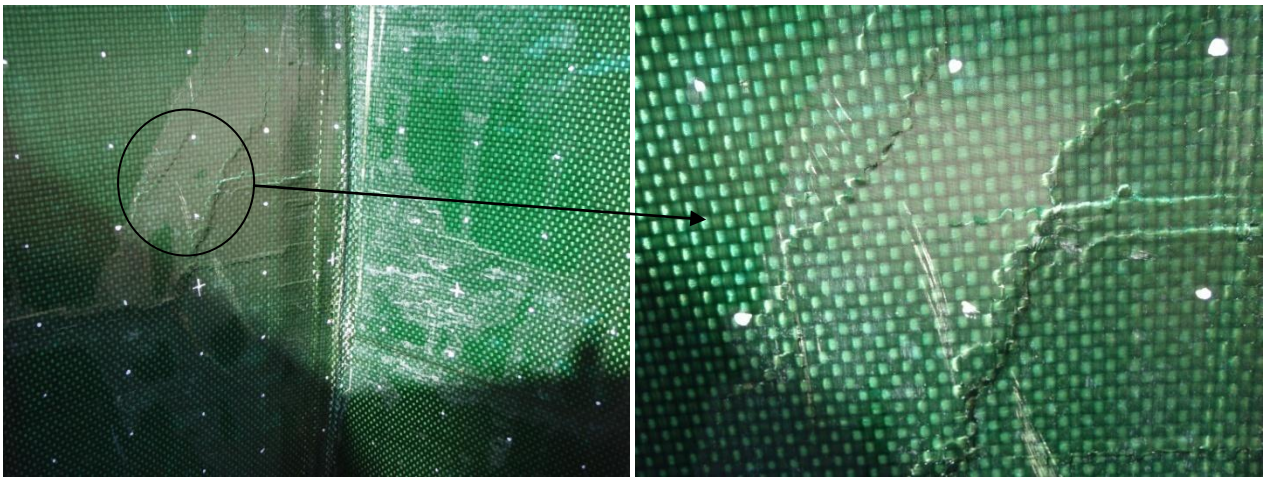

Figure 5-24 Cracking of E-glass test pan D

After the first of these experiments, due to the hull being much closer to the blast, the frame supporting the hull bent out of shape and the welds at the corners cracked. As a result, the frame was modified by attaching bracing in a diamond across the frame, see Figure 5-25 below. This will have provided some extra stiffness to the test pans in comparison to the work done in

experiments 1 and 2 discussed previously, however, as these results are not to be compared to the previous ones it was deemed an acceptable alteration.

Figure 5-25 Bracing of frame supporting test pans

A drawback of adding the bracing to the frame is that it made it difficult to get a clear video of the inside of the hull during the blast as tracking points would disappear from view. However every effort was made to get as close to the centre of the hull as possible.

Measured values								Adjusted values					
Pan	Material	Sand	Centre [mm]	Side [mm] x	Side [mm] y		Distance, d	Camera angle, a	Centre [mm]	Side [mm] x	Side [mm] y		Distance, d
A	S2	Wet	Not able to track	5.1	31.1		31.52	34	Not able to track	5.1	37.5		37.85
B	S2	Wet	59	16.6	48.4		51.17	34	71.2	16.6	58.4		60.7
C	S2	Wet	36.8	20.4	32.9		38.71	31	43	20.4	38.4		43.48
D	S2	Wet	Not able to track	73.7 7.7	95.2 23.8	Left side Right side	120.4 25	32	Not able to track	73.7 7.7	112.3 28	Left side Right side	134 29
A	E glass	Wet	Data not captured				-	Data not captured					-
B	E glass	Wet	Data not captured				-	Data not captured					-
C	E glass	Wet	97.3	15	50		52.2	32	114.7	15	59		60.88
D	E glass	Wet	112	57.8	118		131	40	146	57.8	154		164
A	Steel	Wet	Data not captured				-	Data not captured					-
B	Steel	Wet	118	30	100		104	37	147	30	125		128
C	Steel	Wet	110	3	115		115	40	144	3	150		150
D	Steel	Wet	Data not captured				-	Data not captured					-

Table 5-8 Maximum dynamic deflections experiment 3

As would be expected the test pans in experiment 3 moved further than in experiments 1 and 2, though in exactly the same manner, with the majority of movement appearing at the sides and delamination occurring on the inside at the centre of the V with the composite pans.

Table 5-8 shows clearly that the S2 glass composite deformed much less dynamically than either of the other materials. Again the values of displacement will include the displacement done by the delaminating layers of fabric. This is definitely the case with the E-glass test pans, for example in the video footage of test pan D when the top layers delaminate they move so much that the material folds over the tracking spots. Figure 5-26 shows the before and during shots from the video camera.

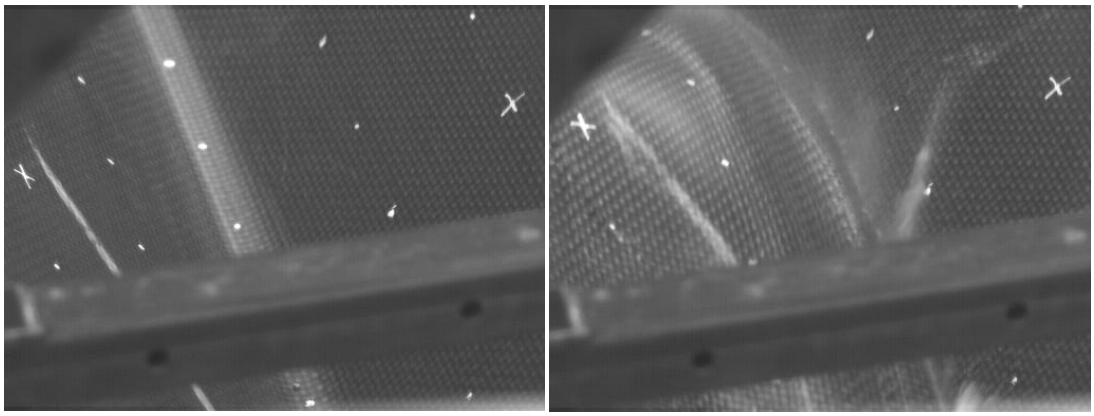

Figure 5-26 E-glass test pan D delamination effects during blast loading

As a result of the problems with the camera views more consideration is given to the permanent damage done to the test pans for this set of experiments.

Figure 5-27 E-glass hull D after testing in experiment 3

Although every effort was made to ensure that the charge was placed directly below the centre of the V, on one of the tests it emerged afterwards that it had been placed slightly

over to one side. Although this makes it difficult for comparison purposes the results were interesting. Hull D manufactured from the S2 glass was subjected to a slightly off-centre blast. As would be expected the dynamic deformation was greater on the one side, but the hull itself withstood the blast effectively, with no perforations and only slightly more delamination on the one side, as shown in Figure 5-28. Although not very clear in the picture there was a definite 'dent' in the side of the test pan as a result of the blast which led to a permanent deformation value in Table 5-9, which was not seen on any other samples.

PAN	MATERIAL	SAND	DEFLECTIONS [MM]	
			CENTRE	SIDE
A	Steel	Wet	11	45
B	Steel	Wet	12	52
C	Steel	Wet	10	37
D	Steel	Wet	8	32
A	S2 Glass	Wet	-	-
B	S2 Glass	Wet	-	-
C	S2 Glass	Wet	-	-
D	S2 Glass	Wet	-	14
A	E Glass	Wet	-	-
B	E Glass	Wet	-	-
C	E Glass	Wet	-	-
D	E Glass	Wet	-	-

Table 5-9 Permanent deflections from experiment 3

Figure 5-28 S2-glass test pan D experiment 3 - off centre blast

5.2.3 DISCUSSION OF EXPERIMENTAL RESULTS

This section will discuss the results obtained and form comparisons between the different materials and the different shapes.

COMPARISONS BETWEEN STEEL AND COMPOSITE

The aim of this part of the testing and of the project was to compare and contrast the differences of composites against steel under blast loading.

As previously mentioned the steel test pans all moved in the same way as the composites, but they moved further and deformed plastically.

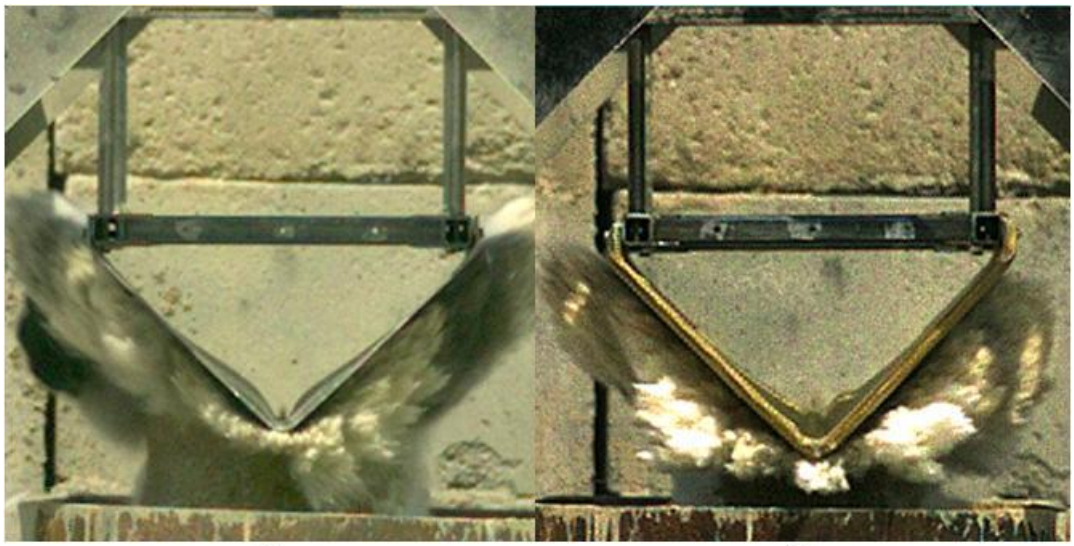

Figure 5-29 Comparison between steel (a) and composite (b) test pan C during experiment 1

Figure 5-29 above shows how the two materials deformed during testing. The figure clearly shows that the steel pan moves much further than the composite one, these stills are taken after roughly the same amount of elapsed time. The composite also returns to its original position after the blast has dissipated, whilst the steel remains deformed.

The following images are taken after experiment 3 and are of the centre of each test pan for each of the different materials. At first glance it is clear that the steel has fared much worse than either of the composites in terms of the resultant damage. However as previously mentioned the E-glass suffered a loss of structural integrity and the amount of delamination on each of the test samples eclipsed that seen by the S2-glass by far.

Looking solely at the S2-glass samples very little damage can be seen at the bottom of the test pan. In particular shape C suffered no visible delamination along the entire length. Shapes A and B suffered a small amount in the middle, whereas shape D had a large amount, in comparison, to one side. Though as previously mentioned this is most likely due to the fact that the blast was off centre, and as a result would not have been deflected as effectively. It is also perhaps important to mention that this delamination did not extend along the whole length of the test pan, just slightly more than halfway.

Figure 5-30 E glass, S2 glass and steel pan A after testing - experiment 3

Figure 5-31 E-glass S2-glass and steel pan B after testing - experiment 3

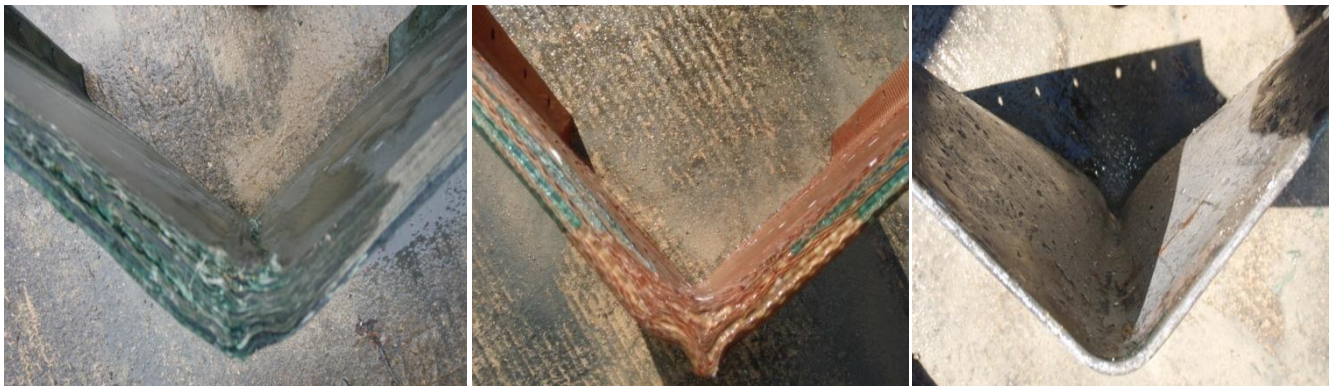

Figure 5-32 E-glass S2-glass and steel pan C after testing - experiment 3

Figure 5-33 E-glass S2-glass and steel pan D after testing - experiment 3

In all cases for the composite it was noticed that some damage was done to the outside of the test pan, the amount varied between the two materials. This damage consisted of a few frayed fibres no more than two layers deep, caused by the particles in the sand impacting the surface. Figure 5-34 shows this in more detail. If a composite solution were to be employed in the future for blast protection it would be recommended that a thin steel 'skin' be applied over the outside to protect the composite from rocks and other debris kicked up whilst driving.

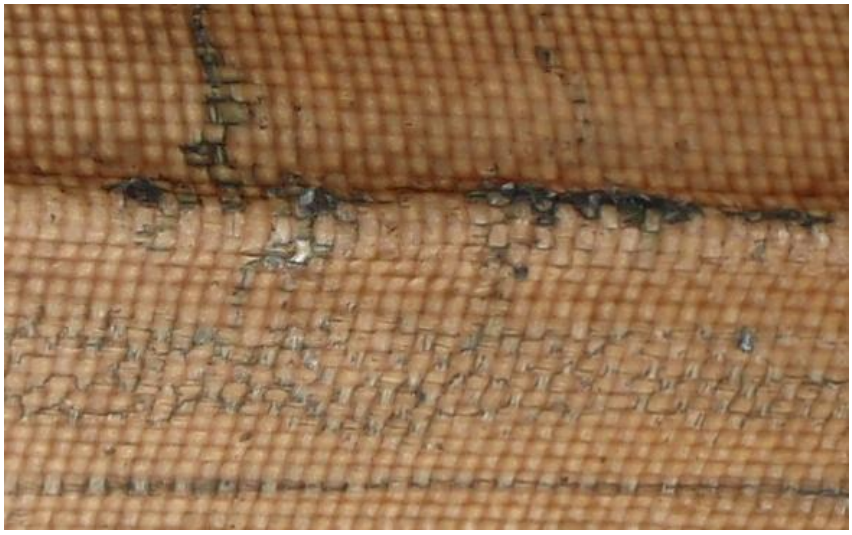

Figure 5-34 Fraying of odd fibres on outside of hull due to sand impact

Table 5-10 shows the relative displacements between the steel and the two composites for comparison purposes.

PAN	POSITION	STEEL	COMPOSITE EXPERIMENTS 1&2		COMPOSITE EXPERIMENT 3	
			S2	E	S2	E
A	Centre	1	0.71	-	-	-
	Side	1	0.37	-	-	-
B	Centre	1	0.43	-	0.48	-
	Side	1	0.28	-	0.47	-
C	Centre	1	0.57	-	0.3	0.78
	Side	1	0.51	-	0.29	0.48
D	Centre	1	0.97	0.91	-	-
	Side	1	0.40	0.69	-	-
C2	Centre	In relation to steel C after first firing	0.78	-	-	-
	Side		0.59	-	-	-
C3	Centre		-	-	-	-
	Side		1.57	-	-	-

Table 5-10 Relative hull displacement in relation to steel after experiments 1, 2 and 3

Table 5-10 clearly shows that the composite outperformed the steel in all tests. The one odd result comparing that the central displacements of pan D were looked at in more detail. The video footage of the S2 glass test pan showed a lot more delamination occurring along the inside central spine. This has been included in the displacement calculation as it was not possible to subtract this movement from the actual hull movement. An idea of the vertical movement can be gathered from the y component of the side movement, D, see Figure 5-22. On S2 glass test pan B, where there was very little delamination during the test, the y component of the side movement is much closer in value to the displacement occurring at the centre of the V, than the other tests where delamination did occur. By using the vertical component the comparative results are even better than those shown in Table 5-10. See Table 5-11 below.

PAN	POSITION	STEEL	COMPOSITE EXPERIMENTS 1&2		COMPOSITE EXPERIMENT 3	
			S2	E	S2	E
A	Centre	1	0.46	-	-	-
B	Centre	1	0.35	-	0.4	-
C	Centre	1	0.4	-	0.76	0.41
D	Centre	1	0.54	0.95	-	-

Table 5-11 Recalculated relative hull displacements

SHAPE VS. STAND-OFF

The aim of this part of the testing was to discover which has the greater impact, the shape or the ground clearance. Tremblay (Tremblay, 1998) conducted a study into the impulse seen by a blast deflector.

The graph in Figure 5-35 is taken from Tremblay and shows how the total impulse increases with the internal angle of an oblique blast deflector. The graph goes from 0°, or a vertical plate to 180° or a flat plate.

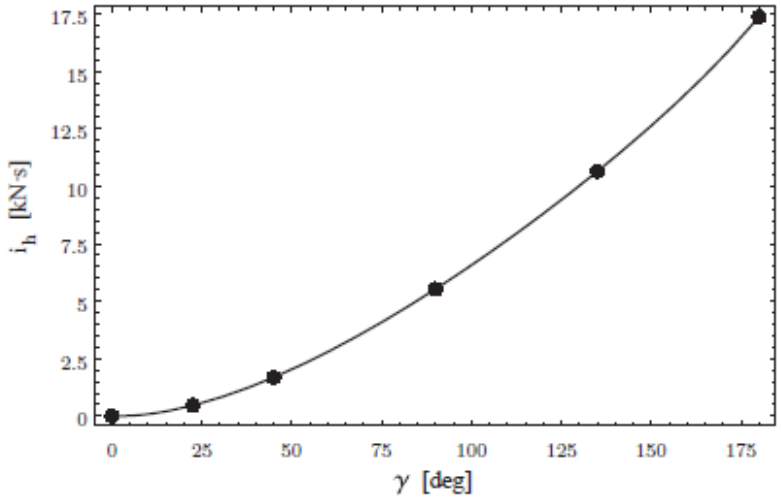

Figure 5-35 Graph of angle vs. impulse from (Tremblay, 1998)

However Tremblay also stated that the vertical impulse decreases rapidly with stand-off, as shown in Figure 5-36

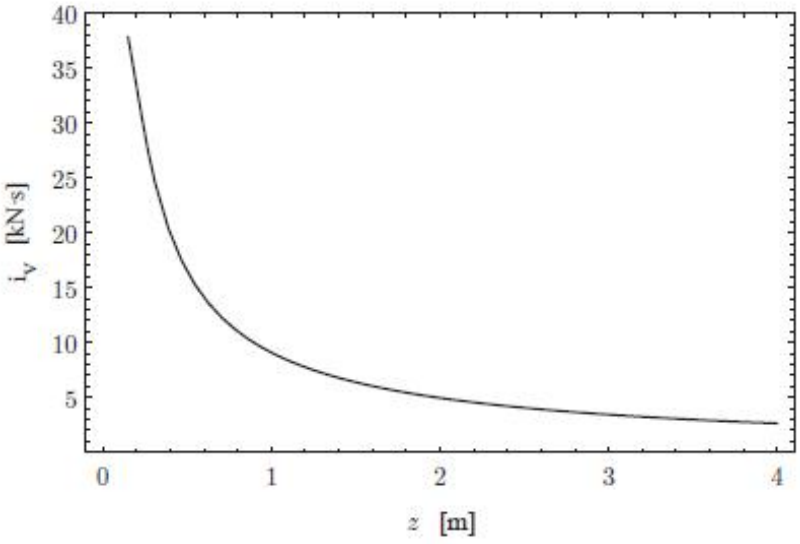

Figure 5-36 Impulse as a function of stand-off (Tremblay, 1998)

As it is not possible to have a stand-off distance of the magnitude displayed by the latter stages of this graph on an armoured vehicle, a compromise must be made.

In order to get a sharp V-shape under a vehicle, it is invariable that the ground clearance has to be reduced to compensate thereby running the risk that the impulse seen by the vehicle will increase.

EXPERIMENTS 1 &2					
MATERIAL	POSITION	A	B	C	D
STEEL	Centre	1	1.4	1.33	0.83
	Side	1	1.43	0.87	0.91
S2 GLASS	Centre	1	0.85	1.08	1.13
	Side	1	1.07	1.2	0.99

EXPERIMENT 3					
STEEL	Centre	-	1.02	1	-
	Side	-	0.83	1	-
S2 GLASS	Centre	-	1.66	1	-
	Side	0.87	1.39	1	-
E GLASS	Centre	-	-	1	1.27
	Side	-	-	1	2.7

Table 5-12 Hull movement comparison between shapes after experiments 1, 2 and 3

Table 5-12 shows the relationship between shape vs. stand-off, where A being the largest angle is furthest away from the blast. For experiments 1 & 2 the composite shows that shape A or B could be considered to give the best results in terms of displacements. However the results for A, B and D are very close. For the steel test pans the clear favourite is shape D indicating that the sharper the shape the better for deflection.

Unfortunately for experiment 3 not enough data was captured or was clearly visible from the footage to gain any clear results. However from comparing the hulls afterwards for the S2 glass the delamination appeared to reduce with the angle, with shape C having virtually no damage to inside or outside. Shapes A and B both underwent a small amount of delamination at the centre of the hull. Shape D unfortunately cannot be compared here as was subjected to an off-centre blast.

The amount of permanent deformation also decreased overall with the steel test pans. The E-glass however all suffered from large amounts of matrix cracking and delamination.

Analysing the results as a whole the levels of damage appear to reduce with the angle. This also correlates with work done in the US by Force Protection Ltd which was discussed with Vernon Joynt at a course taken at Cranfield University, Shrivenham.

5.3 SUMMARY

This chapter has described all the experimental work undertaken on behalf of this project work. Results have been analysed and discussed and where possible comparisons have been drawn between the different materials used. It was found that the S2 glass composite was by far the better material, when compared on a weight-for-weight basis. The E glass composite, though it did not move as much as the steel during the experiments, the extent of the delamination was significant enough to cause a loss of structural integrity, in that all the hulls could be easily flexed by hand after the experimental work had been carried out. Failure mechanisms such as delamination and matrix cracking were much more pronounced than in the S2 glass test pans. The steel test pans did not perforate but did deform significantly both dynamically and permanently when compared with the other materials.

"IN ALL SCIENCE ERROR PRECEDES TRUTH AND IT IS BETTER THAT IT SHOULD GO FIRST THAN LAST'

HUGH WALPOLE (1884-1941)

6 MODELLING RESULTS

This chapter will outline the work done in ANSYS AUTODYN in order to replicate previous studies of both experimental and numerical mine blasts and the experimental work done by the author on the range.

It should be noted that for all experimental work done on the range the explosive PE-4 was used whilst for the modelling work the explosive C-4 was used. There are few differences between C-4 and PE-4, C-4 being predominately American whilst PE-4 is British. There is a slight difference in the detonation velocity but the composition of the two explosives is similar, being RDX based to 90% of the mass (Global Security, 2006). The main reason behind this decision is however that C-4 is an option in the in-built library in AUTODYN and has therefore been validated whereas PE-4 is not.

The chapter is broken down into three sections, each with increasing complexity. The first section looks at the mine blast phenomenon in dry sand, using published experimental data for comparison, with the aim to validate the mine blast.

The second section uses the outcome of the mine blast section to look at the effect of a mine blast on a flat composite plate. This is compared with experimental work conducted by the author, with the aim of validating a material model for the composite.

The third section looks at the results from the V-shaped hulls experimental work and compares these results with the numerical models. The validated composite material model from the previous section is used and a steel model from the autodyn library is used for the hulls. Wet sand is also used as the medium in which the explosive is buried, the numerical model for the wet sand is taken from the literature (Grujicic et al., 2009) and is considered acceptable as published in a specialised journal, The Journal of Materials Engineering and Performance. A second sand model was also implemented for comparison purposes, by the same author as the first but a journal reference could not be found (Grujicic et al., 2009A computational of survivability of a pick-up truck).

After each section the results are critically discussed in detail.

6.1 VALIDATION OF MINE BLAST

This section can also be found in (Fiserova, 2006) but was deemed relevant to this work and presented by the author in 2010 (Follett et al., 2010). All simulations have been created by the author and the conclusions are the authors own.

The aim of this section is to validate the mine blast phenomenon within AUTODYN. A model was built that replicated the experimental work done by (Bergeron et al., 1998) and was compared not only with the experimental work but also with work done by (Wang, 2001) on recreating the experimental work in LS-DYNA.

A two-dimensional axial-symmetric model was set up in AUTODYN. The mine was represented by a 100g of TNT, which was described by the JWL EOS, as described in section 4.3.5.

Two deployments were investigated: (a) a buried charge with 30mm of sand coverage, and (b) a flush charge with the top surface level with the sand surface. Measuring gauges were placed at 300mm and 700mm above the ground surface to capture the change in pressure during the simulations. The configurations are shown in Figure 6-1.

A mesh sensitivity study was undertaken using mesh sizes of 4, 2, 1 and 0.5mm. The values of maximum overpressure and specific impulse converged at 1 and 0.5mm mesh sizes. Therefore a mesh size of 1mm was used, this offered both the accuracy and economy of time for the solution to run.

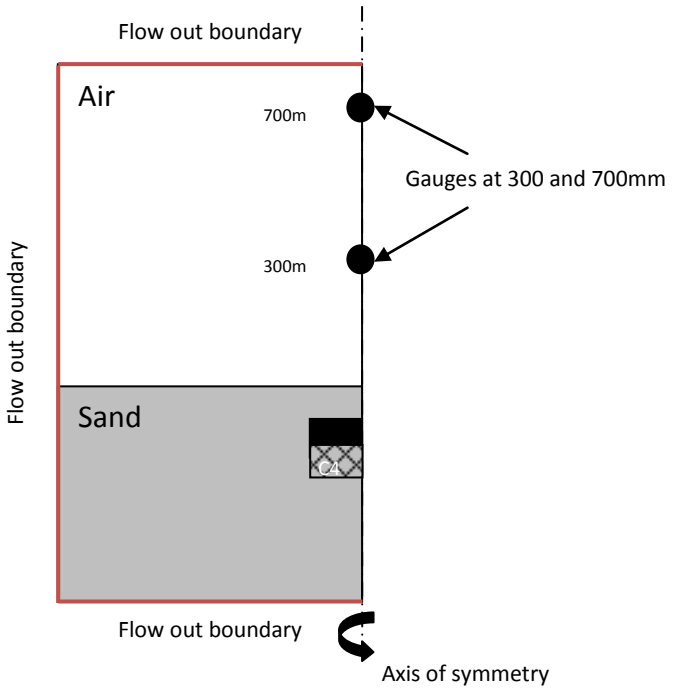

Figure 6-1 Experimental setup in AUTODYN

	PARAMETER	NOTES
2D axi-symmetric model		
Solver	Euler multi-material	
Units	mm, mg, ms	
Mesh dimension ((x1,x2) x (y1,y2)) [mm]	(-700,1000) x (0,500) (-700,0) x (0,500)	Overall mesh dimension Sand mesh dimensions
Cell size	1	
Boundary conditions	Flow out	Applied to three surrounding edges
Explosive Dimensions	C-4 JWL Ø 64 x 20	
Surrounding material	Air, ideal gas	
Soil	Sand	(Laine, L., Sandvik,A., 2001)
Deployment	(a) Flush: DOB = 0mm (b) Buried DOB = 30mm	
Measured parameter	Maximum pressure Specific impulse Time of arrival	

Table 6-1 Model parameters for mine explosion testing in 2D

6.1.1 RESULTS

The shock wave parameters: time of arrival, maximum overpressure and specific impulse from both the numerical methods and the experimental procedures are shown in Table 6-2. These are also shown in Figure 6-2. The error bars show the range of experimental data, so that it is possible to see where the numerical results fall within this range.

***TIME OF ARRIVAL*:** this is the time at which the shock wave front reaches the gauge points at a range of 300 and 700mm. The results show that at a range of 700mm the predictions are in good agreement with the experimental data for both forms of deployment. The values at a range of 300mm however show a 20% discrepancy, overestimated for the buried charge and underestimated for the flush charge. The LS-DYNA predictions are in good agreement for all four cases.

***MAXIMUM OVERPRESSURE*:** Figure 6-2 (b) shows the maximum overpressure at the two measuring locations for both types of mine deployments. There was a wide variance in the experimental data (as shown by the error bar). Except for the flush charge at a range of 300mm, the AUTODYN values fall within the range of measured data. The greatest discrepancy in the data occurred for the 300mm range over the flush charge - about 164% overestimation when compared to the experimental data presented by (Bergeron et al., 1998). This discrepancy is discussed further in the following section, 6.1.2. For the buried charge, however, at the same range there was only a 28% overestimation. The LS-DYNA results were about 50% lower for the flush mine at both stand-off distances and were about 15% and 4% underestimated for the 300m and 700mm distances respectively.

***SPECIFIC IMPULSE*:** This is the area under the pressure time curve for the positive phase duration. It can be approximated (depending on the shape of the curve) by the following equation:

$$i = {}^{1}/_{2}\, tp$$

Equation 6-1

Where *i* is the specific impulse, t is the positive phase duration and p is the maximum pressure.

The specific impulse is important when measuring blast effects as a very high pressure over a very short period of time may be less damaging than a lower pressure over a much longer period of time. This is because the load may have finished acting before significant

deformation has occurred, however if the load were applied over a longer period of time, the structure has time to respond to the full load. The specific impulse allows for comparisons to be drawn and a better idea as to whether a blast wave is survivable.

The specific impulse is shown in Figure 6-2 (c) for the two measuring points and scenarios. At 300mm range the AUTODYN buried charge underestimated the experimental value by 19% and LS-DYNA overestimated by 63%. At the same distance the flush charge gave a 14% higher value for the AUTODYN simulation and the LS-DYNA model was in very good agreement. At 700mm, both AUTODYN and LS-DYNA results do not fall within the measured data and are overestimated. AUTODYN overestimated by about 19% and 46% for the buried and flush mines respectively, LS-DYNA overestimated by 36% and 18% respectively.

TIME OF ARRIVAL [µS]						
POSITION ABOVE SOIL [MM]	BURIED, DOB = 30MM			FLUSH, DOB = 0MM		
	MEASURED	LS-DYNA	AUTODYN	MEASURED	LS-DYNA	AUTODYN
300	266	270	318	94.8	90	76
700	784	710	774	285.6	300	295

MAXIMUM OVERPRESSURE [KPA]						
POSITION ABOVE SOIL [MM]	BURIED, DOB = 30mm			FLUSH, DOB = 0mm		
	MEASURED	LS-DYNA	AUTODYN	MEASURED	LS-DYNA	AUTODYN
300	724.8	613.3	929.7	2797	1359	7380
700	304.5	290.1	334.1	1189	580.8	1409

SPECIFIC IMPULSE [KPA.MS]						
POSITION ABOVE SOIL [MM]	BURIED, DOB = 30mm			FLUSH, DOB = 0mm		
	MEASURED	LS-DYNA	AUTODYN	MEASURED	LS-DYNA	AUTODYN
300	106.8	174.5	86.1	85.8	86	98
700	57.2	77.9	68	116.4	137.5	169.6

Table 6-2 Shockwave parameters, measured results taken from (Bergeron et al., 1998) **and LS-DYNA results taken from** (Wang, 2001)

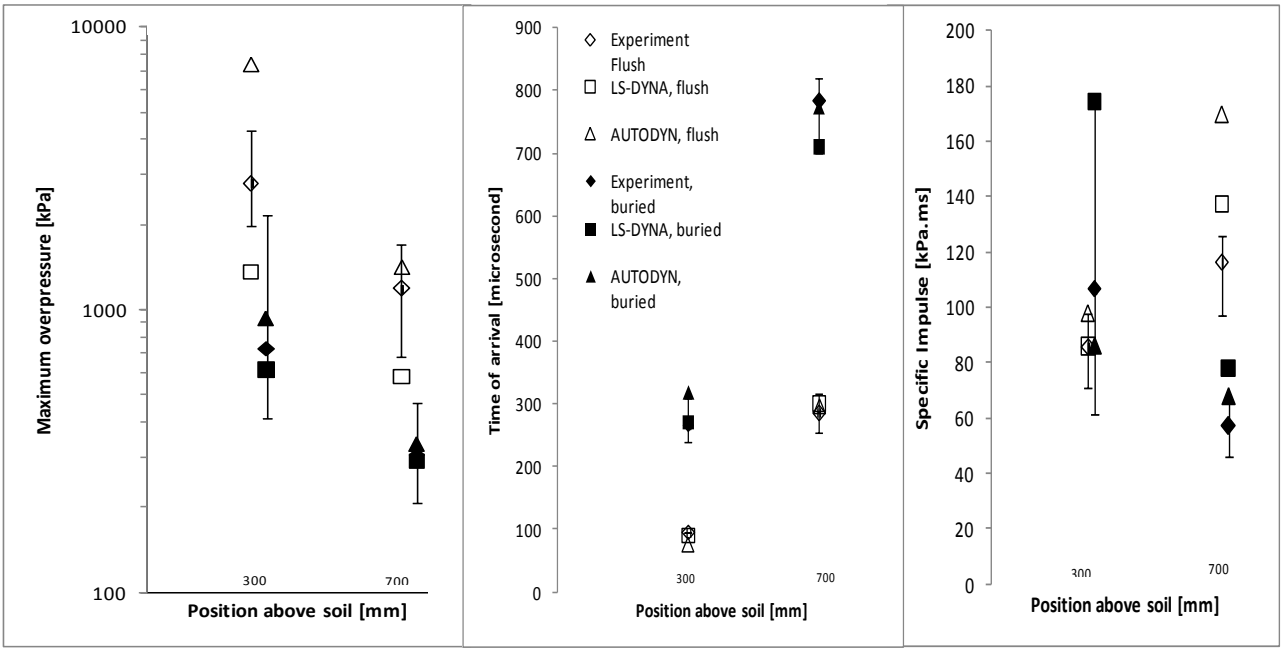

Figure 6-2 Shockwave parameters results

6.1.2 DISCUSSION OF RESULTS

The numerical results obtained by using AUTODYN, for the 700mm range are in better agreement with the experimental data than for the 300mm range. This is consistent with previous findings, by (Fiserova et al., 2003), that the convergence of numerical results with experiment occurs with increased range from the centre of the charge.

Since numerical solutions are used as a tool for improving the design of vehicles subjected to mine blasts, it is important to consider the results obtained with this in mind. When determining severe loading and the worst case scenario, conservative estimates are much preferred than non-conservative estimates.

Generally damage to a target can be caused by the following modes as discussed by (Held, 1990):

Overpressure can be responsible for damage if the vibration period of the target is short relative to the positive phase duration.

The AUTODYN results vary from 10 to 164% discrepancy from the measured data but in overestimation. Whilst the LS-DYNA results may have smaller discrepancies (between 5 and 51%) they are all underestimated. In this particular case an overestimation is better suited for design purposes than an underestimation. So the LS-DYNA results could be unsafe when looking at protective design.

It was noted that this figure of 164% was very high and as a result the simulation was looked at in more detail. It was found that the simulation became unstable the longer it ran for with exceptionally small time steps and a large energy error. It was also noted that when the explosive was buried in medium such as sand the simulation ran much more efficiently. The simulation was repeated with the explosive buried 5mm below the sand surface, as would be expected all values reduced but only marginally, the pressure value for the 300mm gauge however reduced considerably, almost by a factor of four, down to 1917kPa. It was also discovered that when a larger mesh size was used for the flush mine, there was much less instability, though more than in the 5mm buried mine, and that simulation produced a maximum over pressure at the 300mm gauge point of 1946kPa. When both of these values are compared to the published experimental data the percentage difference reduces from 164% to 31% for the 5mm buried mine and 30% for the flush mine at a larger mesh size,

both however are underestimates. This shows that the user should be aware of errors that can occur within the software and that not all results are necessarily accurate. Discretion is advised when analysing results from numerical software packages and where possible alternative simulations should be conducted to check the results.

Specific impulse can govern the damage if the vibration period of the target is long relative to the positive phase duration.

Both numerical models here overestimate, with the exception of the AUTODYN prediction of the buried charge at 300mm, which underestimates at around 19%. Both models here would provide good, though slightly conservative, models for protective design.

Although the peak pressure was greater for the flush mine than for the buried mine, the buried mine will usually have a greater impact on the structure above, in that the debris from the ground is propelled upwards at considerable speed. The blast will also cause a crater to form in the ground where it was placed or buried. The depth and size of this crater will very much depend upon the depth of burial of the mine. Instability in the ground can lead to further damage as a result of the structure collapsing or turning over. For further comparisons between the soil ejecta, crater size and the detonation products cloud can be found in (Fiserova, 2006) with reasonably good agreement between experimental data and all numerical data.

In reality it would be highly unusual to use a flush mine, they are almost always going to be buried or hidden somehow. Unfortunately as the data was compared with previous work conducted both experimentally and numerically it was essential to recreate what had been done previously.

6.2 FLAT PLATE TESTING

The following tests were conducted using an axial symmetric 2-D model. An equivalent surface area was calculated to relate the plate from the square plates used during testing into a round plate for the model. This was done in order to save simulation time and to allow a much smaller mesh size for accuracy. A 3-D model was also created for the 75g test for comparison purposes that produced very nearly identical results, just over a much longer period of time.

6.2.1 MODEL CREATION

The surface area of the plate during the experimental testing was 400 x 400mm^2 or 160000mm^2. In order to convert to a circular plate the area must remain the same, by using the formula for the area of a circle, $A=\pi r^2$ it is possible to calculate r, r = 225mm.

Table 6-3 gives the information required to create the model in AUTODYN, and Figure 6-3 shows the creation of the 75g composite plate model, and the model after it has run to completion of 5ms.

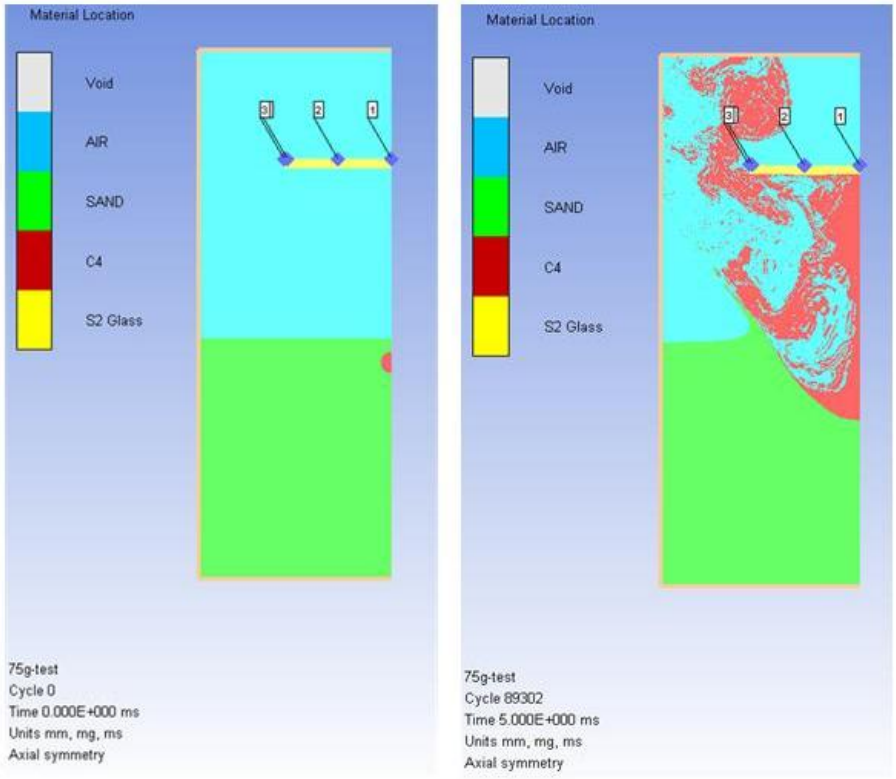

Figure 6-3 Model set-up in AUTODYN

	PARAMETER	NOTES
	2D axi-symmetric model	
Solver	Euler Multi-material Lagrange	Used for air, sand and explosive For plate
Units	mm, mg, ms	
Mesh dimension ((x_1,x_2) x (y_1,y_2)) [mm]	(-500,600) x (0,400) (-500,0) x (0,400)	Overall mesh dimension Sand(Laine, L., Sandvik,A., 2001)
Cell size	1	
Boundary Conditions	Flow out (Euler) Velocity, zero condition in x and y directions	Applied to the three outside edges of air. Applied to outside edge of the plate, as a constraint.
Explosive **Dimensions**	C-4, JWL 75g r = 22mm 130g r = 27mm 185g r = 30mm 240g r = 33mm 300g r = 35.5mm	With 50mm of sand above the top of the spherical charge. Location is at ((-50-r),0) (x,y).
Plate, Composite	S2 Glass (354,374) x (0,225)	Mesh size reduced to 0.5mm over the depth of the composite plate
Gauge Placement	3 gauges equally spaced along top surface of plate. With a 4^{th} located just inside the constrained edge	Positions are at 0, 125, 225 and 220mm from the symmetry axis. History plots to include x and y co-ordinates and pressure.

Table 6-3 Model parameters for flat plate testing in 2D

After the model has run to completion, it is possible to look at history plots from the gauges. In this case the x co-ordinate of the gauge has been used to calculate displacement, though a variety of other parameters could be set, depending upon what is required. Figure 6-4 shows the gauge history, taken from AUTODYN after the simulation had finished, for the 75g test of the movement in the x-direction.

In AUTODYN 2D the x-axis is the symmetry axis. It should be noted that the images in Figure 6-3 above have been rotated by 90° and the x-axis lies vertical.

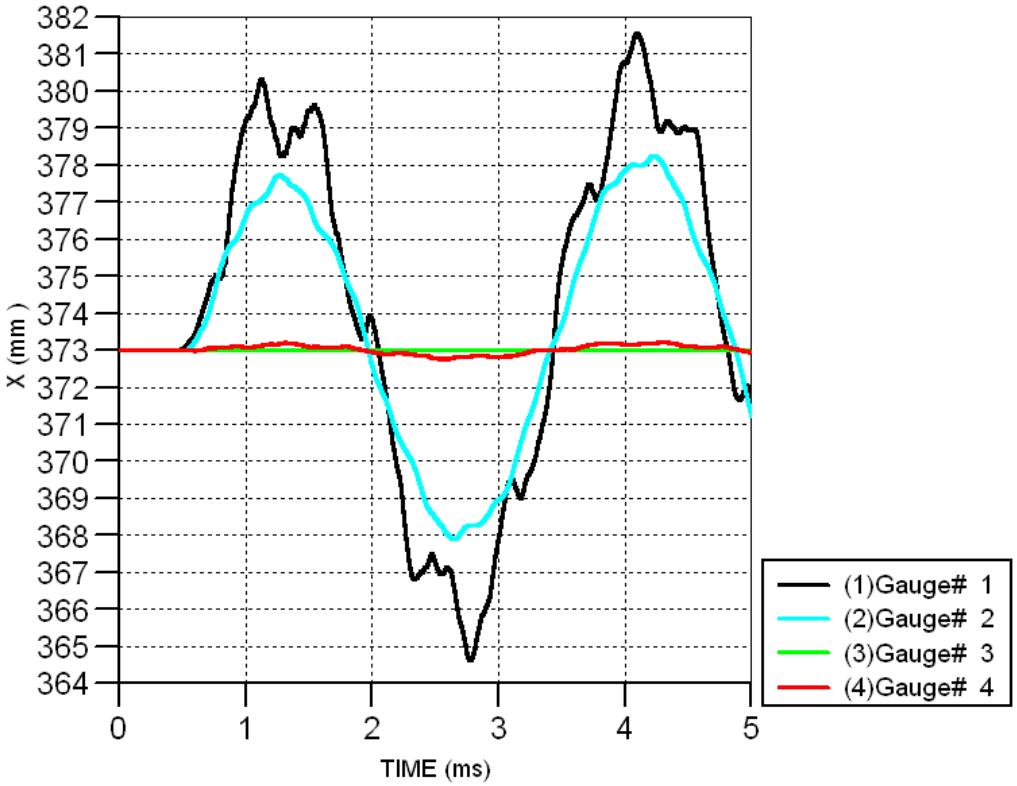

Figure 6-4 75g Gauge History x-position

The plate in this example oscillates as the blast passes around it. This was also witnessed on all the experimental video footage.

The above process was re-created for each charge weight and plate material. The following section gives the results from the numerical modelling and compares them with the experimental results in chapter 5. Unfortunately the 75g experimental video did not save during the testing and therefore cannot be compared to the numerical results.

6.2.2 RESULTS

75G TEST			
GAUGE NUMBER	NUMERICAL MAX DISPLACEMENT [MM]	ACTUAL MAX DISPLACEMENT [MM]	% DIFFERENCE
1	8.5	Results not captured	-
2	5	"	-
3	0	"	-
4	0.25	"	-

Table 6-4 75g Test Results

130G TEST			
GAUGE NUMBER	NUMERICAL MAX DISPLACEMENT [MM]	ACTUAL MAX DISPLACEMENT [MM]	% DIFFERENCE
1	16	15.8	1.27
2	11	11.34	-2.99
3	0	3.55	-
4	0.5	6.38	-92.16

Table 6-5 130g Test Results

185G TEST			
GAUGE NUMBER	NUMERICAL MAX DISPLACEMENT [MM]	ACTUAL MAX DISPLACEMENT [MM]	% DIFFERENCE
1	20	26.9	-25.65
2	14	16.05	-12.77
3	0	6.00	-
4	0.8	6.02	-86.71

Table 6-6 185g Test Results

240G TEST			
GAUGE NUMBER	NUMERICAL MAX DISPLACEMENT [MM]	ACTUAL MAX DISPLACEMENT [MM]	% DIFFERENCE
1	21.5	28.39	-24.27
2	16	22.90	-30.13
3	0	13.52	-
4	1	14.20	-92.96

Table 6-7 240g Test Results

300G TEST			
GAUGE NUMBER	NUMERICAL MAX DISPLACEMENT [MM]	ACTUAL MAX DISPLACEMENT [MM]	% DIFFERENCE
1	40	44.80	-10.71
2	28	35.48	-21.08
3	0	15.51	-
4	1	19.87	-94.97

Table 6-8 300g Test Results

6.2.3 DISCUSSION OF RESULTS

The percentage differences shown are the differences from the actual displacement to the numerical displacement, calculated by: $\frac{Numerical-Actual}{Actual} \times 100\%$

The large differences between gauges 3 and 4 are a result of the plate in AUTODYN being fully constrained and unable to move at all at gauge 3. Whereas during the experiment the two steel plates clamping the composite, did actually move a small amount, as shown in Figure 6-5.

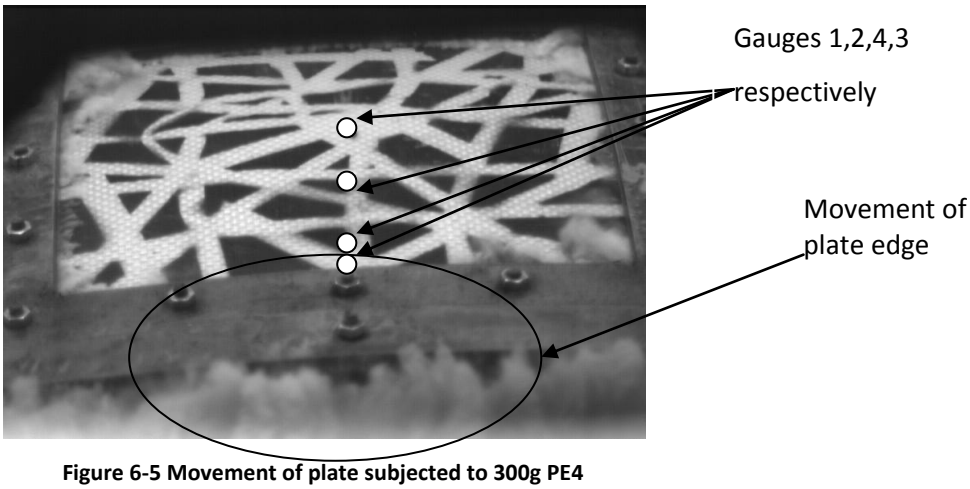

Figure 6-5 Movement of plate subjected to 300g PE4

However as it is not possible to recreate this movement within AUTODYN, and it would not be an accurate representation to subtract the outer movement from all the others, it is important to be aware and to take into account when analysing the results. The results are shown graphically for the maximum displacement in Graph 6-1. Another factor that could be contributing to the errors at gauges 2 and 4 is the way that the angle correction has been applied. For example in Figure 6-6, the maximum displacement calculation is correct as the tangent to the movement is horizontal, however when measuring the movement at the side by applying the angle correction the displacement that is measured is that depicted in Figure 6-6, whereas the numerical model is measuring the vertical movement.

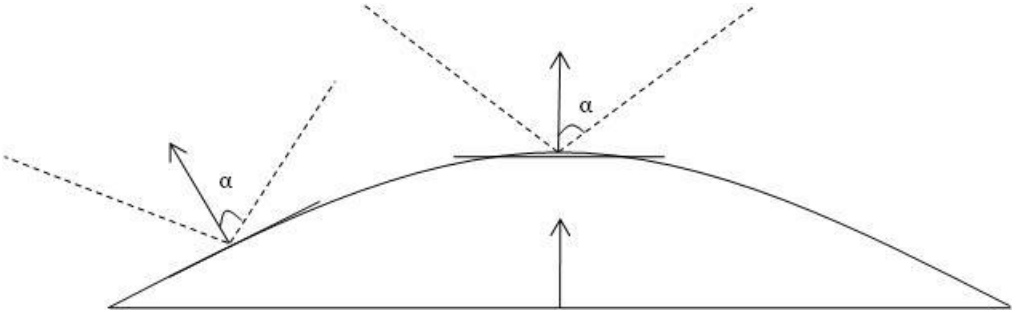

Figure 6-6 Angle correction errors

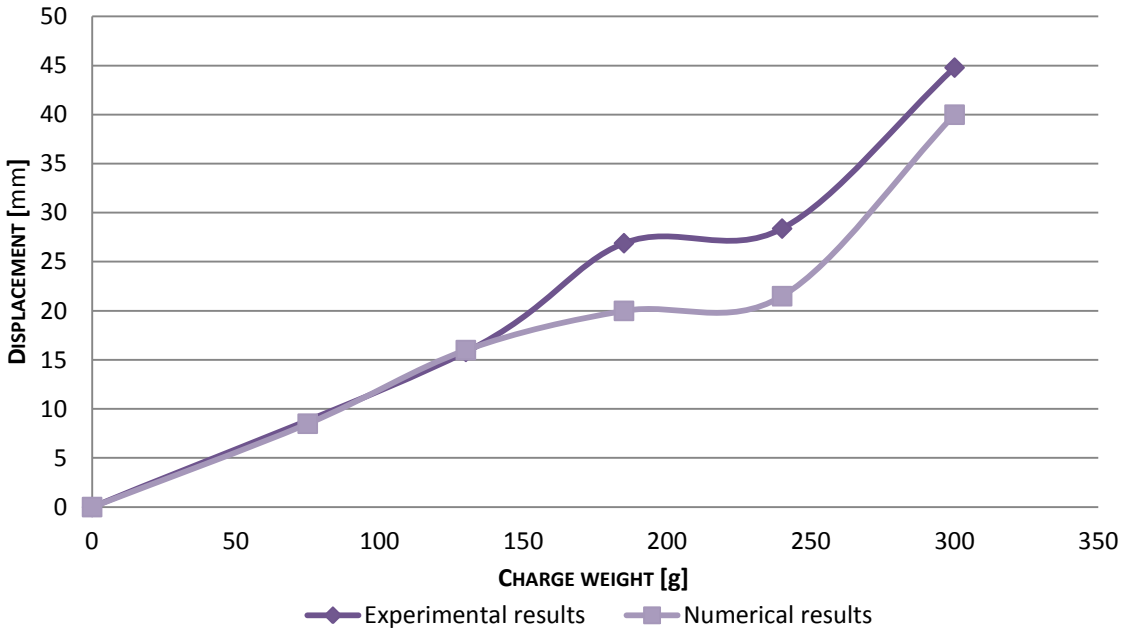

Graph 6-1 Charge weight vs. maximum displacement

Again these results include the displacement seen by the frame and are not as constrained as the numerical results. As would be expected the higher the charge size the more movement seen by the edge of the plate during the experiment and as a result affects the discrepancy between numerical and experimental results.

Looking at the maximum displacement the percentage differences range from 1-30%, however these are all underestimates, rather than as discussed in the previous section for a design approach an overestimate would be more useful. The only parameter that was measured for this case was the displacement, if future work were to take this stage further then other parameters like pressure, impulse, and strain rates could be measured, unfortunately due to cost restraints this was not possible for this study.

If it had been possible to capture more data from the experiments then the blast wavefront parameters could have been compared with those from the AUTODYN model. For the purposes of interest and for use if future work is carried out, the blast wave parameters have been considered here, but for the AUTODYN model only. Also the differences between a blast in a) air b) buried in dry sand and c) buried in wet sand have been compared and presented. The blast wave parameters include the wavefront velocity, the air density behind the wavefront and the maximum dynamic pressure and these are all calculated from the

maximum overpressure. They have all been calculated for the different charge sizes used and for the three mediums in which they are detonated. The model setup and the mesh parameters remain the same as for the flat plate simulations, minus the composite plate.

First using a TNT equivalency of 1.3 (Weckert and Anderson, 2006) it is possible to calculate the scaled distance, Z by; $Z = {}^{R}/_{W^{1}/_{3}}$ where R is the distance from the centre of the charge and W is the TNT equivalency weight of the charge.

Table 6-9 shows the scaled distances for all the charge sizes used in these experiments.

CHARGE WEIGHT [g]	R [m]	W [kg]	Z [m/kg^1/3]
0	-	-	-
75	0.43	0.10	0.93
130	0.43	0.17	0.78
185	0.43	0.24	0.70
240	0.44	0.31	0.64
300	0.44	0.39	0.60

Table 6-9 Scaled distances for different charge weights of PE4

AUTODYN simulations were run with the blast in air, dry sand and wet sand, and the pressures were obtained at the plate location. It is then possible to compare the pressure levels experienced by a structure when buried in these mediums. The results are shown in Table 6-10.

Z [m/kg$^{1/3}$]	AUTODYN P_s [BAR]		
	AIR	DRY SAND	WET SAND
0.93	11.73	1.5	3.15
0.78	17.67	2.78	5.14
0.70	21.42	4.41	7.40
0.64	25.33	5.98	9.32
0.60	28.66	7.01	9.99

Table 6-10 Values of peak static overpressure for Z from AUTODYN when in air, and buried in dry and wet sand

As can be seen and as expected the air blast gives much higher pressure readings than either the dry or wet sand. The wet sand also as expected gives greater pressure readings than the dry sand. For comparative purposes these results have been put into graph format in Graph 6-2. It should be noted that although an air blast will give higher pressure during the blast it will have reduced specific impulse. This is because when the blast interacts with the soil the progression of the blast is slowed down. By increasing the time the blast acts over the structure is given more time to deform. Whereas in air the blast dissipates very quickly and has less time to inflict damage to a structure.

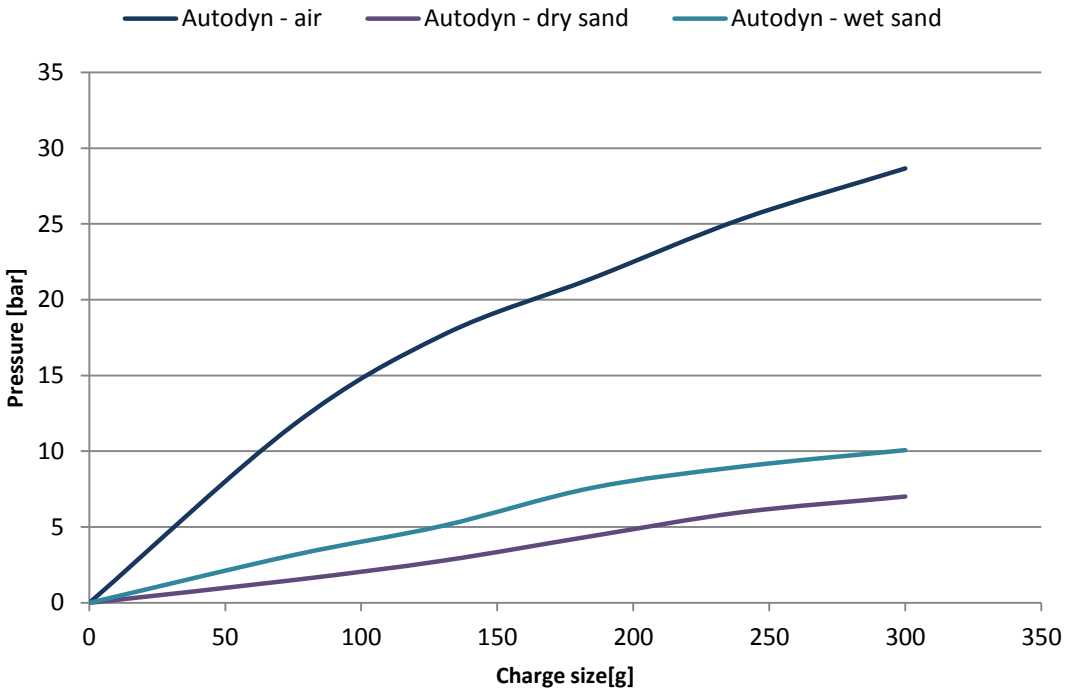

Graph 6-2 Pressure differences

Using these values it is then possible to calculate the blast wavefront velocity, U_s the air density behind the wavefront, ρ_s and the maximum dynamic pressure, q_s from the following equations taken from (Smith and Hetherington, 1994):

$$U_s = \sqrt{\frac{6p_s + 7p_0}{7p_0}} . a_0$$

Equation 6-2

$$\rho_s = \frac{6p_s + 7p_0}{p_s + 7p_0} . \rho_0$$

Equation 6-3

$$q_s = \frac{5p_s^2}{2(p_s + 7p_0)}$$

Equation 6-4

Where, p_s is the peak static overpressure, p_0 is the ambient air pressure ahead of the blast wave, ρ_0 is the density of the air at ambient pressure ahead of the blast wave and a_0 is the speed of sound at ambient pressure. These values are shown in Table 6-11.

Z [m/kg$^{1/3}$]	AIR BLAST			DRY SAND			WET SAND		
	U_s [ms^{-1}]	ρ_s [kgm^{-3}]	q_s [bar]	U_s[ms^{-1}]	ρ_s [kgm^{-3}]	q_s [bar]	U_s [ms^{-1}]	ρ_s [kgm^{-3}]	q_s [bar]
0.93	1130.4	87.4	18.4	514.0	12.3	0.7	654.0	24.4	2.4
0.78	1366.2	131.1	31.6	625.3	21.7	2.0	790.5	39.0	5.4
0.70	1496.0	158.7	40.4	743.3	33.6	4.3	921.3	55.6	9.5
0.64	1620.3	187.4	49.6	841.5	45.2	6.9	1019.4	69.7	13.3
0.60	1719.1	211.9	57.6	900.1	52.7	8.8	1051.4	74.7	14.7

Table 6-11 Wavefront parameters

Again as expected an air blast gives much greater values than for either wet or dry sand. This is due to there being nothing in the way that the blast wave must travel through and lose some of its energy. A charge buried in wet sand would do significantly more damage than a charge buried in dry sand by looking at these figures. This was also seen during some of the experimental work where hulls A and B were subjected to a blast in dry sand for comparative purposes, see Table 5-6 in chapter 5 Experimental Work.

Unfortunately as previously mentioned it is only possible to compare the air blast wave front parameters with the literature, see (Henrych, 1979; Brode, 1955), as there is no other information for this charge size buried under these conditions and the data was not captured during the experimental work.

However it is possible to calculate the speed of the shock wave from the video files if the shockwave is caught on camera. By using the following expression it is then possible to calculate the side on pressure (Smith and Hetherington, 1994):

$$P_s = \frac{\left(2\gamma\left({}^{v_s}/_{a}\right)^2 - (\gamma+1)\right)}{(\gamma+1)P_{atm}}$$

Equation 6-5

Where a is sound speed in air, v_s is shock wave speed, γ is adiabatic constant for air (1.4) and P is pressure (side on and atmospheric). This could then be compared with the values in the table above. Unfortunately it was not possible to capture the shockwave during the flat plate experiments due to the position of the camera.

6.3 MODELLING OF V-SHAPED HULLS

For these tests the model was created in the 3-D environment with symmetry in both the x and y axes, i.e. a ¼ model. Shell elements were used in order to reduce simulation time. The geometry was simplified slightly in that the curve at the bottom of the V was not modelled this was to allow shell elements to be used. Shell elements were used to so that the steel hulls, which are quite thin, could be modelled without interaction problems. Shell elements as mentioned in chapter 4 Modelling using ANSYS AUTODYN, section 4.3.1 allow the user to set artificial thicknesses so that a surrounding Euler mesh does not have to be very small that could then require more nodes than the licence allows for or take a considerable amount of time to run to completion. By using shell elements not only was individual layer data for the composite modelled but the previous issues did not arise.

The explosion in wet sand was created first as an axial symmetrical model in AUTODYN. This was then saved as a datafile and remapped onto the 3-D model. This reduced the simulation time significantly and enabled a spherical charge to be modelled using an Euler grid. Table 6-12 gives the model parameters used for the 2D explosion to be remapped later, whilst Table 6-13 gives the parameters for the 3D model. A 5mm mesh size is also applied to the shell. The dimensions are not listed in the table because they change depending upon the angle of the hull. The shell is first created as a part in the xy plane and then rotated to the corresponding angle and moved through the translate command into the correct position. The rotate and translate commands can be found in the parts menu → zoning → transformations.

	PARAMETER	NOTES
Solver	Euler 2D multi-material solver	
Units	mm, mg, ms	
Mesh dimension ((x_1,x_2) x (y_1,y_2))	(-300,250) x (0,340)	Overall mesh dimension
Cell size	1mm	
Boundary conditions	Flow out (Euler)	Applied to three outside edges
Explosive **Dimensions and centre of charge/detonation**	C-4, JWL 240g r=33mm (-83,0)	After creating part filled with air, can then fill by block for the sand and by geometrical shape for the explosive.
Sand **Dimensions**	(Grujicic et al., 2009) (-300,0) x (0,150)	
Simulation controls	Model allowed to run until sand and explosive products are close to where the bottom of hull would lie, approximately 0.4ms.	

Table 6-12 Model parameters for explosion

	PARAMETER	NOTES
Solver	Euler Multi-material Shell	Used for air, sand and explosive For hull
Units	mm, mg, ms	
Mesh dimension (x_1,x_2) x (y_1,y_2) x (z_1,z_2)	(0,300) x (0,300) x (-300,550)	Overall mesh dimension
Cell size	5mm	
Boundary Conditions	Flow out (Euler) Velocity, zero condition in x, y and z directions.	Applied to the three outside edges of air (not applied to bottom surface to allow for a rigid surface). Applied to top edge of the hull, as a constraint.
Hull, Composite	S2 Glass	Shell filled with composite →40 layers, 0.5mm thick, S2 Glass
Hull, Steel	Steel 4340	Steel shell thickness set to 5mm
Gauge Placement	Gauges equally spaced along the two symmetry planes of the V.	Arranged as a block along j and k lines each 10 cells apart. History plots include x and y displacement and pressure.
Simulation controls	Model ran until displacement levelled out or dropped significantly	

Table 6-13 3D model parameters

In order to remap the 2D simulation onto the 3D, there are a number of steps that must be followed:

1. Open 2D model that is to be remapped, in this case the blast in wet sand
2. Go to the cycle that is at the required position in time
3. Under parts → Fill → Additional fill options → datafile
4. Then write datafile giving it desired name
5. Open up model where remap is to take place
6. Ensure that all materials from the 2D explosion are present in material library

7. Create part filled with air as described in Table 6-13.
8. Under parts → Fill → Additional fill options → datafile
9. Check option to read datafile
10. Browse to location of datafile and open
11. Select the materials to be remapped
12. State where the origin from the 2D file is to be located, in this case also at origin
13. Finally select which axis is to be the symmetry axis, in this case the z-axis
14. Ok message about changing from 2D to 3D

This will import the data from the explosion simulation onto the structural simulation. The following figures show how it appears in AUTODYN. Figure 6-7 shows the 2D explosion in the wet sand, and Figure 6-8 shows the 3D model before and after the remap has taken place as well as part way through a simulation.

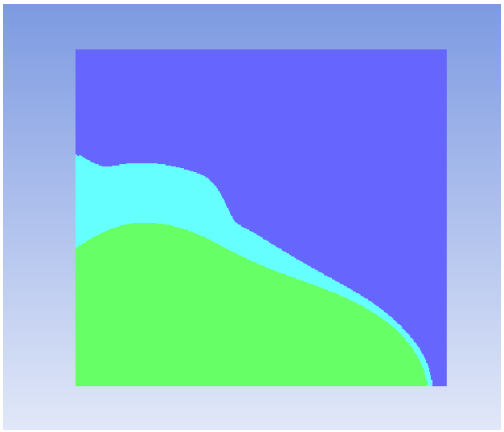

Figure 6-7 2D explosion

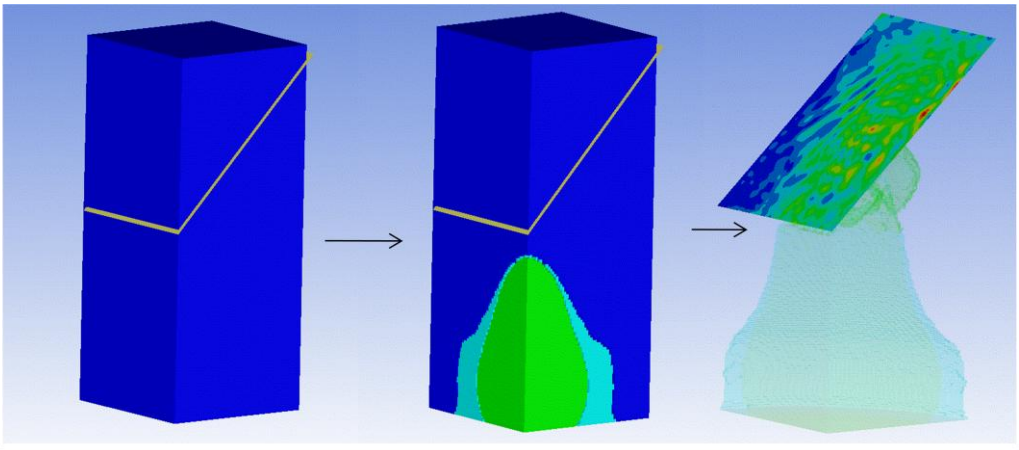

Figure 6-8 Remapping into 3D

6.3.1 RESULTS

Table 6-14 to 6-17 show the numerical results after the first set of simulations had been conducted. Section 6.3.2 Discussion of results discusses these further and makes changes to the model set-up in order to improve accuracy.

HULL	MAX CENTRE DISPLACEMENT [MM]		MAX SIDE DISPLACEMENT [MM]	
	NUMERICAL	ACTUAL	NUMERICAL	ACTUAL
A	3.92	53.15	18.41	67.12
B	2.39	74.40	14.54	95.75
C	3.52	70.75	20.04	58.45
D	3.11	43.95	17.29	61.35

Table 6-14 Steel hulls maximum displacement results at high stand-off

HULL	MAX CENTRE DISPLACEMENT [MM]		MAX SIDE DISPLACEMENT [MM]	
	NUMERICAL	ACTUAL	NUMERICAL	ACTUAL
A	0.21	37.57	1.7	24.68
B	0.2	32.10	1.45	26.48
C	0.145	40.41	1.8	29.58
D	0.171	42.46	1.9	24.45

Table 6-15 Composite hulls maximum displacement results at high stand-off

HULL	MAX CENTRE DISPLACEMENT [MM]		MAX SIDE DISPLACEMENT [MM]	
	NUMERICAL	ACTUAL	NUMERICAL	ACTUAL
A	3.78	Not captured	22.5	Not captured
B	3.87	147	21.8	128
C	2.97	144	20.22	150
D[1]	7.66	Not captured	30.93	Not captured

Table 6-16 Steel hulls maximum displacement at low stand-off

HULL	MAX CENTRE DISPLACEMENT [MM]		MAX SIDE DISPLACEMENT [MM]	
	NUMERICAL	ACTUAL	NUMERICAL	ACTUAL
A	0.69	Not seen	3.35	37.85
B	0.98	71.2	3.25	60.7
C	1.02	43	3.51	43.48
D	1.16	Not seen	3.75	134 (left side) 29 (right side)

Table 6-17 Composite hulls maximum displacement at low stand-off

[1] Odd result: Simulation parameters compared to previous simulations and no identifiable reason was discerned as to why this was the case. However still very large discrepancy between the experimental results.

6.3.2 *DISCUSSION OF RESULTS*

From looking at the simulations of the V-shaped hulls, the way the hull moves corresponds to what was seen during the experimental work, with the sides moving upwards and inwards towards each other as shown by Figure 6-9. The position of the maximum displacement also corresponded to what was seen experimentally. The maximum displacement seen at the sides of the hulls was just below the halfway point, also depicted in Figure 6-9.

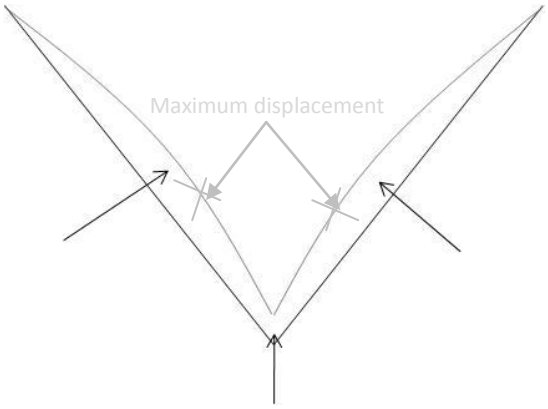

Figure 6-9 Hull movement during blast

It was also obvious that the composite out performs the steel significantly, which was again shown experimentally. However an issue arose when the values of the displacements were compared.

After the first set of simulations had been completed it was noticed that according to the numerical model there was negligible deformation to both the steel and composite hulls. The discrepancy between the composite hull data could also be explained, in some part, to the delamination caught by the cameras, which will contribute to the measured deflection presented in the tables of results, see Table 5-6 and Table 5-8.

As a result the steel model used was the first area of consideration for what could be wrong. The steel used in the experiments was a mild structural steel to BS EN 10025:1993, Grade S275. The steel used in AUTODYN was also a structural steel (steel 4340) but there were some differences in the properties. In order to check that this was not causing a significant error in the calculations a simple flat plate over an air blast was set up in AUTODYN 2D with gauges placed at intervals to measure the deflections. The test was repeated with every steel model available in the AUTODYN library. Table 6-18 shows the yield strengths and shear moduli of these different steels.

After the simulations had run for a short amount of time, the gauge plots were compared and can be seen in Graph 6-3. It is clear from this that any differences between the steels are negligible according to AUTODYN when under this kind of loading, and are certainly not enough to explain the differences seen between the model and the experiment.

MATERIAL	YIELD STRENGTH [GPA]	SHEAR MODULUS [GPA]
Steel v250	1.56	71.8
Steel s-7	1.537	81.8
Steel 4340	0.792	81.8
Steel 1006	0.35	81.8

Table 6-18 Yield strengths and shear moduli of steels in AUTODYN

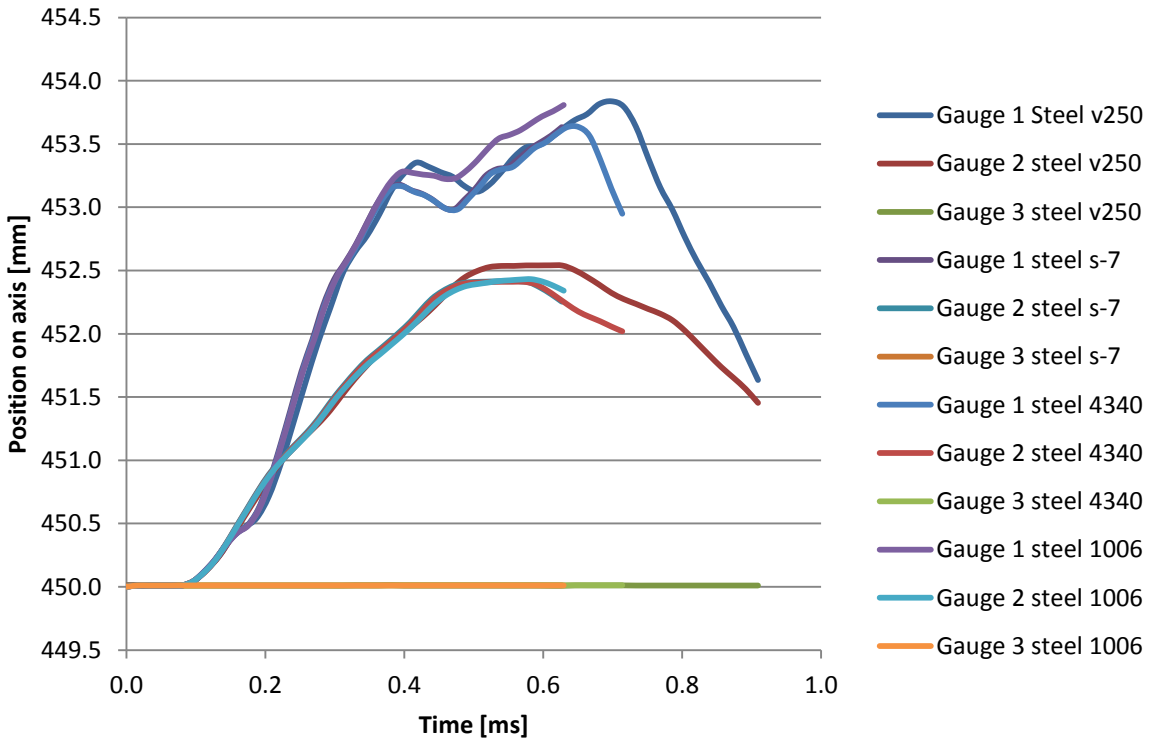

Graph 6-3 Steel models comparison

Aware that the mine blast model in dry sand and the material model had been verified during previous work, it was considered that there may be a problem with the wet sand model and so this was the next area for consideration.

Going back to the paper where the model was taken from (Grujicic et al., 2009) it was noticed that there was an inconsistency with the units used. In a graph the units of pressure were displayed in GPa whilst in the table they were labelled in MPa when they were in

actual fact in GPa. As a result the 2D simulation with altered values for the pressure was re-run and then again re-mapped onto all the 3D hull models for them to run again. Graph 6-2 in the previous section shows the pressure differences using the updated wet sand model, as do the results presented in Table 6-14 and Table 6-15.

The models were re-run and the gauge measurements again compared with the experimental data.

After the models were re-created it was again found that the displacement in the steel hull was significantly less than the experimental data, but was increased from the results mentioned above.

A second sand model was found, created by the same author see (Grujicic et al., 2009A computational survivability of a pick-up truck subject to mine detonation loads) the model details can be found in Appendix 5, though very little difference was found in the numerical results when run on some of the composite hulls.

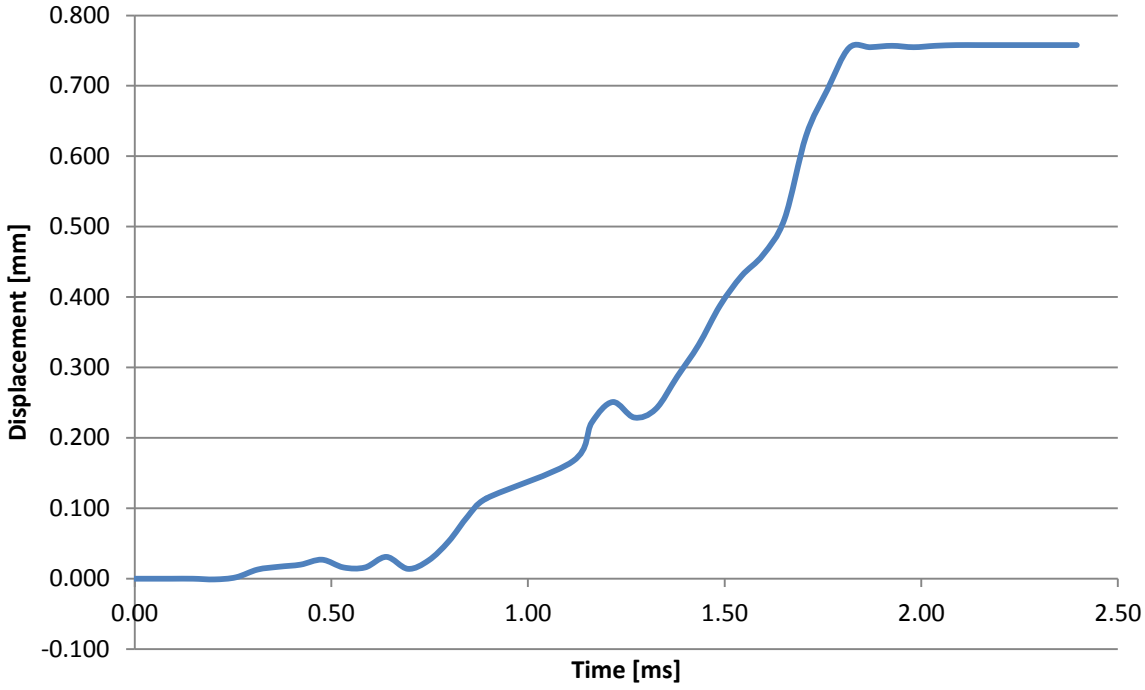

Graph 6-4 Maximum centre displacement steel hull A with updated sand model – higher stand-off

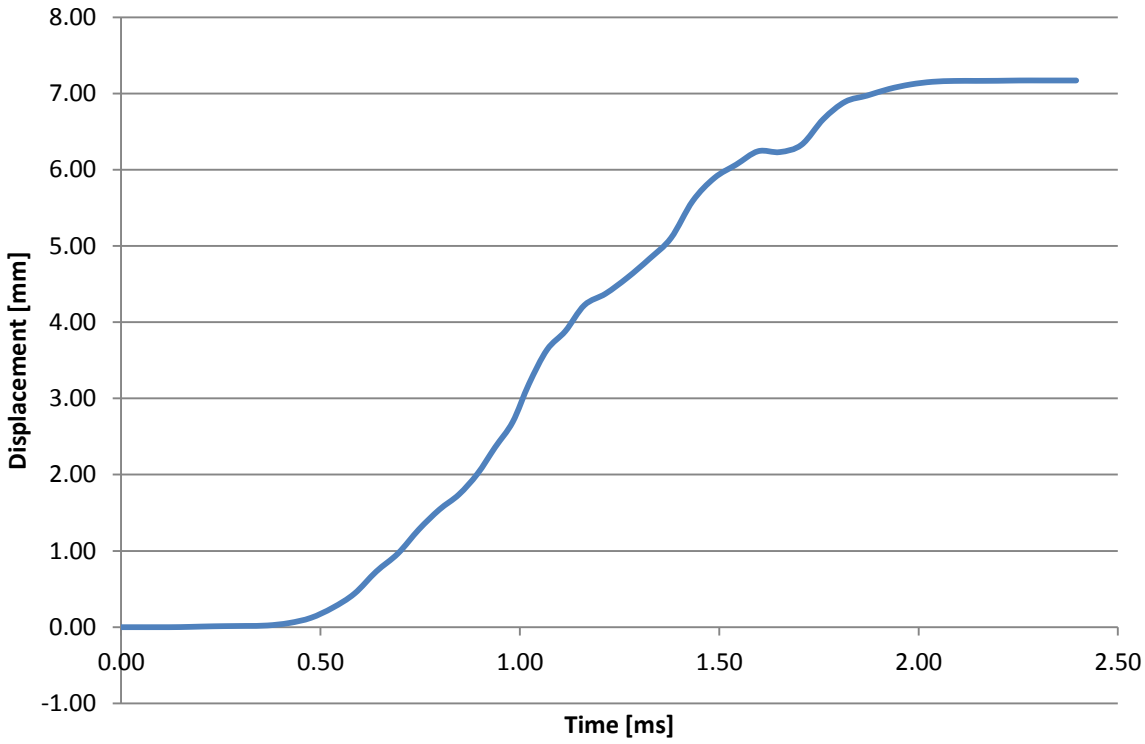

Graph 6-5 Maximum side displacement steel hull A with updated sand model – higher stand-off

In order to try and discover what could be wrong with the model the simulations were again re-run but this time using a blast in air. Although this should create less deformation than what would be seen from a buried charge, if the air blast shows more damage than the buried blast then there is something else wrong with the sand model that has not been identified, or there could be a problem with the way the sand model interacts with the hull part during the simulation.

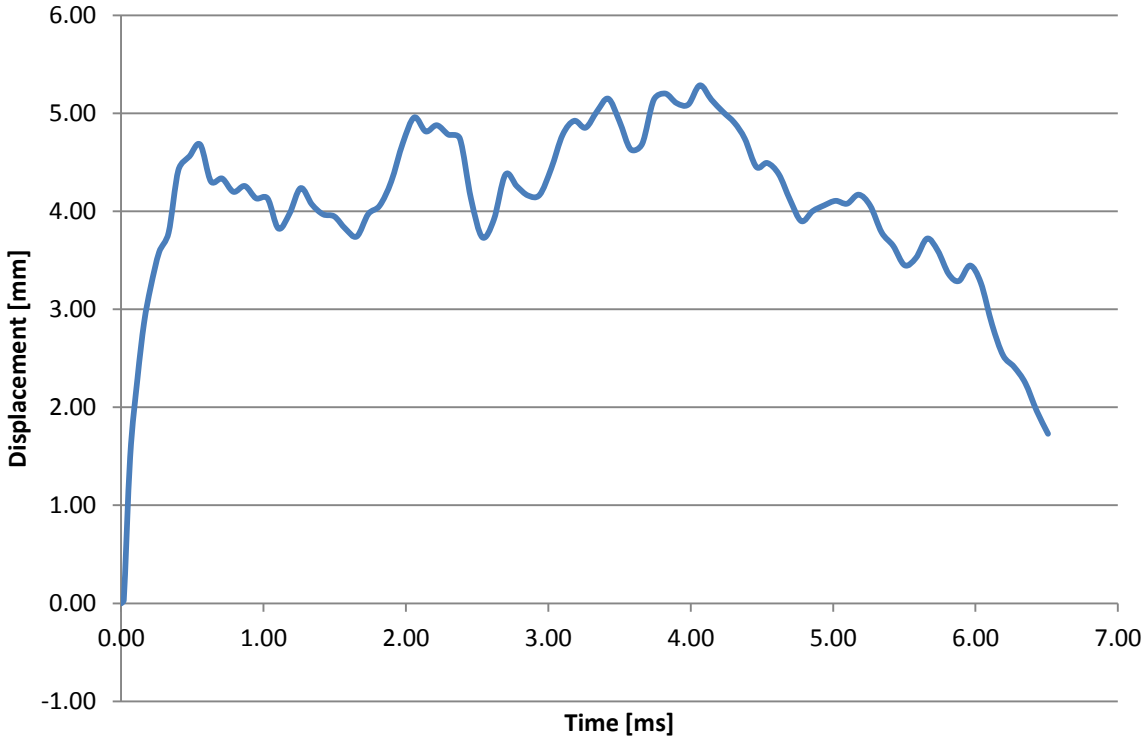

Graph 6-6 Centre displacement steel hull A air blast – higher stand-off

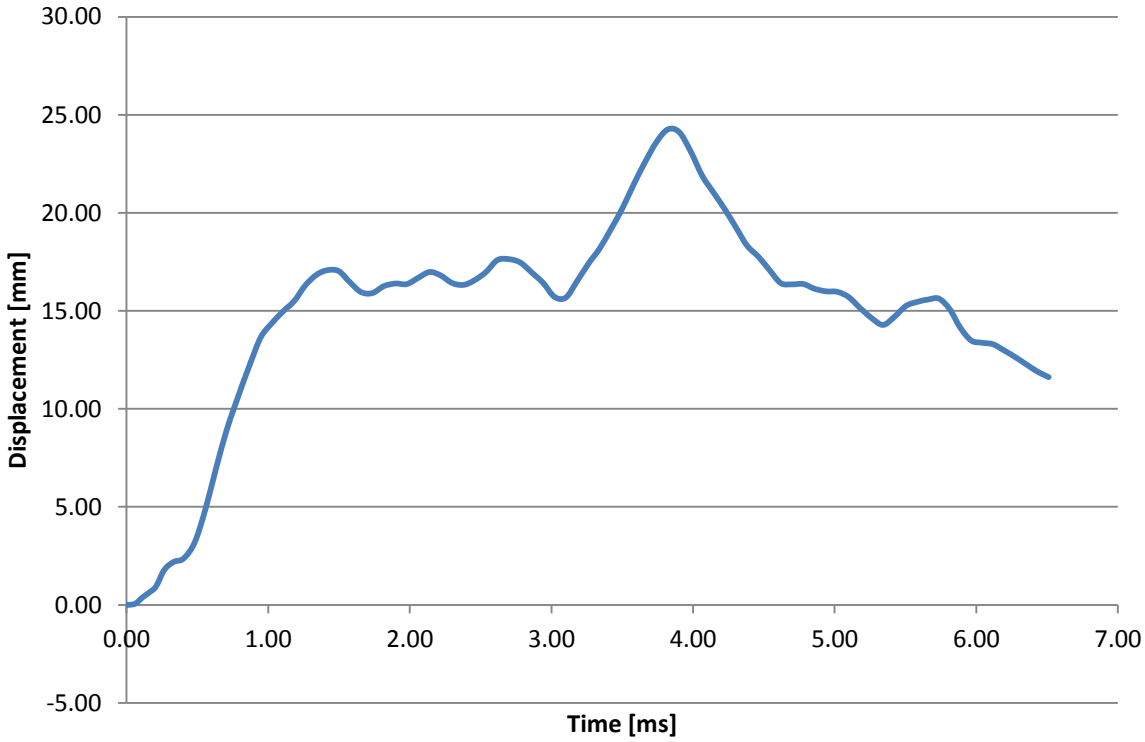

Graph 6-7 Side displacement steel hull A air blast – higher stand-off

The air blast clearly shows that the deformation is much greater and correlates considerably better with the experimental results however as should be expected there is still a large

discrepancy, especially when looking at the displacement occurring right at the centre of the V hull (a factor of 5), see Graph 6-8 and Graph 6-9. This could be down to a number of issues, mainly that of the reduced specific impulse from an air blast rather than a buried blast, but others as well such as; the simplified geometry in autodyn means that there is a much sharper V at the centre than on the actual hulls. This would split and deflect the blast much more effectively than a softer more rounded shape, as what was used for the experimental work. Realistically however it is impossible to manufacture such a sharp shape.

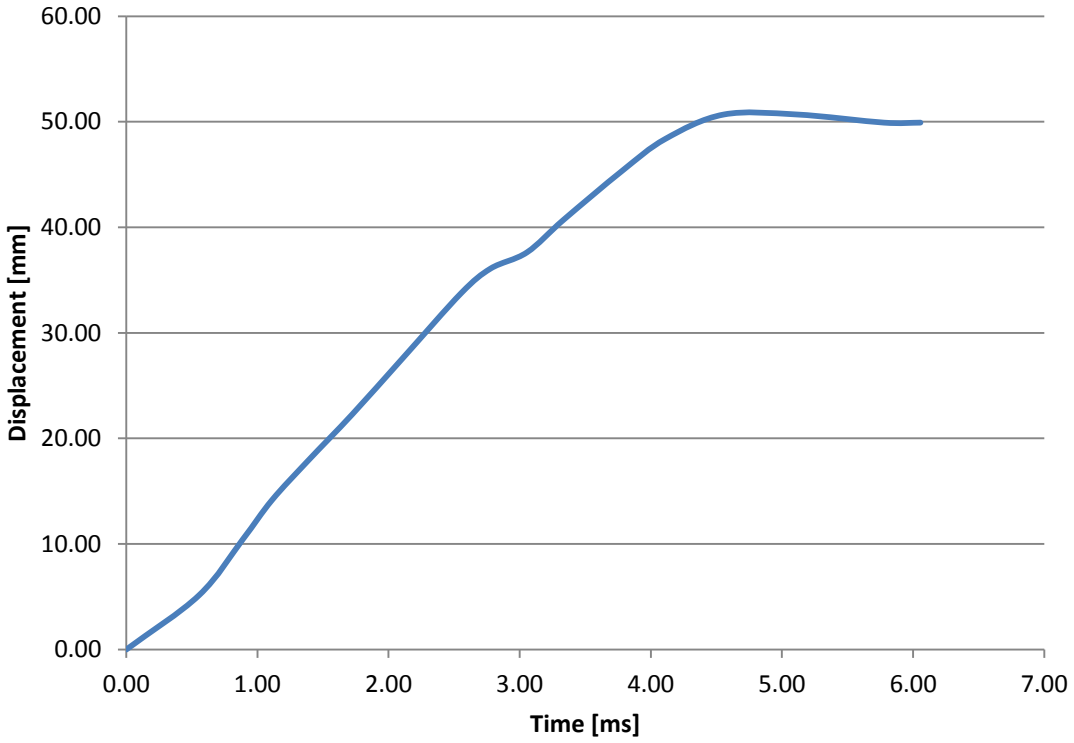

Graph 6-8 Experimental central displacement steel hull A – higher stand-off

It should be noted that the time axis is not indicative of the actual time elapsed. The camera is triggered manually during the experiments and due to variances by the user can be triggered at different times, and can capture a lot of still footage at the beginning of the experiment. For the numerical results graphs the time axis shows how far along the simulation has progressed, due to the remapping of the explosion up to a point the time is again not indicative of the actual time elapsed during the experiment. The time axes are shown for the purposes of seeing how far along the simulation proceeded before termination.

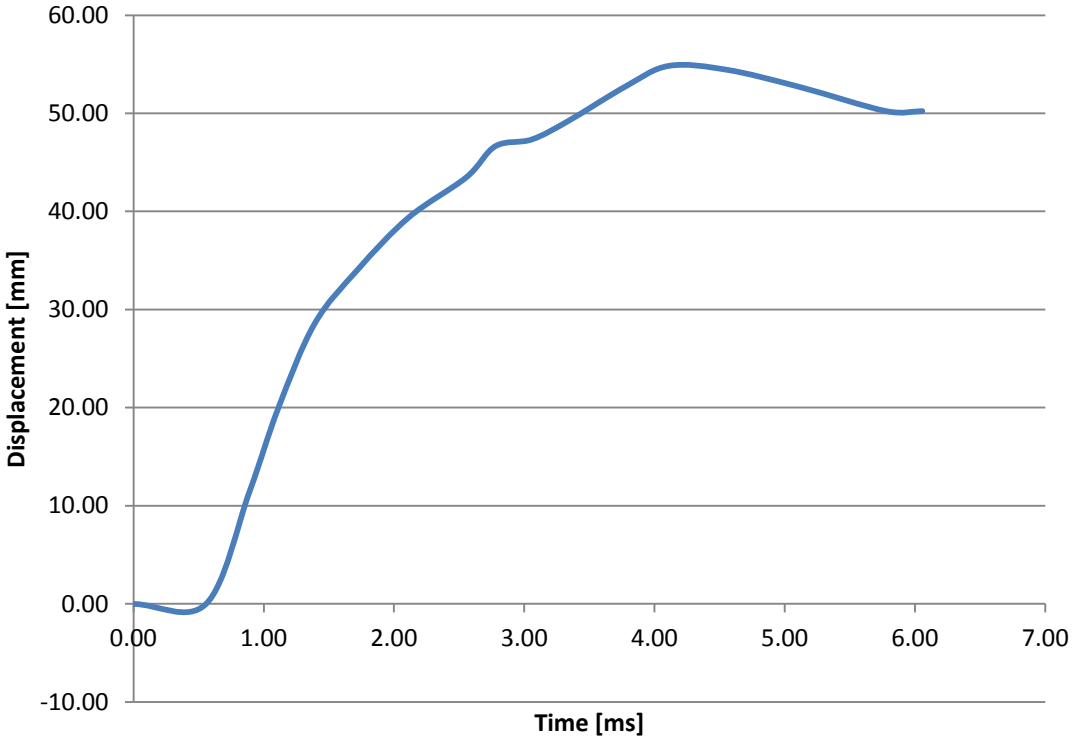

Graph 6-9 Experimental side displacement steel hull A – higher stand-off

A model was created for steel hull A only that was an exact model of the test pan in order to discover how much of an effect the shape has on the model. In order to be able to model the test pan, a mesh that is smaller than the thickness of the part is required for the air. Unfortunately having a very fine mesh throughout the air is not possible due to computer and licence limits, therefore the mesh was made coarse at the bottom and top of the air but refined over the middle in order to allow for the interaction between the solid part and the Euler mesh. It was built in the Design Modeller feature of Ansys Workbench and then after being transferred into meshing, was imported into AUTODYN, where the air and the explosion were added, Figure 6-10 shows the model ready to run in AUTODYN. Again the wet sand model was discarded for this purpose and only the air blast was considered.

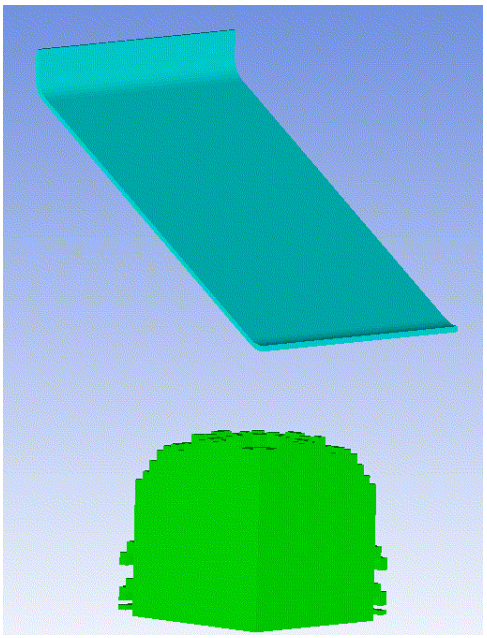

Figure 6-10 Steel Hull A exact model with air blast – higher stand-off

A few attempts had to be made with perfecting the mesh size and distribution. If the Euler mesh size is too large then the blast fails to interact properly with the solid Lagrange part, see Figure 6-11. There has to be at least two Euler cells covering the thickness of the Lagrange mesh.

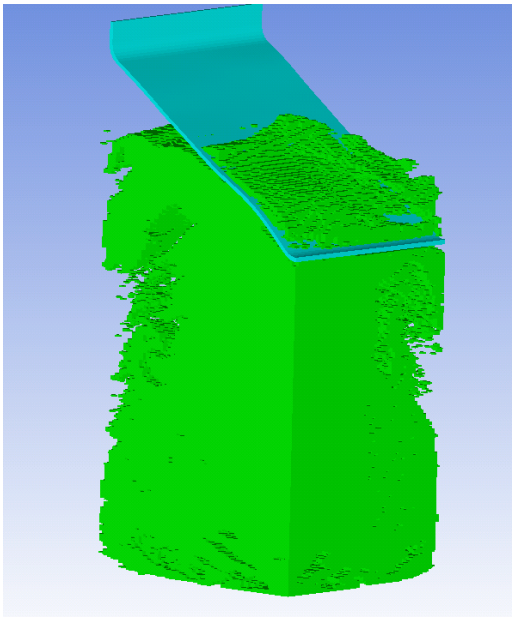

Figure 6-11 Interaction considerations in AUTODYN

Unfortunately due to the size of the model and the constraints of the computer it was impossible, in this instance, to fully eradicate all problems with the interaction. However there was enough to give a supposedly definitive result on the shape of the hull having a significant effect. Figure 6-12 shows the hull model in AUTODYN after the blast has occurred.

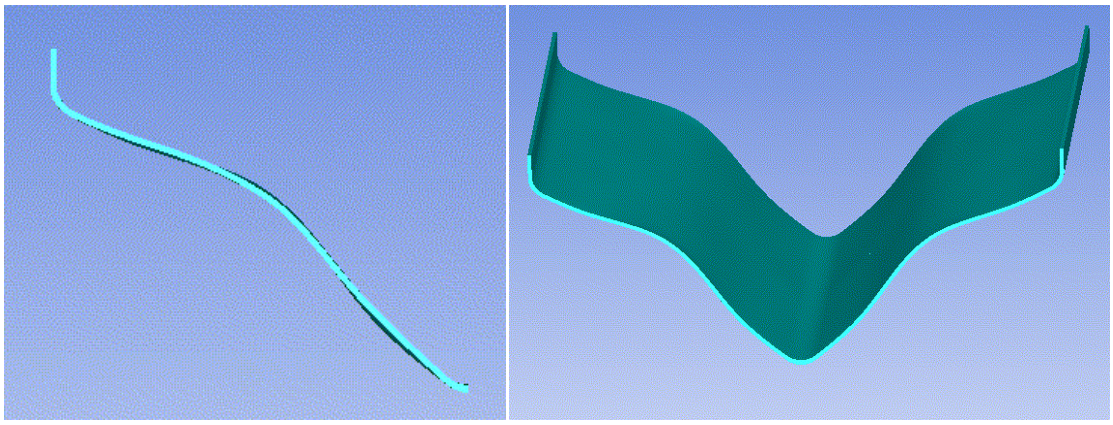

Figure 6-12 Actual shape steel hull A under air blast loading

Graph 6-6 and Graph 6-7 shows the centre and side displacement respectively of a shell model of steel hull A under an air blast. In comparison Graph 6-10 below shows the side displacement when the actual shape was used.

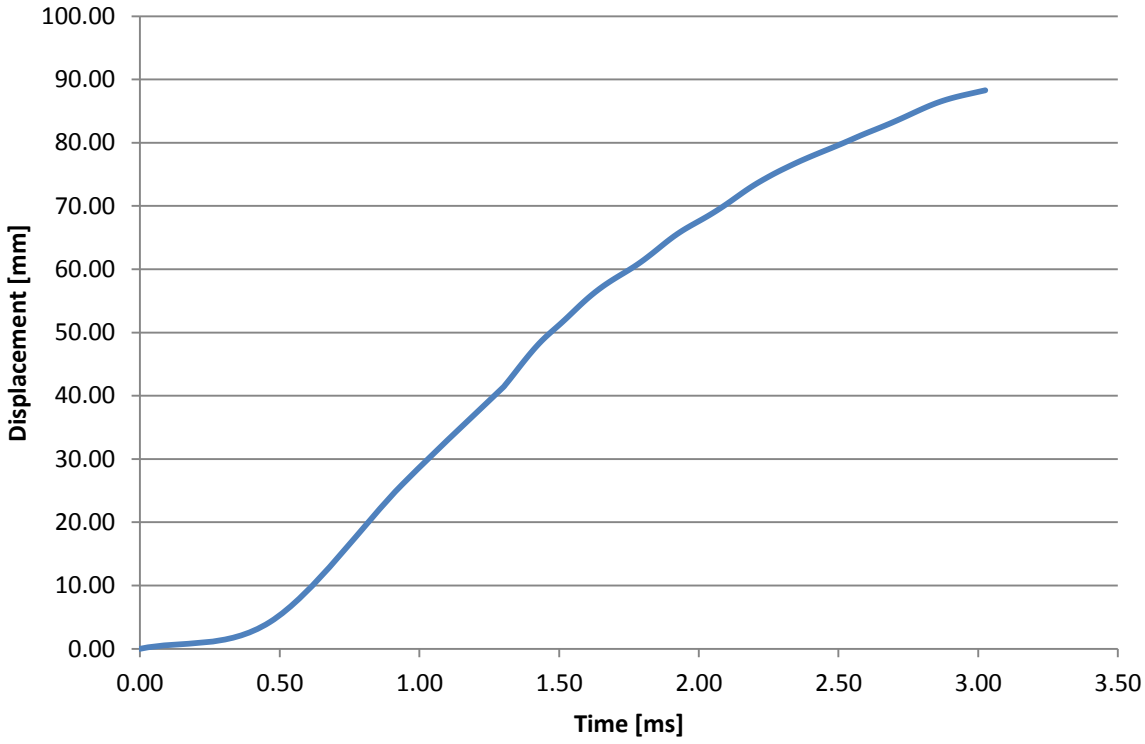

Graph 6-10 Side displacement of actual shape steel hull A under air blast

There were some difficulties with running this model due to the size of the files. This is why it has only run for 3ms whereas in Graph 6-7 it ran for more than twice that time, but it can be seen that the graph appears to start levelling off after 3ms.

These results show that the shape has had a significant effect on the displacement seen in the numerical model. After 3ms the steel shell model had a maximum side displacement of about 16mm and a total maximum displacement of 24mm whereas the actual shape model

gave a maximum side displacement of just under 90mm, after only 3ms. This is considerably greater than that shown by the wet sand model in Graph 6-4 and Graph 6-5 and is much more indicative of the experimental results. In fact it gives a greater value for the displacement occurring at the side than what was seen experimentally, which as previously stated is good for design purposes.

Unfortunately due to the element co-ordinate system it is not possible to model the composite in this way. Figure 6-13 shows the material directions for the x, y and z axes respectively. Although the x axis lies in the correct plane the y and z axes do not. Unless the shape is built within AUTODYN rather than in the design modeller the element co-ordinate system matches the global co-ordinate system and will not follow the shape of the solid model.

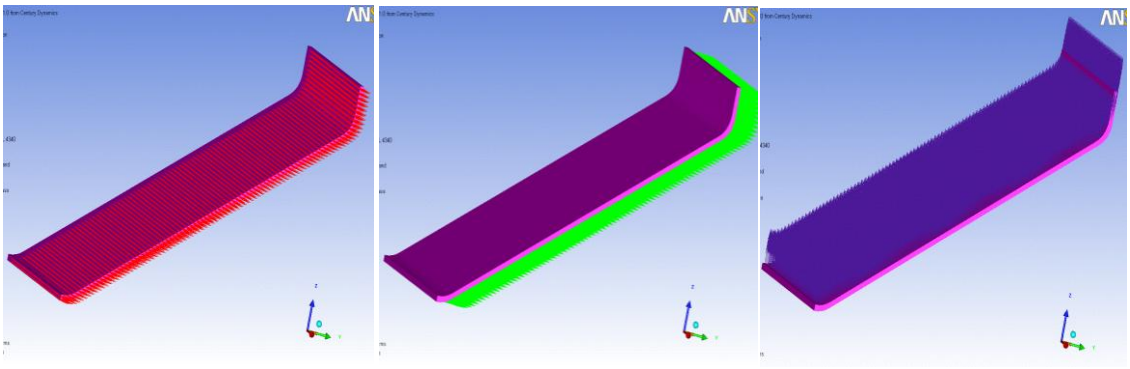

Figure 6-13 Material directions for orthotropic material in AUTODYN

In order to build the model in autodyn the shape has to be constructed out of an eight point shape. It is possible to create a number of these and then join them together, using the join matrix in the setup menu.

A simulation was run using this technique on hull shape A for the composite, Figure 6-14 shows what the model looked like before the simulation was left to run. It has a much straighter bottom edge than the actual curve that did exist, but should give a better idea as to the movement of the structure under a blast load. The blast load applied was again that of a blast in air, instead of applying the wet sand model.

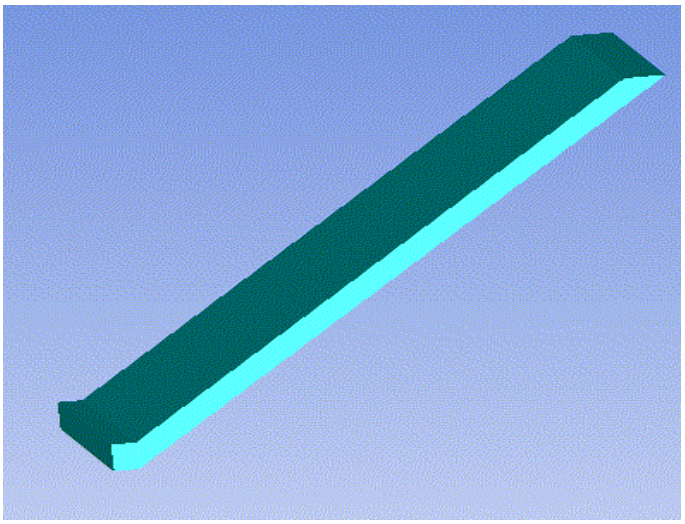

Figure 6-14 Solid composite hull shape A modelled in AUTODYN

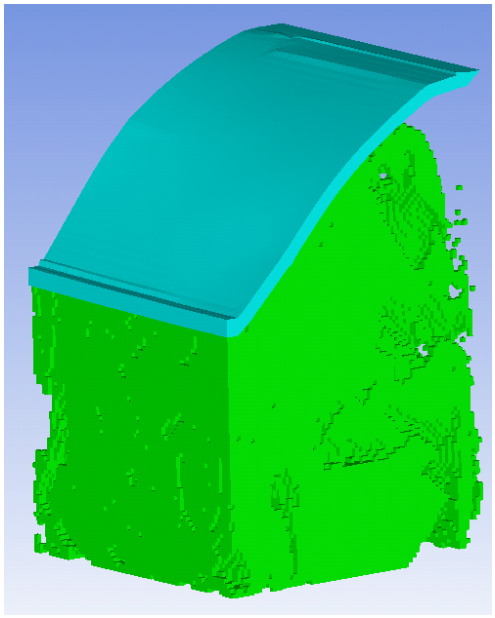

Figure 6-15 Solid composite hull A during simulation – higher stand-off

Again it appears that the shape has had an effect on the movement of the hull. However with both the adapted shapes there is one other significant difference and that is the fact that they have not been modelled using shell elements. Although this should not make a difference a check was conducted by repeating one of the flat plate simulations in 3D with shell elements (unfortunately it is not possible to model composites as shells in 2D) to ensure that the simulations gave the same results. By modelling in 3D more elements are used therefore the mesh size needs to be increased, in this case from 1mm to 5mm. The simulation time also increased significantly due to the number of elements in the mesh, so some discrepancy would be expected. The actual results however were very surprising in that for the 130g flat plate that was recreated the shell model moved approximately 2mm

whereas the solid model previously conducted moved approximately 16mm at the maximum displacement. It was thought that this could have been an error in how the composite lay-up model was created so as a check a quick simulation was conducted on a steel plate subjected to a blast load. The results again are surprising and are shown in Graph 6-11 where it can be clearly seen that the solid model experienced almost twice as much deformation than the shell model.

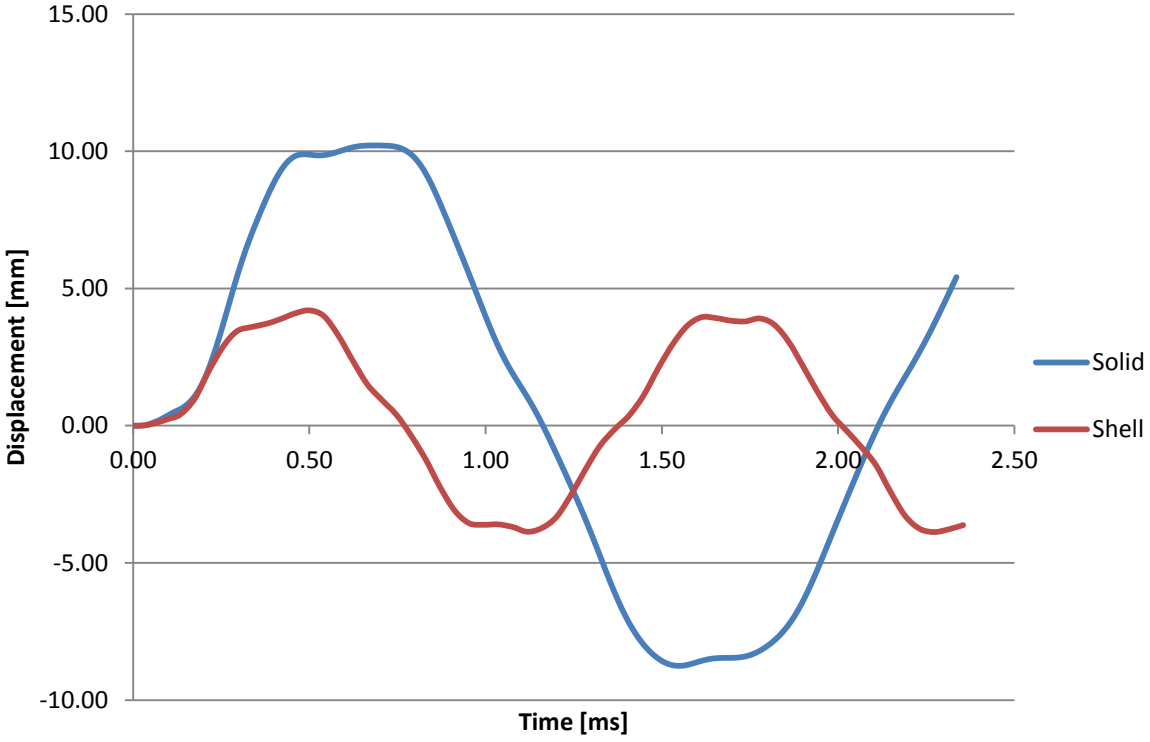

Graph 6-11 Comparison between shell and steel flat plate model

The simulations for all the hulls were repeated using a solid shape rather than shells and the results again analysed. It was however found that again there were interaction problems with the steel hulls as it was not possible to get the mesh of the surrounding air small enough to enable full interaction. Also as the hull angle decreased and became sharper the simulations became progressively more unstable, with large energy errors, too small time-steps and degenerate cell warnings. It was then realised that the flow_out boundary condition surrounding the Euler grid, was far too close to the Lagrange hull, which was causing the errors to occur, this is discussed in section 4.4 Step 3. By increasing the size of the Euler grid, there were again issues with the mesh size, in that the computer did not have enough memory to allow the whole grid to have a mesh size of 5mm. This was addressed by concentrating the small mesh around the hull and letting it expand out towards the

boundary. The new Euler mesh set up is as detailed in Table 6-19 and depicted in Figure 6-16:

	CO-ORDINATES (X_1,X_2)	NUMBER OF CELLS	ZONING CRITERIA		
			DX	NX	REGION
X	(0 , 500)	80	5	60	Lower i
Y	(0 , 500)	80	5	60	Lower j
Z	(-150 , 500)	100	5	80	Central k

Table 6-19 Updated Euler grid sizing

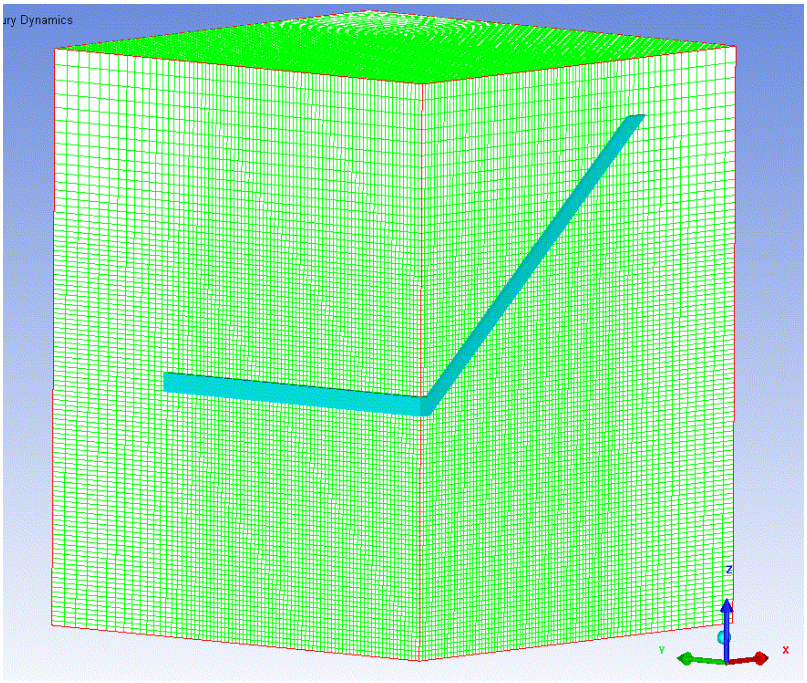

Figure 6-16 Zoning of surrounding Euler grid around Hull B

All composite simulations were repeated again so that comparisons could be drawn with the experimental data. Due to the problems surrounding the interactions with the steel hulls, these were not created as solids. The results of the S2-glass composite hulls are outlined in Table 6-20. The numerical results are again of the hulls undergoing a purely air blast rather than the wet sand because of the previously identified errors and uncertainties in the model.

HULL A - S2 GLASS [MM]	HIGHER STAND-OFF – EXPERIMENTS 1 & 2		LOWER STAND-OFF – EXPERIMENT 3	
	CENTRE	SIDE	CENTRE	SIDE
Numerical	4.00	12.54	2.00	13.75
Experimental	37.60	24.68	-	37.85
Percentage difference	-89.10%	-49.20%	-	-63.67%
HULL B - S2 GLASS				
Numerical	2.50	9.78	2.50	14.46
Experimental	32.10	26.48	71.20	60.70
Percentage difference	-92.20%	-63.00%	-96.50%	-76.20%
HULL C - S2 GLASS				
Numerical	2.02	10.67	1.00	9.89
Experimental	40.41	29.58	43.00	43.48
Percentage difference	-95.00%	-63.90%	-97.70%	-77.20%
HULL D - S2 GLASS				
Numerical	2.00	11.57	1.08	9.86
Experimental	42.46	24.45	-	29 & 134 (due to off-centre blast)
Percentage difference	-95.29%	-52.70%	-	-

Table 6-20 Composite hulls comparable results of maximum dynamic displacements

For these results the percentage difference is calculated by:

$$\frac{numerical-experimental}{experimental} x100\%.$$

Although the discrepancy is again relatively large, it is much closer than the previous modelling results conducted throughout this chapter. What is interesting about these results however is that the percentage difference between the experimental values and the numerical values remains relatively constant for both the displacement at the side and at the centre. This could be taken as a sign that the model is working and giving a reasonable

representation of what is occurring beneath the delamination. However without experimental data to back this up, it would just be conjecture.

The fact that an air blast was used rather than a buried blast for the modelling will have had an effect on the results tabulated above. By burying a charge energy is lost during the initial stages when interacting with the surrounding medium. As a result the time over which the pressure wave acts is slowed down, by slowing the pressure-time history down the area under the graph increases and therefore so does the specific impulse. It is the specific impulse that can cause more damage than the pressure, as a structure is given more time to react and deform as a result of the forces acting upon it.

Ideally further work would have been undertaken to create a sand model that accurately represented the wet sand used during the experimental phase. However time constraints were again an issue.

An important factor to also note is that the experimental displacement values also include the movement of the delaminating layers, whereas the model cannot currently account for this phenomenon. As has been previously mentioned the inside layers of the hulls delaminated away from the structure during the blast tests and the high speed cameras were set up so at to capture the inside movement of the hulls. As a result the displacements seen by the cameras will have included that of the delaminating layers and are not indicative of the hull movement as a whole. As will be discussed further in the following chapter, by including more data capture techniques within the experimental phase a much more accurate representation of what was occurring could have been documented and a more reliable model may have been created.

6.4 SUMMARY

This chapter has conducted a comprehensive study into the modelling techniques available in the numerical software AUTODYN, with the purpose of comparing various models with experimental data conducted throughout the course of this project.

Although the numerical data does not give a good agreement with the experimental work conducted on the V-shaped hulls a very good agreement was found when comparing the flat plate experiments. There are also identified reasons why this disagreement might be the case, such as the delaminating fabric moves further than the hull itself and unfortunately

there was no way to either compare this with the numerical data or to remove the effect from the experimental data.

The numerical models showed that the composite was a better choice than the steel and showed how the hull would move under the loading. They also identified the impact that the shape at the bottom of the V would have on the deflection.

"SCIENCE…..

NEVER SOLVES A PROBLEM

WITHOUT CREATING TEN MORE"

GEORGE BERNARD SHAW (1856 –1950)

7 DISCUSSION SUMMARY AND FURTHER WORK

7.1 INTRODUCTION

This chapter is a summary of the work presented in this thesis and will assess the work done throughout the course of this project and critically analyse the methods and results obtained against the aims of the project. The aims were to discover if composite materials could be used as an alternative to steel for the V-shaped blast deflectors on vehicles and if it was possible to simulate these results using numerical analysis software.

Experiments on the hulls were conducted in three stages: Experiment 1 consisted of steel and S2-glass V-shaped hulls of three different shapes with a weight-for-weight equivalency with a distance of 590mm from the top of the hull to the surface of the sand.

Experiment 2 introduced a new material, E-glass for another shape alongside the S2-glass and steel hulls with the distance from the top of the hull to the sand surface remaining the same at 590mm.

Experiment 3 used all three materials for all four shapes but at a lower distance of 480mm from the top of the hull to the sand surface.

The chapter is split into sections covering these aims of the thesis and presents directions for future work.

7.2 CONDUCTING EXPERIMENTAL WORK

This section addresses the first aim of the project – to discover if it would be possible to use composites for blast deflectors on vehicles and what level of comparative protection could they provide.

For all experimental work conducted the damage levels experienced by the various materials differed greatly between materials. All the composite test pans used retained their outside shape as a result of a centrally located blast, whereas the steel underwent enough deflection to induce permanent deformation, in the form of ‘dents’ on the side panels of the test pan.

Unfortunately due to data not being captured and the delaminating composite folding over the tracking markers it has not been possible to compare dynamic deformations to the same extent for experiment 3 as it was for experiments 1 and 2. However looking at the test pans

afterwards, it could still be clearly seen that the S2-glass was by far the better material with very little damage, sustaining its shape throughout, even when subjected to a number of tests. Test pan D which was accidentally subjected to a side impact blast even stayed intact with no perforation and only a small amount of deformation to the one side.

The E-glass also retained its shape fully during all tests, however the delamination was much more pronounced and on all hulls there was a loss of integrity in the structure in that they could all be easily flexed by hand afterwards. There was also a lot more cracking of the matrix up the sides of the test pan. Matrix cracking is assumed to occur due to manufacturing defects in the matrix material and the weakness in the fibre-matrix interface bonding (ASM International, 1993). Weaknesses in the fibre matrix interface are more likely to be the cause here as both composites were manufactured under the same conditions.

The steel test pans underwent a significant amount of deflection during the blast and as a result experienced a certain amount of residual deformation on the side panels, where the force of the blast has pushed the sides of the test pan towards each other. The way in which the hulls moved was the same for each test with the majority coming from these side panels and the rest from the bottom of the V.

Based on the above discussion it is clear that the results from all the experimental work has led to the main conclusion that the S2 glass composite would be a better material to use for blast deflector plates under vehicles. They significantly out-performed the steel in all tests and it may be possible to use a lighter version to offer a similar level of protection currently available from the steel.

The results regarding the shape vs. stand-off show that the shape appears to be the more important factor, in this case. However this could change if looked at a wider variety of angles. Tremblay (Tremblay, 1998) stated that the impulse delivered to a plate not only decreases rapidly with stand-off, but would also decrease when looking at angles between 0°, for a flat plate, and 180°, for a vertical plate. Therefore there could be an ideal shape within the limits of vehicle design. However more testing would have to be conducted to discover where the ideal shape and position lies, and this would probably change depending on the size of the blast and the medium in which the explosive was buried.

Ideally if these experiments were to be conducted again, then attaching gauges to the hull to measure displacement, pressure and strain would have significant advantages, especially

when comparing to the numerical results conducted in chapter 6 Modelling Results. Unfortunately due to cost restraints it was not possible for this project, as the gauges are likely to be ruined with each test. Another option would be to use dampers instead of the steel bars for the support structure holding the frame to the rig. This would allow for a measurable vertical movement. However this would then be difficult to compare with numerical results unless there was an option in the constraints for this movement.

7.2.1 MATERIAL PROPERTIES

When the properties of the two types of composites are compared it is possible to see why there are such differences between the two test results.

E-glass is a family of glasses with a calcium aluminoborosilicate composition and a maximum alkali content of 2%. They are used as general purpose fibres when strength and high electrical resistivity are required. S-glass has a magnesium aluminosilicate composition, which demonstrates high strength and is therefore used where high tensile strength is required (ASM International, 1993). S2-glass is of the same composition as S-glass with a different coating and is a trademark of AGY composites. The mechanical properties of both S2 and E glass are outlined in Table 7-1 below.

PROPERTY	S2-GLASS FIBRE	E-GLASS FIBRE
Density (g/cm^3)	2.46	2.58
Tensile strength (MPa)	4890	3445
Tensile modulus (GPa)	87	72.5
Elongation (%)	5.7	4.8
Fibre diameter range (μm)	5-9	4-25

Table 7-1 Differences between the mechanical properties of E and S2 glass fibres (Fecko, 2006)

Table 7-1 shows that the S2 glass fibres have a much higher tensile strength than that of the E-glass. This is down to silica content of the fibres. S2-glass has a silica content of around 65% whereas E-glass has only around 54%. This silica content is also one of the reasons why S2-glass is more expensive, silica has a very high melting temperature and therefore manufacturing techniques and equipment are more complex and time consuming for the S2-glass.

7.3 MODELLING IN AUTODYN

A lot of the problems encountered throughout this chapter of work are as a result of available computer power and licences and the licence terms. With more licences available, errors could have been rectified quicker as more simulations could have been conducted.

Numerical models can only tell so much; in order for them to be considered accurate they need to be compared with experimental work and/or other published literature. It is also important to note that they are only as accurate as the information that is put into them. Any errors with material models, mesh sizing and even the general model set-up will be carried throughout the simulation and into the results. For example during this work the small error found in the paper containing the wet sand model

There are usually a variety of methods available in order to model a scenario, what was found throughout this work was these different methods may give different solutions to the problem. User discretion is advised and by testing different methods it should be possible to find the one that works best with the available data.

If using the software to predict events then it would be advisable to create similar models that can be compared with experimental data. This would enable the user to gauge the accuracy of the model for the predictive work.

Although the numerical and experimental results are comparatively not in good agreement, there are positives from the work carried out. The mine blast phenomenon was modelled in autodyn and found to give a realistic representation of the occurrence. There were some discrepancies, but that is to be expected when they are so many variables and unpredictable events occurring. The material model gave an accurate representation of the deformation when modelled as a flat plate subjected to a charge of varying sizes buried in dry sand. Again the discrepancies encountered during these simulations were few and those that were, were due to the differences in the rigid constraints imposed between the experiment and the numerical model. There are a number of reasons as discussed in chapter 6 Modelling Results as to why the lack of cohesion between the two sets of results, but unfortunately without definitive results from the experimental work, the numerical model can raise doubts. It does however predict the movement of the hulls, where the maximum displacement occurs and that there is no deformation to the outside shape of the S2 glass

composite hulls. It also gives a relatively good assessment of the fact that the composite will withstand the blast effectively.

It is possible that with more time and more computer power that a more accurate result could be obtained however in the interim, these results do provide an idea of what results could be expected from material comparisons. They do not appear to give a representation of the effect of the angle, though this could be due to inherent instabilities within the model, as discussed in section 6.3.2 where as the angle decreased in some instances the model became unstable with large energy errors and small time steps.

7.4 THROUGH LIFE MANAGEMENT IMPLICATIONS

It is not possible to simply introduce a piece of equipment into the armed services no matter how good it may be. There are processes and their inherent implications that must be considered and methods put in place as to how to deal with them.

The experimental work conducted as part of this project showed that the S2-glass out-performed the steel by a large margin. With regards to the implications of this for the through life and the defence lines of development the areas that would need to be considered are:

- Training – to assess the levels of damage, in some instances during the experimental work damage done to the outside of the hull looked minimal yet the inside it was possible to see the extent of delamination that occurred. The inside of the hull will be hidden from view therefore training needs to occur that teaches the user how to assess the levels of damage even when they might not be seen.

  It was shown during experiment one that the composite was capable of being subjected to multiple blasts but the damage became significantly more extensive each time. This must be avoided, therefore it would be suggested that the hull is removed and checked over thoroughly using the eye or other non-destructive techniques such as ultra-sonic testing and/or tap testing.
- Equipment – if a composite hulled vehicle was taken up and these various methods for testing were implemented then the equipment to allow for these must also be co-located with the vehicle. This would also increase the costs associated with the implementation of the vehicle and must be taken into account when predicting the total through life costs of the vehicle.

- Logistics – there must be a location that this testing can be carried out in and this may need to be a clean room with all the necessary equipment to hand.

  Whilst the hull is being checked over for damage and repair work carried out if possible, the vehicle is not able to be used. Therefore the consideration of spare hulls should be taken into account, else the vehicle is redundant. This would then have implications on the supply chain and manufacturers again contributing to the overall through life cost of the vehicle.

This is just a sample demonstration of the issues that may arise due to one aspect. There are others that would need to be looked at in detail and processes put in place to combat difficulties.

Ideally any new equipment should require little to no changes in the way the service currently works, yet should perform better, cost less and look good. However this is not always possible and progress will inevitably lead to changes.

7.5 FUTURE WORK

If this work were to be continued further, there are many areas that could be explored. These areas are broken down into sections that cover the various areas of the project work.

7.5.1 EXPERIMENTAL WORK

Experimentally there are a number of improvements that could be made to the original set-up, Such as:

- Using extra equipment to gain a more thorough representation of the material response to the blast. As previously mentioned, pressure and strain gauges could be placed on the inside surface of the hull to capture data during the blast. Instead of using rigid supports, dampers could be used, with a known resistance and allowable movement so that upward movement could be calculated. Using lasers to capture the movement of the test pan during the blast is another option. However all these options cost a considerable amount of money and use up valuable time during the experimental setup. Therefore making sure that they capture what is required would be of paramount importance.

- Repeating the experiments as they stand but looking more at the equivalent stiffness. What is the minimum weight of the composite that could be used to give the same level of protection currently employed by the steel on the mine protected armoured vehicles. Are there any alternative composites that could provide similar levels of protection, such as aramid or even carbon fibres, however these are generally more expensive to manufacture than glass fibre composites.
- What would happen to the composite if subjected to an off centre blast. One experiment was conducted, purely accidentally but with very interesting results. This could be taken further and again compared back to the steel equivalent.

7.5.2 MODELLING WORK

- As computer technology increases it will become possible to model much more intricately than was possible with this work. The steel hulls could be remodelled and compared with the results published in this work.
- Material data that was not provided for the E-glass, could be calculated by conducting various experiments, such as the tensile test, and then the E-glass hulls could be modelled numerically.
- Using different software may well produce different results, as was shown with the comparisons between LS-DYNA and AUTODYN for the mine blast modelling in chapter 6 section 6.1 Validation of Mine Blast.

7.5.3 OTHER WORK

Other work that was intended for this project but not carried out due to time constraints, would be further material model validation.

- Recreating the flat plate experiments but using wet sand instead of dry, would give a better understanding of how the model and material behaved.
- Using the gas guns to shock flat plates and then calculating the shock equation of state for the material and modelling in a numerical package for comparison purposes. Because this experiment is much more controlled with very few variables it would give a much more accurate representation of the material.

- Other experiments that could be conducted are impact and penetration tests. Again these are very controlled experiments that would be relatively straightforward to recreate in a numerical modelling package.

"A learning experience is one of those things that says, "You know that thing you just did? Don't do that.""

Douglas Adams (1952-2001)

8 CONCLUSIONS

This work began with two main questions: “Could composites be used to replace steels for blast deflectors on mine protected vehicles?” and “How effective and realistic is numerical analysis in predicting the material response of these blast deflectors?” In the course of this project the questions have been addressed by the following means:

i) In chapter 5 the experimental work conducted for this investigation found that the S2-glass composite could be used as a better alternative to steel. In all cases there was significantly less dynamic deformation than the steel and no permanent deformation for the centrally located blast. Whereas the steel had significant levels of both. There was some damage done to the composite test pans, delamination being the main cause. However the outside of the test pan retained its shape and was even capable of a multi-hit capacity with no perforations. The other composite tested, E-glass, did not stand up as well as the S2-glass with a lot more delamination and the presence of matrix cracking became clearly visible. There was again little dynamic and permanent deformation in comparison to the steel, but there were concerns over the structural integrity of the material after the tests.

ii) The other factor that was considered during the experimental work was the argument of shape vs. stand-off. The lower stand-off results could only be fully compared after the testing as the delamination on the videos made comparisons very difficult. Due to the multi-hit experiment carried out on one of the hulls during the higher stand-off experiments comparing permanent damage afterwards was very difficult. Although no definitive result for this was found. The results from the experiments conducted did lean towards shape being the more prominent factor.

During a conversation with Vernon Joynt of Force Protection Incorporated (Joynt, 2011), who manufacture the Mastiff, Ridgeback and Buffalo vehicles, it was discovered that from testing that they have done in America that they found that the sharper the angle the better the survivability prospects. The blast, although closer to

the structure, was apparently deflected much better without causing as much damage.

iii) In chapter 6 Modelling Results, a mine blast model was created and compared with published experimental work and data from another numerical software package. When modelling mine blast phenomenon there are bound to be discrepancies due to the amount of variables that can occur during the experimental work. Two different scenarios were compared: a mine that is flush with the surface and a mine that is buried in dry sand. The shock parameters, time of arrival, maximum overpressure and specific impulse were compared and on the whole were found to be in reasonable agreement with the data. One result that produced an error of 164% was looked at in more detail, and a number of models with slight differences were created to show that it was a small error inherent in the software for that particular set-up and this error was reduced to 34%

iv) In chapter 6 Modelling Results section 6.2 a material model was devised and a simple flat plate model was created and compared with experimental work done in chapter 5. The experimental work consisted of constrained flat plates subjected to various charge sizes. The deformation was recorded using high speed video cameras and then used to validate the material model. Dry sand was used in both the experiment and the material model, as has been validated in the past (Laine, L., Sandvik,A., 2001). Despite a small issue with the constraints in the experiment not being as rigid as would be liked there was a good correlation between the experimental work and the numerical model.

v) Again in chapter 6 section 6.3, the V-shaped hulls were created and tested and then compared with the experimental data from chapter 5. Errors in the set up and the sand material-model forced development of the numerical model until a working model was created. When compared with the experimental data, it was found to be quite a long way out. However reviewing the video footage it is obvious that the delamination experienced by the test pan is included in the measured deformation

and unfortunately this is not shown by the numerical model, however the percentage error is comparatively consistent across the results.

The steel hulls proved very difficult to model using solid elements, due to the interaction problems that occur between Lagrange and Euler elements, the steel hull was too thin and the surrounding Euler grid, as it was so large, could not have a small enough mesh size to enable full interaction. One model was created and left to run for a number of weeks that did show, even with interaction problems, the movement of the steel. The values of the displacements in this case were in fact greater than the experimental results, though the numerical model was conducted using an air blast rather than a blast buried in wet sand, which could account for this difference.

The numerical modelling work did eventually give a representation of what occurred during the experimental work, and could, if applied correctly, be used to predict other events such as side impact or larger blasts.

It is a fact that data acquisition from explosive experiments is very difficult, and unfortunately if something goes wrong or if data is not captured it is not easy, or cost effective to repeat the experiment. During this work, some data was not captured by the camera, and on others the movement during the test interfered with the tracking markers making it impossible to calculate the deformation at that point. Ideally other data acquisition techniques would have been employed, such as strain and pressure gauges unfortunately due to cost restraints this was not possible. Other options include using lasers to track the hull movement but again cost implications interfered. Another factor to consider that by employing these extra techniques the time taken to set up for each experiment would have been significant, resulting in the possibility of fewer tests being conducted.

The biggest challenge encountered during the course of this work has been the learning of the numerical software. As a result of this learning process the author has discovered that a numerical model can only be as good as the person using it. Numerical software must be

fully understood in order to be used effectively. Discretion is advised when looking at the results, if something does not appear right, the chances are it is not. Create models that have one small thing changed and compare, it could be that there was a small inherent error that has been magnified upon the running of the model.

Numerical modelling, for the scenarios presented in this work, can give a relatively good idea of where a solution could lie. However, with all the variables and discrepancies inherent in the assumptions made during the creation of these models, you can never be certain until verified with experimental work.

REFERENCES

Absil, L.H.J., Verbeek, H.J. and Weerheijm, J., (1997), *Combined Experimental and Numerical Study of Mine Detonations in the Vicinity of Vehicles*, DRDB, Defence Research Establishment, Suffield, Banff, Canada.

Adamik, V., Trzcinski, W. A. and Vagenknecht, J. (2004), "Investigation of the Behaviour of Steel and Laminated Fabric Plates Under Blast Wave Load", .

Airbus (2011)*, A330-300*, available at: http://www.airbus.com/aircraftfamilies/passengeraircraft/a330family/a330-300/ (accessed February 18th).

Alem, N. M., Strawn,G.D. (1996), *Evaluation of an Energy Absorbing Truck Seat for Increased Protecttion from Landmine Blast,* , Technical report, U.S. Army Aeromedical Research Laboratory, Fort Rucker, Alabama, USA.

Armedforces.co.uk (2012)*, Defence Projects: Bowman - Tactical C41 Radio System*, available at: http://www.armedforces.co.uk/projects/raq3f55e10b63f0e (accessed January 2012).

Army Guide *, T-64 Main Battle Tank*, available at: http://www.army-guide.com/eng/product100.html (accessed November 2nd).

ASM International (1993), *Composites,* .

Baker, W. E., Cox, P. A., Westine, P. S., Kulesz, J. J. and Strehlow, R. A. (1983), *Explosion hazards and evaluation,* Elsevier, Amsterdam.

Barney, J. (1991), "Firm Resources and Sustained Competitive Advantage", *Journal of Management,* vol. 17, no. 1, pp. 99-120.

Batra, R. C. and Hassan, N. M. (2008), "Blast resistance of unidirectional fiber reinforced composites", *Composites Part B: Engineering,* vol. 39, no. 3, pp. 513-536.

Battletanks.com (2010)*, T-64 Soviet Main Battle Tank*, available at: http://www.battletanks.com/t-64.htm (accessed 5th July).

BBC News (2009)*, Q&A: Snatch landrovers*, available at: http://news.bbc.co.uk/1/hi/uk/7703703.stm (accessed January).

BBC News (2010)*, Inquest hears vehicle in Afghan blast 'not adequate'*, available at: http://news.bbc.co.uk/1/hi/uk/8545227.stm (accessed January).

Bergeron, D.M. and Tremblay, J.E., (2000), *Canadian Research to Characterise Mine Blast Output*, Cranfield University [RMCS], Shrivenham, UK.

Bergeron, D. M., Walker, R. and Coffey, C. (1998), *Detonation of 100g Anti-Personnel Mine Surrogate Charges in Sand: A Test Case for Computer Code Validation,* .

Bird, R., (2001), *Protection of Vehicles against Landmines*.

Boris, J. P. and Book, D. L. (1973), "Flux-corrected transport. I. SHASTA, a fluid transport algorithm that works", *Journal of Computational Physics,* vol. 11, no. 1, pp. 38-69.

Boris, J. P. and Book, D. L. (1997), "Flux-Corrected Transport", *Journal of Computational Physics,* vol. 135, no. 2, pp. 172-186.

Brannen, K. (2010)*, 'Chimney' deflects IEDs*, available at: http://www.defensenews.com/story.php?i=4996368 (accessed 2/3).

British Army (2010)*, Personal Armour*, available at: http://www.army.mod.uk/equipment/personal/1456.aspx (accessed August 27th).

Brode, H. L. (1955), "Numerical solution of spherical blast waves", *Journal of Applied Physics,* vol. 26, no. 6.

Century Dynamics Limited, *Autodyn Training Course: Training Manual*.

Century Dynamics Limited, (1998), *AUTODYN user's documentation*, Horsham, UK.

Century Dynamics Limited, (2005), *Autodyn: Release notes, version 4.2*.

Chassillan. (2004), *VBCI* .

Cheng, Q.H., Lu, C., Tan, X.M. and Tham, C.Y., (2002), *Response of a Box-Like Structure to Nearby Explosion*, Defence Science and Technology Agency, Singapore.

Child, C. (2009), *Blast Effects on Vehicle Hull Shapes* (unpublished MSc project report thesis), Cranfield University, Shrivenham Campus, .

Christensen, R. M. (1979), *Mechanics of Composite Materials,* John Wiley & Sons, Livermore, California, USA.

Christopher, M. (2005), *Logistics and Supply Chain Management: Creating value adding networks,* 3rd ed, Pearson Education Limited, Harlow.

Christopher, M. and Holweg, M. (2011), "“Supply Chain 2.0”: managing supply chains in the era of turbulence", *International Journal of Physical Distribution & Logistics Management,* vol. 41, no. 1, pp. 63-82.

Comtois, J. L. R., Edwards, M. R. and Oakes, M. C. (1999), "The effect of explosives on polymer matrix composite laminates", *Composites Part A: Applied Science and Manufacturing,* vol. 30, no. 3, pp. 181-190.

Daniel, I. M. and Ori, I. (2006), *Engineering Mechanics of Composite Materials,* Oxford University Press.

Defence Management.com (2009)*, HMS Daring's voyage of discovery*, available at: http://www.defencemanagement.com/feature_story.asp?id=13324 (accessed 04/13).

Department of Trade and Industry (2006)*, Recycling Carbon Fibre*, available at: http://www.bis.gov.uk/files/file34992.pdf (accessed February 18).

Dobratz, B. M., Crawford,P.C. (1985), *LLNL Explosive Handbook: Properties of Chemical Explosives and Explosive Simulants,* , California, USA.

Dorn, M.R., Rees, S.J. and Docton, M.K., (1999), *Improving Vehicle Resistance to Blast*, Cranfield University [RMCS], Shrivenham, UK.

Fairlie, G. and Bergeron, D., (2002), *Numerical Simulation of Mine Blast Loading on Structures*, Las Vegas, Nevada, USA.

Fecko, D. (2006)*, High strength glass reinforcements still being discovered*, available at: http://www.reinforcedplastics.com/view/1682/high-strength-glass-reinforcements-still-being-discovered (accessed June 7).

Fiserova, D. (2006), *Numerical Analyses of Buried Mine Explosions with Emphasis on Effect of Soil Properties on Loading* (unpublished PhD thesis), Defence College of Management and Technology, Cranfield University.

Fiserova, D., Hameed, A., Rose, T.A., Hetherington, J.G. and Prochazka, S., (2003), *Systematic Study of Simulated Mine Explosions Using AUTODYN*, University of Pardubice, Paradubice, The Czech Republic.

Follett, S., Hameed, A., Darina, S. and Hetherington, J. G. (2010), "Numerical simulations as a reliable alternative for landmine explosion studies: The Autodyn approach", 12-18 November 2010, Vancouver, .

Force Protection Incorporated, (2010), *Ocelot*.

French, M., (2010), *Composite Materials for Military Vehicles*, Battlespace Online.

French, M. and Lewis, M. (1996), "The advanced composite armoured vehicle platform (ACAVP) programme", *Journal of defence science,* vol. 1, no. 3.

Gibson, R. F. (1994), *Principles of Composite Material Mechanics,* McGraw-Hill, Wayne.

Global Security (2006), *Explosives - Compounds*, available at: http://www.globalsecurity.org/military/systems/munitions/explosives-compositions.htm (accessed October 19th).

Global Security (2010), *Global Security: Improvised Explosive Devices (IEDs) / Booby Traps*, available at: http://www.globalsecurity.org/military/intro/ied.htm (accessed March 3rd).

Gray, B. (2009), *Review of acquisition for the secretary of state for defence,* .

Greuter, A., (2004), *MOWAG - mine protection solution LAV's PIRANHA/EAGLE IV*, Cranfield University [RMCS], Shrivenham, UK.

Grujicic, M., Bell, W. C., Marvi, H., Haque, I., Cheeseman, B. A., Roy, W. N. and Skaggs, R. R. (2009), *A computational of survivability of a pick-up truck subject to mine detonation loads*, available at: http://myweb.clemson.edu/~gmica/Publications/Ref_172x.pdf (accessed June/16).

Grujicic, M., Pandurangan, B. and Cheeseman, B. A. (2006), "The effect of degree of saturation of sand on detonation phenomena associated with shallow-buried and ground-laid mines", *Shock and Vibration,* vol. 13, no. 1, pp. 41-61.

Grujicic, M., Pandurangan, B., Coutris, N., Cheeseman, B. A., Roy, W. N. and Skaggs, R. R. (2008), "Computer-simulations based development of a high strain-rate, large-deformation, high-pressure material model for STANAG 4569 sandy gravel", *Soil Dynamics and Earthquake Engineering,* vol. 28, no. 12, pp. 1045-1062.

Grujicic, M., Pandurangan, B., Coutris, N., Cheeseman, B. A., Roy, W. N. and Skaggs, R. R. (2009), "Derivation, Parameterization and Validation of a Sandy-Clay Material Model for Use in Landmine Detonation Computational Analyses", *Journal of Materials Engineering and Performance,* , pp. 1-17.

Grujicic, M., Pandurangan, B., Huang, Y., Cheeseman, B. A., Roy, W. N. and Skaggs, R. R. (2007), "Impulse loading resulting from shallow buried explosives in water-saturated sand", *Proceedings of the Institution of Mechanical Engineers, Part L: Journal of Materials: Design and Applications,* vol. 221, no. 1, pp. 21-35.

Grujicic, M., Pandurangan, B., Qiao, R., Cheeseman, B. A., Roy, W. N., Skaggs, R. R. and Gupta, R. (2008), "Parameterization of the porous-material model for sand with different levels of water saturation", *Soil Dynamics and Earthquake Engineering,* vol. 28, no. 1, pp. 20-35.

Gupta, A.D., (2002), *Modelling and Analysis of Transient Response in a Multilayered Composite Panel due to Explosive Blast*, Orlando, Florida, USA.

Hall, R. (2011), *First A400M support contract nears*, available at: http://www.aviationweek.com/aw/generic/story_channel.jsp?channel=defense&id=news/asd/2011/10/03/05.xml (accessed January/15).

Held, M., (1990), *Similarities of Shock Wave Damage in Air and in Water*.

Held, M., (2002), *Momentum Distribution of Anti-Tank Mines*, Orlando, USA.

Henrych, J., (1979), *The Dynamics of Explosion and its Use*, Elsevier Science Publishers, Amsterdam.

Hetcher, B., (2004), *The Value of Landmine Protection Simulation in Vehicle Design*, Cranfield University [RMCS], Shrivenham, UK.

Hirsch, H. (1992), *Numerical Computation of Internal and External Flows,* Wiley - Interscience, Great Britain.

Hogg, I. (1977), *The Tank Story,* Phoebus Publishing Company/BPC Publishing Ltd., London.

Holland, S., (2001), *The Application of the TABRE attenuation System to Vehicles for Enhanced Underside Blast Protection*, Cranfield University [RMCS], Shrivenham, UK.

House of Commons Committee of Public Accounts (2003), *Ministry of Defence: Building an air manoeuvre capability: the introduction of the Apache Helicopter,* Forty sixth report of session 2002-03, pp 6, London: The Stationary Office Ltd, London.

House of Commons Committee of Public Accounts (2007), *Ministry of Defence: Delivering digital tactical communications through the Bowman CIP Programme,* Fourteenth Report of Session 2006-07, pp 8, London: The Stationary Office Limited, London.

House of Commons Defence Committee (2007), *Strategic Lift: Eleventh report of session 2006-07,* HC 462, London Stationary Office, London.

iCasualties (2011), *iCasualties: Operation Enduring Freedom*, available at: http://www.icasualties.org/OEF/ (accessed February 18th).

International Campaign to Ban Landmines (2009), "Landmine Monitor Report 2009: Toward a mine-free world.", [Online], available at: http://lm.icbl.org/index.php/publications/display?url=lm/2009/es/major_findings.html.

International Institute for Strategic Studies (2010), *Deal saves Europe's transport aircraft*, available at: http://www.iiss.org/publications/strategic-comments/past-issues/volume-16-2010/march/deal-saves-europes-transport-aircraft/ (accessed August).

Chris Irvine. (2010) "History of the snatch land rover", *Daily Telegraph (online),* 9 March 2010, .

Ishikawa, T. and Chou, T. -. (1982), "Stiffness and strength behaviour of woven fabric composites", *Journal of Materials Science,* vol. 17, pp. 3211--3220.

Jacko, M. and Bella, V., (2002), *The Simulation of Charge Detonation Action on Armour Plate*, Waplewo, Poland.

Jane's Information Group, (1999), *Composite amoured vehicles are shaping up, weapons and equipment*.

John, V. (2003), *Introduction to Engineering Materials,* Palgrave Macmillan.

Johnson G. R., Cook W. H. (1983), "A constitutive model and data for metals subjected to large strain rates and high temperatures", *7th International Symposium on Ballistics,* April 1983, The Hague, Netherlands, .

Joynt, V., (2011), .

Khare, A. (2010), *Blast Effects on Shaped Composites* (unpublished MSc thesis), Cranfield Unversity Defence Academy College of Management and Technology, Shrivenham.

Laine, L., Ranestand, O., Sandvik, A., Snekkevik,A. (2001), "Numerical Simulation of Anti-Tank Mine Detonations", *12th APS Topical Group Conference on Shock Compression of Condensed Matter,* Atlanta, USA, .

Laine, L., Sandvik,A. (2001), "Derivation of Mechanical Properties for Sand", Proceedings of the 4th Asia-Pacific Conference on Shock and Impact Loads, Singapore, pp. 361.

Leonardo Da Vinci, (1487), *Pen Drawing of Armoured Car*.

Mercedes Benz (2011)*, Mercedes Benz Pictures*, available at: http://www.mercedesbenzpic.com/mercedesbenz/car/pictures/2010/08/mercedes-benz-slr-mclaren-roadster-titel1.jpg (accessed 2/18).

Ministry of Defence, Acquisition Operating Framework (2009a)*, Defence Lines of Development*, available at: http://www.aof.mod.uk/aofcontent/srategic/guide/sg_dlod.htm (accessed June).

Ministry of Defence, Acquisition Operating Framework (2009b)*, What is Through Life Capability Management*, available at: http://www.aof.mod.uk/aofcontent/operational/business/capabilitymanagement/capabilitymanagement_whatis.htm (accessed June).

Ministry of Defence, Acquisition Operating Framework (2011)*, Through life capability management (TLCM): Introduction*, available at: https://www.aof.mod.uk/aofcontent/tactical/tlcm/content/introductiontotlcm.htm.

MOD (2010), *Armoured Fighting Vehicles*, available at: http://www.army.mod.uk/equipment/fighting-vehicles/default.aspx (accessed July 13).

National Audit Office (2002), *Building an Air Manoeuvre Capability: The Introduction of the Apache Helicopter,* HC 1246, pp 25-27, London: The Stationary Office, London.

National Audit Office (2004), *Press Release - Ministry of defence: Major Projects report 2003,* HC195, London Stationary Office, London.

National Audit Office (2006a), *Delivering digital tactical communications through the Bowman CIP programme,* HC 1050, pp 1-3, London: The Stationary Office, London.

National Audit Office (2009), *The Major Projects Report,* HC-85 I, pp 7, London Stationary Office, London.

National Audit Office (2011), *Major Projects Report 2011,* HC1520-I, London Stationary Office, London.

NATO (2010), *North Atlantic Treaty Organization: Standardization Agreements*, available at: http://www.nato.int/cps/en/SID-8BF0F167-D3248540/natolive/stanag.htm (accessed 3/3).

NATO Standardization Agency, (2004), *STANAG 4569: Protection Levels for Occupants of Logistic and Light Armoured Vehicles*, 1st ed.

Nell, S., (2000), *Test and Evaluation of Landmine Protected Wheeled Vehicles*, Cranfield University [RMCS], Shrivenham, UK.

Net Resources International (2010), available at: http://www.army-technology.com/projects/buffalo/buffalo1.html (accessed 5th July).

Niekerk, B., (2001), *Landmine Protection - Dealing with the Uncertainties*, Cranfield University [RMCS], Shrivenham, UK.

Ogorkiewicz, R. M. (1968), *Design and Development of Fighting Vehicles,* Macdonald & Co Ltd, London.

Ogorkiewicz, R. M. (1991), *Technology of Tanks,* Janes Information Group Limited, UK.

Ogorkiewicz, R. M. (1994), *World-wide trends in the development of armoured fighting vehicles,* 6, Jane's Information Group, Surrey.

Oran, E. S. and Boris, J. P. (2000), *Numerical Simulation of Reactive Flow,* 2nd ed, Cambridge University Press, UK.

Raju, I. S. and Wang, J. T. (1994), "Classical Laminate Theory Models for Woven Fabric Composites", *Journal of Composites Technology and Research,* vol. 16, no. 4, pp. 289--303.

Ramasamy, A., Hill, A. M., Bull, A. M. J. and Clasper, J. C. (2009), "Blast mines: Physics, injury mechanisms and vehicle protection", *Journal of the Royal Army Medical Corps,* vol. 155, no. 4.

Ravid, M. and Ziv, D., (2004), *Protection and Survivability of Light AFV and Support Vehicles*, Cranfield University [RMCS] Shrivenham, UK.

Ricardo *, Latest Project: Ocelot*, available at: http://www.ricardo.com/en-gb/Engineering-Consulting/Defense-Systems-and-Technologies/Latest-Project/ (accessed July 5th).

Ricardo (2009)*, Image of Ocelot LPPV*, available at: https://www.ricardo.com/en-gb/News--Media/Press-releases/News-releases1/2009/Ricardo-and-Force-Protection-Europe-unveil-Ocelot-the-next-generation-in-defence-vehicle-performance-and-crew-protection/ (accessed July 14th).

Smith. (2009), *Blast waves produced by the detonation of high explosive materials in air.*(unpublished Course notes), .

Smith, P. D. and Hetherington, J. G. (1994), *Blast and Ballistic Loading of Structures,* Butterworth-Heinemann Ltd, Oxford.

Supacat (2010)*, SPV400*, available at: http://www.supacat.com/products/spv400/ (accessed July 13th).

SYEN *, HUMS*, available at: http://www.syen.co.uk/HUMS.htm (accessed October 25).

Terry, T. W., Jackson, S. R., Ryley, C. E. S., Jones, B. E. and Wormell, P. J. H. (1991), *Fighting Vehicles,* BPCC Wheatons Ltd, Exeter.

Think Defence (2010)*, The Light Protected Patrol Vehicle*, available at: http://www.thinkdefence.co.uk/2010/03/the-light-protected-patrol-vehicle/ (accessed July 13th).

TPI Composites (2007)*, TPI Composites and Armor Holdings Unveil Army's First All-Composite Military Vehicle*, available at: http://www.tpicomposites.com/press-room/press-release-archive/tpi-composites-and-armor-holdings-unveil-armys-first-all-composite-military-vehicle.aspx (accessed Jaunary 18th).

Tremblay, J. E. (1998), *Impulse on blast deflectors from a landmine explosion,* , Defence Research Establishment, Valcartier, Quebec.

Vasiliev, V. V. and Morozov, E. V. (2001), *Mechanics and Analysis of Composite Materials,* Elsevier Science Ltd, Oxford, UK.

Wang, J. (2001), *Simulation of Landmine Explosion Using LS-DYNA Software: Benchmark Work of Simulation of Explosion in Soil and Air,* , Australia.

Wasserbly, D., (2010), *USMC looks to armoured capsules for Humvees*.

Weckert, S. and Anderson, C. (2006), *Preliminary comparison between TNT and PE4 landmines,* , Weapon Systems Division, DSTO, Edingburgh, South Australia.

Wharton, R. K., Formby, S. A. and Merrifield, R. (2000), "Airblast TNT equivalence for a range of commercial blasting explosives", *Journal of hazardous materials,* vol. 79, no. 1-2, pp. 31-39.

White, A., (2007), *Armor, TPI have light touch for HMMWV*, Jane's Information Group.

Williams, K., Poon,K.A. (2000), *A Numerical Analysis of the Effect of Surrogate Anti-Tank Mine Blasts on the M113,* , Valcartier, Canada.

Williams, J., (1999), *Anti-Tank Landmines - The Threat*, Cranfield University [RMCS], Shrivenham, UK.

X Coy 45 Commando Op Herrick 9, (2008), *IEDs in Afghanistan*.

APPENDIX 1

- ASME Conference paper
- GEMS presentation
- LTN Poster

ASME 2010 International Mechanical Engineering Congress and Exposition

IMECE2010
November 12-18, 2010, Vancouver, British Columbia, Canada

IMECE2010-40435

NUMERICAL SIMULATIONS AS A RELIABLE ALTERNATIVE FOR LANDMINE EXPLOSION STUDIES: THE AUTODYN APPROACH

Stephanie Follett Cranfield University Shrivenham, Wiltshire, UK	**Amer Hameed** Cranfield University Shrivenham, Wiltshire, UK
S. Darina Cranfield University Shrivenham, Wiltshire, UK	**John G. Hetherington** Cranfield University Shrivenham, Wiltshire, UK

ABSTRACT

In order to validate the numerical procedure, the explosion of a mine was recreated within the non-linear dynamics software, AUTODYN. Two models were created and analysed for the purposes of this study – buried and flush HE charge in sand. The explosion parameters – time of arrival, maximum overpressure and specific impulse were recorded at two stand-off distances above the ground surface. These parameters are then compared with LS-DYNA models and published experimental data.
The results, presented in table format, are in reasonable agreement.

Keywords: mine explosion, sand, numerical simulation

NOMENCLATURE

p	pressure
v	specific volume
T,	temperature
i	specific impulse
t	time

INTRODUCTION

The landmine is considered to be one of the most dangerous weapons in use during armed conflicts. In armed conflicts over the last decade, US military losses attributed to landmines were 59% in Persian Gulf War and 60% in Somalia [1]. Landmine Monitor, despite data collection issues, has identified at least 73,576 casualties of landmines , Explosive Remnants of War (ERW), and victim activated improvised explosive devices in 119 states and areas in the past ten years [2].

With the advent of conflicts in Iraq and Afghanistan the landmine has been usurped by the improvised explosive device, commonly known as an IED. IED's accounted for just over 61% of all fatalities in Afghanistan in 2009 [3].
As a result, blast protection features are now a pre-requisite on all armoured vehicles. In particular crew survivability remains paramount when designing vehicles. Reducing crew mortality still remains a great challenge for vehicle manufacturers [4-7].
There have been some initiatives over recent years into the understanding of mine blast loading behaviour in order to enhance demining equipment and mine resistant armoured vehicles. This research can be divided into three inter-dependant areas:

(a) *Prediction of the blast load* – dealing with the shock wave propagation through soil and air by taking into account the characteristics of the explosive and the nature of the soil such as moisture content, soil particle sizes and their linkages.
(b) *Response of the structure* – investigating the structural and kinematic responses of the demining equipment and vehicle, including the shape of the vehicle's chassis and the blast attenuation material.
(c) *Vulnerability of human being* – assessment of the effects caused by the high shock pressures, the spalling of materials and the vertical and lateral motion of the vehicle as a result of the explosion.

The research in these three areas can generally be split into two approaches; numerical and experimental.

Experimental activities: Experiments have been conducted to investigate the response of a vehicle subjected to a mine explosion in order (i) to analyse the gross motion and damage to the vehicle, (ii) to assess effects on the occupants and (iii) to evaluate attenuation materials [1;8-10]. These experimental results have led to design proposals, in earlier vehicles, such as deflector plates fitted under the wheel wells and fuel tanks placed in rear of vehicle. More recent developments have wheels located outside of the crew compartment and the V-shaped hull designed to fit in between. Experiments studying explosion output have shown that mine deployment and soil compositions, especially moisture content, have a significant effect on the magnitude of vehicle loading. The most severe loading is obtained from explosion of mines buried in a cohesive soil, such as clay [11-13].

Numerical Simulations: Finite Element Analysis (FEA) is widely used in defence related engineering problems, high velocity impact and penetration problems being some of the more common analyses. In preliminary works empirical formulae were implemented in simulation format to model the explosion process [14-15]. Following on from this [16-18] conducted bespoke simulations which can now allow for the study of the explosion process from the initiation of the charge. Table 1 outlines studies looking at the simulation of mine explosions, focusing on the parameters dominant to explosion loading.
The focus of this paper is on determining the severe loading caused by a mine explosion. The degree of loading varies depending on the way the mine is implemented. Figure 1 shows the different methods of deployment. They are either (a) spread on the surface of the ground, (b) laid flush with the ground level or (c) buried in the soil (20mm – 60mm, uniquely 400mm [19]. Two or more mines may also be stacked in the same place.
For every deployment of a mine the soil conditions will have an effect on the result of the explosion, even though part of the explosive energy will be dissipated through the soil. The soil impinging on the target will considerably contribute to the loading that the target sees. Depth of burial and soil composition, therefore have significant roles in the loading magnitude.

This paper looks at the numerical analysis of a mine explosion using the commercially available software AUTODYN. In order to validate the simulation model the experimental work conducted by Bergeron *et al.* [12] was replicated. These AUTODYN results were then compared with other results obtained using LS-DYNA, another finite element program, from Wang [23]. The experiments modelled were of a buried and flush high explosive charge in sand.
The remainder of this paper is organised in the following format. The next section covers the rudiments of explosion modelling, and the subsequent sections discuss the simulation framework proposed and the numerical results obtained from the simulation runs. The paper concludes with a discussion of the results.

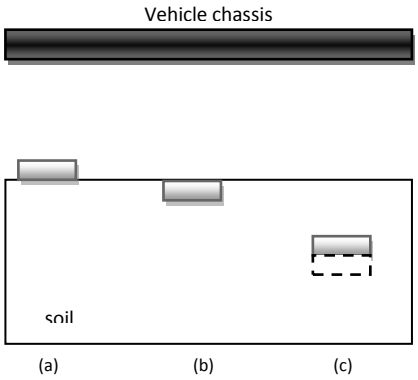

Figure 1: The scheme of mine deployment: (a) surface laid mine, (b) flush mine, (c) buried mine

Table 1 Overview of numerical modelling of a mine explosion

Source	Code	Mesh size (mm)	Explosive EOS	Soil model	Stand-off distance (m)	Note
Laine *et al*. [18]	AUTODYN	8	10.4kg Composition B: JWL EOS	Sand [20]	0.4 till 1; 100mm soil cover	Analysis of pressure and impulse magnitude were conducted for buried, flush and surface laid charge.
Fairlie *et al*. [17]	AUTODYN	25 (air)	1kg C-4 Ideal gas EOS	Sand [20]	0.4; 50mm soil cover	Total momentum imparted to the pendulum was observed and compared with experiments
Grujicic *et al*[21]	AUTODYN	-	C-4 JWL	CU-ARL[22]	0 – 0.4; 0.1-0.8 soil cover	The impulse delivered to a vertical impulse measurement fixture (VMIF) was measured and compared with experimental results.
Wang [23]	LS-DYNA	-	100g C-4 JWL	Sand	0.3 and 0.7	Pressure and ejecta forming were investigated and compared with experiments[12].
Cheng *et al*. [16]	AUTODYN & MSC. Dytran	10	5kg TNT: JWL	Rigid surface	0.56	Output parameter was the deflection of box
Williams *et al*. [24]	LS-DYNA	-	7.5kg C-4	ρ= 2170kg.m^{-3}	-	Blast was introduced through initial velocity boundary condition obtained from *empirical impulse* model. Output parameter was floor deflection
Gupta [14]	LS-DYNA	-	907.2g Pentolite	-	1.52	CONWEP algorithm was implemented into LS-DYNA to generate blast pressure loading. Response of composite panel was investigated.
Niekerk [25]	MSC. Dytran	-	800g pentolite	Rigid surface	0.5	Pressure analysis resulted in 24% underestimated prediction. Experiment data varies from 38-81MPa.
Absil *et al*. [26]	AUTODYN	2	475g Composition B	-	0.2	Impact of fragments from steel casing on aluminium plates was investigated.
Dorn *et al*. [27]	FLUENT & LS-DYNA	Interaction of blast wave with vehicle and occupant injuries (DYNAMAN model)				
Jacko *et al*. [28]	AUTODYN		500g TNT			Response of armour plate subjected to contact explosion, was studied.

EXPLOSION MODELLING

Using the laws of conservation of mass, momentum and energy a general system of equations can be formulated to describe an explosion.

There are supplementary equations that can be used to describe detonation theory such as the Chapman-Jouguet equation [29-30], and include material properties of the explosive products, soil and air.

These material models play an important role in linking the stress to the deformation and internal energy. The explosive products and the surrounding air is modelled using an equation of state (EOS). This equation represents the relationship between the pressure, p, the specific volume, v, and the temperature, T, for example:

$$p = f(v, T) \quad \textbf{(1)}$$

Additional components are needed for modelling the soil. These components are known as strength and failure models. The strength model describes the materials resistance to shear and is represented by yield criterion, which describes the transition between the elastic and plastic regimes. The failure model used here is a simple one that covers the tensile strength limit which the material can withstand.

High explosives are generally modelled using an equation of state that can be classified into one of two types outlined below:

(a) Equations of state *without explicit chemistry* for a particular composition of explosive are based on experimental data to derive the formulae.
(b) Equation of state *with explicit chemistry* contain individual equations for the component molecules and rules for their combining together to give an EOS for any composition of explosive.

In choosing the appropriate equation of state the application, the required accuracy and the method

of solution are the main factors to take into account.
The empirical Jones-Wilkins-Lee (JWL) EOS calculated without explicit chemistry, is widely used in mine blast calculations. It has been implemented in codes such as LS-DYNA and AUTODYN. To derive this EOS a cylinder expansion test was implemented (see [31]). This test comprises a copper tube containing explosive which is detonated and the cylinder wall acceleration caused by the explosive products is captured on high speed camera, until the cylinder wall has reached three times its original diameter.

The resulting empirical equation is a pressure-volume relationship independent of temperature. In AUTODYN the JWL EOS is implemented as shown in equation (2) below:

$$p = A\left(1 - \frac{\omega}{R_1 V}\right)e^{-R_1 V} + B\left(1 - \frac{\omega}{R_2 V}\right)e^{-R_2 V} + \frac{\omega E}{V} \quad (2)$$

Where A [Pa], B [Pa], R_1, R_2 and ω are coefficients which depend upon the composition of the explosive. The variable $V = {}^{v}/_{v_0}$ is the expansion of the explosive products and E [J.m^{-3}] is the detonation energy per unit volume.

The surrounding air was assumed to be an ideal gas whose equation of state is in the form:

$$p = (\gamma - 1)e\rho$$

Where γ, is the adiabatic exponent, e [J.kg^{-1}] is the specific internal energy and ρ [kg.m^{-3}] is the density.

The sand model used was of a porous material derived by Laine *et al.* [20]. The EOS describes the compaction, a granular strength model, the yield surface dependence on pressure and assumes negligible tensile strength.

This model was derived for the use of modelling sand with a dry density of 1,574kg.m^{-3} and an average water content of 6.57% [20].

SIMULATION SETUP

In order to validate the numerical procedure the models replicated the experiments conducted by Bergeron *et al.* [12]. A two-dimensional axi-symmetric model was set up in AUTODYN. The mine was represented by a 100g of C-4, which was described by the JWL EOS [32].

Two deployments were investigated: (a) a buried charge with 30mm of sand coverage, and (b) a flush charge with the top surface level with the ground surface. Measuring gauges were placed at 300mm and 700mm above the ground surface. The configurations are shown in Figure 2.
A mesh sensitivity study was conducted with mesh sizes of 4, 2, 1 and 0.5mm. The values of maximum overpressure and specific impulse converged at 1 and 0.5mm mesh sizes. Therefore a mesh size of 1mm was used.

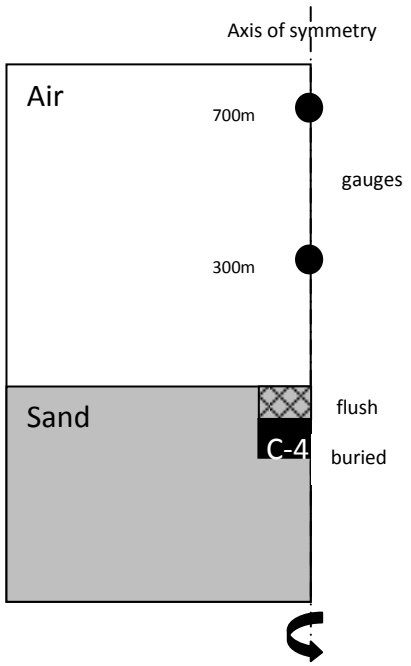

Figure 2 Experimental setup in AUTODYN

RESULTS

The results have been compared with the experimental data from Bergeron *et al.* [12] and with the numerical results from Wang [23] obtained using the software LS-DYNA.

The shock wave parameters: time of arrival, maximum overpressure and specific impulse from both the numerical methods and the experimental procedures are shown in Table 2. These are also shown in Figure 3. The error bars show the range of experimental data, so that it is possible to see where the numerical results fall within this range.

Time of arrival: this is the time at which the shock wave front reaches the gauge points at a range of 300 and 700mm. The results show that at a range of 700mm the predictions are in good agreement with the experimental data for both forms of deployment. The values at a range of 300mm, however show a 20% discrepancy, overestimated for the buried charge and underestimated for the flush charge. The LS-DYNA predictions are in good agreement for all four cases.

Maximum overpressure: 3(b) shows the maximum overpressure at the two measuring locations for both types of mine deployments. There was a wide variance in the experimental data (as shown by the error bar). Except for the flush charge at a range of 300mm, the AUTODYN values fall within the range of measured data. The greatest discrepancy in the data occurred for the 300mm range over the flush charge - about 164% overestimation. For the buried charge, however, at the same range there was only a 28% overestimation. The LS-DYNA results were about 50% lower for the flush mine at both stand-off distances and were about 15% and 4% underestimated for the 300m and 700mm distances respectively.

Specific Impulse: This is the area under the pressure time curve for the positive phase duration. It can be approximated (depending on the shape of the curve) by the following equation:

$$i = {}^{1}/_{2}\, tp$$

Where *i* is the specific impulse, T is the positive phase duration and p is the maximum pressure.

The specific impulse is important when measuring blast effects as a very high pressure over a very short period of time may be less damaging than a lower pressure over a much longer period of time. The specific impulse allows for comparisons to be drawn and a better idea as to whether a blast wave is survivable.

The specific impulse is shown in Figure 3(c) for the two measuring points and scenarios. At 300mm range the AUTODYN buried charge underestimated the experimental value by 19% and LS-DYNA overestimated by 63%. At the same distance the flush charge gave a 14% higher value for the AUTODYN simulation and the LS-DYNA model was in very good agreement. At 700mm, both AUTODYN and LS-DYNA results do not fall within the measured data and are overestimated. AUTODYN overestimated by about 19% and 46% for the buried and flush mines respectively, LS-DYNA overestimated by 36% and 18% respectively.

Table 2 Shock-wave parameters

Position above soil [mm]	**Time of arrival [µs]**					
	BURIED, DOB = 30mm			**FLUSH, DOB = 0mm**		
	Measured	LS-DYNA	AUTODYN	Measured	LS-DYNA	AUTODYN
300	266	270	318	94.8	90	76
700	784	710	774	285.6	300	295

	Maximum Overpressure [kPa]					
	BURIED, DOB = 30mm			**FLUSH, DOB = 0mm**		
	Measured	LS-DYNA	AUTODYN	Measured	LS-DYNA	AUTODYN
300	724.8	613.3	929.7	2797	1359	7380
700	304.5	290.1	334.1	1189	580.8	1409

	Specific Impulse [kPa.ms]					
	BURIED, DOB = 30mm			**FLUSH, DOB = 0mm**		
	Measured	LS-DYNA	AUTODYN	Measured	LS-DYNA	AUTODYN
300	106.8	174.5	86.1	85.8	86	98
700	57.2	77.9	68	116.4	137.5	169.6

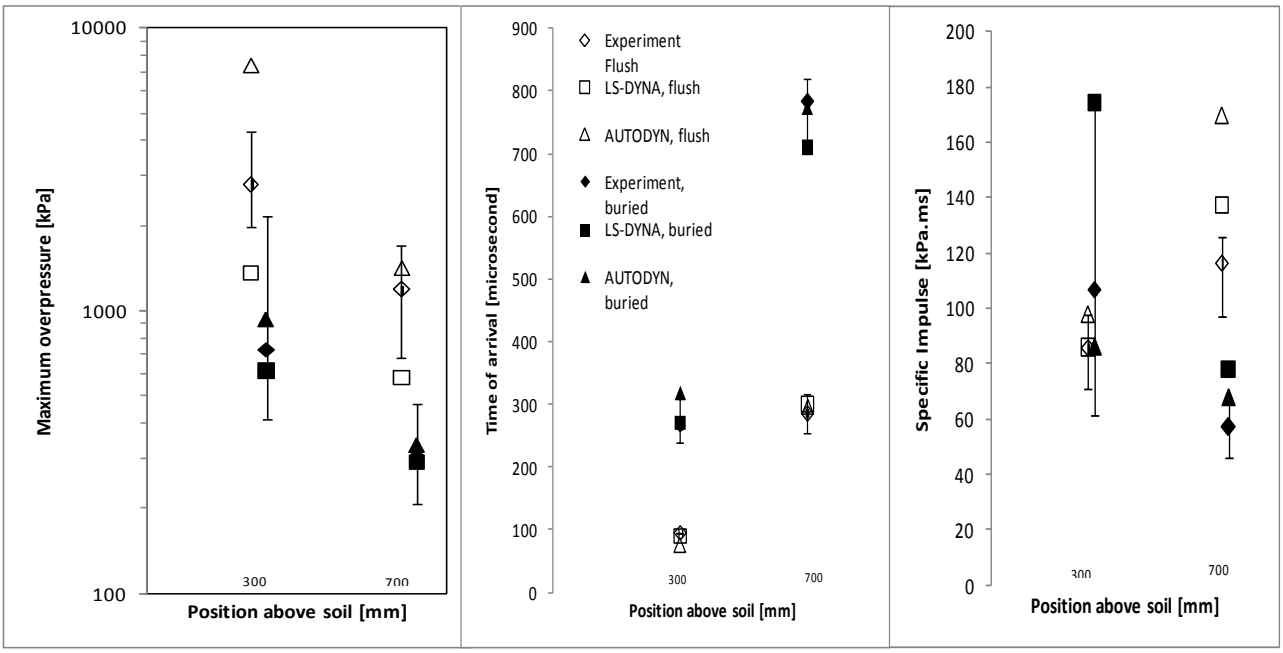

(a) Time of arrival **(b) Maximum overpressure** **(c) Specific impulse**

Figure 3 Shockwave parameters

DISCUSSION

The numerical results obtained by using AUTODYN, for the 700mm range are in better agreement with the experimental data than for the 300mm range. This is consistent with previous findings, by some of the authors, that the convergence of numerical results, with experiment occurs with increased range from the centre of the charge [33].

The blast output is commonly assessed in terms of scaled distance, which is defined by;

$$Z = {}^{R}/_{W^{1}/_{3}} \qquad \textbf{(5)}$$

Where R[m] is the distance from charge centre and W [kg] is the TNT equivalent charge mass. The simulations here, where 100g of C-4 is assessed at 300 and 700mm ranges, correspond to scaled distances of 0.636 and 1.484m.kg$^{-1/3}$ respectively.

Since numerical solutions are used as a tool for improving the design of vehicles subjected to mine blasts, it is important to consider the results obtained with this in mind. When determining severe loading and the worst case scenario, conservative estimates are much preferred than non-conservative estimates.

Generally damage to a target can be caused by the following modes [34]:

Overpressure can be responsible for damage if the vibration period of the target is short relative to the positive phase duration. The AUTODYN results vary from 10 to 164% discrepancy from the measured data but in overestimation. Whilst the LS-DYNA results may have smaller discrepancies (between 5 and 51%) they are all underestimated. In this particular case an overestimation is better suited for design purposes than an underestimation. So the LS-DYNA results could be unsafe when looking at protective design.

Specific impulse can govern the damage if the vibration period of the target is long relative to the positive phase duration. Both numerical models here overestimate, with the exception of the AUTODYN prediction of the buried charge at 300mm, which underestimates at around 19%. Both models here would provide good, though slightly conservative, models for protective design.

CONCLUSIONS

This paper has introduced non-experimental, numerical techniques for modelling mine blast and the subsequent interactions with surrounding material. The results obtained, on the whole, have been compared favourably with published experimental data. As a result of this we believe that using numerical modelling to simulate mine explosions offers a cheaper alternative, especially in the early stages of testing, to experimental work.

Shock-wave parameters were investigated for the two types of mine deployments in sand. Apart from in one instance (maximum pressure at 300mm for the flush mine) the AUTODYN results are in good agreement with the experimental data. The LS-DYNA results are all underestimated apart from the Specific impulse at 300mm from the buried mine, which is around 65% overestimated.

REFERENCES

[1] Bird, R., (2001), *Protection of Vehicles against Landmines*.

[2] International Campaign to Ban Landmines (2009), "Landmine Monitor Report 2009: Toward a mine-free world.", [Online], available at: http://lm.icbl.org/index.php/publications/display?url=lm/2009/es/major_findings.html.

[3] , *iCasualties: Operation Enduring Freedom* (2010), available at: http://www.icasualties.org/OEF/ (accessed March 4th).

[4] Chassillan, M. V. (2004), In *9th European Armoured Fighting Vehicle Symposium*, .

[5] Greuter, A., (2004), *MOWAG - mine protection solution LAV's PIRANHA/EAGLE IV*, Cranfield University [RMCS], Shrivenham, UK.

[6] Hetcher, B., (2004), *The Value of Landmine Protection Simulation in Vehicle Design*, Cranfield University [RMCS], Shrivenham, UK.

[7] Ravid, M. and Ziv, D., (2004), *Protection and Survivability of Light AFV and Support Vehicles*, Cranfield University [RMCS] Shrivenham, UK.

[8] Alem, N. M., Strawn,G.D. (1996), Evaluation of an Energy Absorbing Truck Seat for Increased Protecttion from Landmine Blast, , Technical report, U.S. Army Aeromedical Research Laboratory, Fort Rucker, Alabama, USA.

[9] Holland, S., (2001), *The Application of the TABRE attenuation System to Vehicles for Enhanced Underside Blast Protection*, Cranfield University [RMCS], Shrivenham, UK.

[10] Nell, S., (2000), *Test and Evaluation of Landmine Protected Wheeled Vehicles*, Cranfield University [RMCS], Shrivenham, UK.

[11] Bergeron, D.M. and Tremblay, J.E., (2000), *Canadian Research to Characterise Mine Blast Output*, Cranfield University [RMCS], Shrivenham, UK.

[12] Bergeron, D.M., Walker, R. and Coffey, C., (1998), *Detonation of 100g Anti-Personnel Mine Surrogate Charges in Sand: A Test Case for Computer Code Validation*.

[13] Held, M., (2002), *Momentum Distribution of Anti-Tank Mines*, Orlando, USA.

[14] Gupta, A.D., (2002), *Modelling and Analysis of Transient Response in a Multilayered Composite Panel due to Explosive Blast*, Orlando, Florida, USA.

[15] Williams, J., (1999), *Anti-Tank Landmines - The Threat*, Cranfield University [RMCS], Shrivenham, UK.

[16] Cheng, Q.H., Lu, C., Tan, X.M. and Tham, C.Y., (2002), *Response of a Box-Like Structure to Nearby Explosion*, Defence Science and Technology Agency, Singapore.

[17] Fairlie, G. and Bergeron, D., (2002), *Numerical Simulation of Mine Blast Loading on Structures*, Las Vegas, Nevada, USA.

[18] Laine, L., Ranestand, O., Sandvik, A., Snekkevik,A. (2001), "Numerical Simulation of Anti-Tank Mine Detonations", *12th APS Topical Group Conference on Shock Compression of Condensed Matter*, Atlanta, USA, .

[19] Colin, K., (1997), , Jane's Information Group Ltd, Coulsdon, UK.

[20] Laine, L., Sandvik,A. (2001), "Derivation of Mechanical Properties for Sand", Proceedings of the 4th Asia-Pacific Conference on Shock and Impact Loads, Singapore, pp. 361.

[21] Grujicic, M., Pandurangan, B., Huang, Y., Cheeseman, B. A., Roy, W. N. and Skaggs, R. R. (2007), "Impulse loading resulting from shallow buried explosives in water-saturated sand", *Proceedings of the Institution of Mechanical Engineers, Part L: Journal of*

Materials: Design and Applications, vol. 221, no. 1, pp. 21-35.

[22] Grujicic, M., Pandurangan, B. and Cheeseman, B. A. (2006), "The effect of degree of saturation of sand on detonation phenomena associated with shallow-buried and ground-laid mines", *Shock and Vibration*, vol. 13, no. 1, pp. 41-61.

[23] Wang, J. (2001), Simulation of Landmine Explosion Using LS-DYNA Software: Benchmark Work of Simulation of Explosion in Soil and Air, , Australia.

[24] Williams, K., Poon,K.A. (2000), A Numerical Analysis of the Effect of Surrogate Anti-Tank Mine Blasts on the M113, , Valcartier, Canada.

[25] Niekerk, B., (2001), *Landmine Protection - Dealing with the Uncertainties*, Cranfield University [RMCS], Shrivenham, UK.

[26] Absil, L.H.J., Verbeek, H.J. and Weerheijm, J., (1997), *Combined Experimental and Numerical Study of Mine Detonations in the Vicinity of Vehicles*, DRDB, Defence Research Establishment, Suffield, Banff, Canada.

[27] Dorn, M.R., Rees, S.J. and Docton, M.K., (1999), *Improving Vehicle Resistance to Blast*, Cranfield University [RMCS], Shrivenham, UK.

[28] Jacko, M. and Bella, V., (2002), *The Simulation of Charge Detonation Action on Armour Plate*, Waplewo, Poland.

[29] Ficket, W., Davis,C.W., (1979), *DetonationID - 49*, University of California Press.

[30] Henrych, J., (1979), *The Dynamics of Explosion and its Use*, Elsevier Science Publishers, Amsterdam.

[31] Dobratz, B. M., Crawford,P.C. (1985), LLNL Explosive Handbook: Properties of Chemical Explosives and Explosive Simulants, , California, USA.

[32] Century Dynamics Limited, (1998), *AUTODYN user's documentation*, Horsham, UK.

[33] Fiserova, D., Hameed, A., Rose, T.A., Hetherington, J.G. and Prochazka, S., (2003), *Systematic Study of Simulated Mine Explosions Using AUTODYN*, University of Pardubice, Paradubice, The Czech Republic.

[34] Held, M., (1990), Similarities of Shock Wave Damage in Air and in Water.

A COMPARISON BETWEEN STEEL AND COMPOSITE V-SHAPED HULLS UNDER BLAST LOADING: AN EXPERIMENTAL APPROACH

STEPHANIE FOLLETT

CRANFIELD UNIVERSITY, SHRIVENHAM, UK.
S.FOLLETT@CRANFIELD.AC.UK
+ (44) 7793 151 102

OVERVIEW

- Experimental set-up
- Videos
- Outline of results

EXPERIMENTAL SETUP

- Third scale experiment
- Saturated sand
- Spherical 240g PE-4 buried 50mm beneath sand surface – blast scaling laws corresponds to ≈ 6.5kg
- Four different V shapes (varying angles)
- Distance from top of V to sand surface kept constant
- Displacement measured from high speed video footage

EXPERIMENTAL SETUP CONTD.

HULL CONFIGURATION

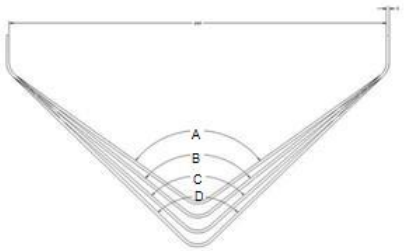

VIDEO RESULTS – SHAPE C

VIDEO RESULTS – SHAPE C

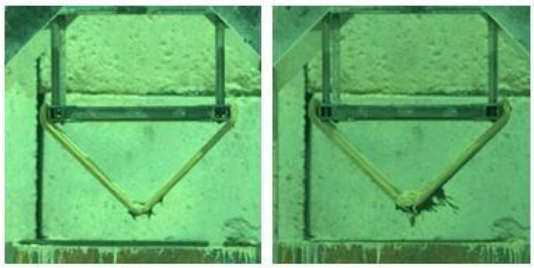

SHAPE C

SHAPE C

College of Management and Technology

SHAPE C

Composite Hull

- Poured water over underside of hull
- No perforation after three firings
- More damage to one side due to manufacturing process

Steel Hull

- No perforation, but only one firing
- Lots of deformation in comparison to composite

College of Management and Technology

RESULTS

- Using high speed video camera footage
- Tracked points on the inside of the hull to measure deformation

Correcting for camera angle and using known distances on the film can calculate displacement

Measured maximum deflection at base and at the sides

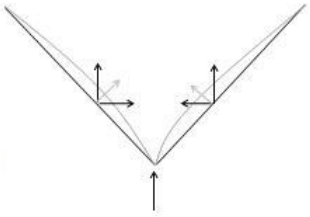

College of Management and Technology

RESULTS CONTD.

Found that: -

- *The steel V hulls exhibited at least twice the dynamic deformation of the S2 glass phenolic constructions*

College of Management and Technology

Cranfield UNIVERSITY

Department of Engineering Systems and Management

Contact: Miss S. Follett, Dr. A. Hameed, Dr. A. Motta,

s.follett@cranfield.ac.uk, a.hameed@cranfield.ac.uk, a.motta@cranfield.ac.uk,

Soil Moisture Content Effects on Blast Modelling

Numerical Modelling and Simulation - Autodyn

Technology

Simulation of soils with different composition and moisture contents and its influence on the impulse delivered to a structure caused by land mines.

Existing applications

Mine protection features for vehicles.

Opportunities for companies

Measures to mitigate blast effects on vehicles operating in different environments.

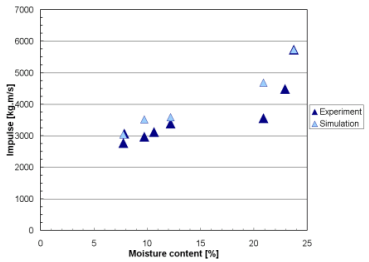

100mm depth 1kg C-4, prairie soil

Material Options

Steel vs. Composites

Technology

Composites provide a light-weight alternative when compared to steel.

Existing applications

Ballistic protection for vehicle and personnel (body armour).

Opportunities for Companies

Development and application of materials in vehicle and personnel blast protection.

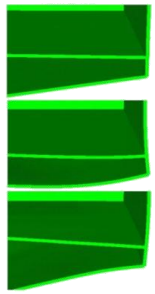

Hull Optimisation

Design: LS-DYNA & Autodyn

Technology

Simulation of vehicles with single, double floor and V-shape bottoms when submitted to blast loads.

Parametric analysis: Stand-off distance, optimum v, panel gap, hull material, panel thickness, etc.

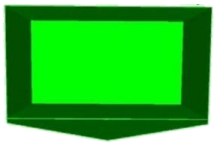

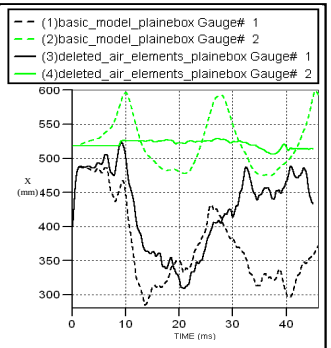

Composite Hull Design

Numerical Modelling - Autodyn

Technology

Full range of blast modelling, covering different soil mixture contents and armour materials; material assessment based on blast mitigation performance.

Existing Applications

Composite as add-on armours.

Opportunities for companies

Application of hybrid and full composite armours as structural parts with improved geometries for optimal performance.

APPENDIX 2

- STANAG 4569
- AEP 55 Vol 2 Annexe C

NATO/PFP UNCLASSIFIED

STANAG 4569
(Edition 1)

NORTH ATLANTIC TREATY ORGANIZATION
(NATO)

NATO STANDARDIZATION AGENCY
(NSA)

STANDARDIZATION AGREEMENT
(STANAG)

SUBJECT: PROTECTION LEVELS FOR OCCUPANTS OF LOGISTIC AND LIGHT ARMOURED VEHICLES

Promulgated on 24 May 2004

J. MAJ
Brigadier General, POLAR
Director, NSA

-i-

NATO/PFP UNCLASSIFIED

STANAG 4569
(Edition 1)

RECORD OF AMENDMENTS

No.	Reference/date of amendment	Date entered	Signature

EXPLANATORY NOTES

AGREEMENT

1. This NATO Standardization Agreement (STANAG) is promulgated by the Director, NSA under the authority vested in him by the NATO Military Committee.

2. No departure may be made from the agreement without consultation with the tasking authority. Nations may propose changes at any time to the tasking authority where they will be processed in the same manner as the original agreement.

3. Ratifying nations have agreed that national orders, manuals and instructions implementing this STANAG will include a reference to the STANAG number for purposes of identification.

RATIFICATION, IMPLEMENTATION AND RESERVATIONS

4. Ratification, implementation and reservation details have been provided to NSA. They are available on request or through the NSA websites (internet hrrp://nsa.nato.int ; NATO Secure WAN http://nsa.hq.nato.int).

FEEDBACK

5. Any comments concerning this publication should be directed to NATO/NSA - Bvd Leopold III, 1110 Brussels-BE

STANAG 4569
(Edition 1)

NATO STANDARDISATION AGREEMENT (STANAG)

PROTECTION LEVELS FOR OCCUPANTS OF LOGISTIC AND LIGHT ARMOURED VEHICLES

ANNEXES: A. Protection levels for logistic and light armoured vehicle occupants against KE and Artillery Threats
B. Floor protection levels for logistic and light armoured vehicle occupants against grenade and blast mine threats

RELATED DOCUMENTS:

STANAG 4164: Test Procedures for Armour Perforation Tests of Anti-Armour Ammunition

STANAG 4190: Test Procedures for Measuring Behind-Armour Effects of Anti-Armour Ammunition

MIL-P-46593A: Military Specification: Projectile, Calibre's .22, .30, .50 and 20 mm Fragment-Simulating

MIL-STD 662E: V_{50} Ballistic Test for Armour

AEP – 55: Procedures for evaluating the protection level of logisitc and Light Armoured Vehicles

AIM

1. The aim of this Agreement is to standardise protection levels for logistic and light armoured vehicle occupants to ensure that:

(a) commanders in the field can select the right equipment to fulfil a mission under a given threat;

(b) nations have a planning guide to deploy the appropriate equipment to address theatre specific threats; and

(c) nations can develop and upgrade their equipment to match given threats.

AGREEMENT

2. Participating nations agree to adopt the two lists of protection levels outlined in Annexes A and B and to use the appropriate designation when describing their protective capabilities to other NATO nations. This will ensure interoperability in multinational missions by using equipment with matching protection levels against a given threat.

3. The protection level list is based on a 90% probability of providing protection to the occupants at the given threat. The criteria used to determine protection probability and test procedures is up to the individual countries, using STANAG 4164 as guidance for the test procedures. An update of this STANAG (4569) will be produced within 3 years, when greater guidance may prove possible.

DEFINITIONS

4. The following terms and definitions are used for the purpose of this agreement:

(a) Logistic vehicle

Vehicles designed to carry miscellaneous cargo ranging from a unit's basic load of essential classes of supplies, through field maintenance/repair assets, to personnel welfare items (reference: AC/225(Panel II)WP/63).

(b) Light armoured vehicle

Vehicles which provide protection from weapons up to a maximum of 25 mm calibre.

IMPLEMENTATION OF THE AGREEMENT

5. This STANAG shall be considered to be implemented when a nation has issued the protection level lists to commanders in the field, to those responsible for deploying equipment (vehicles) and to development or testing agencies, in all instances requiring its use when describing the protection level of a national light vehicle to another NATO nation.

ANNEX A to
STANAG 4569
(Edition 1)

PROTECTION LEVELS FOR LOGISTIC AND LIGHT ARMOURED VEHICLE OCCUPANTS

Level	KE-Threat	Reference - Artillery - Threat
5	Automatic Cannon: APDS Ammunition Distance: 500 m Angle: frontal arc to centerline: ± 30° sides Included; elev. 0°	Artillery: 155mm Estimated range of burst: 25 m Angle: all around Elev. 0° - 90°
	Ammunition: 25 mm x 137 APDS-T, PMB 073 V500: 1258 m/sec; Vo: 1335 m/sec **	
4	Heavy Machine Gun: AP Ammunition Distance: 200 m Angle: azimuth 360°; elev. 0°	Artillery: 155mm Estimated range of burst: 25 m Angle: all around Elev. 0° - 90°
	Ammunition 14,5 mm x 114 API/B32; V=911 m/sec**	
3	Assault and Sniper rifles: AP tungsten carbide core Distance: 30m Angle: azimuth 360°; elev. 0°-30° Ammunition: 7,62 mm x 51 AP (WC); V=930 m/sec** 7,65 mm x 54R B32 API; V= 854 m/sec**	Artillery: 155mm Estimated range of burst: 60m Angle: azimuth 360° Elev. 0°-30°

** V = Figures are mean values: tolerance of striking velocity for an individual shot is ± 20 m/sec

ANNEX A to
STANAG 4569
(Edition 1)

2	Assault Rifles: Armour piercing steel core Distance: 30 m Angle: azimuth 360°; elev. 0°-30°	Artillery: 155 mm Estimated range of burst: 80 m Angle: azimuth 360° Elev. 0°-22°
	Ammunition: 7,62 mm x 39 API BZ; V-695 m/sec**	
1	Assault Rifles: Ball Ammunition Distance: 30 m Angle: azimuth 360°; elev. 0°-30°	Artillery: 155mm Estimated range of burst: 100m Angle: azimuth 360° Elev. 0°-18°
	Ammunition: 7,62mm x 51 NATO ball; V=833 m/sec 5,56 mm x 45 NATO ss 109; V= 900 m/sec 5,56 mm x 45 NATO M 193; V= 937 m/sec**	

** V = Figures are mean values: tolerance of striking velocity for an individual shot is ± 20 m/sec

ANNEX B to
STANAG 4569
(Edition 1)

FLOOR PROTECTION LEVELS FOR LOGISTIC AND LIGHT ARMOURED VEHICLE OCCUPANTS FOR GRENADE AND BLAST MINE THREATS

Level		Grenade and Blast Mine Threat	
4	4b	Mine Explosion under center	10 kg (explosive mass) Blast AT Mine
	4a	Mine Explosion pressure activated under any wheel or track location	
3	3b	Mine Explosion under center	8 kg (explosive mass) Blast AT Mine
	3a	Mine Explosion pressure activated under any wheel or track location	
2	2b	Mine Explosion under center	6 kg (explosive mass) Blast AT Mine
	2a	Mine Explosion pressure activated under any wheel or track location	
1	Hand grenades, unexploded artillery fragmenting submunitions, and other small anti personnel explosive devices detonated anywhere under the vehicle.		

ANNEX C DEFINITION OF TESTING CONDITIONS

C1 SURROGATE TNT MINE BURIED IN WATER SATURATED SANDY GRAVEL

Tests shall be conducted in soil with the following specifications:

Soil type: sandy gravel

Particle size analysis: 100% passing the 40 mm sieve, maximum 10% passing 80 µm, and a typical particle size curve for a sandy gravel is provided at Figure C1.

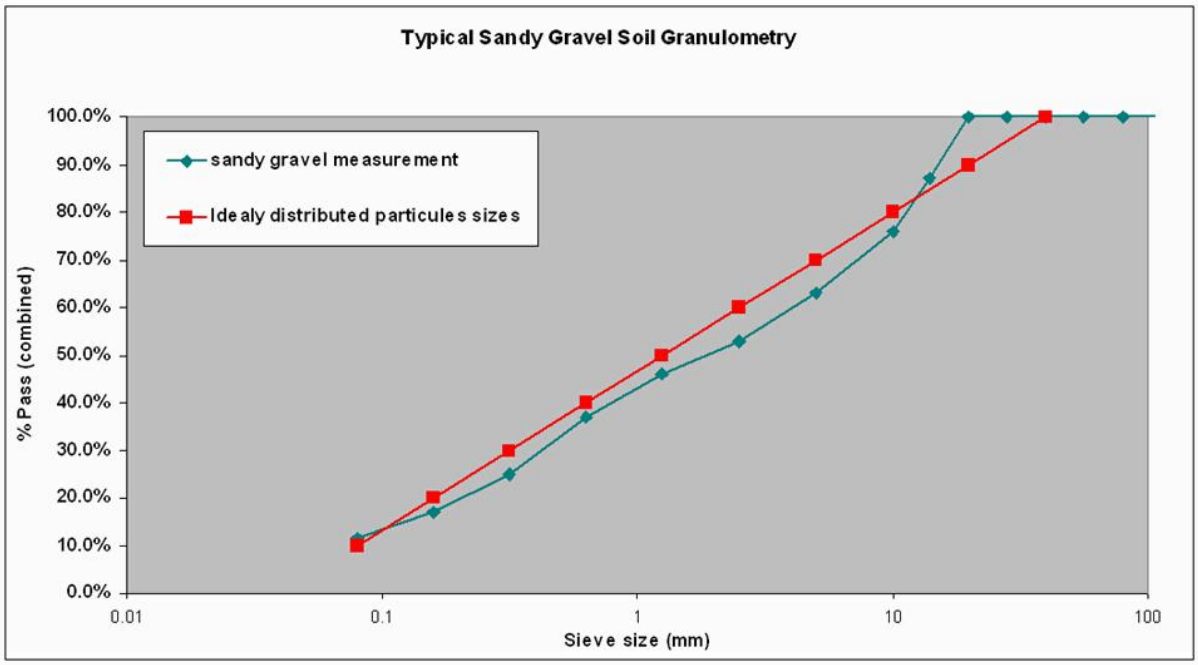

Table C1 Typical Sandy Gravel Soil Granulometry

Soil total (wet) density: 2200 +/- 100 kg/m³

The sandy gravel shall be saturated with water prior to testing. Total soil density shall be calculated using dry density measurement and soil humidity measurement. Standard methods for measuring dry density and humidity are provided in ASTM D2922-01 and ASTM D3017-01. Equivalent methods may be applied.

On-site soil measurements, pre-detonation, shall be included in the test report.

The dimensions of the test bed must be at a minimum of 2x2 m² area with a minimum depth of 1.5 m.

A constant soil quality over the entire test bed should be given.

APPENDIX 3

- Material data sheets for S2 Glass in phenolic resin
- Material data safety sheets
- Safety data sheets – phenolic resin

Section E – Properties

MECHANICAL PROPERTIES – Phenolic System (HJ1)

Property	Standard	Average
Specific Gravity	ASTM D792	1.96
Water Absorption	ASTM D570	1% (max)
Loss on Ignition	ASTM D2584	16-23%
Tensile Strength ---Modulus ---Elongation	ASTM D638	70 KSI (485 MPa) 3.6 MSI (25 Gpa) 4%
Poisson's Ratio		0.26
Flexural Strength ---Modulus	ASTM D790	26 KSI (180 MPa) 4.2 MSI (29 MPa)
Flexural Strength, wet ---Modulus, wet		18 KSI (124 MPa) 3.9 MSI (27 MPa)
Short Beam Shear	ASTM D2344	2.1 KSI (14.5 MPa)
Bearing Strength	ASTM D953	38 KSI (262 MPa)
In-plane Compressive ---Strength ---Modulus	ASTM D695	 24 KSI (165 MPa) 4.4 MSI (30 Gpa)
Normal (0°/90°) Compressive ---Strength ---Modulus		 109 KSI (750 MPa) 0.5 MSI (3.4 Gpa)

Note: Mechanical properties were determined from specimens of one half-inch thickness rather than thicknesses called out in ASTM standards.

Section E – Properties

MECHANICAL PROPERTIES – S-2 Glass®

Property	ASTM Standard	Uniply Structural	Woven Structural	Woven Ballistic
Elastic Constants		**10^6 PSI**	**10^6 PSI**	**10^6 PSI**
Longitudinal Modulus, E_L	D3039, D638	7.7 – 8.5	4 .0– 4.8	3.6 – 4.4
Transverse Modulus, E_T	D3039, D638	2.3 – 2.9	4 .0– 4.8	3.6 – 4.4
Axial Shear Modulus, G_{LT}	D3518	0.9 – 1.3	0.6 – 0.9	0.5 –0.7
Poisson's Ratio,	D3039	0.26 – 0.28	0.24 – 0.26	0.24 –0.26
Strength Properties		**10^3 PSI**	**10^3 PSI**	**10^3 PSI**
Longitudinal Tension	D3039, D638	230 – 290	80 – 120	70 - 100
Longitudinal Compression	D3410, D695	100 – 180	40 – 90	30 – 50
Transverse Tension	D3039, D638	6 – 12	80 – 120	70 – 100
Transverse Compression	D3410, D695	16 - 29	40 – 90	30 – 50
In-Plane Shear	D3518	9 – 24	17 – 50	17 – 30
Interlaminar Shear	D2344	8 – 15	4 – 6	2 – 4
Longitudinal Flexural	D790	180	47 – 90	25 – 35
Longitudinal Bearing	D953	68 – 80	50 – 80	38 – 48
Ultimate Strains		**%**	**%**	**%**
Longitudinal Tension	D3039	2.7 – 3.5	3.1 – 4.0	3.5 – 4.4
Longitudinal Compression	D3410	1.1 – 1.8	1.0 – 2.0	1.0 – 2.0
Transverse Tension	D3039	0.25 – 0.50	3.1 – 4	3.5 – 4.4
Transverse Compression	D3410	1.1 – 2.0	1.0 – 2.0	1.0 –2.0
In-Plane Shear	D3518	1.6 – 2.5	2.0 – 2.5	2.0 – 2.5
Physical Properties				
Fiber Volume (%)	D2734	57 – 63	61 – 65	61 – 65
Density (lb/in3)	D792	0.071 – 0.073	0.072 – 0.074	0.072 – 0.074
Ply Thickness		0.009 – 0.010	0.019 – 0.020	0.019 – 0.020
Thermal Transition	D4065	230 – 250	220 – 230	208 – 212
Resin Weight (%)		22 – 26	20 – 24	20 – 24

Section E - Properties Database

FIRE/SMOKE PROPERTIES - Low Pressure Polyester

As mentioned in Section C, one of the variations of the low pressure polyester system was developed especially to provide additional fire retardancy. Test panels made by this formulation were subjected to a test simulating a "HEAT" (High Explosive Anti Tank) round threat. One of the panels was filled with alumina trihydrate (35 pph of resin). One sample was unfilled and used as the control. Both materials consisted of 60 percent *S-2 Glass* woven roving by weight. Specimen surfaces were exposed to a 4-1/4-in. flame tip from a propane torch. A description of the test is in the memo reproduced on the next two pages.

Test results follow.

Propane Torch Test, Polyester Low Pressure Systems

	E780FR	E78OTD
Weight prior to test	1,940g	1,610g
Weight after burn	1,935g	1,600g
Weight loss	5g	10g
Flame exposure	10 min.	10.0 min.
Initial surface flame	45 sec.	2.5 min.
Sustained combustion	-0-	Minimal*
Flame breakthrough	-0-	-0-
Time to extinguish after flame removal	-0-	2.5 sec.
Smoke generation after flame removal	Minimal	Moderate
Smoke duration	1-1.5 min.	5 min.
Odor	Yes	Yes

*Combustion supported by two small outgassing points on surface.

Similar burn tests on the exposed cut edge of the panels resulted in almost identical results. It was concluded that the panels passed the test and that even the performance of the unfilled panels was satisfactory.

Section E - Properties Database

FIRE/SMOKE PROPERTIES - HJ1

In recent years, the effects of smoke and toxic gases have been singled out as being one of the leading causes of injury and death in fire. The requirements for interior finish materials onboard U.S. Naval ships are stated in MIL-STD-1623. There are also NAVSEA (Naval Sea Systems Command) requirements for installing aramid-reinforced armor under the FFG-7 armor program. The table below summarizes these requirements for shipboard installations. The source of this information is Naval Surface Weapons Center Report 80-302, "Material Characterization Tests Program":

Test	ASTM Method	Requirement for Index
Flame Spread Index	E-162-75	Less than 25
Oxygen Index	D-2863-74	
(a) 25°C		Greater than 27% oxygen
(b) 150°C		Greater than 27% oxygen
Smoke Obscuration Index	STP-422 (E-662)	
(a) Flaming		Less than 250
(b) Non-flaming		Less than 250

Flammability and Smoke Data

Improved polymer resistance to ignition and reduced rate of burning are key properties to delay or lessen the onset of total obscuration or combustibility for escape and/or rescue. To address this critical area, *S-2 Glass* armor system "HJ1" uses a phenolic resin matrix.

Phenolic resins are fire-resistant materials with low smoke emissions and toxicity levels. In addition, the phenolic polymer structure facilitates the formation of a high carbon form structure, or char, that radiates heat and functions as an insulator.

Section E - Properties Database

Performance Comparison

The following table is a summary comparison of fire/smoke properties of HJI laminate and Aramid-reinforced halogenated vinylester laminates.

	Limiting Oxygen Index		Smoke Obscuration		Flame Spread Index
	23°C	150°C	Flaming	Smoldering	
NAVSEA Guidelines	>27	>27	<250	<250	<25
HJ1*	56	75	30	2	1**
Aramid/ Vinylester***	39	39	405	152	13

*Data from AGY reports and Hardwood Plywood Association Test (copy of latter report at the end of this section of the manual).

**Data from FMI (Fiber Materials, Inc.) literature on typical glass/phenolic systems.

***Data from NSWC (Naval Surface Warfare Center) Report 80-302.

What the Results Mean

The oxygen index is the percent oxygen required to sustain a flame in an oxygen/nitrogen stream of air surrounding a burning 1/8 x 1/4 x 6 in. test specimen. The higher the percent oxygen, the less flammable the material is. The performance of HJI exceeds the guidelines by a 2 to 2.7 factor.

Smoke obscuration index results are expressed in terms of specific optical density, or absorbance. The test method is described in detail in the Hardwood Plywood Manufacturers Association test report at the end of this section of the manual. As noted, HJI far exceeds guidelines established for this test.

Section E - Properties Database

The flame spread index is an indication of the rate a fire may spread. Since the glass is a noncombustible inorganic and the phenolic resin is nonflammable, this specific test was not run by AGY. For reference, a value published by FMI is included.

Toxicity

While there are no formal requirements for tests other than Flame Spread Index, Oxygen Index and Smoke Obscuration Index, additional combustion gas analysis tests were made. The Drager tube gas analysis method was used at the completion of the NBS smoke obscuration test. Data is included in the table below. Data on aramid/vinyl ester is included for comparison.

Substance	Concentration (in-ppm) by system			
	HJ1*		Aramid/Vinyl Ester**	
	F	NF	F	NF
Carbon monoxide	250	60-100	1000	70
Hydrogen cyanide	1	0	10	trace
Hydrogen chloride	0	0	1.6	2
Nitrogen oxides	10+	3-5		Not tested
Hydrogen fluoride	0	0		Not tested
Carbon dioxide	1.2	0.1	0.6	0.1
Phenol	>5	>5		Not tested
Formaldehyde	3-10	0		Not tested
Isopropyl alcohol	4	2		Not tested

Note: F = flaming and NF = non-flaming.

*Hardwood Plywood Manufacturers Association Report (at the end of this section of the manual)

**NSWC TR80-302, "Material Characterization Tests Program, ASTM Flammability and Fire Shielding Test for Candidate Kevlar Reinforced (KRP) Armor for DDG 993 Class of Ships"

Section E - Properties Database

The nitrogen oxide concentration in the flaming mode exceeded the range of the specific Drager tubes used. But the relatively low level in non-flaming mode would indicate low levels in the flaming mode. Phenol concentrations also exceeded the range of the specific Drager tubes available. But the reporting personnel noted that it was also relatively low, based on the reaction of the tubes used. Carbon monoxide is at a low level and equal to or below levels of current aramid-reinforced ballistic armor laminates.

CHEMICAL AND CORROSION RESISTANCE

The U.S. Army's Belvoir Research, Development and Engineering Center at Fort Belvoir, Va., conducted a series of CARC (Chemical Agent Resistant Coating) tests on various laminate constructions. The test report (at the end of this section of the manual) points out water absorption and blistering problems with aramid composites but not with glass fiber composites.

ELECTRICAL PROPERTIES

Limited testing was performed to determine electrical properties of ballistics materials. Results follow.

	Dielectric Constant	**Loss Tangent**
Laminate	14 GHz, 75F	14 GHz. 75F
E780CM	3.6	0.012
HJ1	4.3	0.040

The ballistic materials are considered transparent to most of the electromagnetic spectrum with minimal loss of signal -- less than one decibel (<1 dB). These materials can incorporate aluminum flake, carbon black, metal facing and other additives and combinations to enhance electrical conductivity, electromagnetic interference, and similar requirements.

Section E - Properties Database

THERMAL - MECHANICAL PROPERTIES

The following pages contain results of Dynamic Mechanical Analysis (DMA) of various laminates. A comparison of E780CM polyester resin and HJI Phenolic resin samples 1 and 2 reveals the different characteristics of the two resin types. The polyester resin exhibits a well-defined transition in both its GI and GI' profile. This indicates a narrow molecular weight distribution. The phenolic resin, on the other hand, exhibits a broader transition but maintains a higher G' value beyond 130°C.

Dynamic mechanical proper ties were measured as a function of temperature in a rectangular torsion mode on the Rheometrics Dynamic Spectrometer (RDS). G' (shear storage modulus), G" (shear loss modulus), and Tan Delta (G"/G') were measured at 5°C increments from -50°C to 350°C for samples 1 and 2 and -50°C to 180°C for the E780CM polyester. Following completion of this initial temperature scan, the specimen was recooled to -50°C and a second temperature sweep conducted.

Comparisons of these "first scan" and "second scan" temperature profiles were then made to determine the polyester's initial degrees of cure. No "second scan" temperature sweeps were conducted on the other two (phenolic) samples. Rather, the HJ1 samples reflect the range in resin content, 18 percent and 23 percent, respectively. Each test was conducted at a constant strain of 0.1 percent and a constant frequency of 10 hertz. The glass transition temperature (T_g) of each sample is determined from the extrapolated onset of its GI transition.

The broad transition of HJ1 begins to drop at 300°C. The HJ1 system retains mechanic properties up to 260°C. This is also outlined in the phenolic resin Mil Spec MIL-L-9299.

Thermal Gravimetric Analysis (TGA) of the HJ1 system (phenolic 229) was conducted in air at a 30mL/minute flow rate. Substantial decomposition (weight loss) did not occur in the HJ1 system until about 350°C. The high thermal oxidative stability of HJ1 coincides with its higher fire resistance and smoke obscuration, reported elsewhere in this section.

agy

MATERIAL SAFETY DATA SHEET

Section 1: Product and Company Information

Product Name(s): **Beta®** Fibers, Cardable Fiber, Chopped Strand, Conductive Roving, Multitex, **S Glass®** Fibers, **S-2 Glass®** Fibers, Wax Bonded Strand, Polyester Combination Yarn, **VeTron™** Fibers, Yarns, or **ZenTron®** Fibers.

Manufacturer:
AGY World Headquarters
2556 Wagener Rd.
Aiken, SC 29801.
Telephone: 1-803-643-1367 (8am to 5pm ET, weekdays)

Emergency Contacts:
CHEMTREC (24 hours everyday): 1-800-424-9300

Health and Technical Contacts:
1-888-434-0945 (8am to 5pm ET, weekdays)

Beta® is a trademark of AGY
S Glass® is a trademark of AGY
S-2 Glass® is a trademark of AGY
ZenTron® is a trademark of AGY

Section 2: Composition and Ingredient Information

Common Name	CAS No.	Wt. %
Fiber Glass (non respirable)*1	65997-17-3	98 - 100
Size*2	NA	0 -2 %

Note: *1 – As manufactured continuous filament glass fibers are not respirable. Continuous filament glass products that are chopped, crushed or severely mechanically processed during manufacturing or use may contain a very small amount of respirable particulate, some of which may be glass shards. See Section 8 of Material Safety Data Sheet for exposure limit data.
*2 - See Section 15 of MSDS for concentrations of California Proposition 65 chemicals and other regulatory information relative to this product(s).

Component Related Regulatory Information
This product may be regulated, have exposure limits or other information identified as the following: glass wool fiber, fibrous glass and nuisance particulates.

Component Information/Information on Non-Hazardous Components
No additional information available.

agy

MATERIAL SAFETY DATA SHEET

Section 3: Hazards Identification

Emergency Overview

No unusual conditions are expected from this product

Appearance and Odor: White/off-white colored solid with no odor.

Primary Route(s) of Exposure: Inhalation, lungs, skin, eye

Potential Health Effects:

Inhalation:
Dusts and fibers from this product may cause mechanical irritation of the nose, throat and respiratory tract.

Skin Contact:
Dusts and fibers from this product may cause temporary mechanical irritation to the skin.

Eye Contact:
Dusts and fibers from this product may cause temporary mechanical irritation to the eyes.

Ingestion:
Ingestion of this product is unlikely. However, ingestion of product may produce gastrointestinal irritation and disturbances.

Medical Conditions Aggravated by Exposure:
Chronic respiratory and skin conditions may temporarily worsen from exposure to this product.

Chronic Conditions:
See Section 11 for additional information.

agy

MATERIAL SAFETY DATA SHEET

Section 4: First Aid Measures

Inhalation:
Move person to fresh air. Seek medical attention if irritation persists.

Skin Contact:
For skin contact, wash with mild soap and cold water. Do not wash with warm water because this will open up the pores of the skin, which will cause further penetration of the fibers. Use a washcloth to help remove fibers. To avoid further irritation, do not rub or scratch affected areas. Rubbing or scratching may force fibers into skin. If irritation persists get medical attention.

Eye Contact:
Immediately flush eyes with plenty of running water for at least 15 minutes. If irritation persists get medical attention.

Ingestion:
Ingestion of this material is unlikely. If it does occur, watch the person for several days to make sure that intestinal blockage does not occur.

Section 5: Fire Fighting Measures

Flash Point:	None	**Flash Point Method:**	Not determined
Upper Flammability Limit:	None	**Lower Flammability Limit:**	None
Flammability Classification:	Non-flammable	**Vapor Density (Air = 1):**	Not Applicable

Extinguishing Media: Water fog, foam, carbon dioxide($CO_{2)}$ or dry chemical.

Unusual Fire and Explosion Hazards: None known.

Fire Fighting Instructions: Use self-contained breathing apparatus (SCBA) and full bunker turnout gear in a sustained fire.

Hazardous Combustion Products: Primary combustion products are carbon monoxide, hydrogen, carbon dioxide and water. Other undetermined compounds could be released in small quantities.

agy

MATERIAL SAFETY DATA SHEET

Section 6: Accidental Release Measures

Containment Procedures: This material will settle out of air. If concentrated on land, it can be scooped up for disposal as non-hazardous waste. This material will sink and disperse along the bottom of waterways and ponds. It cannot easily be removed after it is waterborne; however, the material is non-hazardous in water.

Clean-Up Procedures: Scoop up material and put into a suitable container for disposal as a non-hazardous waste.

Response Procedures: Isolate area. Keep personnel away.

Special Procedures: None.

Section 7: Handling and Storage

Handling Procedures: Keep product in its packaging, as long as practicable to minimize potential dust generation. Keep work areas clean. Avoid unnecessary handling of scrap materials. Wear PPE as described in Section 8.

Storage Procedures: No special procedures.

Section 8: Exposure Controls and Personal Protection

Exposure Guidelines:
A: General Product Information: Follow all applicable exposure limits.

B: Exposure Limits:

Fiber Glass Continuous Filament (65997-17-3)

Ingredient	OSHA PEL (8-hr TWA)	ACGIH TLV (8-hr TWA)
Non-respirable fibers and particulate	15 mg/m^3 (total dust)(a)	5 mg/m^3 (inhalable fraction)
Respirable particulate	5 mg/m^3 (respirable dust)(b)	None
Respirable particulate with fiber like dimensions (glass shards)	None Established	None Established

agy

MATERIAL SAFETY DATA SHEET

Ventilation: General dilution ventilation and/or local exhaust ventilation should be provided as necessary to maintain exposures below occupational exposure limits.

PERSONAL PROTECTIVE EQUIPMENT

Respiratory Protection: A properly fitted NIOSH approved N 95 series disposable dust respirator such as the 3M model 8210 (model 8271 in high humidity environments) or equivalent should be used when high dust levels are encountered, the level of glass fibers in the air exceeds the occupational exposure limits, or if irritation occurs.

Skin Protection: Normal work clothing (long sleeved shirts and long pants) is recommended. Use gloves. Skin irritation is known to occur chiefly at pressure points such as around neck, wrists, waist, and between fingers.

Eye/Face Protection Equipment: Wear safety glasses, goggles or face shield.

Section 9: Physical and Chemical Properties

Appearance:	White/off-white Solid	**Odor:**	None
Physical State:	Solid	**pH:**	Not Applicable
Vapor Pressure (mm Hg @ 20°C):	Not Applicable	**Vapor Density (Air = 1):**	Not Applicable
Boiling Point:	Not Applicable	**Solubility (H_2O):**	Insoluble
Specific Gravity (Water=1):	2.60	**Freezing Point:**	Not Applicable
Evaporation Rate (n-Butyl Acetate = 1):	Not Applicable	**Viscosity:**	Not Applicable
VOC:	< 0.4%	**Melting Point:**	> 800°C

Physical Properties: Additional Information
No additional information available.

agy

MATERIAL SAFETY DATA SHEET

Section 10: Chemical Stability and Reactivity Information

Stability: This is a stable material.

Conditions to Avoid: None known.

Incompatible Materials: None known.

Hazardous Decomposition Products: Sizings or binders may decompose in a fire. See Section 5 of MSDS for information on hazardous combustion products.

Hazardous Polymerization: Will not occur.

Section 11: Toxicological Information

Acute Effects:

General Product Information

Dusts may cause mechanical irritation of the eyes and skin. Ingestion may cause transient irritation of throat, stomach and gastrointestinal tract. Inhalation may cause coughing, nose and throat irritation, and sneezing. People with pre-existing respiratory conditions, may experience difficulty breathing, congestion and chest tightness.

Carcinogenicity:

Fiber Glass Continuous Filament: The International Agency for Research on Cancer (IARC) in June, 1987, categorized fiber glass continuous filament as not classifiable with respect to human carcinogenicity (Group 3). The evidence from human as well as animal studies was evaluated by IARC as insufficient to classify fiber glass continuous filament as a possible, probable, or confirmed cancer causing material.

The American Conference of Governmental Industrial Hygienists (ACGIH) A4 classification, not classifiable as a human carcinogen, for respirable continuous filament glass fibers is based on inadequate data in terms of its carcinogenicity in humans and/or animals.

For respirable continuous filament glass fibers, a TLV-TWA of 1 fiber/cc was adopted to protect workers against mechanical irritation. The TLV-TWA of 5 mg/m3 was adopted for nonrespirable glass filament fiber, measured as inhalable dust, to prevent mechanical irritation of the upper respiratory tract.

Note: There are no known chronic health effects connected with long-term use or contact with these products.

agy

MATERIAL SAFETY DATA SHEET

Products that are chopped, crushed or severely mechanically processed during manufacture or use may contain a very small amount of respirable glass fiber-like fragments. NIOSH defines "respirable fibers " as greater than 5 microns in length and less than 3 microns in diameter with an aspect ratio of ≥ 5:1(length-to-width ratio).

Chronic Study in Animals

A laboratory test was conducted with a different product (special application glass fiber) with comparable composition and durability. Test animals breathing very high concentrations of respirable fibers on a long-term basis developed fibrosis, lung cancer and mesothelioma.

About 23% of the rats (n=43) exposed to 1022 f/cc for 5 hrs/day, 7 days/week for 52 weeks developed lung tumors (adenoma and carcinoma). Five percent (5%) of the unexposed control group (n=38) developed lung tumors (adenoma and carcinoma).

Five percent (5%) of the rats in the exposed group developed mesothelioma and 12.5% developed advanced fibrosis. None of the rats in the unexposed control group developed mesothelioma and 0.6 % developed advance fibrosis.

A second group of rats was exposed to a similar concentration of asbestos (respirable amosite fibers) for 5 hours/day, 7 days a week for 52 weeks. 38% of the rats developed lung tumors (adenoma and carcinoma) and 5 % developed mesothelioma. 14.5 % developed advance fibrosis.

Importantly, this result, that is similar disease rates for the special application fiber and amosite asbestos, had been predicted in a 1996 scientific paper (Inhal. Tox. 8:323-343, 1996 ref). That paper specifically stated that in rats all fibers which were durable enough to remain in a rat lung for two (2) years or more, would produce the same disease rates if the exposures were the same. While the special application fiber is much less durable than asbestos, it is stable enough to remain in the rat lung for more than the two (2) year time period. The results of the current study are therefore not unexpected, and they do not indicate that similar disease rates would be seen in longer lived species or humans, exposed to these fibers.

B: Component Carcinogenicity

Fiber Glass Continuous Filament (65997-17-3)

ACGIH: A4 – Not classified as a human carcinogen.

IARC: Group 3 "not classifiable as to its carcinogenicity to humans" October 2001 meeting

Section 12: Ecological Information

No data available for this product. This material is not anticipated to harm animals, plants or fish.

agy

MATERIAL SAFETY DATA SHEET

Section 13: Disposal Considerations

US EPA Waste Number & Descriptions:

A: General Product Information

Material, if discarded, is not expected to be a characteristic hazardous waste under RCRA.

B: Component Waste Numbers

No EPA Waste Numbers are applicable for this product's components.

Disposal Instructions

Dispose of waste material according to Local, State, Federal, and Provincial Environmental Regulations.

Section 14: Transport Information

US DOT/TDG (Canada) Information

Shipping Name:	Not regulated for transport
Hazard Class:	None
UN/NA #:	None
Packing Group:	None
Required Labels:	None

Additional Transportation Regulations:

No additional information available.

agy

MATERIAL SAFETY DATA SHEET

Section 15: Regulatory Information

US Federal Regulations:
A: General Product Information
No additional information available.

B: Component Analysis
No additional information available.

The following is provided to aid in the preparation of SARA 311 and 312 reports.

SARA 311/312

Acute Health Hazard: Yes
Chronic Health Hazard: No
Fire Hazard: No
Sudden Release of Pressure Hazard: No
Reactive Hazard: No

C: Clean Air Act
The following components appear on the Clean Air Act – 1990 Hazardous Air Pollutants List:
None

State Regulations:
A: General Product Information
No additional information available.

B: Component Analysis – California

California Proposition 65: Chemical	CAS Number:	Concentration - Parts Per Billion (PPB) Maximum
1, 4-Dioxane	123-91-1	< 5.0
Acetaldehyde	75-07-0	< 5.0
Ethylene Oxide	75-21-8	< 5.0
Formaldehyde	50-00-0	< 12.1

Other Regulations:

A: General Product Information
No additional information available.

B: Component Analysis - Inventory

Component	CAS #	TSCA	DSL	EINECS
Fiber Glass (Continuous Filament)	65997-17-3	Yes	Yes	266-046-0

agy

MATERIAL SAFETY DATA SHEET

C: Component Analysis – WHMIS IDL

The following components are identified under the Canadian Hazardous Products Act Ingredient Disclosure List:
None

WHMIS Status: Not controlled

WHMIS Classification: None

D: Other Government Regulations

Continuous filament glass products are not classified as a "Dangerous Substance" or a "Dangerous Preparations" under the EU Directive 88/379/EEC.

1. **Classification and Labeling (EEC)** – This product is not required to be labeled under Council Directives 88/379EEC, 67/548/EEC, Annex I, and 97/69/EC.
2. **CERTIFICATION STATEMENT for:**
   Directive 2002/95/EC for RoHS and Directive 2002/96/EC for WEEE
   Based on our current glass analyses, AGY certifies that our fiberglass yarns are well below the requirements of both of these Directives.

Section 16: Other Information

HMIS and NFPA Hazard Ratings:

Category	HMIS	NFPA
Acute Health	1	1
Flammability	0	0
Reactivity	0	0

NFPA Unusual Hazards: None.

HMIS Personal Protection: To be supplied by user depending upon use.

Reasonable care has been taken in the preparation of this information, but the manufacturer makes no warranty of the merchantability or any other warranty, expressed or implied, with respect to this information. The manufacturer makes no representations and assumes no liability for any direct, incidental or consequential damages resulting from its use.

agy

MATERIAL SAFETY DATA SHEET

MSDS Change Log

Effective Date	Revisions to Section:	Supercedes
August 09.1999		**NEW**
August 31, 1999	1 – Added Trade Mark ® names	August 09, 1999
March 14, 2001	Reviewed entire MSDS & added California Proposition Chemicals data in Section 15	August 31, 1999
April 12, 2002	Reviewed entire MSDS & added VeTron ™ Trade Mark in Section 1	March 14, 2001
April 14, 2004	Reviewed entire MSDS & Changed name to "**AGY**"	April 12, 2002
April 12, 2005	Reviewed entire MSDS & added "Other Chemicals" data to Section 15	April 14, 2004
May 22, 2006	Reviewed entire MSDS & amended "Other Chemicals" data in Section 15 to remove use of Tributyl Tin Oxide (TBTO) compounds and to update per modified European Directive on Restriction of Hazardous Substances.	April 12, 2005
June 18, 2007	Added certification statement for RoHS & removed large table from Section 15. Length reduced from 15 pages to 13 pages.	May 22, 2006
October 23, 2007	Clarified certification statements for Directive 2002/95/EC for RoHS and Directive 2002/96/EC for WEEE. Length reduced from 13 pages to 11 pages.	June 18, 2007

REVISION DATE: 26/01/2009

REV. NO./REPL. SDS GENERATED :

Advanced Composites Group

SAFETY DATA SHEET
SL385 PHENOLIC PREPREG

1 IDENTIFICATION OF THE SUBSTANCE/PREPARATION AND OF THE COMPANY/UNDERTAKING

PRODUCT NAME	SL385 PHENOLIC PREPREG
PRODUCT NO.	SL385/00
APPLICATION	Phenolic resin Pre-preg
SUPPLIER	ACG Manchester Ltd Grimshaw Lane Middleton Manchester, M24 2AE Tel: +44 (0)161 6534876 (UK Office hours Only) Fax: +44 (0)161 6553673 sds@acg.co.uk

2 HAZARDS IDENTIFICATION

Not regarded as a health or environmental hazard under current legislation.

HUMAN HEALTH

The product contains small amounts of organic solvents. The hazardous properties of the product are considered limited. However, the product contains a small amount of sensitising substance which may provoke an allergic reaction among sensitive individuals.

3 COMPOSITION/INFORMATION ON INGREDIENTS

Name	EC No.	CAS-No.	Content	Classification
PHENOL	203-632-7	108-95-2	< 1%	Muta. Cat. 3;R68 T;R23/24/25 C;R34 Xn;R48/20/21/22
FORMALDEHYDE ...%	200-001-8	50-00-0	< 0.25%	Carc3;R40 T;R23/24/25 C;R34 R43

The Full Text for all R-Phrases are Displayed in Section 16

4 FIRST-AID MEASURES

INHALATION

Impregnated fabric. Unlikely to be hazardous by inhalation because of the low vapour pressure of the substance at ambient temperature. The manufactured articles. Dust may irritate respiratory system or lungs.

INGESTION

Immediately rinse mouth and drink plenty of water (200-300 ml). Do not give victim anything to drink if they are unconscious. Do not induce vomiting.

SKIN CONTACT

Remove contaminated clothing immediately and wash skin with soap and water. Contact physician if irritation continues.

EYE CONTACT

Promptly wash eyes with plenty of water while lifting the eye lids. Continue to rinse for at least 15 minutes and get medical attention.

SL385 PHENOLIC PREPREG

5 FIRE-FIGHTING MEASURES

EXTINGUISHING MEDIA
Fire can be extinguished using: Water spray, fog or mist. Foam, carbon dioxide or dry powder.

SPECIAL FIRE FIGHTING PROCEDURES
Containers close to fire should be removed immediately or cooled with water. Keep run-off water out of sewers and water sources.

UNUSUAL FIRE & EXPLOSION HAZARDS
Fire causes formation of toxic gases.

SPECIFIC HAZARDS
By fire, toxic gases may be formed (COx, NOx).

PROTECTIVE MEASURES IN FIRE
Self contained breathing apparatus and full protective clothing must be worn in case of fire.

6 ACCIDENTAL RELEASE MEASURES

PERSONAL PRECAUTIONS
Wear protective clothing as described in Section 8 of this safety data sheet.

ENVIRONMENTAL PRECAUTIONS
Avoid discharge into drains, water courses or onto the ground. Collect and dispose of spillage as indicated in section 13.

SPILL CLEAN UP METHODS
Recover the product and place in a suitable container for reuse, or Transfer to a container for disposal.

7 HANDLING AND STORAGE

USAGE PRECAUTIONS
Good personal hygiene is necessary. Wash hands and contaminated areas with water and soap before leaving the work site. Harmful vapours may be liberated during curing. Mechanical ventilation or local exhaust ventilation may be required. Ventilate well, avoid breathing vapours. Use approved respirator if air contamination is above accepted level. Do not eat, drink or smoke when using the product.

STORAGE PRECAUTIONS
Keep in original container. Store at specified temperature. Freezing. - 18 °C. Keep away from food, drink and animal feeding stuffs.

STORAGE CLASS
Chemical storage.

8 EXPOSURE CONTROLS/PERSONAL PROTECTION

Name	Std	TWA - 8 hrs		STEL - 15 min		Notes
FORMALDEHYDE ...%	WEL	2 ppm	2.5 mg/m3	2 ppm	2.5 mg/m3	
PHENOL	WEL	2 ppm(Sk)				

WEL = Workplace Exposure Limit.

INGREDIENT COMMENTS
WEL = Workplace Exposure Limits

PROTECTIVE EQUIPMENT

SL385 PHENOLIC PREPREG

PROCESS CONDITIONS
Use engineering controls to reduce air contamination to permissible exposure level.

ENGINEERING MEASURES
Observe Workplace Exposure Limits and minimise the risk of inhalation of vapours.

RESPIRATORY EQUIPMENT
Harmful vapours may be liberated during curing. If ventilation is insufficient, suitable respiratory protection must be provided.

HAND PROTECTION
Barrier cream applied before work may make it easier to clean the skin after exposure, but does not prevent absorption through the skin. Use protective gloves made of: Rubber (natural, latex). Butyl rubber or polyvinyl acetate.

EYE PROTECTION
Wear approved, tight fitting safety glasses where splashing is probable.

OTHER PROTECTION
Wear appropriate clothing to prevent repeated or prolonged skin contact.

HYGIENE MEASURES
Remove contaminated clothing and wash the skin thoroughly with soap and water after work. Wash contaminated clothing before reuse. When using do not eat, drink or smoke.

SKIN PROTECTION
Use barrier creams to prevent skin contact. Wear apron or protective clothing in case of splashes.

ENVIRONMENTAL EXPOSURE CONTROLS
Avoid release to the environment. Dispose of waste and residues in accordance with local authority requirements.

9 PHYSICAL AND CHEMICAL PROPERTIES

APPEARANCE	Viscous liquid Impregnated fabric.
ODOUR	Slight odour
SOLUBILITY	Insoluble in water

10 STABILITY AND REACTIVITY

STABILITY
Stable under normal temperature conditions and recommended use. Harmful vapours may be liberated during curing.

CONDITIONS TO AVOID
Avoid excessive heat for prolonged periods of time.

HAZARDOUS POLYMERISATION
Polymerises when heated.

POLYMERISATION DESCRIPTION
Polymerises easily with evolution of heat. Keep cool.

MATERIALS TO AVOID
Strong acids. Strong alkalis. Strong oxidising substances.

HAZARDOUS DECOMPOSITION PRODUCTS
Thermal decomposition or combustion may liberate carbon oxides and other toxic gases or vapours.

11 TOXICOLOGICAL INFORMATION

SL385 PHENOLIC PREPREG

GENERAL INFORMATION
Contains small amounts of organic solvents. Extensive use of the product in areas with inadequate ventilation may result in hazardous vapour concentrations.

SKIN CONTACT
The product contains a small amount of sensitising substance which may provoke an allergic reaction among sensitive individuals after repeated contact.

12 ECOLOGICAL INFORMATION

MOBILITY
The product is insoluble in water.

BIOACCUMULATION
Bioaccumulation is unlikely to be significant because of the low water solubility of this product.

DEGRADABILITY
This product is not expected to be readily biodegradable.

13 DISPOSAL CONSIDERATIONS

GENERAL INFORMATION
Waste is suitable for incineration. Waste is classified as hazardous waste. Disposal to licensed waste disposal site in accordance with the local Waste Disposal Authority.

DISPOSAL METHODS
Dispose of waste and residues in accordance with local authority requirements. INCINERATE. Recover and reclaim or recycle, if practical.

WASTE CLASS
Waste is classified as hazardous waste.

14 TRANSPORT INFORMATION

GENERAL

The product is not covered by international regulation on the transport of dangerous goods (IMDG, IATA, ADR/RID).

No transport warning sign required.

15 REGULATORY INFORMATION

RISK PHRASES

NC	Not classified.

SAFETY PHRASES

P14	Contains FORMALDEHYDE ...%. May produce an allergic reaction.

EU DIRECTIVES
Dangerous Substance Directive 67/548/EEC. Dangerous Preparations Directive 1999/45/EC.

APPROVED CODE OF PRACTICE
Safety Data Sheets for Substances and Preparations.

NATIONAL REGULATIONS
The Chemicals (Hazard Information and Packaging for Supply) Regulations 2002. No. 1689. The Carriage of Dangerous Goods and Use of Transportable Pressure Equipment Regulations 2007 (CDG 2007)

16 OTHER INFORMATION

GENERAL INFORMATION
The recommended curing procedures must be followed.

REVISION DATE: 26/01/2009 REV. NO./REPL. SDS GENERATED :

SL385 PHENOLIC PREPREG

ISSUED BY
Product Safety Officer

REVISION DATE 26/01/2009

SDS NO. 11152

SAFETY DATA SHEET STATUS
Approved.

DATE 26/01/2009

RISK PHRASES IN FULL

R23/24/25	Toxic by inhalation, in contact with skin and if swallowed.
R34	Causes burns.
R37	Irritating to respiratory system.
R40	Limited evidence of a carcinogenic effect.
R43	May cause sensitisation by skin contact.
R48/20/21/22	Harmful: danger of serious damage to health by prolonged exposure through inhalation, in contact with skin and if swallowed.
R68	Possible risk of irreversible effects.

APPENDIX 4

- Wet sand material models
- S2-glass material model

FIELD DEPENDANT VARIABLES	UNITS	PIECE-WISE MODEL RELATIONS									
Reference density	Kg/m^3	2080.5									
COMPACTION EQUATION OF STATE											
Density	Kg/m^3	1758.7	1760.5	1762.2	1764	1765.7	1767.5	1769.2	1770.9	1772.7	1774.4
Pressure	*MPa*	0	17.8	35.5	53.3	71.1	88.9	106	124	146	160.1
Sound speed	*m/s*	3189.2	3189.2	3189.2	3189.2	3189.2	3189.2	3189.2	3189.2	3189.2	3189.2
MO GRANULAR STRENGTH MODEL											
Pressure	*MPa*	0	17.8	35.5	53.3	71.1	88.9	106	124	146	160.1
Yield stress	*MPa*	0.556									
Density	Kg/m^3	1758.7	1760.5	1762.2	1764	1765.7	1767.5	1769.2	1770.9	1772.7	1774.4
Shear Modulus	*MPa*	133.33	133.33	133.33	133.33	133.33	133.33	133.33	133.33	133.33	133.33
PMIN FAILURE MODEL											
Hydro Tensile Limit	*kPa*	88.89									
EROSION											
Instantaneous Geometric Strain	-	2.0									

Table A5-1: Saturated sandy clay material model taken from (Grujicic et al., 2009) **used in first part of AUTODYN modelling**

FIELD DEPENDANT VARIABLES	UNITS	PIECE-WISE MODEL RELATIONS									
Reference density	Kg/m^3	2641.0									
COMPACTION EQUATION OF STATE											
Density	Kg/m^3	2046	2052	2058	2063	2069	2075	2081	2086	2092	2156
Pressure	*MPa*	0	72.28	144.58	216.8	289.1	361.4	433.7	506.3	578.3	1510
Sound speed	*m/s*	3812	3812	3812	3812	3812	3812	3812	3812	3812	3812
MO GRANULAR STRENGTH MODEL											
Pressure	*MPa*	0	30.77	61.53	92.3	123.1	153.8	184.6	215.37	246.13	-
Yield stress	*MPa*	0	9.952	32.81	68.6	117.3	178.9	253.5	253.5	253.5	-
Density	Kg/m^3	2060	2101	2442	2502	2656	2928	2954	2991	2997	3156
Shear Modulus	*MPa*	76.9	869.4	4030	4910	7770	14800	16600	36700	37300	37300
PMIN FAILURE MODEL											
Hydro Tensile Limit	*kPa*	67									
EROSION											
Instantaneous Geometric Strain	-	2.0									

Table A5-2: Saturated sand model taken from (Grujicic et al., 2009) **used for final part of AUTODYN model**

FIELD DEPENDANT VARIABLES	UNITS	ENGINEERING CONSTANTS IN DIRECTION					
		11	22	33	12	23	31
Reference density	g/cm^3	1.96					
ORTHOTROPIC EQUATION OF STATE							
Young's Modulus	kPa	$3.034e^7$	$3.034e^7$	$3.4e^6$			
Poisson's ratio	-				0.26	0.26	0.26
Shear Modulus	kPa				$4.83e^6$	$4.83e^6$	$4.83e^6$
Material axes: ijk space							
ELASTIC STRENGTH MODEL							
Shear Modulus	kPa	$6.9e^6$					
MATERIAL STRESS/STRAIN FAILURE MODEL							
Tensile Failure Stress	kPa	$6.9e^5$	$6.9e^5$	$2.07e^5$			
Max Shear Stress	kPa				$2.07e^5$	$2.07e^5$	$2.07e^5$
Tensile Failure Strain	-	0.045	0.045	0.045			
Max shear strain	-				0.05	0.05	0.05
Post failure op: Isotropic							
EROSION							
Instantaneous Geometric Strain	-	5.0					

Table A5-3: S2 Glass material model used in AUTODYN modelling

APPENDIX 5

- Drawings of equipment used for testing
- Frame as used previously, for details of rig construction and the technical drawings please see (Child, 2009).

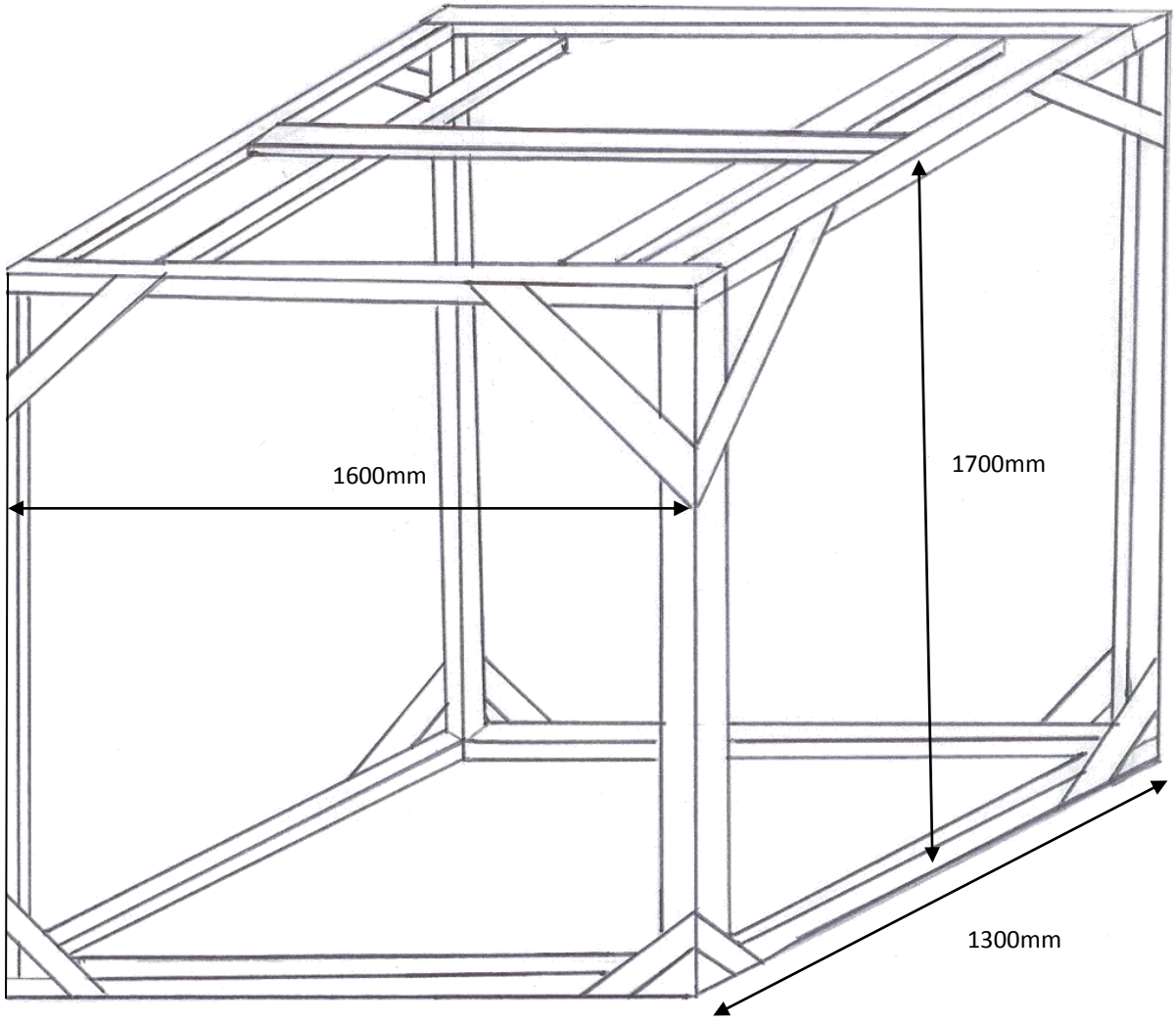

Test rig as used in previous work. For all dimensions and construction details please see {{132 Child, C. 2009}}. The frame is constructed from 5mm thick 100mm box section mild steel. With overall dimensions of 1300 x 1600 x 1700mm

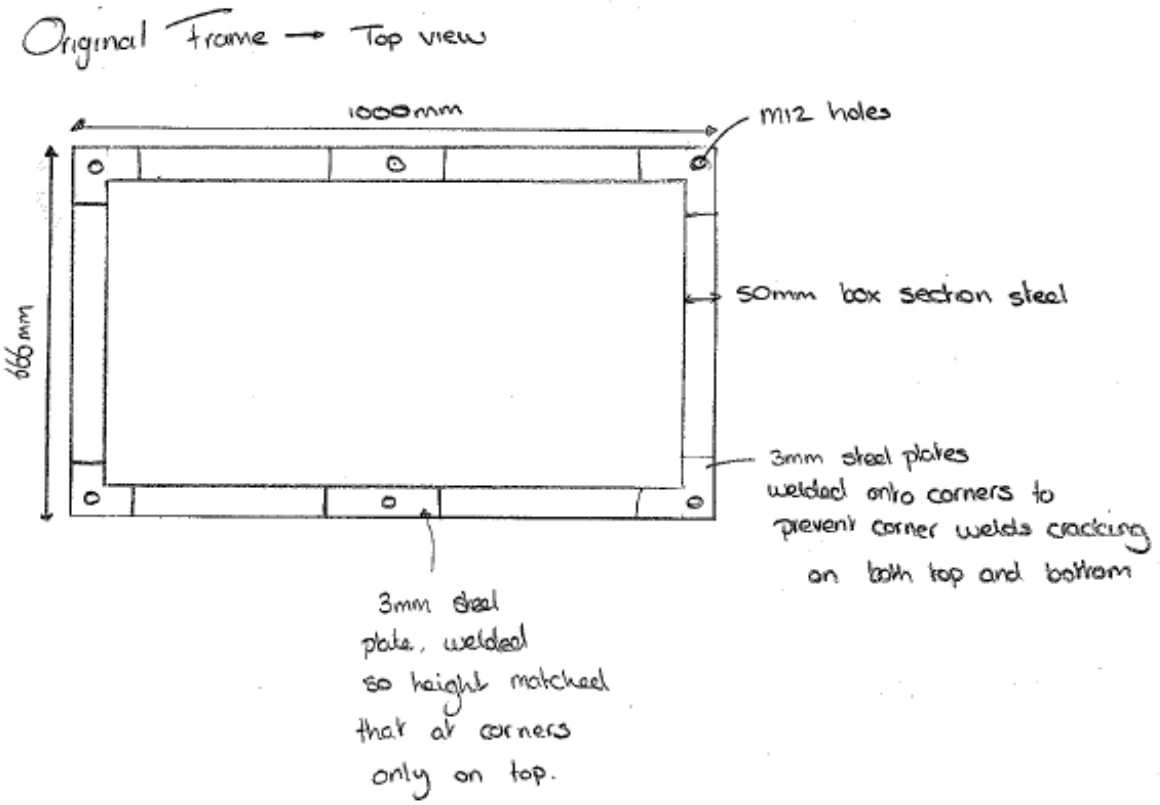

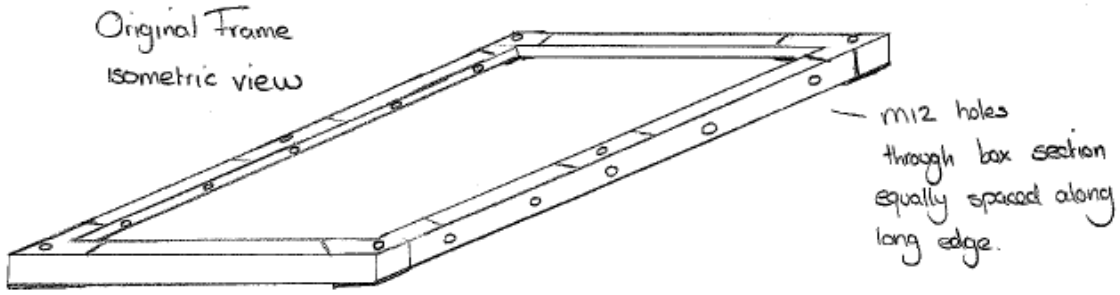

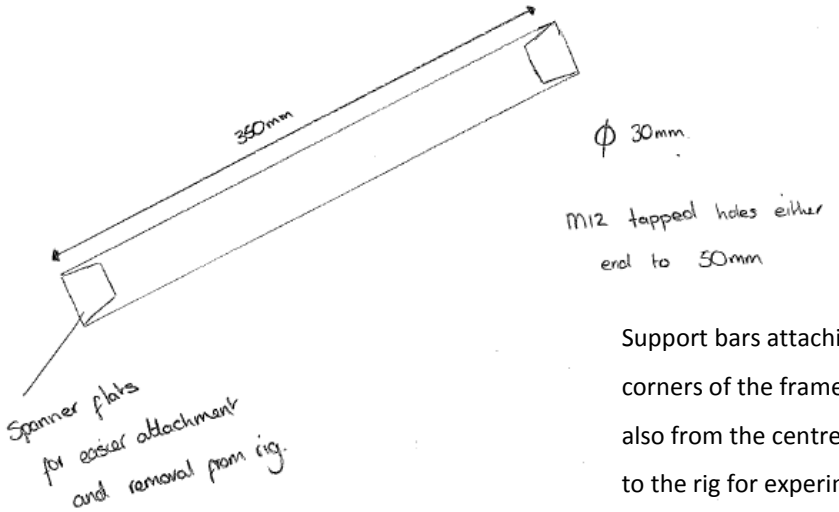

Support bars attaching frame to rig at the four corners of the frame for experiments 1 & 2 and also from the centre of the long edge of the frame to the rig for experiment 3.

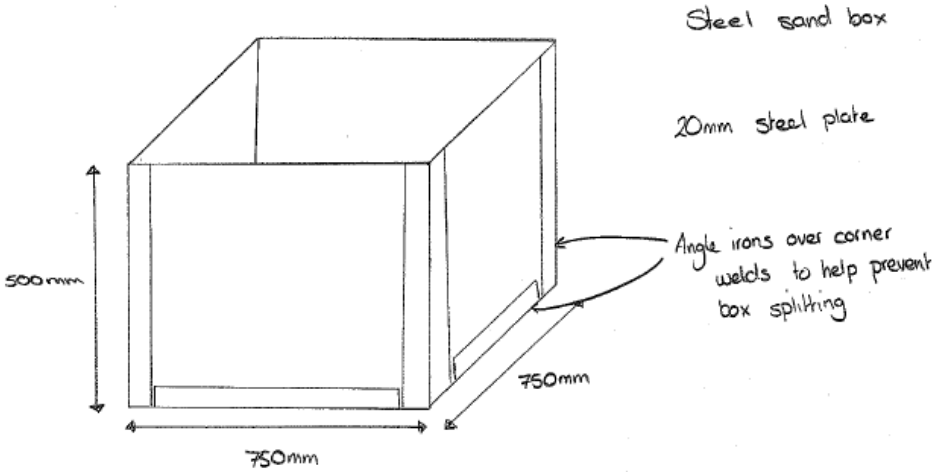

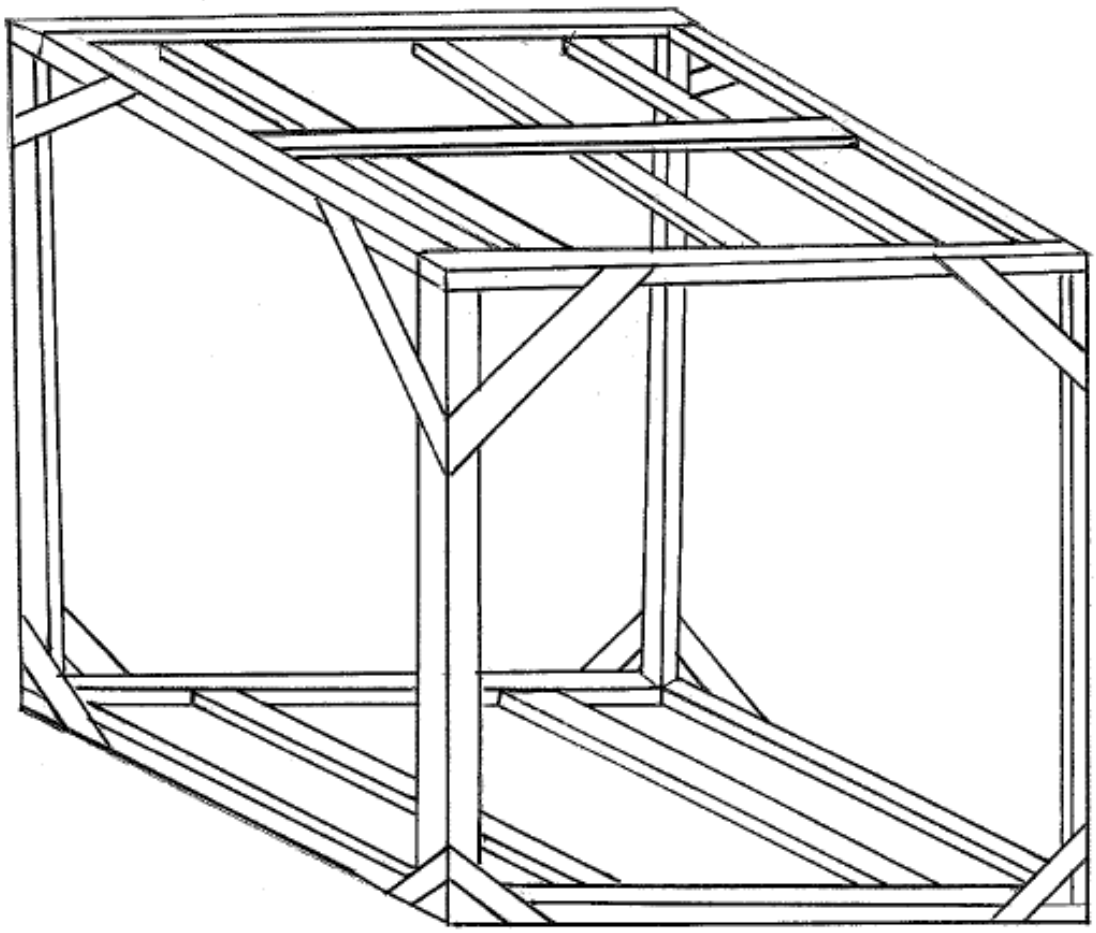

Modified rig, to include support bars on floor to make it easier to lift the steel sand container in and out of place with the forklift truck. An extra support bar on the top of the rig was also added so that the extra support bars holding the frame could be attached to the rig. All made from the same 100mm box section mild steel 5mm thick.

Modified Frame used for Experiment 3.

Top View

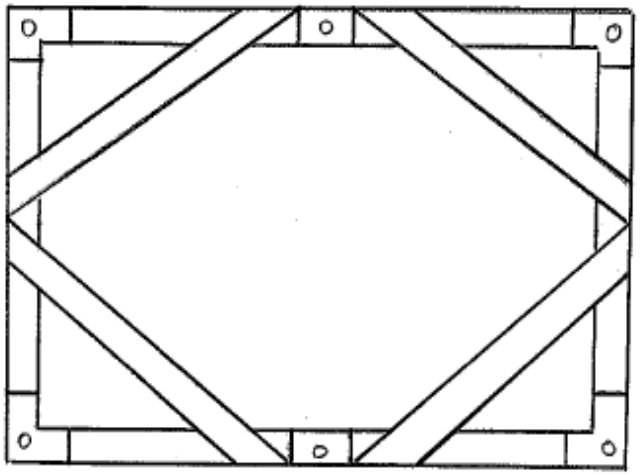

50 mm wide x 5mm thick steal bracing applied in a diamond over the top and bottom of the frame and welded in place.

Isometric view

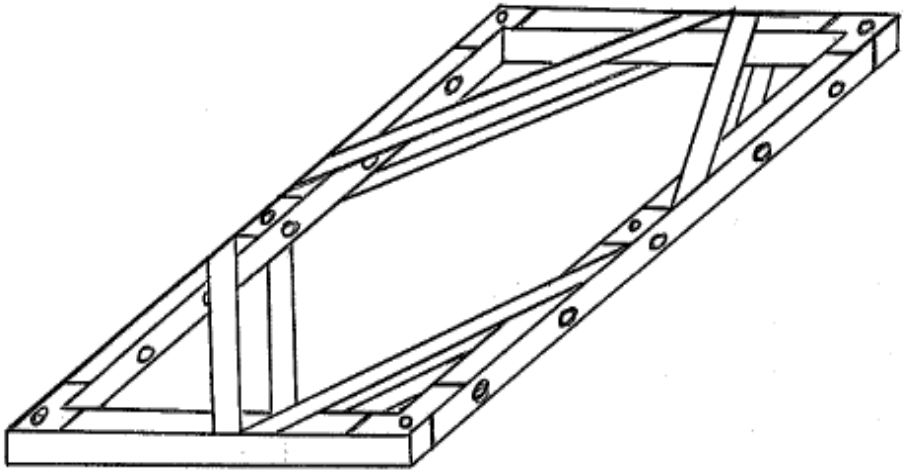

APPENDIX 6

- Flat plates range plan
- V-shaped hulls – experiment 1
- V-shaped hulls – experiment 2
- V-shaped hulls – experiment 3

Blast Testing on Composite Flat Plates

May 2010

Aim

As part of EngD work, testing will be conducted on a selection of flat composite plates in order to validate a numerical model.

The amount of explosive will vary: 75g, 130g, 185g x2, 240g and 300g, and will be buried in sand. The explosive will act upon an exposed composite plate 400x400mm (exposed dimensions) held in place within a purpose built test rig. The aim is to compare the results with numerical data in order to validate a material model and to then see if composites can be used for blast protection.

Location

Testing will be conducted outside at the ERDA on the hard standing. The plates will be secured in a test rig built by Cranfield University workshops.

Test Date

Starting the 18th May 2010 for two days

Personnel

Stephanie Follett

Professor Ian Horsfall

Graeme Creighton

Helen Jones

Equipment

The following equipment will be required to complete the testing:

1. Blast rig, delivered Monday 17th May 2010
2. Six composite plates, 500x500mm supplied by NP Aerospace and machined to be held in blast rig
3. Spherical test charges PE4 totalling 1.115kg
4. Six L2A2 detonators
5. Sharp sand for burying charge
6. Pre-built container for holding sand and locating charge
7. High speed video camera

Test Conduct

All tests will use the same procedure

1. The composite plate will be located in the test rig and secured with sixteen M10 bolts
2. The stand-off distance will be kept the same for each test

3. The high speed video camera will be set up at one end of the test rig to capture the complete process
4. The sand container will be placed below the rig in the centre
5. The sand container will be filled with sharp sand
6. The spherical charge will be located 50mm below the surface of the sand, directly beneath the centre of the plate
7. Only one charge will be detonated beneath each plate

Blast Testing on Steel and Composite V shaped hulls

May 2010

Aim

As part of EngD work, testing will be conducted on a selection of V-shaped hulls made from S2 glass composite and steel in order to determine if the composite is a viable alternative to steel for blast protection. The hulls will be scaled to 1/3rd of intended size.

240g of PE4 will be buried in fully saturated sand. This will act upon the underside of a V-shaped hull held in place in a purpose built blast test rig, with the aim of producing a numerical model to predict the material response.

Location

Testing will be conducted outside at the ERDA on the hard standing. The test pans will be secured in a test rig built by Cranfield University workshops.

Test Date

Following after flat plate tests for approximately three days.

Personnel

Stephanie Follett

Professor Ian Horsfall

Graeme Creighton

Helen Jones

Atul Khare

Equipment

The following equipment will be required to complete the testing:

1. Blast rig, delivered Monday 17th May 2010
2. Three composite V-shaped hulls, provided by NP Aerospace and three steel hulls, provided by Cranfield University workshops, at three different angles
3. Spherical test charges PE4 totalling 1.44kg
4. Six L2A2 detonators
5. Sharp sand for burying charge, and water for saturating the sand
6. Pre-built container for holding sand and locating charge
7. High speed video camera

Test Conduct

All tests will use the same procedure

1. The test pan will be located in the test rig and secured with ten M12 bolts, five along each side.

2. The stand-off distance will vary for each test but the distance from the top of the test pan to the sand will be kept constant.
3. The high speed video camera will be set up at one end of the test rig to capture the complete process
4. The sand container will be placed below the rig in the centre
5. The sand container will be part filled with sharp sand and then fully saturated in water
6. The spherical charge will be located 50mm below the surface of the sand, directly beneath the centre of the hull
7. Only one charge will be detonated beneath each hull

Blast Testing on Steel and Two Types of Composite V shaped hulls

November 2010

Aim

As part of EngD work, testing will be conducted on one V-shaped hull made from S2 glass composite E-glass composite and steel in order to determine if the composite is a viable alternative to steel for blast protection. The hulls will be scaled to 1/3rd of intended size.

240g of PE4 will be buried in fully saturated sand. This will act upon the underside of a V-shaped hull held in place in a purpose built blast test rig, with the aim of producing a numerical model to predict the material response.

Location

Testing will be conducted outside at the ERDA on the hard standing. The test pans will be secured in a test rig built by Cranfield University workshops.

Test Date

November/December 2010 one day only

Personnel

Stephanie Follett

Graeme Creighton

Alan Peare

Mike Teagal

Equipment

The following equipment will be required to complete the testing:

1. Blast rig, already in place on ERDA
2. One S2-glass composite hull, one E-glass composite hull and one steel hull all at the same angle
3. Spherical test charges PE4 totalling 0.72 kg
4. Three L2A2 detonators
5. Sharp sand for burying charge, and water for saturating the sand
6. Three plastic boxes for containing saturated sand
7. Pre-built container for containing the plastic box
8. High speed video camera

Test Conduct

All three tests will use the same procedure

1. The test pan will be located in the test rig and secured with ten M12 bolts, five along each side.
2. The stand-off distance will vary for each test but the distance from the top of the test pan to the sand will be kept constant.
3. The high speed video camera will be set up at one end of the test rig to capture the complete process
4. The plastic box will be placed inside the steel container below the rig in the centre
5. The plastic box will be part filled with sharp sand and then fully saturated in water
6. The spherical charge will be located 50mm below the surface of the sand, directly beneath the centre of the hull
7. Only one charge will be detonated beneath each hull

Blast Testing on Steel and Two Types of Composite V shaped hulls

May 2011

Aim

As part of EngD work, testing will be conducted on a variety of V-shaped hulls, four shapes in three different materials totalling twelve tests. The hulls will be scaled to 1/3rd of intended size.
240g of PE4 will be buried in fully saturated sand. This will act upon the underside of a V-shaped hull held in place in a purpose built blast test rig, with the aim of producing a numerical model to predict the material response.

Location

Testing will be conducted outside at the ERDA on the hard standing. The test pans will be secured in a test rig built by Cranfield University workshops.

Test Date

May 23rd for four days

Personnel

Stephanie Follett

Graeme Creighton

Helen Jones

Alan Peare/Mike Teagal/Dave Miller

Equipment

The following equipment will be required to complete the testing:

1. Blast rig, already in place on ERDA
2. Twelve test pans, four different shapes in three materials, all composites supplied by NP Aerospace and the steel by the Cranfield University workshops.
3. Spherical test charges PE4 totalling 2.88 kg
4. Twelve L2A2 detonators
5. Sharp sand for burying charge, and water for saturating the sand
6. Twelve plastic boxes for containing saturated sand
7. Pre-built container for containing the plastic box
8. High speed video camera

Test Conduct

All tests will use the same procedure

The test pan will be located in the test rig and secured with ten M12 bolts, five along each side.

1. The stand-off distance will vary for each test but the distance from the top of the test pan to the sand will be kept constant.
2. The high speed video camera will be set up at one end of the test rig to capture the complete process
3. The plastic box will be placed inside the steel container below the rig in the centre
4. The plastic box will be part filled with sharp sand and then fully saturated in water
5. The spherical charge will be located 50mm below the surface of the sand, directly beneath the centre of the hull
6. Only one charge will be detonated beneath each hull

APPENDIX 7

- Experimental graphs
    - Experiments 1 & 2
    - Experiment 3
- AUTODYN graphs
    - Experiments 1 & 2
    - Experiment 3

Experiment	Dates	Description	Who was responsible
Flat plates	May 2010	Six flat S2-glass composite plates 500mm^2 subjected to varying PE4 charge sizes buried in dry sand	Author, MSc student was presented though this experiment not shared.
1	May 2010	Steel and S2-glass V-shaped hulls shapes A-C, see Figure 5-9. 240g PE4 buried in wet sand with high stand-off	Author and MSc Student and results shared, see (Khare, 2010).
2	December 2010	Steel, S2-glass and E-glass shape D. 240g PE4 buried in wet sand with high stand-off	Author
3	May 2011	Steel, S2-glass and E-glass. Shapes A-D. 240g PE4 buried in wet sand with low stand-off	Author

EXPERIMENTAL GRAPHS – EXPERIMENTS 1 &2

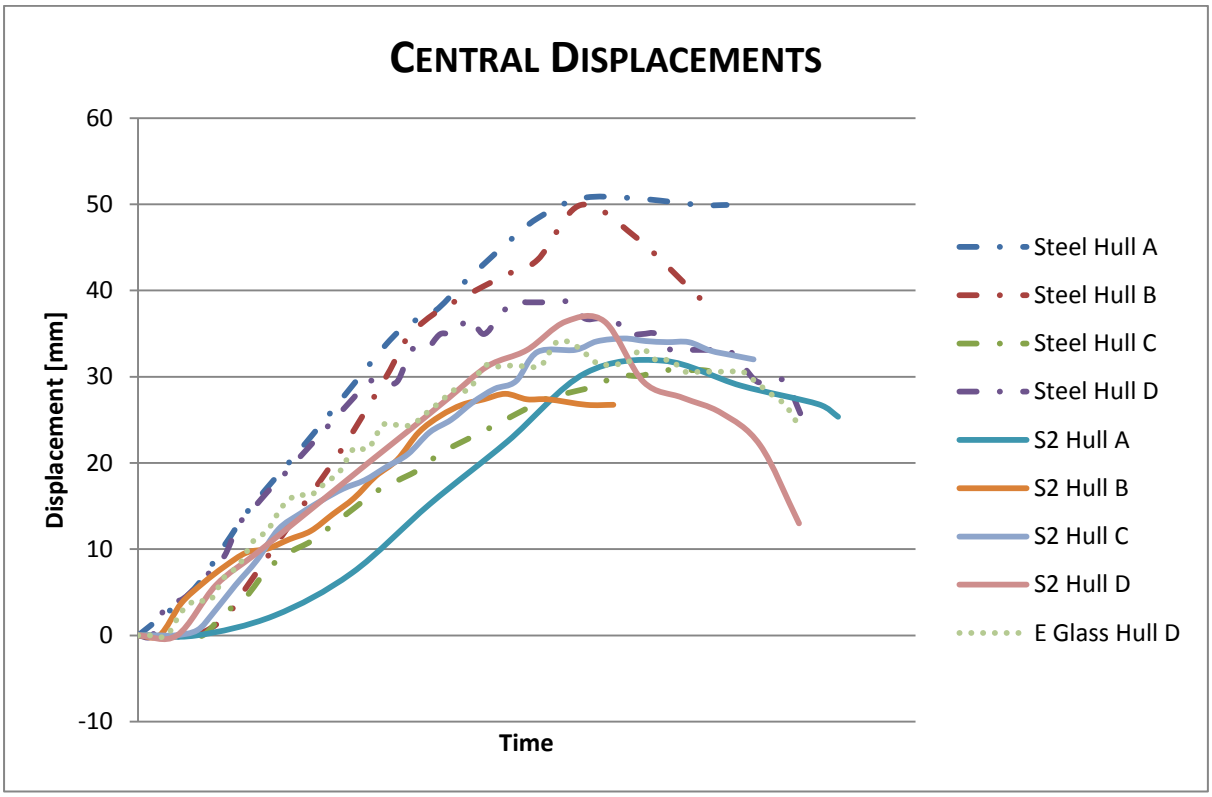

Graph A7-1 Central displacements of all hulls in experiments 1 & 2

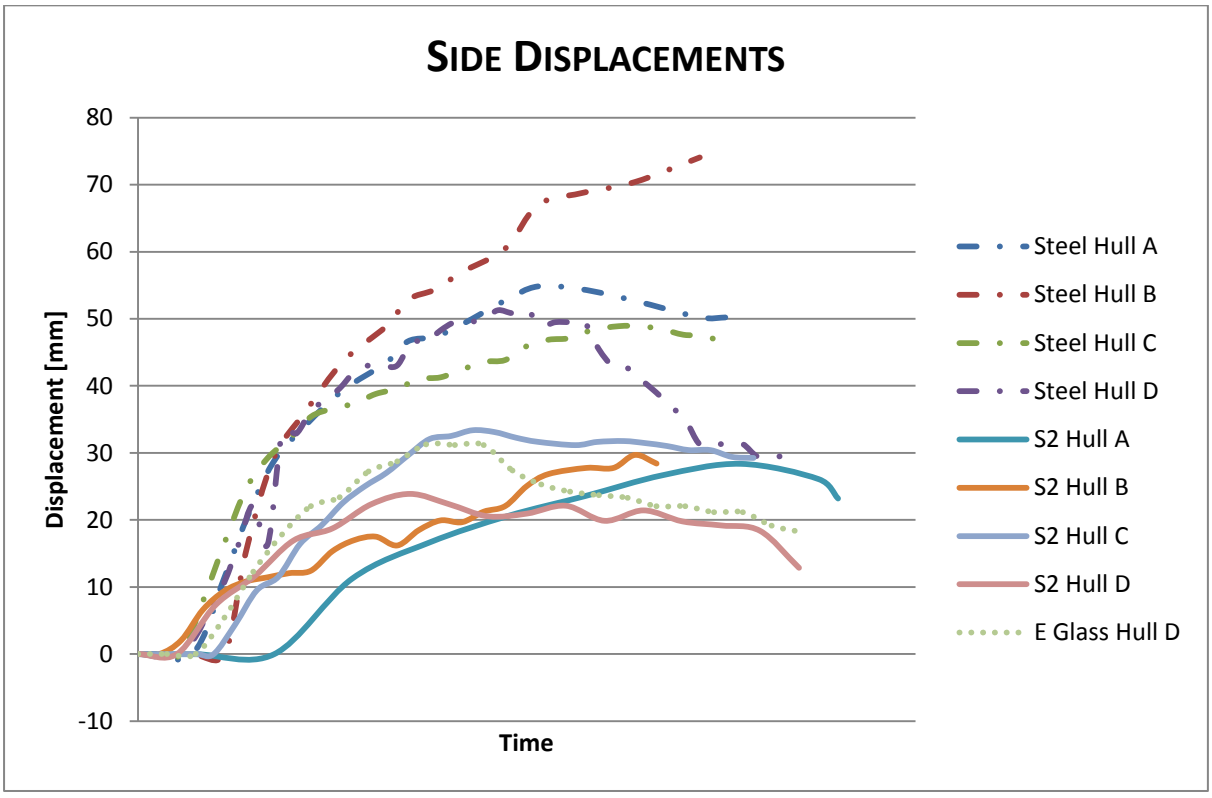

Graph A7-2 Side displacements of all hulls in experiments 1 & 2

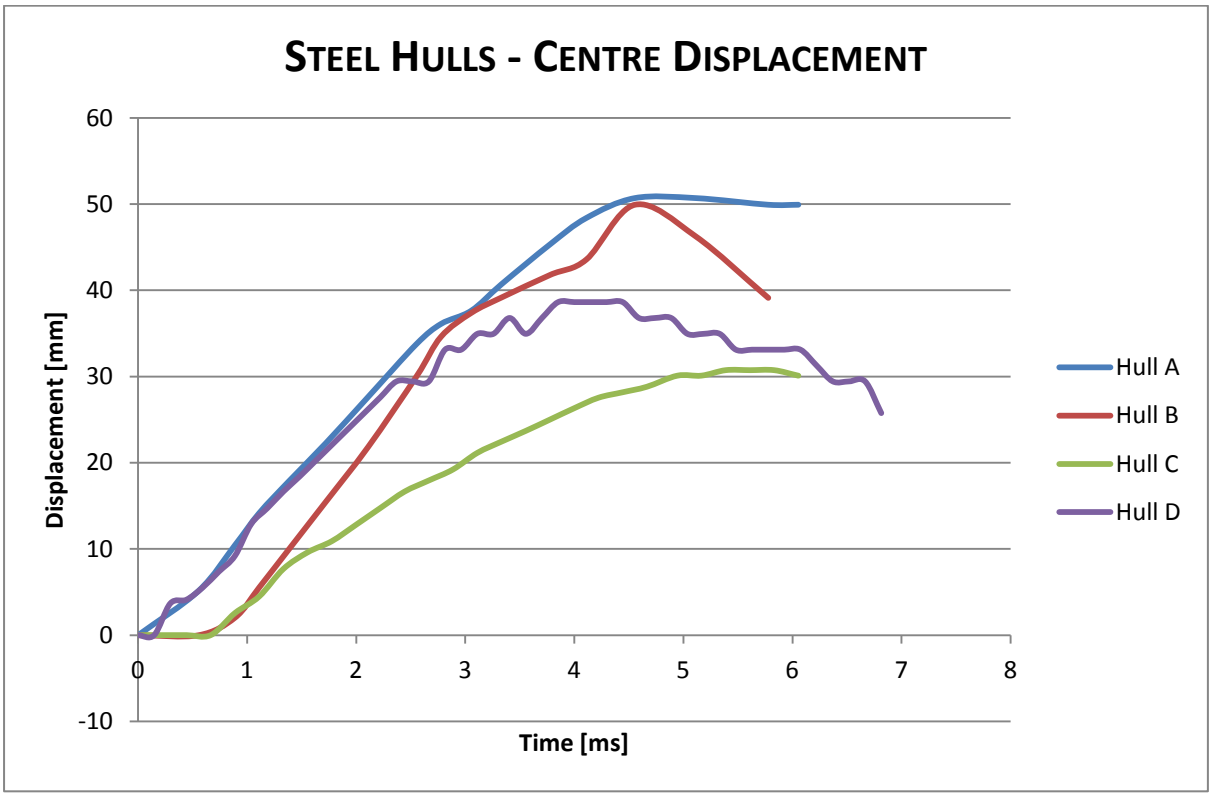

Graph A7-3 Central displacements of steel hulls in experiments 1 & 2

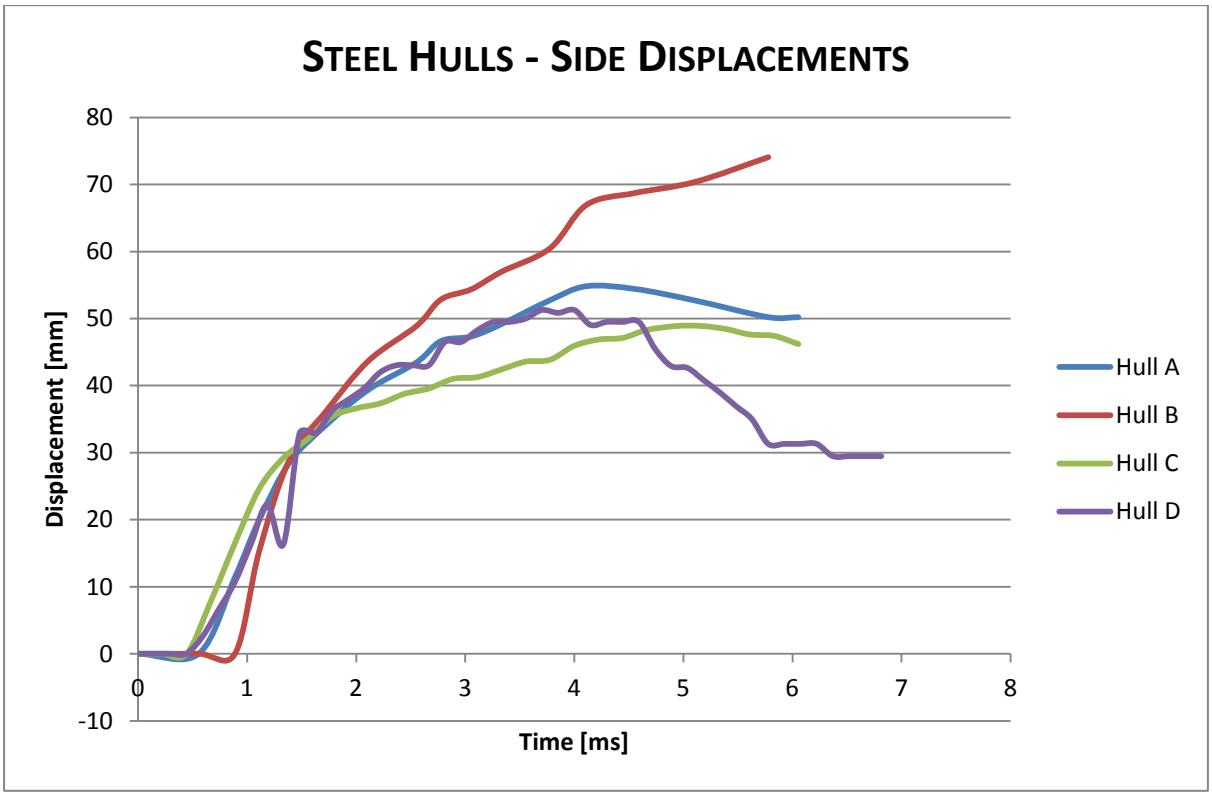

Graph A7-4 Side displacements of steel hulls in experiments 1 & 2

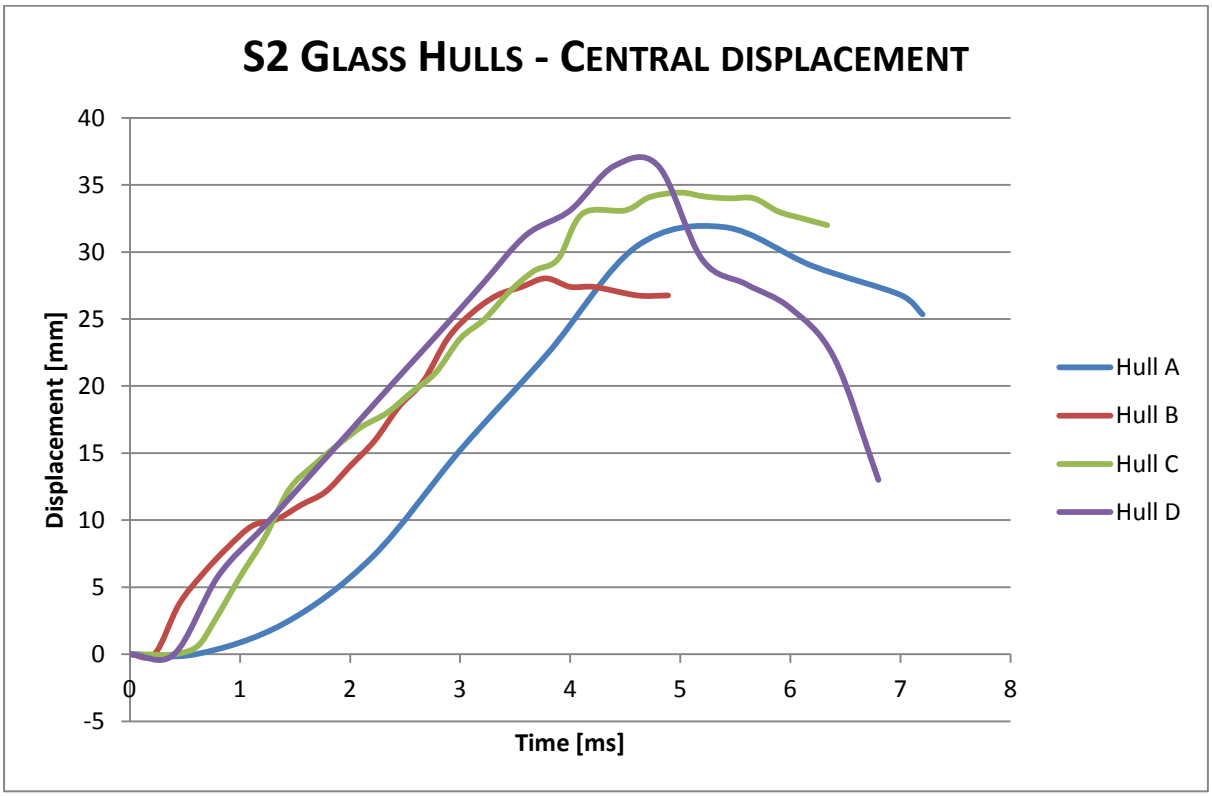

Graph A7-5 Central displacements of S2 glass hulls in experiments 1 & 2

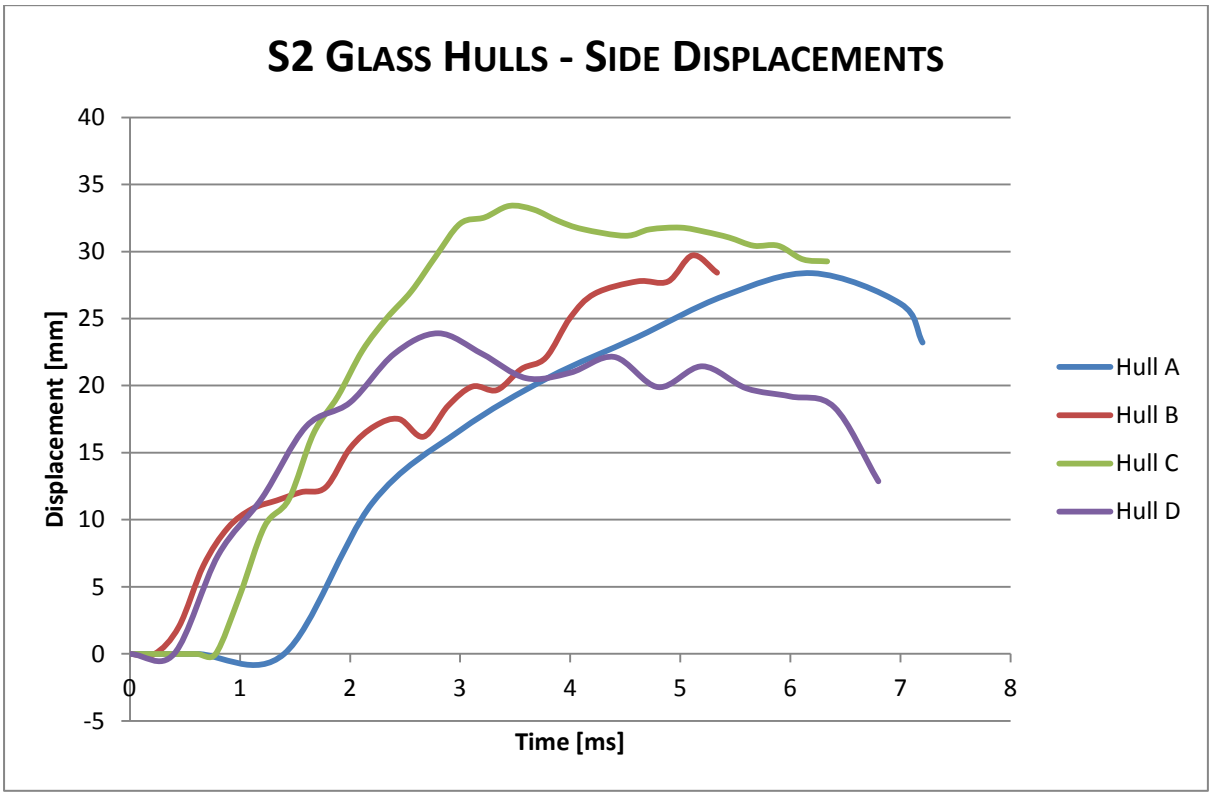

Graph A7-6 Side displacements of S2 glass hulls in experiments 1 & 2

EXPERIMENTAL GRAPHS – EXPERIMENT 3

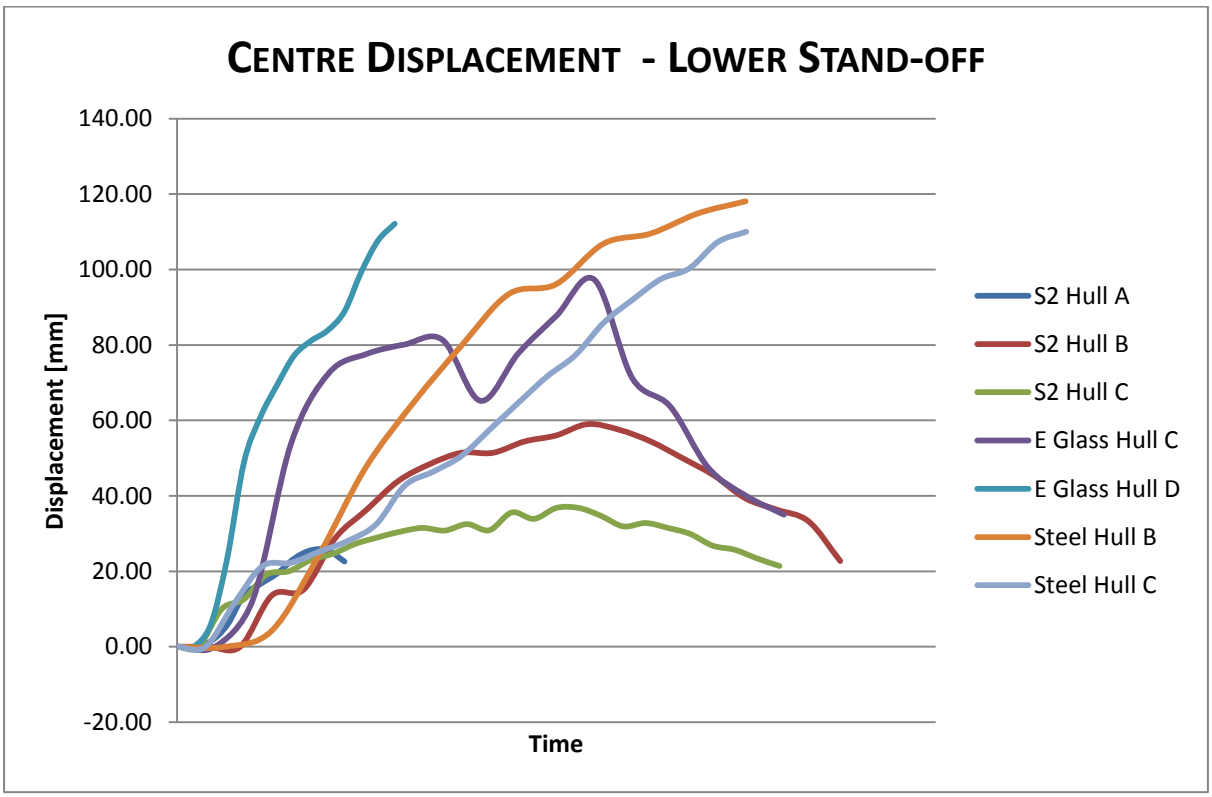

Graph A7-7 Central displacements of all hulls in experiment 3

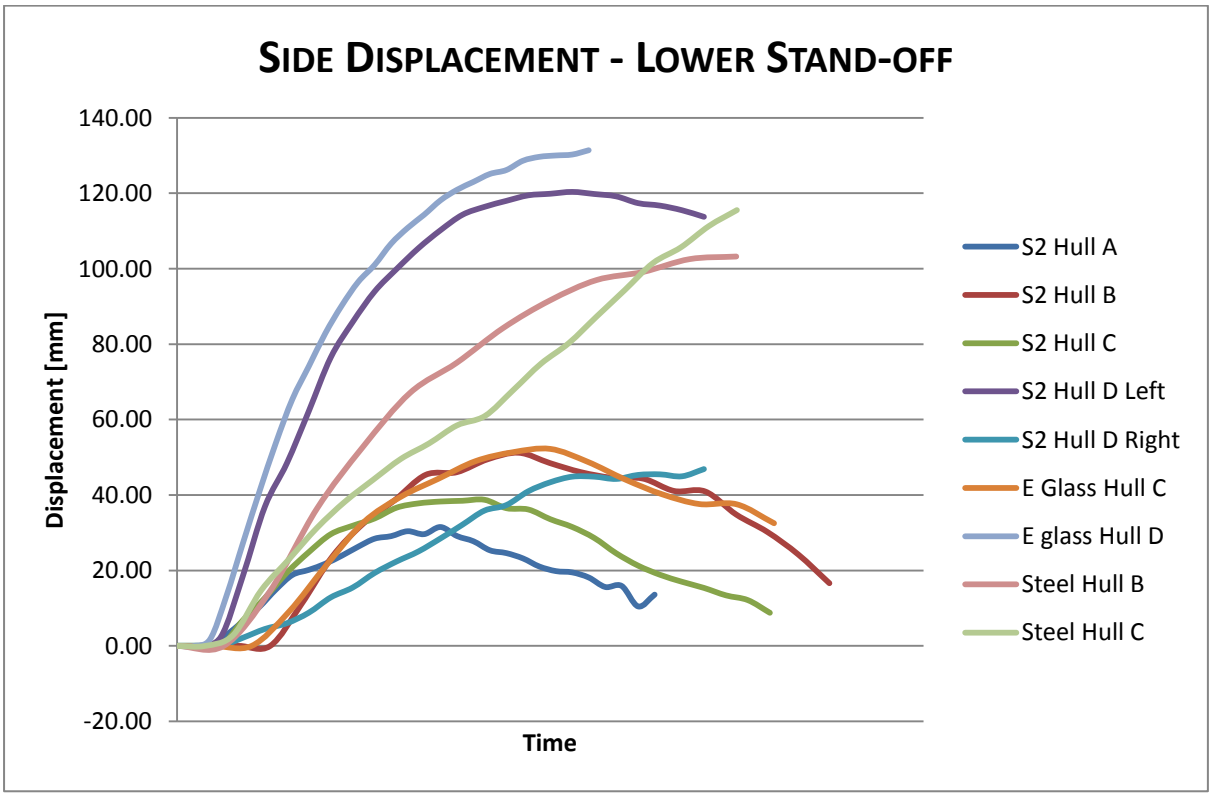

Graph A7-8 Side displacements of all hulls in experiment 3

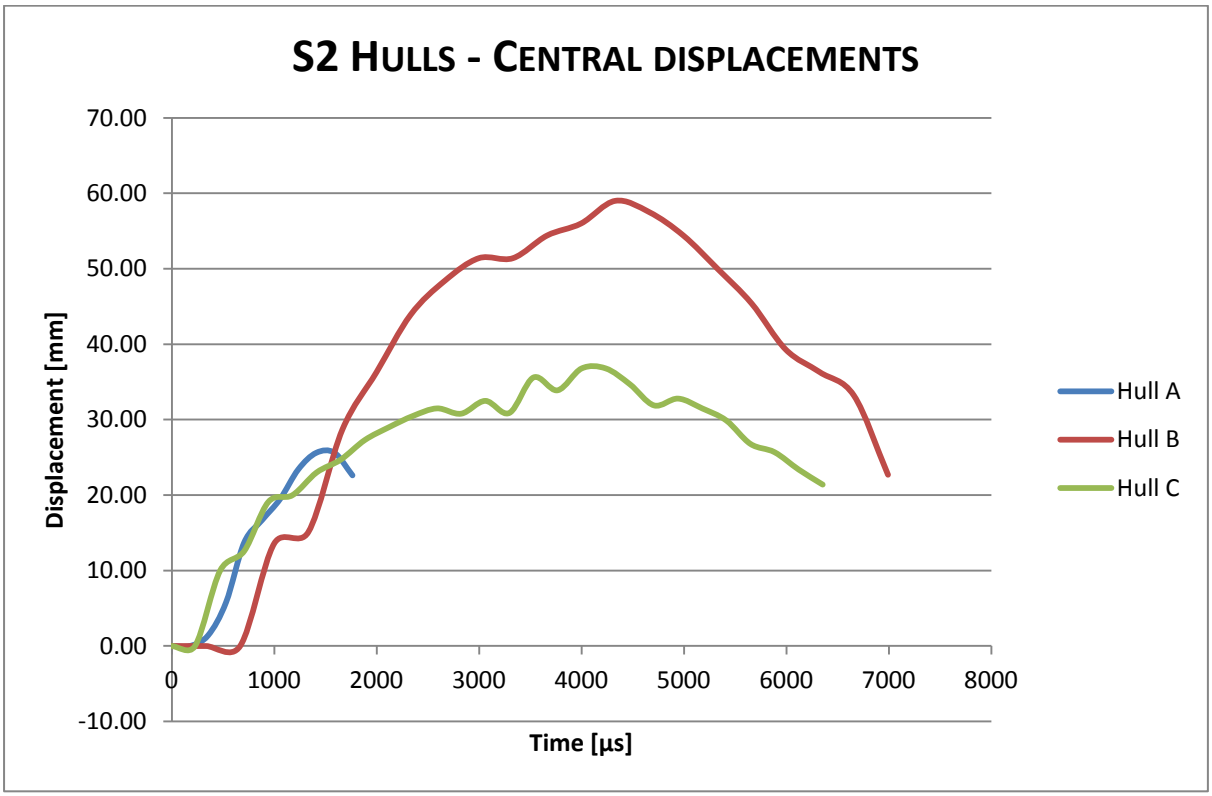

Graph A7-9 S2 central displacements of hulls in experiment 3

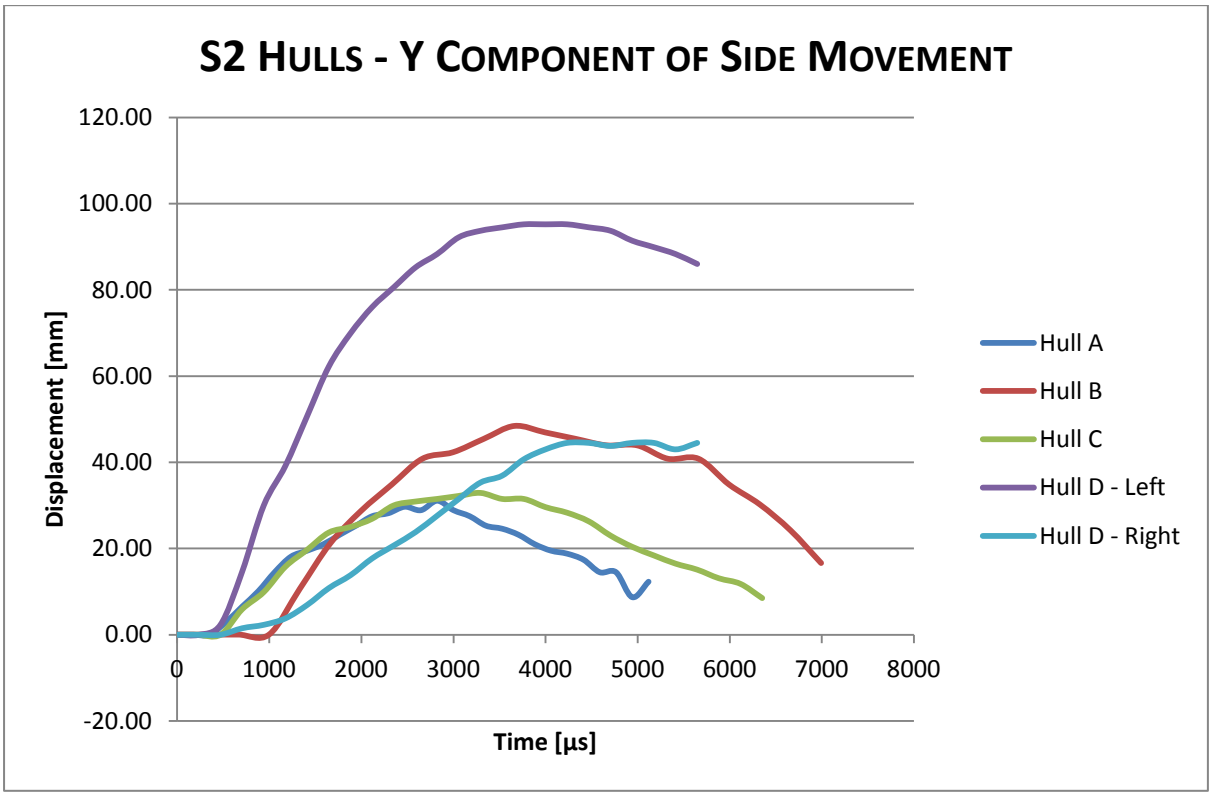

Graph A7-10 Y component of S2 hulls in experiment 3

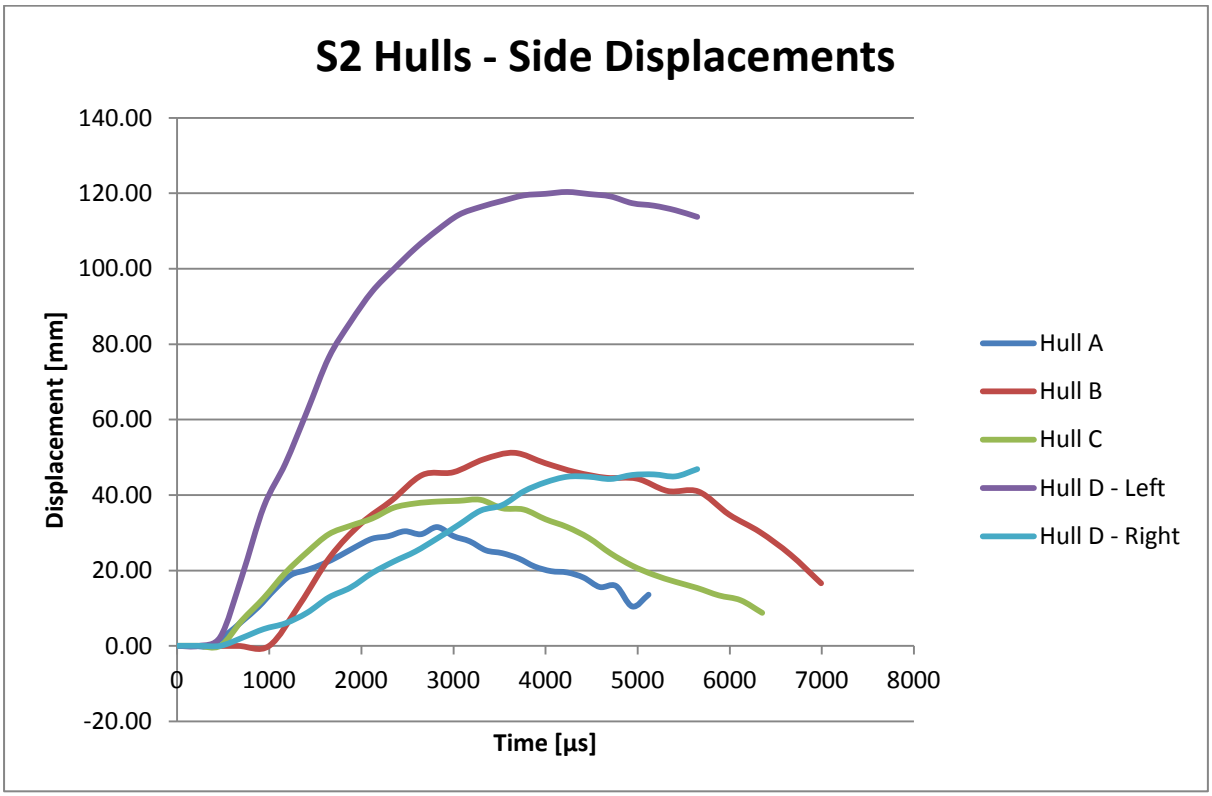

Graph A7-11 Side displacements of S2 hulls in experiment 3

All AUTODYN graphs shown below are the final maximum displacement values during the simulations.

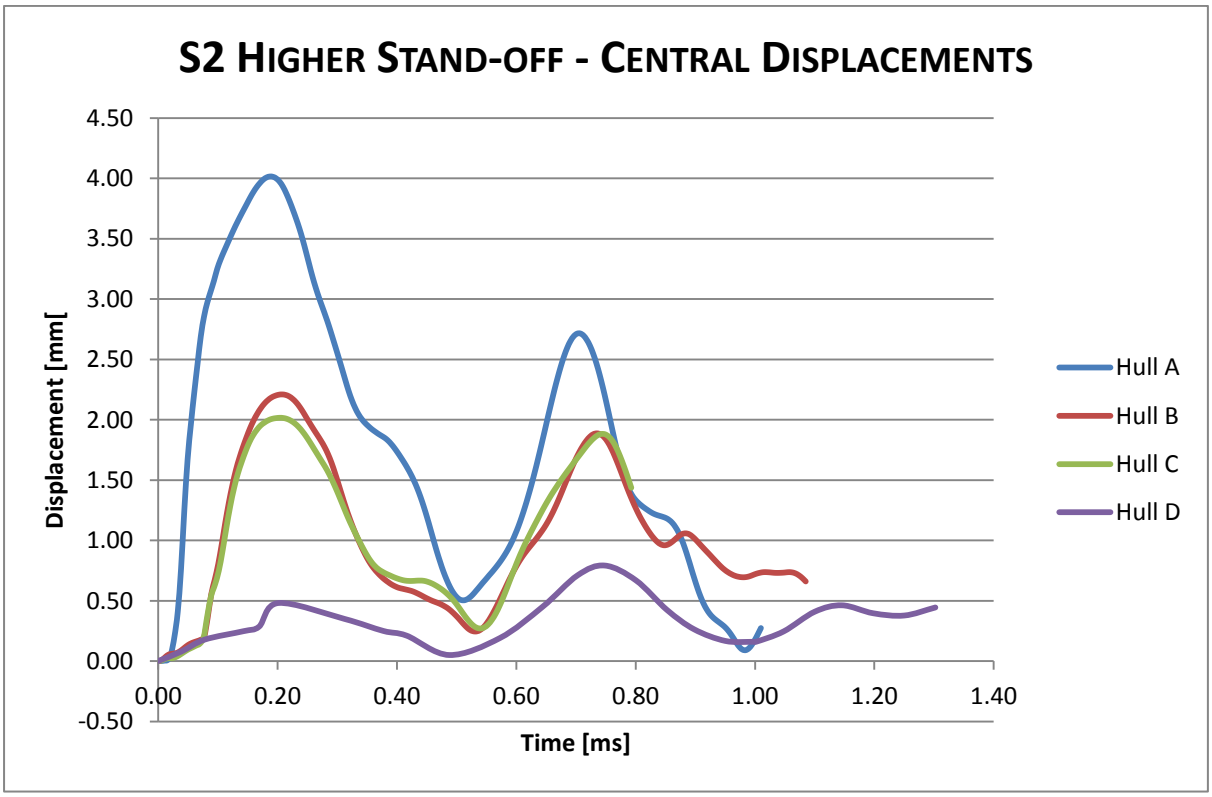

Graph A7-12 S2 glass hulls central displacement from AUTODYN model – air blast

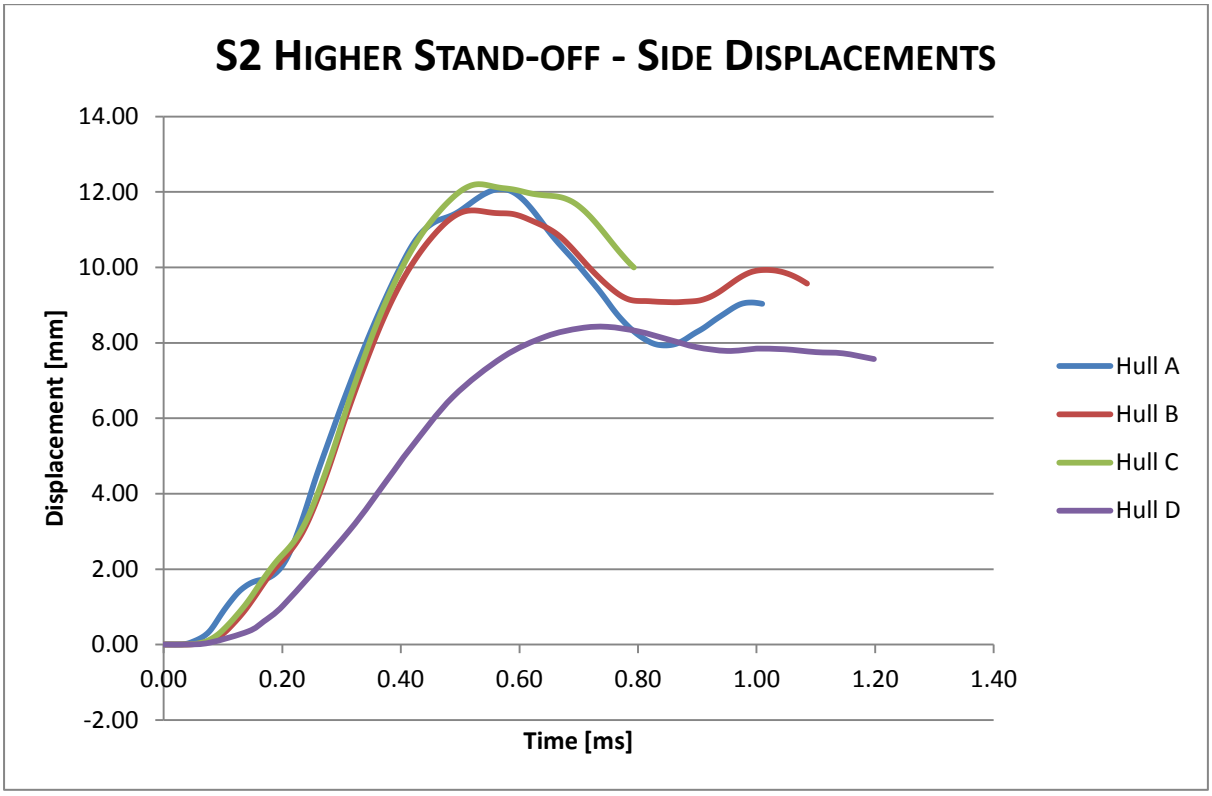

Graph A7-13 S2 glass hulls side displacement from AUTODYN model – air blast

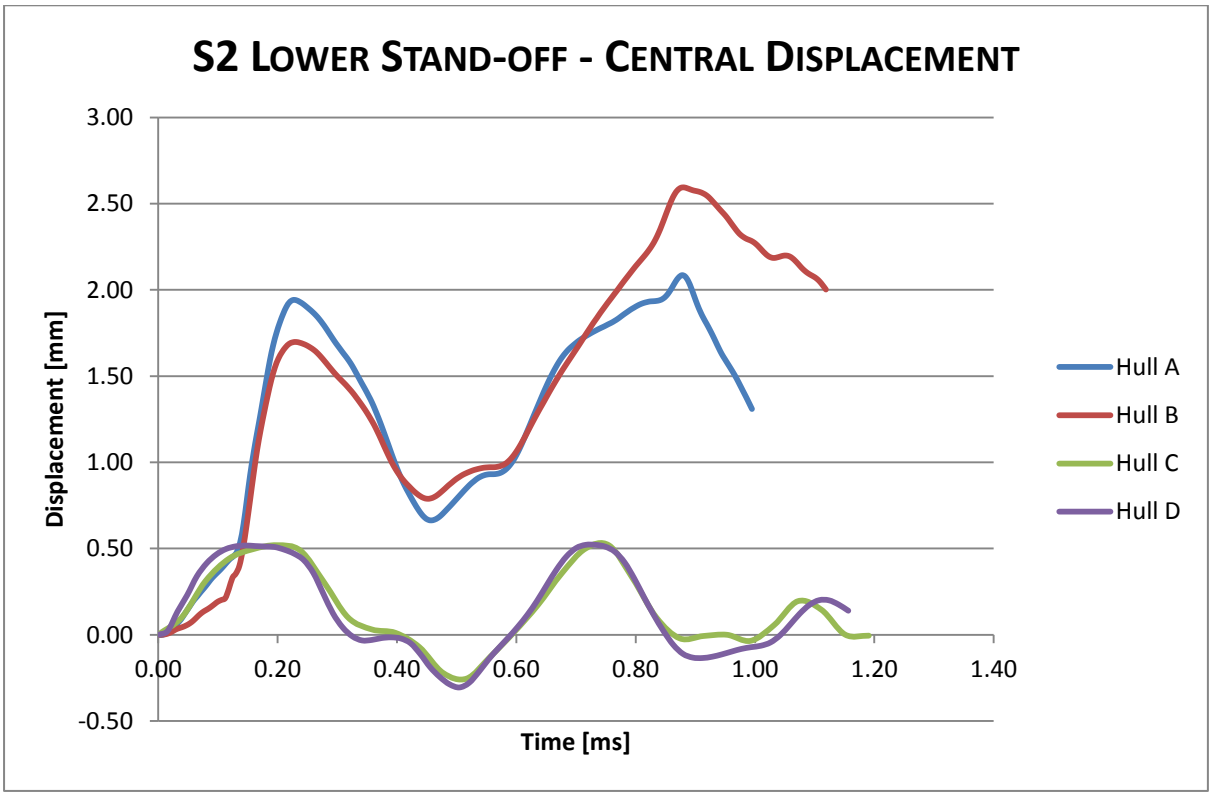

Graph A7-14 S2 glass hulls central displacement from AUTODYN model – air blast

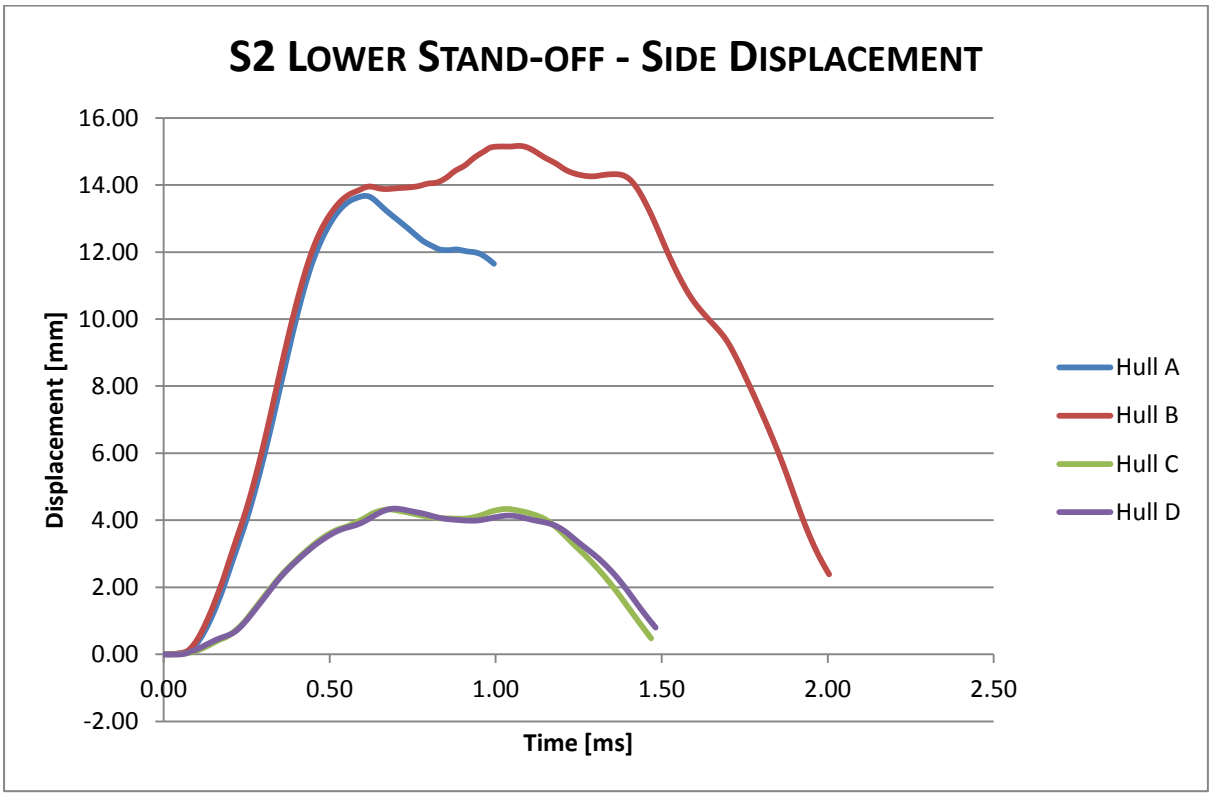

Graph A7-15 S2 glass hulls side displacement from AUTODYN model – air blast

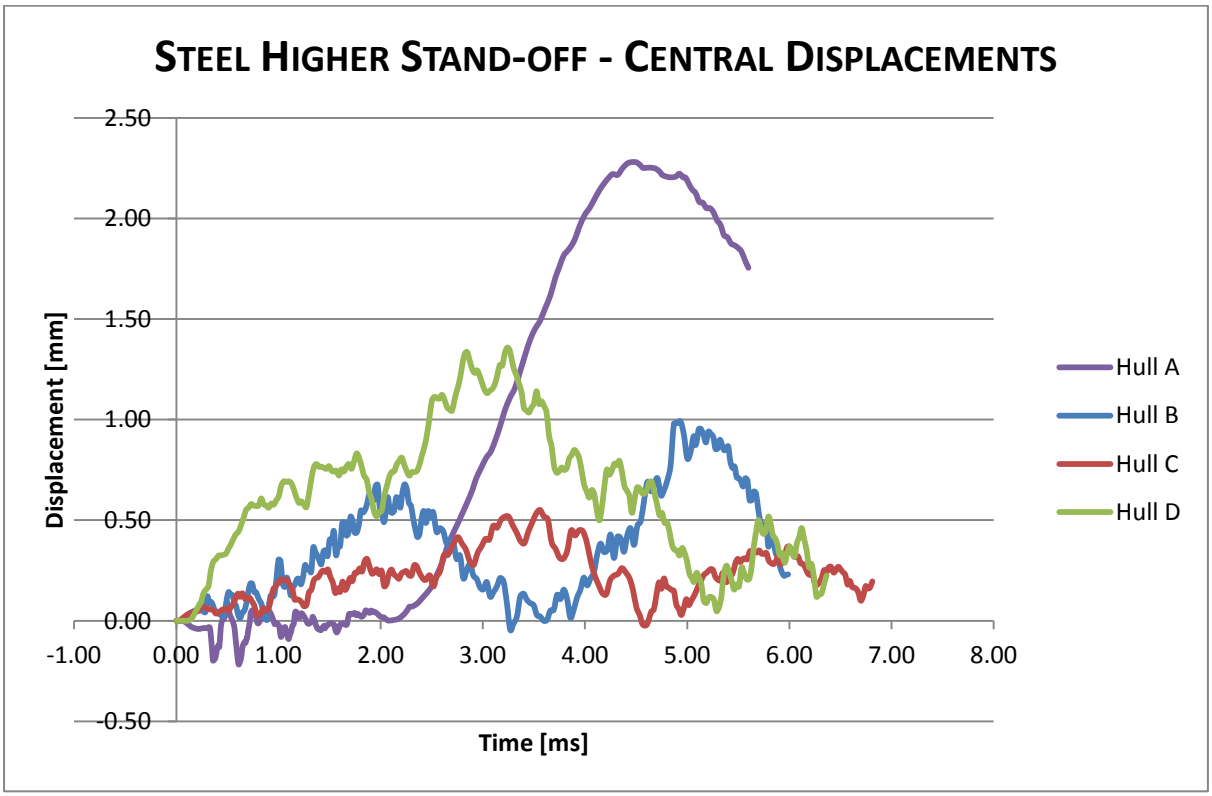

Graph A7- Steel hulls central displacement from AUTODYN model – wet sand

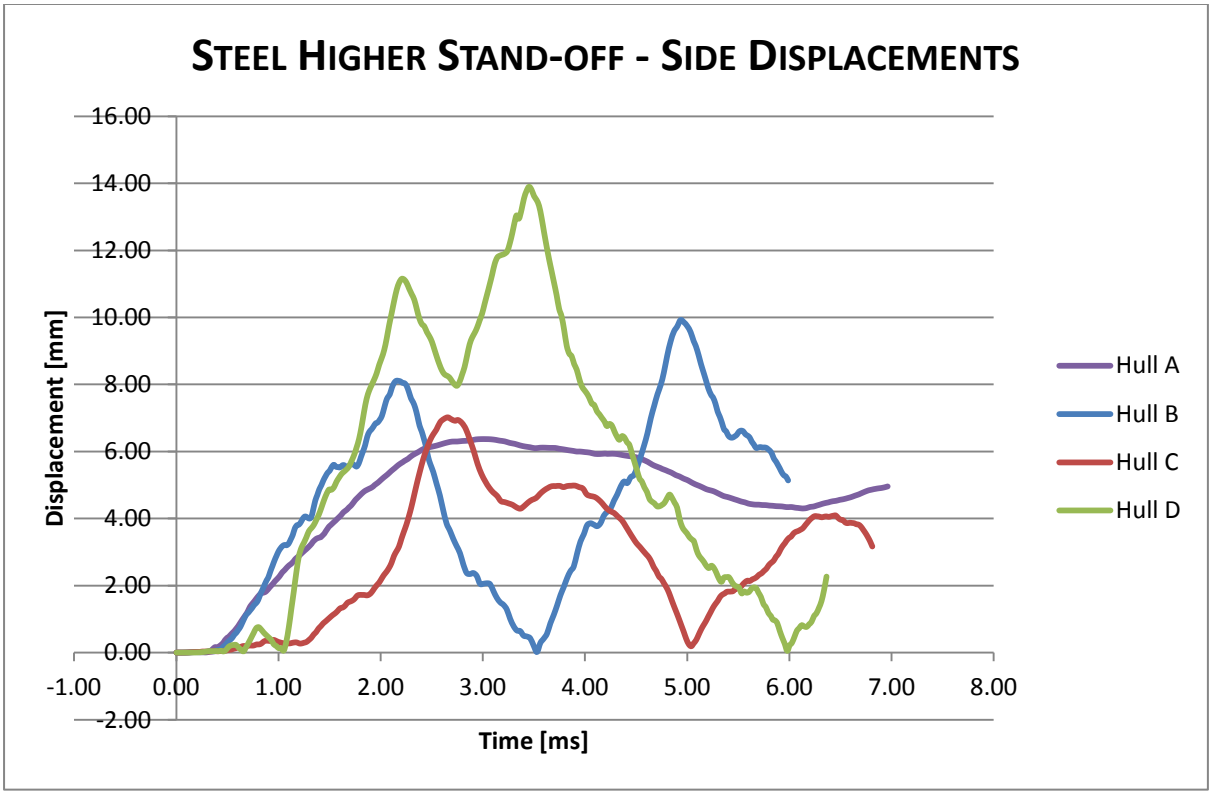

Graph A7- Steel hulls side displacement from AUTODYN model – wet sand

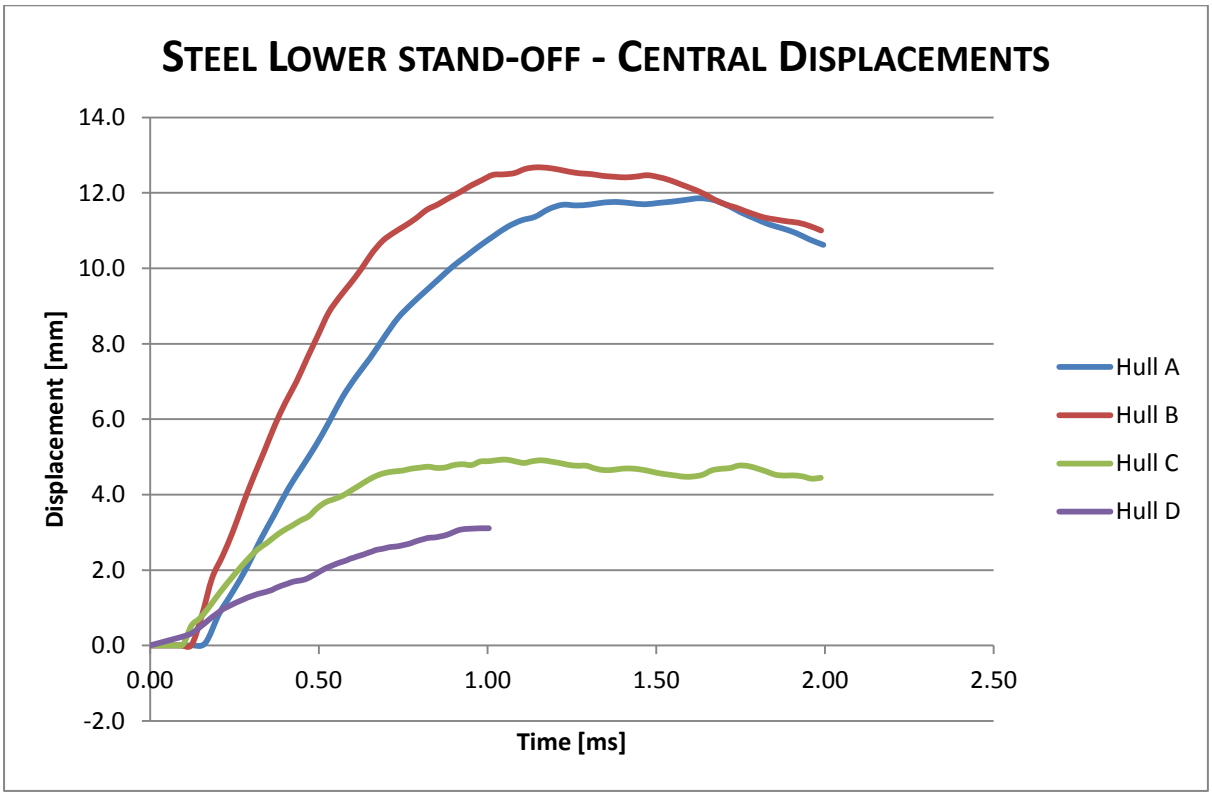

Graph A7- Steel hulls central displacement from AUTODYN model – wet sand

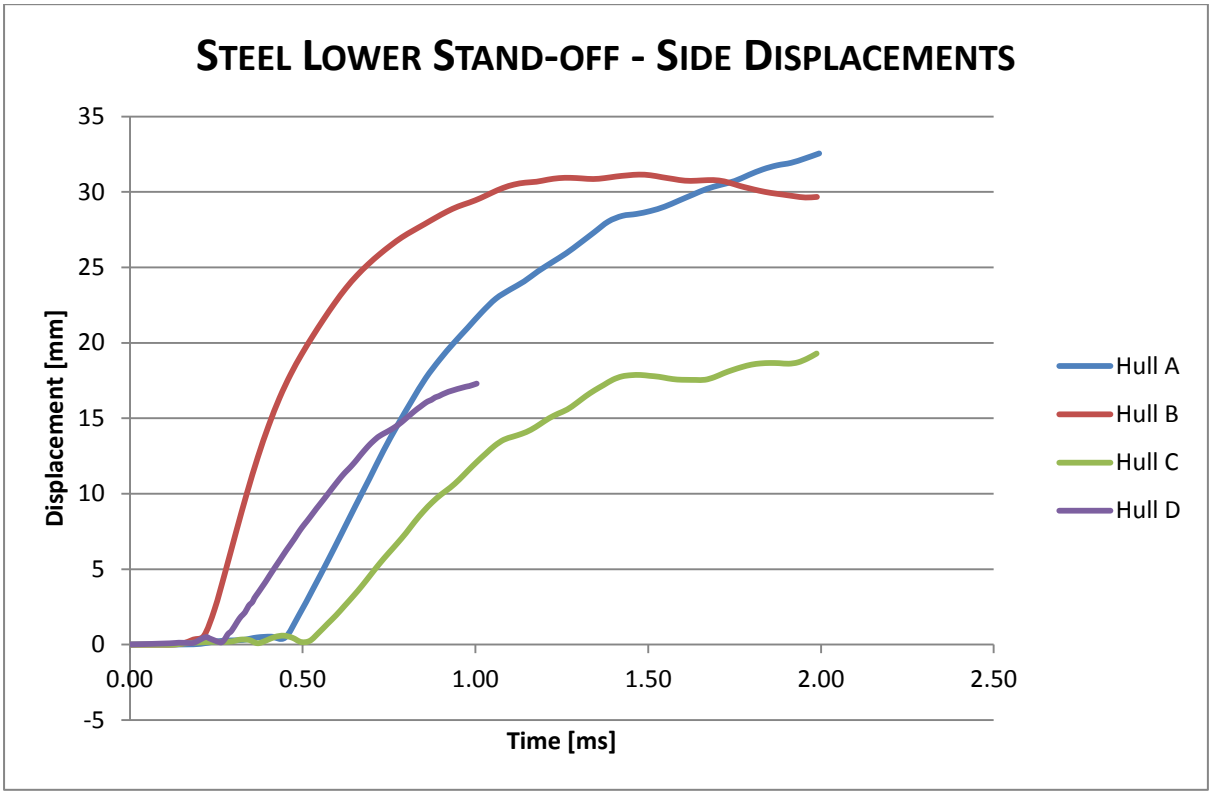

Graph A7- Steel hulls side displacement from AUTODYN model – wet sand

AUTODYN GRAPHS

"NOW THIS IS NOT THE END. IT IS NOT EVEN THE BEGINNING OF THE END. BUT IT IS, PERHAPS, THE END OF THE BEGINNING"

WINSTON CHURCHILL (30 NOVEMBER 1874 – 24 JANUARY 1965)